ELECTRON PARAMAGNETIC RESONANCE STUDY OF AMMONIUM IODIDE SINGLE CRYSTALS DOPED WITH Cu^{2+}, Mn^{2+}, AND VO^{2+} IONS

By

PREM CHAND

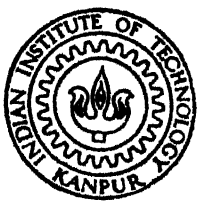

DEPARTMENT OF PHYSICS

INDIAN INSTITUTE OF TECHNOLOGY, KANPUR

JANUARY, 1983

ELECTRON PARAMAGNETIC RESONANCE STUDY OF AMMONIUM IODIDE SINGLE CRYSTALS DOPED WITH Cu^{2+}, Mn^{2+} AND VO^{2+} IONS

A Thesis Submitted
In Partial Fulfilment of the Requirements
for the Degree of
DOCTOR OF PHILOSOPHY

By
PREM CHAND

to the
DEPARTMENT OF PHYSICS
INDIAN INSTITUTE OF TECHNOLOGY, KANPUR
JANUARY, 1983

TO FOND MEMORY OF MY MOTHER

AND

TO MY FATHER

CERTIFICATE

This is to certify that the work presented in this thesis entitled, 'Electron Paramagnetic Resonance Study of Ammonium Iodide Single Crystals Doped with Cu^{2+}, Mn^{2+}, and VO^{2+} Ions', is the original work of Mr. Prem Chand, carried out under my supervision and has not been submitted elsewhere for a degree.

(G.C. Upreti)
Assistant Professor
Department of Physics
Indian Institute of
Technology, Kanpur-208016, India

January, 1983

ACKNOWLEDGEMENTS

I feel elated in placing on record my deep sense of gratitude and indebtness to Dr. G.C. Upreti for his allround guidance in the inception, execution and completion of this work. His words of encouragement in times of stress, his lively interest and ideal approach to the problems and his constructive criticism made him a balanced blend of a 'friend, philosopher and guide'.

Sincere thanks are due to Monash University, Clayton, Victoria, for sending me a copy of the Ph.D. thesis of Dr. T.E. Freeman. I am also grateful to Prof. N.J. Trappeniers for sparing a copy of Dr. S.H. Hagen's Ph.D. thesis. I would like to express my special thanks to the Head, RSIC, IIT, Madras, for his kind permission to record Q-band spectra and to Mrs. R. Geetha for the help in recording the Q-band spectra.

It is a pleasure to thank Professors R.M. Singru, Y.R. Waghmare, V.K. Deshpande, H.D. Bist, G.N. Rao and T.M. Srinivasan for their encouragement and interest in the progress of the work. I am really grateful to Dr. S.K. Sharma for his help in times of need. Thanks are also due to Dr. K.K. Sharma for his interest in the progress of work.

I am morally bound to express my thanks to all of my friends at IIT/K for their co-operation and company which had been a perennial source of pleasure for me. Special thanks are due to Drs. M.B. Patel, S.K. Khosa, and R.S. Saraswat,

for their help in processing of this thesis. I am indebted to late Dr. A.K. Jain for his help in learning the intricacies of the computer programmes used in this thesis. It gives me a pleasure to express my thanks to M/s M. Pal, G.D. Tiwari, B.P. Singh and Dr. A.K. Singh for help in solving many problems faced by us.

The timely help from Physics Workshop, Electronic Shop and Low Temperature Laboratory is gratefully acknowledged. I am grateful to Mr. J.S. Sharma of Physics Workshop for the tremendous help he has given to me during the completion of this thesis.

I appreciate Mr. K.N. Islam for his patient and neat typing, M/s Lallu Singh and H.K. Panda for cyclostyling. I am also thankful to M/s S.L. Kannaujia, Ram Prakash and D.K. Kannaujia for assistance in laboratory and elsewhere.

On behalf of my family I would like to express our sincere thanks for the kind cooperation and pleasant company to the families of Dr. G.C. Upreti, Dr. S.K. Sharma and Prof. M.S. Tyagi. A deep sense of emotion prevails in expressing our thanks to Mrs. and Mr. O.P. Rama for friendship and brotherly affection. Their cheerful disposition and pleasant compa ny has gone a long way in facing many problems.

It is not sufficient but necessary to express my heartiest thanks to the members of my family especially, to my wife Indra and to my daughters Shweta and Swati for

their cooperation and tolerance shown especially during the experimental phase of this work, when I used to work during the odd hours for long periods.

I am grateful to UGC for providing me a teacher fellowship and to the Principal, R.K. College Shamli for granting me leave to undertake this project. I am also thankful to the Director, IIT Kanpur for providing all facilities and help.

In the end I would like to thank all those persons collectively from whom I have received any sort of assistance or scientific information useful for the completion of the present work.

Prem Chand

Prem Chand

TABLE OF CONTENTS

SYNOPSIS

ELECTRON PARAMAGNETIC RESONANCE STUDY OF AMMONIUM IODIDE SINGLE CRYSTALS DOPED WITH Cu^{2+}, Mn^{2+} AND VO^{2+} IONS

PREM CHAND
Ph.D.
DEPARTMENT OF PHYSICS
INDIAN INSTITUTE OF TECHNOLOGY, KANPUR 208016, INDIA

When divalent cation impurities substitute for monovalent cation hosts, an equal number of cation vacancies are created for over all charge compensation. Such cation-vacancy pairs have been extensively studied in alkali halides by EPR using the transition metal ions as impurity cations. EPR has been found to give a direct insight into various processes of ion-vacancy pair formation, because of the identification of type of ion-vacancy complex through their characteristic EPR spectra. As a simple extension of such studies in other similar lattices ammonium halides have attracted much attention. The ammonium halides are in fact more interesting because of their various polymorphic phase transitions. The extensively studied ammonium halides are NH_4Cl: (Cu^{2+}, Mn^{2+}, VO^{2+}, Co^{2+}, Ni^{2+}, Fe^{3+} and Cr^{3+}) and NH_4Br (Cu^{2+}). The only other ammonium halide studied by EPR is $NH_4F:Cu^{2+}$. Of all the ammonium halides ammonium iodide

is rather interesting because it furnishes an opportunity of studying two structural phase transitions below room temperature ($\sim$300K). With the above points in mind EPR study of Ammonium Iodide single crystals doped with transition metal ions has been undertaken. For doping the divalent ions Cu^{2+}, Mn^{2+}, VO^{2+}, Co^{2+} and Ni^{2+} and the trivalent ions Fe^{3+}, Cr^{3+} and Gd^{3+} were tried, out of which, only Cu^{2+}, Mn^{2+} and VO^{2+} EPR spectra could be observed in the temperature range 573K to 77K available in our lab. A detailed EPR study of these ions in ammonium iodide single crystals over the temperature range 573K to 77K has been carried out. The whole work can be broadly divided into three parts, viz. computational analysis of the EPR spectra, study of ion-vacancy complexes and study of the phase transitions in Ammonium Iodide.

Chapter I describes in brief, a general introduction to the subject of EPR in solids, particularly in single crystals. A brief mention of various fields of applications of EPR in interdisciplinary areas has also been made.

Chapter II has been divided into four sections. Section A deals with a brief theory of EPR, the crystal field effects and the Spin-Hamiltonian formalism. The discussion is restricted to iron group transition metal ions in general. Section B presents Spin-Hamiltonian analysis, computational methods and analysis of forbidden hyperfine transitions. Section C briefly describes the application of EPR as a technique to study phase transitions in solids. The last section D presents the crystal

structures of Ammonium Iodide in all its three phases, models for these transitions and the transition temperatures obtained through various experimental techniques.

Chapter III contains a brief description of the experimental set up used in the studies - a Varian E-line X-band EPR spectrometer (E-102), a continuous flow crystat fitted with a Varian E-257/WL-257 variable temperature controller, a two axis crystal rotating device, and a Varian E-500 Gaussmeter for calibration of the magnetic field. The techniques used for growing good quality single crystals doped with paramagnetic impurities have also been described.

In chapter IV results of EPR study of Ammonium Iodide doped with Mn^{2+} have been given. The studies were made at Q-band frequencies at RT and at X-band frequencies in the temperature range 573K to 77K. The parameter b_2^o ($\equiv$ D) was found to be very large ($\sim$1612 Gauss) due to which the X-band spectra were complicated and Q-band studies became desirable. The temperature dependence of the Spin-Hamiltonian parameters and the line widths is presented. The spectra of polycrystalline samples at X-band and at Q-band are also discussed. The strong angular dependence of hyperfine forbidden transitions and the model for ion-vacancy complex has been discussed. The concept of coexisting phases on passing through the I transition temperature below room temperature has also been discussed on the basis of the observed large thermal hysteresis and temperature dependence of Spin-Hamiltonian parameters and linewidths.

Chapter V presents the results of a detailed study of copper doped Ammonium Iodide single crystals in the temperature range 573K to 77K at X-band. Three distinct types of magnetic complexes have been observed. The Spin-Hamiltonian parameters, their temperature variation and the nature of phase transitions have been discussed in this chapter. The possible models for each ion-vacancy complex have also been discussed.

Chapter VI contains the results of the EPR study of Vanadyl ion in Ammonium Iodide. The molecular ion has been found to exhibit a behaviour in NH_4I similar to that in liquids. The observed room temperature and the low temperature spectra have been explained on the basis of the tumbling motion of V-O bond. The applicability of Kivelson's theory of linewidths in liquids has been discussed and used to explain the observed linewidths.

Chapter VII contains the rather complementary results of EPR study of Mn^{2+} and VO^{2+} ions in NH_4Br single crystals. As the EPR study of Cu^{2+}, VO^{2+} and Mn^{2+} in NH_4I single crystals yielded ample information and it was observed that these ions show more or less similar behaviour in NH_4I and NH_4Cl, it was felt interesting to study Mn^{2+} and VO^{2+} in NH_4Br. The results of the EPR study of VO^{2+} and Mn^{2+} in Ammonium Bromide in the temperature range 400K to 77K and their comparison with those in NH_4Cl and NH_4I have been summarised.

Chapter VIII gives a comparative summary of results presented in Chapter IV through VII. The conclusions drawn and the scope for further studies have been discussed.

Each chapter has been written in a manner to be more or less self-contained, therefore, as such repetitions of some statements is expected. The errors in parameters are indicated by numbers inside parenthesis placed after the last significant digit, for example, g = 2.456(5) is equivalent to g = 2.456 ± 0.005. This system is adopted for the purpose of space-economy. The tables and figures for each chapter are placed serially at the end of the related chapter after the reference. Books on the subject of EPR, which were consulted mostly, in writing the thesis are given as 'General References' at the end of the Chapter I.

At the end ~~of~~ two appendices are included. Appendix A contains a literature survey of magnetic resonance and relaxation studies on Ammonium halides and Appendix B contains the algorithm of the method used for calculation of the Spin-Hamiltonian parameters for Mn^{2+} ion.

CHAPTER I

INTRODUCTION

Abstract: The phenomena of Electron Paramagnetic Resonance (EPR) is introduced briefly. A list of electronic systems that can be studied by EPR and the results one can obtain respectively from single crystal studies are discussed briefly. Various applications of the EPR technique are enumerated.

In 1945 Zavoisky[1] discovered the phenomenon, predicted by Gorter and Karonig as early as 1936[2], that the paramagnetic ions in a crystal are capable of absorbing energy from a high frequency magnetic field superimposed on a constant magnetic field to which the crystal is subjected. Soon afterwards, experiments were reported by Cummerow and Halliday[3], and by Bleany and Penrose[4]. Many and varied have been the uses of magnetic resonance techniques since 1945.

The main progress in the techniques of measurement came from the Oxford groups of Bleany and Griffith and their co-workers. The theoretical background was developed by Pryce and his co-workers, Abragam, Stevens, Elliot and Judd in the early stages.

Electron paramagnetic resonance (EPR) is different from simple microwave spectroscopy in the sense that it is highly selective being concerned with paramagnetic materials only, whose energy levels may be tuned by the application of a magnetic field so as to resonate at a chosen frequency. In principle EPR technique can be applied to any paramagnetic system paramagnetic atoms or ions, colour centres donors or acceptors in semiconductors, organic radicals etc. Thus EPR spectroscopy is a technique for detecting unpaired electrons

and for studying the interaction of these electrons with their surroundings. Being a sensitive technique, wherever applicable, it yields accurate and detailed information unobtainable with other methods. This method can give information about the concentration of free radicals, establishes their identities and helps one to learn a great deal about the nature of the chemical bonds within a molecule. The change in molecular motion can be deduced from reversible changes in hyperfine pattern and yields information about trapping and diffusion techniques. Quantitative information about the hyperfine structure reveals the detailed molecular orbit of the unpaired electron and the distribution of the spin density over the molecule. This enables predictions to be made on the reactivity of the different groups in the molecule. There is quite a variety of information to be obtained from free radical studies[5] and the field of investigation is widening all the time. The carbon bonding, carbon heat treated conditions and effects in thermoelectricity can be investigated by means of EPR study of free radicals. The kinetics of radical reactions can be studied by measuring either concentration of free radicals or the relative concentrations of one radical to another. By the latter relationship enzymes have been studied in biochemical work. Chemical kinetics at various temperatures can be followed and intermediates in catalytic analysis be studied. Oxidation reduction systems, corrosion and role played by free radicals in producing corrosion

effects are the other fields of study by EPR for chemists. In biology and associated sciences such as biomedical, biophysical and biochemical, there are numerous uses for EPR. In fact most of the EPR machines are found in the biosciences, where they study enzyme reactions, behaviour of free radicals in living tissues and their carcenogenic effects, effects of radiation on biological materials[5]. Much may be learnt about the phenomenon of photosynthesis and the study of growth by observing the paramagnetic ions needed by some organisms to grow. Essentially all the information, obtained on radicals stabilized in irradiated biomolecules such as nucleic acids[5,6] and proteins[5,7] have been obtained from EPR spectroscopy. EPR has successfully been tried as a diagonestic tool for cancer, jaundice, etc.[5,8,9] by studies of free radicals in the living tissues. Transistors and other semiconductor devices like tunnel diodes, ruby and many more materials of great importance in solid state physics have been investigated using EPR techniques and the investigation has lead to the improved components. Recent development of electron spin resonance imaging of paramagnetic centres in solids[10] has offered the possibility of examining the distribution of paramagnetic centres in samples. Possible applications include radiation damage, diffusion and implantation in solids. Particularly favourable cases are single substitutional nitrogen in diamond and phosphorus in silicon. Variations of the method may permit the observation of spin labels in small biological specimens. The last but not the least

is the interesting use of the EPR technique in dating archeological materials[11]. Very recently Ikeya and Miki[12] have reported a new dating method with a digital EPR, suitable for dating of food or other materials of relatively young age and will be helpful for legal medicine or forgery detection.

EPR is a very powerful tool and has been most widely used in solid state research, especially in single crystals. The concept of 'diluting' a paramagnetic complex by an isostructural diamagnetic medium[13,14] and of forming mixed crystals with diamagnetic compounds[15], enhanced to a great extent the details obtained by EPR (like observation of fine structure, hyperfine structure and in some cases superhyperfine structure). EPR has contributed valuable information concerning the energy levels lying within a few cm^{-1} from the ground state of a paramagnetic system and to the understanding of various interactions in solids. Many magnetic and structural informations may be obtained through the transition ions (Iron group, palladium group, rare earth group, platinum group, and actinide group), where the paramagnetism arises due to electrons in an unfilled d or f shell. Some of them are listed hereunder:

(a) EPR determines the accurate magnitude of the level separation between the energy levels lying within few cm^{-1} from the ground level of a paramagnetic system. The study of these levels by susceptibility measurements requires experimentation at very low temperatures ($kT \sim 1\ cm^{-1}$). The above information is useful in interpreting bulk properties e.g. susceptibility

and specific heat; especially at very low temperatures, when such properties depend only on the levels within a few cm^{-1} of the ground level.

(b) Dilute solid solutions of paramagnetic ions have increased the details obtained by EPR studies. This has made possible to study the fine, hyperfine and superhyperfine interactions of the paramagnetic complex. The hyperfine structure arises due to interaction between electron and nucleus, thus is one direct method for finding the magnitude of nuclear spin in its ground state and approximate values of the nuclear magnetic dipole and electric quadrupole moments can be found.

(c) The sensitivity of the observed EPR spectrum to the symmetry and strength of local electrostatic field provides useful information regarding the symmetry and sites of paramagnetic complex in single crystal study. The number of preferential and 'magnetically inequivalent' sites, the point group symmetry in some cases and the occurence of phase and structural transitions[16] in single crystals are obtained from EPR studies.

(d) The determination of accurate 'g' values contributes in estimating the interaction with high lying levels[17], the nature of chemical bonding and magnetic effects of paramagnetic host ions.

(e) The existence of covalent bonding can be directly observed in EPR spectrum as a superstructure on the EPR transitions[17]. Covalent bonding also leads to a reduction in the

strength of hyperfine interaction.[18]

(f) The saturation of forbidden hyperfine transitions obtained in EPR, is one of the most effective means of polarizing nuclei.

(g) Useful information, is sometimes, obtained about the band structure of solids e.g. in the case of graphite, EPR provides the values of some band parameters which were not available from the previous experimental work.

(h) In a well resolved EPR spectrum, the widths of resonance lines depend on a number of factors e.g. spin lattice relaxation time i.e. the rate at which the microwave energy absorbed by spins is transferred into thermal energy (lattice vibrations), the magnetic dipole interaction between neighbouring magnetic ions and the exchange interaction between neighbours. Thus the information about these factors can be obtained from the observed line widths in EPR spectra.

(i) The study of defects in single crystals by EPR is of great interest. It has been possible to characterize the complex lattice defects and colour centres in single crystals with EPR. Interesting data concerning the properties of conduction electrons in metals and semiconductors have been obtained through EPR[19].

(j) Photosensitive charge transfer processes important in luminiscence and photoconductivity can be investigated by EPR. The first observation of charge transfer by visible light was of Fe^{2+} into Fe^{3+} in Cds[20]. The charged

states observed by EPR are generally produced or enhanced by the trapping of free electrons or holes created during illumination of the crystal with light of energy near to that of the band gap, and diminished with light of energy less than that of the band gap. However, Ni^{3+} were produced with light of energy less than that of band gap by Holten et al[21].

(k) EPR has found important applications in radio engineering in the construction of low noise amplifiers and also in solid state maser materials.

Most of the above mentioned information can be obtained from well resolved EPR spectra. The observation of EPR in concentrated materials is hindered by the broadening of resonance lines due to magnetic interactions between paramagnetic ions and thus makes them unpopular for EPR studies. Of late, however, it has been found that it is possible to get well resolved EPR spectra in paramagnetic hosts satisfying certain criteria and in such cases it is possible to get information about the host crystal.[22] Following are the electronic systems that can be used in studies by EPR.

(1) atoms having an odd number of electrons, like Nitrogen or Hydrogen
(2) ions having partly filled inner electron shells for example transition ions (iron group, palladium group, rare earth group, platinum group and actinide group)
(3) molecules having an odd number of electrons, such as NO

(4) free radicals (compounds possessing unpaired electrons like CH_3), which may often be produced by nuclear radiation

(5) colour centers which involve, in the main, trapped electrons or holes

(6) conduction electrons in metals and semiconductors

(7) a small number of molecules with an even number of electrons but having a resultant angular momentum, as an oxygen molecule.

REFERENCES

1. E. Zavoisky, J. Phys. USSR 9, 211 (1945); ibid 10, 170 and 197 (1946).
2. C.J. Gorter and R. de L. Kronig, Physica 3, 1009 (1936).
3. R.L. Cummerow and D. Halliday, Phys. Rev. 70, 433 (1946).
4. B. Bleany and R.P. Penrose, Nature 157, 339 (1946).
5. D.J.E. Ingram 'Free radicals as studied by ESR', Butterworths, London (1958).
   Pshezhetskii, V.K. Millinchuk, V.A. Roginski and V.I.Tupikov 'EPR of free radicals in radiation chemistry', translated from Russian by P. Shelnitz and edited by T. Pick, John-Wiley & Sons, New York (1974).
   W. Gordy 'Symposium on information theory in biology', Pergmon (1958).
   H.M. Swartz, J.R. Bolton and D.C. Borg 'Biological applications of ESR', Wiley-Interscience,New York (1972).
   S.J. Wyard 'Solid state biophysics', McGraw Hill, New York (1969).
6. A. Muller, Prog. Biophys. Mol. Biol. 17, 491 (1967).
7. W. Gordy, W.B. Ard and H. Shields, Proc. Natl. Acad. Sc. 41, 983 (1955).
8. K.U. Ingold, 'Magnetic resonance in chemistry and biology', Inc.,New York (1975).
9. A.J. Vithayathil, J.L. Ternberg and B. Commoner, Nature 207, 1246 (1965).
   M.J.R. Hoch, J. Phys. C: Solid State Phys. 14,5659 (1981).

10. M.J.R. Hoch and A.R. Day, Solid State Commun. 30, 211 (1979).

11. M. Ikeya, Nature 255, 48 (1975); Archeometry 20, 147 (1978). J.M.Aitken, 'Phys. and Archeology', Clarendon,Oxford (1974).

12. M. Ikeya and T. Miki, Natur. 67, S. 191 (1980).

13. R.P. Penrose, Nature (London), 163, 992 (1949).

14. B. Bleaney and D.J.E. Ingram,ibid.164, 116 (1949).

15. B. Bleany and D.J.E. Ingram, Proc. Phys. Soc. (London) A63, 408 (1950).

16. F.J. Owens,C.P. Poole Jr. and H.A. Farach, 'Magnetic resonance of phase transitions', Academic,New York (1979).

17. J.H.E. Griffiths, J. Owen and I.M. Ward, Proc. Roy. Soc. (London) A219, 526 (1953).

18. J.S. Van Wieringen, Discuss. Farad. Soc. 19, 118 (1955).

19. B. Henderson and A.K. Garrison, Advances in Phys. 22, 421 (1973).

20. J. Lambe, J. Baker and C. Kikuchi, Phys. Rev. Lett. 3, 270 (1959).

21. W.C. Holton, J. Schreider, and T.J. Estle, Phys. Rev. A133, 1638 (1964).

22. G.C. Upreti and R.S. Saraswat, Mag. Reson. Review 7, 215 (1982).

GENERAL REFERENCES

1. W. Low, 'Paramagnetic Resonance in Solids , Solid State Phys. Supplement 2, Academic, New York (1960).
2. A. Abragam and B. Bleany, 'Electron Paramagnetic Resonance of Transition Ions', Clarendon, Oxford (1970).
3. C.P. Poole Jr. and H.A. Farach, 'The Theory of Magnetic Resonance', Wiley-Interscience (1972).
4. J.W. Orton, 'Electron Paramagnetic Resonance', London, Iliffe Books Ltd. (1968).
5. Ed.: F.J. Owens, C.P. Poole Jr. and H.A. Farach, 'Magnetic Resonance of Phase Transitions', Academic, New York (1979).
6. C.P. Poole and H.A. Farach, 'Relaxation in Magnetic Resonance', Academic, Press N.Y. and London (1971).
7. A.S. Marfunin, 'Spectroscopy', Luminescence and Radiation Centres in Minerals', Springer, Berlin (1979).
8. H.M. Swartz, J.R. Bolton and D.C. Borg, 'Biological Applications of Electron Spin Resonance', Wiley-Interscience, New York (1972).
9. D.J.E. Ingram, 'Biological and Biochemical Applications of ESR', Plenum Press, New York (1969).
10. S.J. Wyard, 'Solid State Biophysics', McGraw Hill New York (1969).
11. 'Biological Magnetic Resonance', Vol. III edited by L.J. Berliner and J. Reuben Plenum New York (1981).
12. A selected bibliography covering literature up to 1972 is available at the end in reference (3).

CHAPTER II

THEORY

Abstract: This chapter has been divided into four Sections. In Section A theory of EPR, the crystal field effects, and the spin-Hamiltonian formalism have been discussed briefly. In Section B the methods of spin-Hamiltonian analysis are described. A general method for fitting the spin-Hamiltonian parameters of a spin-Hamiltonian appropriate to an orthorhombic symmetry of crystalline field for ions with S >1/2 has been described. The computational method for angular variation of EPR spectrum, analysis of hyperfine structure and approximate methods in the treatment of hyperfine forbidden transitions are discussed. Section C deals with the applicability of EPR as a technique in the study of phase transitions in crystals. The last Section D contains a brief review of phase transitions in ammonium halides and the crystal structures in various phases are summarized. The transition temperatures of NH_4I obtained through various experimental techniques are reviewed briefly.

SECTION-A

A.1 RESONANCE CONDITION

The condition necessary for obtaining the resonance is equality of the radiofrequency quantum $h\nu$ and the energy difference $\Delta E = (E_1 - E_2)$ between the spin sublevels. When a free ion with a resultant angular momentum J is subjected to a static magnetic field interaction, then it has 2J+1 energy levels, whose energies are given by :

$$E_{M_J} = g\beta H M_J \qquad \ldots \quad (II\text{-}1.1)$$

where M_J = J, J-1, ... , -J+1, -J, H is the static magnetic field, g is the spectroscopic splitting factor and β is the Bohr magneton.

In electron paramagnetic resonance one is interested in the allowed magnetic dipole transitions between these levels. If the direction of the electromagnetic radiation field is parallel or perpendicular to the magnetic field direction the allowed magnetic dipole transitions are given by the selection rules $\Delta M_J = 0$ or $\Delta M_J = \pm 1$, respectively. Hence when the microwave magnetic field is normal to the applied static magnetic field direction, one observes a single absorption line corresponding to the energy difference, $\Delta E = g\beta H$, between the E_{M_J} levels differing in M_J value by ± 1. Therefore for the microwave quantum with energy $h\nu$, the resonance condition becomes :

$$\Delta E = h\nu = g\beta H \qquad .. \quad (II\text{-}1.2)$$

Further the intensities of these transitions are given by the square of the magnetic dipole transition probabilities P_{M_J} where transition probabilities are given by :

$$P_{M_J \leftrightarrow M_J \pm 1} \propto \left[J(J+1) - M_J(M_J \pm 1) \right]^{\frac{1}{2}} \qquad .. \quad (II\text{-}1.3)$$

It is thus clear that different $M_J \leftrightarrow M_J \pm 1$ transitions will have different intensities.

The expression (II-1.2) establishes a triple dependence :
(i) Magnetic field H, brings forth the appearance of spin sublevels (M_J) with energy difference between them.
(ii) The microwave quantum $h\nu$ causes transition from the lower spin sublevel to the upper one, attended by absorption of energy, and produces an absorption signal.
(iii) The g-factor defines the position of the absorption signal for given H and $h\nu$ and is a characteristic of the system (material) under study. Therefore, there are only two technical variants for the resonance condition, viz. the field and the frequency. The spectrometers where microwave frequency is kept fixed and field is varied between two appropriate values until all the possible resonance signals are obtained, are called field swept and are found to be more convenient. After putting the numerical values of h and β the resonance condition (II-1.2) may be rearranged as :

$$H_{(reson.)}^{(G)} = \frac{714.49\,\nu\,(GHz)}{g} \qquad .. \quad (II\text{-}1.4)$$

where G = Gauss and GHz = 10^9 Hz. For a value of g-factor = 2 and

with a frequency equal to 10 GHz the value of the resonance field is about 3500 G; which is readily attainable. The commercially manufactured EPR spectrometers commonly operate within following band frequencies :

Band	Wavelength (cm)	ν (GHz)	$H_{reson.}$ for g = 2 (KG)
X	3.2	9.3	3.3
K	1.25	24.0	8.5
Q	0.8	37.5	13.0

The technique and equipment for measuring EPR spectra are discussed in detail in a number of excellent monographs[1,2].

A.2 CRYSTAL FIELD EFFECTS

(i) Fine Structure of the EPR Spectra

Splitting of energy levels in EPR occurs, under the effect of two types of fields: internal crystalline field and external applied static magnetic field. While studying paramagnetic ions in diamagnetic host crystal lattices, there are two types of internal interactions: (a) dipolar i.e. between paramagnetic ions and (b) ligand field i.e. between paramagnetic ion and the diamagnetic host neighbours. Former interaction is reduced effectively to a negligible proportion by diluting the paramagnetic ions in the diamagnetic host. Thus each ion may be considered isolated from other paramagnetic ions and interacting only with the ligands. The latter interactions modify the magnetic properties of paramagnetic ions. The crystal field (CF) theory assumes that the paramagnetic ion experiences a crystalline electric potential produced

by the neighbouring ions (point charges) or molecules (point dipoles, e.g. H_2O). The unpaired electrons are under the influence of a force due to this potential and their usual orbital motions get modified. In other words the ligands influence magnetic ion entirely through their electric field at its site and the spin states, can, be split by this crystalline field. This splitting is known as the crystalline field splitting (CFS) or zero field splitting (ZFS), or as initial splitting. The order of its magnitude varies typically from 0.1 cm^{-1} to 1.0 cm^{-1} and is quite negligible in comparison to the optical transitions $10x10^3$ cm^{-1}. However, the energy of the microwave quantum (X-band $\sim$ 0.3 cm^{-1} and Q-band $\sim$ 1.25 cm^{-1}) matches with the ZFS in the case of EPR. Sometimes direct measurements of ZFS can be made by using the so called zero field EPR (ZFEPR) technique. This ZFS is responsible for the fine structure in EPR spectra.

The crystal field interaction is affected by the electrostatic screening of the unpaired electrons if the outer shells are occupied. Depending upon its magnitude relative to other interactions, the crystalline field interaction is generally classified into three categories :

(a) Weak crystal field: When CF interaction is weaker than the spin orbit interaction. This is the case with rare earth and certain actinide compounds. This is attributed to the shielding of the magnetic 4f electrons from the crystalline field due to outer $4s^2, 5s^2, 5p^2$ electrons.

(b) Intermediate crystal field: Here the CF interaction is greater than spin-orbit interaction but is less than the Coulombic

interaction between electrons. The best examples of these are the hydrated salts of the iron group. This situation is often described by the so called 'quenching of orbital angular momentum', where the orbital motion is regarded as clamped by the crystal field so that it is unable to respond to an applied magnetic field. The magnetic properties are almost due to spin only.

(c) Strong crystal field: The CF interaction is of the order of the energy of mutual interaction between electrons. This occurs notably in the cyanides of the iron group and the Palladium (4d) and Platinum (5d) groups. In this case due to strong covalent bonding the crystal field assumption actually does not hold.

(ii) Hyperfine Interaction

An interaction of the magnetic moment of an unpaired electron with the magnetic moment of the nucleus produces an additional small splitting of the electron's spin levels and is manifested in the appearance of the hyperfine structure (HFS) in the EPR spectra. The nuclear magnetic moment produces a magnetic field, $\vec{H}_N$, at the site of magnetic electrons and consequently the modified resonance condition becomes :

$$\Delta E = h\nu = g\beta\ (\vec{H} + \vec{H}_N) \qquad .. \quad (II\text{-}1.5)$$

The hyperfine interaction is highly characteristic one and presents a most convenient means for identification of paramagnetic ions (or centres) by the observed hyperfine structure in the EPR spectra. The interaction of the magnetic electron with nuclei of the ligands gives rise to super hyperfine structure (SHFS).

(iii) Effective Spin and Effective g-factor

In EPR only the spin degeneracy of the lowest orbital state is of interest. The specificity of the action exerted by the crystal field on the spin state consists in the fact that cubic field does not split spin states (with exceptions of ions with $S > 2$), whereas noncubic fields lift the spin degeneracy down to doublets. The noncubic fields lift the spin degeneracy even for orbital singlets, the order of splitting of the spin levels being equal to the splittings by the external magnetic field. In cubic crystalline fields (without ZFS) the spacing between the spin sublevels in an static external magnetic field remains the same and, although the number of magnetic levels depends upon the spin multiplicity (i.e. $2S+1$), the difference between the magnetic levels is the same therefore the resonance condition is satisfied at one and the same field value. Therefore only a single EPR line will be observed which can be described by an effective spin $S' = \frac{1}{2}$ (Fig. II-1 (a)). Moreover the interaction of electron spin with nuclear spin results into $(2S+1) \times (2I+1)$ sublevels where I is the nuclear spin and $m_I (= I, I-1, \ldots, -I+1, -I)$ is the nuclear spin magnetic quantum number ($S = I = 5/2$ for Mn^{2+} ion). The selection rules $\Delta M_S = \pm 1$ and $\Delta m_I = 0$ make 30 transitions possible for Mn^{2+} which in the absence of ZFS give rise to six resonance peaks shown in Fig. II-1(b). In non-cubic fields (i.e. in the presence of ZFS), the partially degenerate spin levels are initially separated and therefore the magnetic field lifts the remaining spin degeneracy and leads to several lines in the EPR spectra referred to as the fine structure. Should the initial splitting of the spin levels

be larger than the microwave quantum used ($h\nu$), the lower level will be considered isolated one with an effective spin S' ($= \frac{1}{2}$ for doublet and 0 for a singlet lower level). For $S'=0$ no EPR will be observed. The low lying doublet separated by energy of more than $h\nu$ from higher levels will be described by an effective g-factor ($= g_{eff}$) and spin S' and the resonance condition will then be :

$$h\nu = g_{eff}\beta HS' \qquad .. \quad (II\text{-}1.6)$$

(iv) Kramers' and Non-Kramers' Ions

The Kramers theorem distinguishes the behaviour in the crystalline field of ions containing an even or an odd number of electrons: Kramers' theorem[3] states that, no crystalline field can split the half integral spin states below the doublet ... e (referred to as Kramers' doublet) and assures the observation of EPR in the so called Kramers' ions (odd number of electrons). In the iron group the Kramers' ions $Ti^{3+}(d^1)$, $Cr^{3+}(d^3)$, $Mn^{2+}(d^5)$, $Co^{2+}(d^7)$ and $Cu^{2+}(d^9)$ have indeed always shown EPR transitions.

(v) The Jahn-Teller Effect[4] (JTE)

The essence of the effect is as follows: if for the given symmetry the ground state of non-linear molecule must be degenerate for certain reasons, the disposition of the nuclei changes in such a way that the symmetry of a complex gets reduced, where upon the degeneracy of the principal term is removed. The additional splitting arising therefrom may considerably effect the magnetic properties. Van Vleck[5] estimated that for iron group a splitting of

few hundred cm^{-1} and for rare earth group about 10^{-2} cm^{-1} may be caused by JTE. It has been customary, in the case of cupric complexes, where distortions from regular octahedron are observed, to attribute at least in part, the cause to JTE.

A.3 THE SPIN HAMILTONIAN

The actual interactions of electronic spins in transition series ions are quite complex. Fortunately the EPR spectra can be represented in most of the cases by a suitable spin-Hamiltonian (SH) with suitable constants known as spin Hamiltonian parameters (SHP). The formalism of the SH is based on the concept of an effective spin. As only transitions between lowest energy levels are observed in EPR, the levels between which transitions occur may be treated as isolated levels, even though these may be influenced considerably by the higher lying levels. For a free ion, a state with quantum number J will split into 2J+1 states in an external magnetic field. Analogously, if the observed transitions are consistent with transitions between 2S'+1 levels, one may define S' as a "fictitious spin" of the system. Thus th levels (2S'+1) may be treated as if originating from a state with "effective spin" or "fictitious spin" equal to S' and the magnetic dipole having 2S'+1 possible orientations. The fictitious spin S' may or may not be equal to the real spin S of the system; for example for Mn^{2+} S = S' = 5/2 and for Cr^{3+} S = S' = 3/2 but for Co^{2+} generally S(= 3/2) $\neq$ S', and S' is found to be 1/2. In Fig. II.2 patterns of EPR spectra of Fe^{3+} and Mn^{2+} are shown and in Fig. II.3 patterns of EPR spectra of the iron group ions are shown. Thus the SH is an energy operator

containing only spin variables. The dependence of SH on the variables other than spin is included in its constants. The derivation of SH in its general form is presented in a number of excellent monographs[6-13].

Generally EPR results from a simultaneous manifestation of several interactions viz. spin orbit, spin-spin, hyperfine, electronic zeeman, nuclear Zeeman and quadrupole interactions. Thus the complete spin Hamiltonian must contain terms describing all possible types of interactions of the magnetic electrons of the impurity ion in a crystal placed in an external magnetic field. These interactions are included in the spin Hamiltonian depending on their strength. The general SH is expressed in the following form :

$$\mathcal{H} = \underbrace{\beta \vec{H}.\tilde{g}.\vec{S}}_{\text{Electronic Zeeman}} + \underbrace{\vec{S}.\tilde{D}.\vec{S}.}_{\text{Fine Structure}} + \vec{S}.\tilde{A}.\vec{I}. + \vec{I}.\tilde{P}.\vec{I}. - \underbrace{\beta_N \vec{H}.\tilde{g}_N.\vec{I}}_{\text{Nuclear Zeeman}} \quad \text{..(II-1.7)}$$

where $\vec{S}$ and $\vec{I}$ are the electronic spin and nuclear spin operators respectively and are equivalent to $\vec{J}$ operators from mathematical point of view and $\tilde{g}$, $\tilde{D}$, $\tilde{A}$, $\tilde{P}$ and $\tilde{g}_N$ are tensor quantities. The detailed discussion of all these terms may be found in many books, for example those by Abragam and Bleany[8] and by Poole and Farach.[12] Sometimes it is found convenient to express the spin-Hamiltonian in terms of the so called equivalent spin operators, each such operator being the equivalent of a combination of spherical harmonics. This has the advantage that the appropriate SH can possibly be written down without detailed calculation, since the SH must reflect the symmetry of the crystal field. The number of such

spin operators is generally limited because of several restrictions viz. non zero matrix elements, invariance under time reversal and higher symmetry of crystalline field. The SH may then be written in the following form[12]:

$$\mathcal{H} = \beta \vec{S}.\tilde{g}.\vec{H} - \beta_N \vec{H}.\tilde{g}_N.\vec{I} + \vec{S}.\tilde{A}.\vec{I} + \sum_{\substack{l=2 \\ \text{even}}}^{2S} \sum_{m=0}^{l} B_l^m O_l^m(S) + \sum_{k=2}^{2I} \sum_{q=0}^{k} C_k^q . O_k^q(I) \quad .. \quad (II\text{-}1.8)$$

where q and m are any integers within the range and l and k are even integers. The form of O_l^m operators are given by Abragam and Bleany[8] (Table 16, Appen.B, page 863) and can also be found in many other books on EPR. The matrix elements have been tabulated by Abragam and Bleany[8] and by Sorin and Vlasova[14]. For $O_l^m(S)$ and $O_k^m(I)$ the operators J_i are replaced by S_i and I_i respectively[12]. The coefficients B_l^m and C_k^q assume definite values for specific interactions. The systematics of the B_l^m parameters depending upon the symmetry, the ion and its spin is listed in Table II.1. The relationship of the B_l^m coefficients with parameters b_l^m, which are also frequently used in EPR, and with the other traditional parameters in use are given below :

$D = 3B_2^0 = b_2^0$; $E = B_2^2 = b_{2/3}^2$ (for orthorhombic ZFS interactions);

$a = 120B_4^0 = 24B_4^4$ =(for fourfold axis coordinate system);

$a = -80B_4^0 = -1600\sqrt{2}B_4^3 = -\frac{80}{3}b_4^3$ (for the threefold axis coordinate system) (cubic ZFS which exists for $S > 3/2$);

$F = 180B_4^0 = 3b_4^0$ (the ZFS which exists for axial distortions for $S > 3/2$)and in general $b_2^m = 3B_2^m$; $b_4^m = 60B_4^m$ and $b_6^m = 1260B_6^m$.

The axial quadrupole term is :

$$P\left[3I_3^2 - I(I+1)\right] = C_2^0 O_2^0(I) \quad .. \quad (II\text{-}1.9)$$

and thus

$$P = \frac{eqQ}{4I(2I-1)} = C_2^0 \quad .. \quad (II\text{-}1.10)$$

where $q = \left(\frac{\partial^2 V}{\partial x^2}\right)$ is the electric field gradient at the nucleus. In lower symmetry the quadrupole interaction term becomes :

$$P\left[3I_z^2 - I(I+1) + \eta(I_x^2 - I_y^2)\right] \quad .. \quad (II\text{-}1.11)$$

which in terms of C_k^q and $O_k^q(I)$ becomes :

$$C_2^0 O_2^0(I) + C_2^2 O_2^2(I) \quad .. \quad (II\text{-}1.12)$$

and thus $C_2^2 = P\eta$ where the parameter η is referred to as the a-symmetry and is thus defined by the ratio $C_2^2/C_2^0 = \eta$. Another completely different way to express the spin Hamiltonian is also employed, adopting the irreducible tensor formalism and leads essentially to the same form of SH and therefore will not be discussed in this thesis. One of the major short-comings of the Steven's operators (O_l^m) is that they do not exactly transform like spherical harmonics under the finite arbitrary rotations[15,16]. Bleany and Stevens[17] and Bowers and Owen[18] have reviewed the application of these phenomenological SHs. Buckmaster[19] has made use of the so called angular momentum tensor operators $T_{lm}(S)$ in place of Stevens operators (O_l^m) and Buckmaster and Shing[20] compared the O-operator and T-tensor formalisms for the paramagnetic Gd^{3+} ion. A comprehensive review of the latter formalism has been given by

Buckmaster et al[21] who found that this latter formalism may be preferred to the former because T-tensors can be transformed consistently using the matrix elements of finite rotation operator even for arbitrary rotation[19-21] whereas O-operators can only be transformed consistently for selected rotations[19]. However this does not pose serious problems as the transformation relations for Stevens operators for rotations have also been completely derived and are available in literature[14]. Therefore we will adhere to the use of O-operators in this thesis.

A.4 ZFS OF S-STATE IONS (Mn^{2+})

The S-state in principle will have no interaction with crystal field, to first order, hence no ZFS. However, small to very large ZFS for Mn^{2+} and Fe^{3+} have been observed in practice. Out of numerous theoretical attempts made to calculate ZFS Mn^{2+} ion, none is found entirely satisfactory and the problem still remains unsolved and challenging to the theoretical workers. We would not attempt any discussion on this point except citing references[22-30], in which attempts have been made towards theoretical explanation of ZFS in S-state ions.

A.5 FORBIDDEN TRANSITIONS

The selection rules when magnetic field is perpendicular to the applied magnetic field are $\Delta M_s = \pm 1$ and $\Delta m_I = 0$, where M_s and m_I are the electrons spin quantum number and nuclear spin quantum number respectively. These are the so called allowed transitions. Fig. II-2 shows the pattern of such transitions in the EPR of Mn^{2+} and Fe^{3+} under various interactions. In certain

cases transitions with $\Delta M_s \neq \pm 1$ and $\Delta m_I \neq 0$ are also observed. These are normally forbidden transitions but when observed become allowed. The transitions with $\Delta M_s \neq \pm 1$ (i.e. $\Delta M_s = \pm 2, \pm 3$ etc.) are referred to "fine-forbidden" transitions while those with $\Delta m_I \neq 0$ (i.e. $\Delta m_I = \pm 1, \pm 2$ etc.) are referred to as "hyperfine forbidden transitions". The fine forbidden transitions become allowed due to the mixing of different M_s states whereas hyperfine forbidden transitions become allowed due to mixing of various m_I states.

SECTION-B

SPIN-HAMILTONIAN ANALYSIS

The EPR spectra of Mn^{2+} ion reported in this thesis have been analysed by the method originally developed by Uhrin[31] and later modified by Jain and Upreti[32]. In this section we will describe this method and related matter for an SH of orthorhombic symmetry which is applicable equally well to cases of higher symmetry also.

(i) The Axes System

For all S-state ions in general and Mn^{2+} in particular $\tilde{g}$ and $\tilde{A}$ are found to be almost isotropic[8] and therefore the asymmetry is often overlooked and the coincidence of principal axes of $\tilde{g}$, $\tilde{A}$ and $\tilde{D}$ tensors is presumed. Further for S-state ions and for iron group ions in general the contributions of the second order CF terms $B_2^0 O_2^0 + B_2^2 O_2^2 = \vec{S}.\tilde{D}.\vec{S}$. are usually an order higher than higher order of CF terms, so that one can assume that the principal axes

of D-tensor (a system of axes in which the tensor is diagonal) will determine the principal axes of the complete SH and consequently those of the EPR spectrum. Neglecting hyperfine interactions the SH (II-1.8) for orthorhombic symmetry can be expressed as :

$$\mathcal{H} = \beta(g_x \mathrm{Sin}\theta\mathrm{Cos}\phi S_x + g_y \mathrm{Sin}\theta\mathrm{Sin}\phi S_y + g_z \mathrm{Cos}\theta S_z).H + B_2^0 O_2^0 + B_2^2 O_2^2 + B_4^0 O_4^0 + B_4^2 O_4^2 + B_4^4 O_4^4 \quad .. \quad (II\text{-}2.1)$$

where θ and ϕ are the usual polar and azimuthal angles respectively with respect to g-tensor principal axes (X, Y and Z) and the axis of quantization has been chosen along one of the principal axes of D-tensor. The Zeeman term can be diagonalized if the axis of quantization is chosen to be the direction of magnetic field $\vec{H}$ and then the SH of II-2.1 assumes the form[32,33] :

$$\mathcal{H} = \beta g_{ii}.H\, S_z' + B_2^0 O_2^{0'} + B_2^2 O_2^{2'} + B_4^0 O_4^{0'} + B_4^2 O_4^{2'} + B_4^4 O_4^{4'} \quad .. \quad (II\text{-}2.2)$$

or alternatively:

$$\mathcal{H} = \beta g_{ii}' H S_z + B_2^{0'} O_2^0 + B_2^{2'} O_2^2 + B_4^{0'} O_4^0 + B_4^{2'} O_4^2 + B_4^{4'} O_4^4 \quad .. \quad (II\text{-}2.3)$$

where the modified primed operators of (II-2.2) are related to unprimed operators by expressions given by Sorin and Vlosova[14]. The relations between the modified constants (primed B_l^m) can alternatively be derived from the relationship between O_l^m and $O_l^{m'}$.

In the principal axes system the term $\vec{S}.\tilde{D}.\vec{S}$. becomes equal to $D_{xx}S_x^2 + D_{yy}S_y^2 + D_{zz}S_z^2$ where $D_{xx} + D_{yy} + D_{zz} = 0$ and thus leads only to two independent parameters viz. $D = 3D_{zz}/2$ and $E = \frac{1}{2}(D_{xx} - D_{yy})$. The axes X, Y and Z can be arbitrarily chosen to label the D-tensor principal axes and will result in different values of D and E[34,35].

There are six different possible ways in which the axes can be labelled and their inter-relationships are given by Hall et al[35]. However, Blumberg[34] suggested a unique characterization for the labelling of axes which is sometimes referred to as standard axis system. The scheme is as follows :

$|D_{xx}| \leq |D_{yy}| \leq |D_{zz}|$ and in notations of D and E the parameter $\lambda (= \frac{E}{D})$ satisfies the inequality $0 \leq \lambda \leq 1/3$.

As the SH and EPR spectrum must reflect the symmetry of the crystalline field, for an orthorhombic symmetry every transition should show an extremum in position when $\vec{H}$ becomes parallel to any of the three principal axes and if the standard axis system of Blumberg[34] mentioned above is used the maximum spread in fine structure will be along Z-axis, the next maximum in fine structure spread along Y axis, whereas the third maximum in fine structure spread will be along the X-axis. The directions of maximum spreads in fine structure will be referred to K_1 , K_2 and K_3 in order of decreasing maximum spreads. For orthorhombic or higher symmetry the directions K_1 , K_2 and K_3 form an orthogonal set of axes (so called magnetic axes) and in addition are coincident with the crystal-field tensor principal axes[36-38]. The relations between the spin Hamiltonian parameters (including fourth order parameters) of SH (II-2.2) in various axis systems (six in all as has been mentioned earlier) with respect to orthogonal magnetic axes (K_1 , K_2 and K_3) have been worked out by Jain[33] and Jain and Upreti[32] and are given in Table II-2. The axis systems are referred to as S_i and are related to the magnetic axes in the following manner :

Axis system	Relative orientations with respect to Principal axes of D-tensor (X, Y and Z).					
S_1	$K_1 \parallel Z$	,	$K_2 \parallel Y$	and	$K_3 \parallel X$	
S_2	$K_1 \parallel X$	,	$K_2 \parallel Z$	and	$K_3 \parallel Y$	
S_3	$K_1 \parallel Y$	,	$K_2 \parallel X$	and	$K_3 \parallel Z$	
S_4	$K_1 \parallel Z$	,	$K_2 \parallel X$	and	$K_3 \parallel Y$	
S_5	$K_1 \parallel Y$	,	$K_2 \parallel Z$	and	$K_3 \parallel X$	
S_6	$K_1 \parallel X$	,	$K_2 \parallel Y$	and	$K_3 \parallel Z$	

The relations, for the three remaining systems viz. S_4 , S_5 and S_6 which are not given in Table II-2 can be obtained simply by changing the signs of total expressions in the rows of B_2^2 and B_4^2 of system S_1 in this Table and g parameters by simple permutations of g-parameters of system S_1. The interchange of X and Y axes is equivalent to reversal of signs of B_2^2 and B_4^2. It may also be mentioned here that the axis system S_1 is the standard axis system of Blumberg and the ratio B_2^2/B_2^0 is always +ve and satisfies the inequality $0 \leq (B_2^2/B_2^0) \leq 1$. The SH (II-2.1) retains the same form in all these axis systems with different values of g_i and B_1^m parameters. From the SH (II-2.1) it is clear that if $\vec{H}$ is confined to ZX plane the secular matrix for (II-2.1) will be real symmetric. The secular matrices of the SH will also be real symmetric if $\vec{H}$ remains confined to the K_1K_3 plane of axis systems S_1 and S_6 , to the K_1K_2 plane of axis systems S_2 and S_4 and to the K_2K_3 plane of axis systems S_3 and S_5. When $\vec{H}$ is confined to the ZX plane in any of these axis systems and the direction of quantization for spin $\vec{S}$ is chosen to be along ξ_j-axis which coincides with $\vec{H}$ then the SH

(II-2.1) which becomes of the following form in ZX plane by setting $\phi = 0$:

$$\mathcal{H} = \beta (g_x \mathrm{Sin}\theta S_x + g_z \mathrm{Cos}\theta S_z) H + \sum_{l,m} B_l^m O_l^m \qquad .. \text{(II-2.4)}$$

is transformed into :

$$\mathcal{H} = \beta g_{\text{eff}} S H + \sum_{l,m} B_l^{m'} O_l^m \qquad .. \text{(II-2.5)}$$

where the relationship between B_l^m and $B_l^{m'}$ can be derived as mentioned before and the SH in this form is very convenient to use for finding the angular dependence of energy eigenvalues for a given system and consequently of the EPR spectrum involved with the energy levels of the given system. Various units of measurement are used in radiospectoroscopy and therefore relationships between some units commonly used are given in Table II-3.

(ii) Computation of Resonance Fields and Determination of Axes and the Angular Variation of EPR Spectra

The EPR transitions result from a matching of energy levels of a spin in a magnetic field by the microwave quantum used. Thus the validity of the phenomenological SH used may be testified by comparing the observed and computed values of resonance fields with the help of the solution of SH matrix (with the known values of parameters) and subsequently matching the possible energy level differences to the microwave quantum. The SH matrix can be solved either by perturbation method or by exact numerical diagnolization on digital computers. The perturbation methods are applicable to the cases where the Zeeman term is dominant and are thus of limited

applicability only to cases with small ZFS and small hyperfine interaction. The forms (II-2.4) and (II-2.5) can be used to diagonalize the SH matrix on a computer. However, in (II-2.4) form a shufling of energy levels takes place when the off diagonal terms are very large, and results in some inconvenience for the scheme of matching of the levels. Therefore the SH (II-2.5) is found to be the most convenient for computer diagonalization because the Zeeman term is always diagonal. The subroutines available in the computer library of the Dec-10 systems at I.I.T., Kanpur were frequently used for diagonalization of real or complex symmetric matrices. A computer subroutine for diagonalization of real symmetric matrices based on the standard Jacobi method[39] was also generated by us and used whenever convenient.

The energy levels giving the fine structure in the EPR are labelled by quantum numbers M_s and those giving the hyperfine structure by m_I. Though the labelling is done as if these are pure quantum numbers, they have no other meaning except their use for labelling. In the perturbation expressions which involve these numbers and treat them as pure quantum numbers an error is introduced due to their real value being different from the pure values. The allowed transitions are defined for $\Delta M_s = \pm 1$ and $\Delta m_I = 0$. The transitions possible in violation of the above rules are termed as forbidden transitions and may involve $\Delta M_s = \pm 2, \pm 3$ etc. and $\Delta m_I = \pm 1, \pm 2$ etc. The resonance fields are calculated from the exact solution of SH matrix and by finding an interval $\langle H, H+\delta H \rangle$ by iterative procedure such that for a value H_j of the magnetic field $F_j\left(=|E_j - E_{j+\Delta M}| - \frac{h\nu}{\beta}\right) \leq 0$ and

for $(H_j - \delta H)$, $F_j \geq 0$ where E_j are the levels involved in the transition, ΔM is a positive or negative integer including zero depending on the transition under consideration being "allowed" or "forbidden", $h\nu$ is the microwave quantum and δH is a small number preselected based on the experimental accuracy of the resonance fields ($\delta H \sim 10^{-1}$-10^{-3} Gauss). The value of H_j thus computed corresponds to the resonance field position for the transition under consideration. The process is repeated until the total number of observed transitions have been considered and their positions computed (in Gauss). The computation of relative intensities is also possible through the eigenvector matrix[40]. The method is equally applicable where the hyperfine terms are also included. However this brute force method becomes extremely time consuming as the number of transitions increases since it involves diagonalizations of SH matrix at sufficiently small intervals of magnetic field intensity over a chosen range. Recently Misra and Vasilopoulos[41] exploited the Feynman's theorem in conjuction with least square fitting using exact numerical diagonalization of SH matrix in developing a new method for quick and accurate computation of resonant magnetic field values corresponding to various orientations of magnetic field in any chosen plane in an EPR experiment.

Through out this thesis, the analysis and calculation of theoretical (computed) angular variation curves was done by exact diagonalization and using the brute force method. Occasionally 36x36 matrices were also diagonalized exactly to refine the

hyperfine constants which are otherwise calculated using the perturbation expressions upto 3rd order in B_2^0 and A[42].

(iii) Fitting of SH Parameters

Various methods for fitting of SH parameters are in use and have been reviewed by Jain and Upreti[32]. Special mention may be made of two excellent fitting methods viz. Uhrin's method[31] modified by Jain and Upreti[32] and the method of Buckmaster et al[43] modified by Smith et al[44]. McGavin et al[45] have also developed an excellent fitting method which takes account of the noncoincidence of the axes of tensors and find its special application in the analysis and refinement of EPR single crystal data involving non coincident axes of tensors. Misra[46,47] has given a useful fitting procedure which has the additional advantage of involving the intensity operators in the exact analysis of EPR data. Since we have made use of the method of Jain and Upreti a brief outline of the method is given below.

The first 2S terms of SH (for example II-2.5) are retained and the SH is expressed in the following form :

$$\mathcal{H} = \sum_{i}^{2S} X_i T_i \qquad .. \quad (II\text{-}2.6)$$

where S is the spin of the system, X_i denote the SH parameters and T_i the equivalent spin operators. For Mn^{2+} ion S=5/2 and for an orientation of $\vec{H}$ parallel to Z axis $X_1=g_z\beta H$, $X_2=B_2^0$, $X_3=B_2^2$, $X_4=B_4^0$, $X_5=B_4^2$ or B_4^4 (depending on the suitability of convergence, generally B_4^2 is found more suitable compared to B_4^4) and $T_1=S_z$, $T_2=O_2^0$, $T_3=O_2^2$, $T_4=O_4^0$ and $T_5=O_4^2$ or O_4^4 (according to the previous choice of X_5).

Initial estimates of X_i parameters are made and are denoted by ($X_i^{(0)}$, i=1 to 2S). Then corresponding theoretical resonance fields are computed by brute force method mentioned earlier for $\Delta M_s = \pm 1$ transitions. These resonance fields are denoted by (H_j^T, j=1 to 2S). The observed resonance fields be denoted by (H_k^0, k=1 to 2S). Expansion or step fields are then calculated in the following manner :

$$\Delta H_j = \frac{H_j^0 - H_j^T}{M}$$

where M is a prechosen integer and

$$H_j^{(L)} = H_j^T + L\Delta H_j \text{ and } L=1,2,\ldots M.$$

Now the theoretical resonance fields are replaced by corresponding $H_j^{(L)}$ starting with L=1. With these and with $X_i = X_i^{(0)}$ the SH matrix (II-2.6) is diagonalised and the wave function (eigenvectors) matrix C is constructed ($C^{\dagger}\mathcal{H}C = \mathcal{H}_{diagonal}$). With the eigenvalues (energy levels) E_k(k = 1,2...2S+1) so determined a function F is constructed as :

$$F = \sum_j^{2S} \left(|E_j - E_{j+1}| - h\nu/\beta \right)^2 \qquad .. \quad (II\text{-}2.7)$$

Using the wavefunctions and the energy levels thus obtained, perturbation theory is then applied to construct a system of linear equations for corrections to the initial estimates of the parameters which may not be the correct parameters. The so called corrected parameters are denoted by $X_i^{(L)}$ (L=1 for the first step) and replaces the initial estimates $X_i^{(0)}$ for next step and satisfy

the solution of the equation for the resonance fields $H_j^{(L)}$ (L=1), with the function $F \leq \delta F$, where δF is a sufficiently small prechosen number. To satisfy the inequality $F \leq \delta F$ for each step L total number n_L (≥ 1) steps may be required.

Now starting with the corrected parameters in step L=1 as new initial estimates for step L=2 the whole procedure for L=1 is repeated for L=2 and better values for initial estimates $X_i^{(2)}$ for next step L=3 are obtained. The process is repeated until the final step L=M is reached such that the corrected parameters are the best estimates for the SH parameters and satisfy the solution of the equation for the experimental resonance fields H_j^0; j=1 to 2S with the inequality $F \leq \delta F$.

Exact details of the method and the algorithm, from which computer programme can be written directly are given as an appendix at the end of the thesis.

(iv) Method for S = 1/2 Ions

For S = 1/2 and I = 3/2 or 7/2 for example Cu^{2+}, Co^{2+} and VO^{2+} the fine structure terms are dropped from the SH and it assumes the simpler form :

$$\mathcal{H} = \beta \vec{S}.\tilde{g}.\vec{H} + \vec{I}.\tilde{A}.\vec{S}. + \vec{I}.\tilde{P}.\vec{I}. - \beta_N \vec{H}.\tilde{g}_N.\vec{I} \quad .. \quad (II\text{-}2.7)$$

In most of the cases the last two terms are found to be very small and may generally be dropped from the spin Hamiltonian. Solution of (II-2.7) for general orientation of magnetic field using perturbation method is given by Golding[48] and can be used to obtain the resonance field values for an arbitrary direction of $\vec{H}$. For axial

symmetry the SH (II-2.7) is sometimes written in terms of more customary symbols in the following form[49] :

$$\mathcal{H} = g_{\parallel}\beta S_z H_z + \beta g_{\perp}(S_x H_x + S_y H_y) + A S_z I_z + B(S_x I_x + S_y I_y) + \\ + Q\left[3I_z^2 - I(I+1)\right] + \beta_N \vec{H}.\vec{I} - R_{\parallel} I_z H_z - R_{\perp}(H_x I_x + H_y I_y) \quad .. \quad (II\text{-}2.8)$$

Bleany[50] in his classic paper has obtained the expressions for the resonance fields applying perturbation method and Low[9] has given the expressions for resonance fields for both the allowed and the forbidden transitions. Extensive discussion of the perturbation method and the above SH may be found in literature[12,48]. For the analysis of Cu^{2+} (S=1/2, I=3/2) and VO^{2+} (S=1/2, I=7/2) EPR spectra the expressions given by Low[9] were used frequently. The parameters thus obtained were next refined by obtaining minimum F ($= \sum_i (H_o^i - H_T^i)^2$) where, H_o^i and H_T^i are the experimentally observed and calculated resonance field values respectively and H_T^i are computed by the 'brute force' method described earlier through the exact numerical diagonalization of a SH matrix (8x8 for Cu^{2+} and 16x16 for VO^{2+}). Probably the best description of the general method for obtaining principal values of g- and A- tensors is presented in the book by Poole and Farach[12].

(v) The Spectrum of a Powder

In powdered (polycrystalline) samples the crystallites have random orientation with respect to the magnetic field $\vec{H}$ and the EPR spectrum will be a superposition of individual EPR spectra typical to each crystallite orientation[9,52] and in the resultant

spectra, to a considerable extent, the details will be lost. Therefore the information extractable from such spectra may be drastically reduced. There have been several successful attempts in analysing the powder EPR spectra using computer techniques[52,53]. The powder spectra though simpler to record experimentally compared to single crystal spectra, pose enormous difficulty in their interpretation especially in cases of high effective spin and low symmetry. In fact only a very few reports of analysis of powder spectra for S = 5/2 are available. The main difficulty lies in the excessive computer time required to simulate such spectra for a particular guess of SH parameters[52]. Veen[52] has discussed the relationship between the EPR spectra of powders and those of single crystals and has obtained the well known observation that the turning points in the angular dependence of the resonance positions of the single crystal determine the peak positions in the corresponding powder spectrum[9]. Due to the above mentioned constraints we have limited our analysis of powder spectra only to a qualitative interpretation.

(vi) Approximate Computational Methods in the Treatment of Forbidden Transitions in EPR

The forbidden hyperfine transitions were first observed by Bleany and Ingram[54] and the first satisfactory explanation for the positions and intensity of such transitions was given by Bleany and Rubins[55]. Since then the subject has attracted the attention of a large number of workers. In general the line positions are calculated by obtaining the corresponding energy values after solving the appropriate spin Hamiltonian using perturbation method.

Depending on the requirements of the situation perturbation calculations have been pushed to higher orders. The expressions for line positions for a field swept EPR experiment are available in literature[55-60] and will not be reproduced here. For identification of forbidden lines we have used the expression given by Lupei et al[60] which are correct to third order of perturbation and involve the general angular variation. The best way of calculating the quadrupole interaction parameter for Mn^{2+} is through the doublet separation of the forbidden hyperfine lines in the central fine structure group which becomes even more convenient if the difference between the doublet separations of the two outermost doublet pairs of the same order ($\Delta m_I = \pm 1$ or ± 2....) is measured[60]. The latter method has been utilized to obtain the quadrupole interaction parameter 'Q' for Mn^{2+}.

The intensity of the forbidden hf transitions is usually found to show large angular dependence. Various theoretical methods have been developed to explain the observed line intensities. A review of these methods has recently been made by Mialhe.[61] We will mention briefly these approximate methods and in some more detail the Bir-Lupei[62,63] method which has been used to explain the spectacular angular dependence of the intensity of hyperfine transitions for $Mn^{2+}:NH_4I$ in this thesis.

(a) Perturbation theory: Bleany and Rubins[55] were the first to give a theoretical interpretation of the observed large anisotropic behaviour of line intensity observed in EPR. The method involves the use of perturbation theory to obtain eigenfunctions of the

Hamiltonian and subsequent computation of the transition probabilities :

$$W_{M_S m_I \,,\, M_S' m_I'} = \left| \langle \psi_{M_S m_I} | S_x | \psi_{M_S' m_I'} \rangle \right|^2 \quad .. \text{(II-2.9)}$$

But this method could only be used satisfactorily for small values of fine and hyperfine structure parameters[61] and must not be used absusively much over the limit of its validity. However, in order to improve the theory other authors, have introduced higher orders of the perturbation, but for large D higher and higher orders have to be taken into account which are not easy to handle.

(b) Effective field method: Bir[56] developed an elegant method to obtain the transition probabilities. Bir's theory gives expressions for the transition probabilities of the allowed and forbidden transitions in terms of the SH parameters and is applicable to the intermediate cases where the condition $g\beta H > D >> A$ still holds and the hyperfine interaction can be treated as a small perturbation. The method is based on the assumption that the eigenfunction $\langle \psi_{M_S m_I} |$ is separable into a pure electronic $\langle \phi_M |$ and a pure nuclear part $\langle \phi_{m_I} |$ so that the transition probability is the product of two factors - electronic transition probability and nuclear transition probability. Later Lupei et al[60] gave pertinent analytic expressions of the effective field method which allowed accurate description of the line intensities even for very large D values but still with $|D|/H_0 < 1$. This later method has been referred to as Bir-Lupei method in the

literature[62,63]. We have used this method to explain the angular variation of the intensity of the allowed and forbidden transitions of the $|M_S = 1/2\rangle \longleftrightarrow |M_S = -1/2\rangle$ transition in $NH_4I:Mn^{2+}$. In the following we describe the Bir-Lupei method.

The effective field created by the electrons at the nucleus is assumed to define the quantization axis rather than the applied magnetic field and the effective fields are obtained by averaging the hyperfine interaction on the exact electronic eigenfunctions (the eigenstates of the SH containing Zeeman and fine structure terms). Consequently the hyperfine interaction becomes equivalent to an effective nuclear Zeeman interaction and can be represented as a product between the nuclear spin and effective magnetic field which will depend on the electronic state $|m_I(M_S)\rangle$ both in magnitude and direction. The nuclear eigenstates form a set of orthogonal vectors within the same electronic quantum number i.e. $M_S = M_S'$ but are not orthogonal to another set corresponding to $M_S' \neq M_S$. The nuclear eigenvectors within two different M_S are connected by the following relationship :

$$|m(M)\rangle = \sum d^{(I)}_{mm'}(G)\,|m'(M')\rangle = \sum P^{(I)}_{mm'}(\mu_{mm'})\,|m'(M')\rangle \quad ..(II\text{-}2.10)$$

where $d^{(I)}_{mm'}(G)$ are the matrix elements of the rotation group G in the irreducible group representation, $\mu_{mm'} = \cos(\vec{H}^M, \vec{H}^{M'})$, $\vec{H}^M$ and $\vec{H}^{M'}$ are the effective fields corresponding to states $|m(M)\rangle$ and $|m'(M')\rangle$, $P^{(I)}_{mm'}(\mu_{MM'})$ are the well known functions[56] :

$$P^{(I)}_{mm'}(\mu) = \frac{(i)^{(2I-3m+m')}}{(I-m)\,(2)^I}\left[\frac{(I-m)!\;(I+m')!}{(I+m)!\;(I-m')!}\right]^{\frac{1}{2}} \frac{(1-\mu)^{\frac{m-m'}{2}}}{(1+\mu)^{\frac{m+m'}{2}}}\, Y^{(I-m')}(\mu)$$

$$..(II\text{-}2.11)$$

where $Y^{I-m'}(\mu) = \frac{\partial^{I-m'}}{\partial \mu^{I-m'}} \left[(1-\mu)^{I-m} (1+\mu)^{I+m} \right]$ .. (II-2.12)

A microwave magnetic field $\perp$ to the external magnetic field will induce transitions between states $|M_s , m_I(M_s)\rangle$ and the probability will be given by :

$$W_{M_s m_I , M_s' m_I'} \propto \left| \langle M_s , m_I(M_s) | S_x | M_s' , m_I'(M_s') \rangle \right|^2$$

$$\propto \left| \langle M_s | S_x | M_s' \rangle \right|^2 \times \left| \langle m_I(M_s) | S_x | m_I'(M_s') \rangle \right|^2$$

$$\propto (W_{M_s , M_s'}) \times (W_{m_I(M_s), m_I'(M_s')}) \quad .. \quad (II-2.13)$$

The composite probability for EPR transitions is thus the product of two probability factors. It can be shown that the second factor $W_{m_I(M_s), m_I'(M_s')}$ which is equivalent to the modulus of the overlap integral is :

$$W_{m_I(M_s), m_I'(M_s')} = \left| \langle m_I(M_s) | S_x | m_I'(M_s') \rangle \right|^2 = \left| P^{(I)}_{m_I m_I'}(\mu_{M_s M_s'}) \right|^2 .$$

.. (II-2.14)

The functions for I = 5/2 can be calculated from analytical expression (II-2.11) and their dependence on μ is shown in Fig. (II-5). The first factor of (II-2.13) for the central transition $M_s = |1/2\rangle \longleftrightarrow |M_s = -1/2\rangle$ for Mn^{2+} in axial symmetry can be shown to be equal to[56,59,60,62]:

$$W_{M_s , M_s'} = \frac{9}{2}\left[1 - \frac{2D^2}{H_0^2}\sin^2 2\theta - \frac{D^2}{2H_0^2}\sin^4\theta + \frac{D^2}{H_0^2}(3\cos^2\theta - 1)\sin^2\theta \right]^2$$

.. (II-2.15)

The effective field $\vec{H}^{M_s}$ by definition is given by :

$$\langle M_s | (\vec{H})_{hf} | M_s \rangle = -\gamma \beta_N \vec{H}^{M_s} . \vec{I} \qquad ..(II-2.16)$$

where $(\vec{H})_{hf}$ represents the part containing hyperfine terms in SH written in a reference frame where electronic Zeeman term is diagonal. The Cosine of the angle between $\vec{H}^{M'_s}$ and $\vec{H}^{M_s}$ may be calculated from :

$$(\mu_{M_s M'_s}) = \frac{\vec{H}^{M_s} \cdot \vec{H}^{M'_s}}{|\vec{H}^{M_s}| \; |\vec{H}^{M'_s}|} \qquad ..(II-2.17)$$

Writing the exact electronic wave functions as a combination of strong field states $|M_s\rangle^0$ in the form :

$$|M_s\rangle = \frac{1}{N}\left[|M_s\rangle^0 + \sum_k A_k |M_s + k\rangle^0 \right] \qquad ..(II-2.18)$$

where N is a normalizing factor and A_k are the admixture coefficients and can be computed by perturbation method, Lupei et al[62,63] obtained following expression for $(\mu_{M_s M'_s})$:

$$(\mu_{M_s M'_s}) = 1 - \frac{A^2B^2}{4K^4}(R_-)^2 \left[1 - \frac{(B^2-A^2)}{K^2} \mathrm{Sin}2\theta (R_+) + \frac{A^2B^2}{K^4} R_{M_s} . R'_{M_s} + \right.$$

$$\left. + \frac{3}{4} \frac{A^2B^2}{K^4}(R_+)^2 \right] + \frac{A^2B^2}{K^4}(R_-)(R_{M_s} . W_{M_s} - R_{M'_s} . W_{M'_s}) \qquad ..(II-2.19)$$

where $K^2g^2 = A^2g^2\mathrm{Cos}^2\theta + B^2g^2\mathrm{Sin}^2\theta$; $g^2 = g_{\parallel}^2 \mathrm{Cos}^2\theta + g_{\perp}\mathrm{Sin}^2\theta$;

$R_{M_s} = \frac{1}{M_s} \langle M_s | S_x | M_s \rangle$; $R_+ = (R_{M_s} + R'_{M_s})$; $R_- = (R_{M_s} - R_{M'_s})$ and

$$W_{M_s} = \frac{1}{M_s} \sum_k (M_s + k) \; |A_k|^2$$

Because the quantity $\mathcal{M}$ has a strong dependence on orientation θ the functions $P^{I}_{M_s M_s'}(\mathcal{M})$ which are strongly dependent on $\mathcal{M}$ will also be highly angular dependent. Finally, therefore, the transition probability given by (II-2.13) shall be highly anisotropic mainly due to the nuclear part (II-2.14) because the electronic part is comparatively a smoother function of θ. The relative intensities of the two hf components belonging to the same group are given by :

$$\frac{\substack{M_s \to M_s' \\ I_{m_I \to m_I'}}}{\substack{M_s \to M_s' \\ I_{m_I'' \to m_I'''}}} = \frac{\left| P^{(I)}_{m_I m_I'}(\mathcal{M}_{M_s M_s'}) \right|^2}{\left| P^{(I)}_{m_{II}'' m_I'''}(\mathcal{M}_{M_s M_s'}) \right|^2} \qquad .. \text{(II-2.20)}$$

(c) Intensity operator method: This method is of special when the zero field and the hf terms are comparable and a separation of eigenfunctions into a nuclear and an electronic part (Bir's method) is not valid[64]. The complete SH with electronic and nuclear spin operators is considered and the effective field at the nucleus is used by considering the actual quantization axes of nuclear and electronic spin operators[64] for deriving the eigenfunction $\psi_{M_s m_I} = C \mid M_s , m_I \rangle$, where C is a coupling operator, and the transition probability is obtained as :

$$W_{M_s m_I , M_s' m_I'} = \left| \langle M_s , m_I | \; C^{\dagger} S_x C \, | M_s' , m_I' \rangle \right|^2 \qquad .. \text{(II-2.21)}$$

where $C^{\dagger}$ is transposed conjugate of C. An intensity operator ρ may then be defined as :

$$\rho = C^{\dagger} S_x C \qquad .. \text{(II-2.22)}$$

order parameter at the transition temperature indicates a first order transition[65]. A comprehensive treatment of the subject has been given by Rao and Rao[67]. Experimental investigations of SPT usually involve a systematic study of variable dependence of a parameter referred to as 'response-parameter', and different variables may be chosen viz. hydrostatic pressure, relative concentrations in solid solutions, temperature and stress. The review articles by Muller[66] give a very useful discussion of the important results obtained for various crystals regarding SPT using EPR as a technique and covers all important works related to SPT studies by EPR till 1971. Very recently Owens[65] has reviewed the applications of EPR of transition ions as probes to study SPT. In addition to paramagnetic ions other defect centres e.g. radiation damage centres are also frequently used as probes to study SPT.

C.2 CHOICE OF PROBE ION

There are several ways in which EPR can be used in SPT studies. As the SPT involves a symmetry change, the effectiveness of an ion as a probe depends on its sensitivity towards symmetry changes (i.e. local crystalline field at the site) which are consequently reflected in the characteristic EPR spectrum. It has been found that $3d^n$ ions with $S > 1/2$ are the most suitable probe ions because of their greater sensitivity to the strength and symmetry of the local crystal field[65]. In the high spin case these ions have nondegenerate orbital ground states and avoids the

undesirable Jahn-Teller distortions. Moreover the long spin-lattice relaxation times of these ions (e.g. Mn^{2+}) in most of the lattices enable the observation of EPR over a wide range of temperature including temperature higher than RT enabling the investigation of high temperature SPTs.

The second determining factor is of course the specific lattice under study. It is desirable that no distortion and no charge compensation be required when a probe ion is incorporated in the host lattice. However, it is not always possible to find a probe that matches the valency and the size of the ion being replaced. In some cases (e.g. Ferro or para magnetic crystals) intrinsic ions can be used to reflect intrinsic dynamical effects of the lattice in the EPR data. However, the underresolved EPR spectra of these systems limits the advantage and the useful informations are usually provided through the line widths, which, may be sensitive to fluctuations of neighbouring ions.

C.3 RESPONSE PARAMETERS FOR SPT BY EPR

In general any feature of the EPR spectrum (viz. SH parameters, line width, intensity, angular dependence of EPR spectrum etc.) which can sense the changes occuring in a crystal when a structural transformation takes place can be used as an experimental response parameter. As the discussion has been restricted to iron group ions, trapped free radicals as probes are not discussed here. Below we discuss in brief some of the experimental response parameters.

C.4 USE OF SH PARAMETERS

(i) Zero Field Splitting Parameter ($B_2^0 = D$)

The ions whose zero field splitting is highly sensitive to and directly dependent on the symmetry and strength of crystalline field are most useful. Thus Cr^{3+} is the obvious choice. The S-state ions (Mn^{2+} and Fe^{3+}), have also been used as probes. However, their interaction with the crystalline field is only indirect[25]. The D parameter for ions such as Cr^{3+}, Fe^{3+} and Mn^{2+} has a functional dependence on temperature generally of the following form[65]:

$$D(T) = D_0 + aT + \sum_i B_i \coth(\omega_i/2kT) \quad .. \text{ (II-3.1)}$$

where D_0 is its value at 0 K, the second term represents the effect of lattice expansion and the third term takes into account the coupling of the ion to the lattice vibrations. Any significant deviation from the normal functional dependence will indicate a structural phase transformation as for example in $Cr^{3+}:KCr(SO_4)_2.12H_2O$[69], $Mn^{2+}:NH_4Cl$,[70] and $Cr^{3+}:NH_4Cl$[71].

(ii) Line Width and Intensity

Various causes are attributed to the line widths in EPR,[8-10,12,13,72,73]- life time broadening (homogenous), spin-lattice relaxation and spin-spin relaxation broadening (inhomogenous), broadening due to crystal imperfections and inhomogeniety of external magnetic field (inhomogenous). As a result of various causes of broadening the line shapes in EPR are neither pure

Gaussian nor pure Lorentzian but are a mixture of both, generally with dominant Lorentzian character. Similarly the line intensities also depend on a number of factors. The resonance line width and the intensity can manifest a structural phase transition through anomalous behaviour near the transition temperature. The line widths are sensitive to the fluctuations of the neighbours (nearest usually). Such fluctuations can be evidenced in EPR data and has been exploited in many cases to manifest a SPT and to gain an understanding about the role of neighbours in such SPT as for example in $Cr^{3+}:KCr(SO_4)_2.12H_2O$[69] and $Mn^{2+}:NH_4Cl$[74].

The line intensity should also in principle manifest the fluctuations of nearest neighbours via spin lattice relaxation which is coupled to the lattice due to the modulation of ligand ion potentials at the paramagnetic ion because of their vibrations. The intensity of the resonance can also be affected by changes in the dielectric behaviour of the crystal. The intensity is observed to be inversely proportional to dielectric constant and can be helpful in studying ferroelectric phase transitions which involve large dielectric changes.

(iii) Line Shapes

These studies have found great use in manifesting incommensurate phase-transitions characteristic to the A_2BX_4 type ferroelectrics. The plane wave incommensurate modulation of the hyperfine interaction causes the hf structure to further split and each hf line shows a splitting in a normal to incommensurate phase

transformation[75]. If a tilt of magnetic axes of paramagnetic ions occurs due to phase transition (for example for Mn^{2+} in trissarcosine calcium chloride[76]) the splitting of the lines may be due to site splitting and indicates an SPT. The temperature dependence of the tilt angle yields important information about the SPT.

(iv) g-values and Hyperfine Parameter

The $3d^9$ ion (Cu^{2+}) has been widely used as a probe to study SPT. It has $S = 1/2$ and $I = 3/2$ and the SH for Cu^{2+} does not contain any crystal field terms (D and E). However for Cu^{2+} in octahedral symmetry with tetragonal distortion the principal g-values and hyperfine constant depend on the particular ground level[8] as determined by the crystal field splitting of the level corresponding to $3d^9$ configurations. These dependences are given in Table II-4. Thus if the SPT involves lowering of symmetry from axial to rhombic the g-values and the hyperfine constants will reflect it in a two fold manner : (I) $g_x \neq g_y$ and $A_x \neq A_y$ and (II) changes in their magnitudes due to different crystal field splittings. These effects are clearly evidenced in the EPR of Cu^{2+} ion and have been successfully used in the detection of SPT in a variety of systems. Special mention may be made over here of some studies of SPT in ammonium halides using Cu^{2+} ion as probe: NH_4Cl[77-81] and NH_4Br[82,83].

(v) Symmetry or Angular Behaviour of EPR Spectrum

Because of the fact that the EPR spectrum should reflect the true symmetry of the crystalline field at the site of the

paramagnetic ion, any changes observed in the angular behaviour of the EPR spectra may be taken as an evidence of SPT. When the symmetry of the crystalline field becomes lower than orthorhombic the effects of lower symmetry are evidenced in the angular behaviour of the EPR spectra.

(vi) Advantages and Disadvantages of EPR as Probe for SPT

The advantage of this technique lies in the fact of high precision common to many EPR spectra and their sensitivity towards the changes in the host lattice under consideration. While in many cases of SPT, a behaviour which remains unnoticed by other techniques can be detected by EPR, as the probe ion is very sensitive to the local environment, in other cases it may be sensitive to only one type of fluctuation and can thus help in discrimination of the dynamical effects. When supplemented by other techniques, it furnishes a deeper insight into the dynamics associated with SPT. Although the value of the EPR technique to probe SPT is well established now, there are certain limitations to its applicability. The restrictions on selecting a lattice and a sensitive ion probe suitable to it, are the greatest handicaps to the universal applicability of this technique. Moreover the presence of impurity ions as probe may have its own effects on the nature of SPT. In fact in many cases transition temperatures are found to be affected by the presence of defects and impurity ions in the pure lattice. However, for sufficiently low concentrations it is expected that these will not affect the nature and dynamics of the phase transition in any appreciable way.

SECTION-D

CRYSTAL STRUCTURE OF NH_4X (X = Cl, Br and I)

Ammonium halides have been reported to undergo various polymorphic phase transitions at different temperatures[84-95]. Ammonium Iodide (NH_4I) lattice has been reported to exist in three arrangements viz. NaCl-type, CsCl-type and a nearly CsCl-type PH_4I-arrangement[85,95] in different intervals of temperature. We will refer to the first arrangement as phase I, to second as phase II and to the last as phase III. While NH_4Cl and NH_4I are known to show two structural phase transitions each at different temperatures NH_4Br is known to show an additional third structural phase transition[84,91] and the structure below this third phase-transition at low temperature will be referred to as phase IV of NH_4Br. Based on the data available in literature a summary of these polymorphic phase transformations for ammonium halides has been given in Table II-5. NH_4F has a different structure[85] (Zincite, P_{6mc}) at high temperature than other ammonium halides (NaCl, Fm3m) and is therefore not included with other ammonium halides. These halides undergo polymorphic phase transitions with hydrostatic pressure and strain also but we will confine the present discussion only to thermal phase transitions at atmospheric pressure. All the halides under consideration have a common structure at high temperatures (NaCl-Fm3m) and the lower temperature phases are all based on CsCl structure. The transition temperatures follow the order of H-bond strength[86] (Cl > Br > I) and the order of anionic

radii in reverse order (I > Br > Cl). On the basis of neutron diffraction[84] results and supported by many other studies[87,88,91] it is now well established that NH_4^+ ions in phase I (referred to as α in Table II-5) undergo complex rotations about one strong H-bond like N-H...X (X = Cl, Br, I) and since this N-H...X bond direction can be one from among the six octahedral bond directions, the structure is highly disordered[86]. Some of the experimental data can also be fitted with a model involving static disorder around the strong N-H...X bond as an alternative to rotation[84]. In Fig. II-6 various models for the NH_4^+ disorder in phase I of NH_4X are shown. The phases II (referred to as β in Table II-5) are doubly disordered with respect to NH_4^+ orientation, because of two possible choices of a set of tetrahedral arrangement of ions to which H-bonds can be formed (Fig. II-7). The two NH_4^+ orientations are energetically equivalent and are occupied randomly.

Phase III of NH_4Cl is different from phases III (referred to as γ in Table II-5) of NH_4I and NH_4Br. In phase III of NH_4Cl (referred to as δ in Table II-5) NH_4^+ assumes ordered orientation (ferro-distortive) in which all of the NH_4^+ ions assume parallel orientation and each Cl accepts four H-bonds tetrahedrally (Fig. II-7). Phase IV of NH_4Br is equivalent to phase III of NH_4Cl. Phases III of NH_4Br and NH_4I are similar and the NH_4^+ ions are ordered parallel to C-axis while NH_4 ions are ordered anti-parallel in the ab plane (antiferrodistortive order). A small distortion along one of the cubic symmetry axes (CsCl - phase II) causes the structure in phase III to be tetragonal with two

molecules per unit cell (Z = 2). These phases III of NH_4I and NH_4Br have been referred to as γ in Table II-5 and in Fig. IV-8, wherein the representations of NH_4^+ orientations in γ and δ phases are shown.

It is interesting to note that both NH_4Br and NH_4Cl are found to exist in their stable forms ($\sim$300K) in β -phase while NH_4I exists in the α -phase around this temperature. The arrangement of NH_4^+ cations and I^- anions in a three dimensional lattice representing α -phase (NaCl-arrangement) is shown in Fig. II-9. It may be noted here that the tetragonal distortion in phase γ from the CsCl arrangement of phase β is only slight and both NH_4I and NH_4Br are nearly cubic (CsCl) in structure in γ -phase. Because the displacements of halide ions (γ -phase) from their corresponding positions in a unit cell in β-phase are found to be $\sim$.04 and 0.12 Å respectively for the iodide and bromide[94] which are within the rms amplitudes of thermal vibrations of the halide ions[93].

The theory of phase transitions in ammonium halides and the nature of various interactions responsible for the phase transitions has been worked out and discussed by many workers[96,97] The transition $\alpha \leftrightarrow \beta$ has been reported to be of first order and is accompanied by a large thermal hysteresis[90]. The transformation II $\beta \longleftrightarrow \gamma$ is of higher order and is usually referred to as λ -transition. These λ-transitions are common to all the three halides under consideration and are believed to be due to the onset of NH_4^+ rotation[98]. The λ -transition is usually attributed

to an order-disorder change in NH_4^+ orientation, though a temperature dependent one dimensional free rotation as a cause of λ-transition has also been suggested in the case of NH_4I[88]. From a correlation of the physical properties with the structure, possible antiferroelectricity in the γ-phase of NH_4Br and NH_4I has been predicted by Sonin[99]. The room temperature of NH_4I is NaCl-type (Fm3m) and transforms to the CsCl-structure (Pm3m) at about 257K. The λ-transition in NH_4I is mostly reported to be around 231K. It is interesting to note the stability range of β-phase in NH_4I is narrow ($\sim$26K) compared to that in the other two halides. In Fig. II-7 the mechanism and the reshuffling of atomic arrangements are shown for NaCl (α) $\longleftrightarrow$ CsCl (β) transformation for NH_4I.

It is worthwhile to mention here that the transition temperatures for NH_4I reported in literature based on the experimental data of various studies have been conflicting (Table II-6). The transformation $\alpha \longleftrightarrow \beta$ depends on the thermal processing of the sample and it has been found that the α-phase can be supercooled to various degrees, dpending on the thermal process and the situation is similar for superheating of β-phase. The thin film studies of NH_4I on LiF substrate by optical absorption[103] revealed supercooling of α phase down to LNT and any phase transformation was absent in this case. Dielectric measurements[104] have been reported to show phase transitions at T_1 = 260K ($\alpha \leftrightarrow \beta$) and $T_2 \sim$ 229K (λ-transition) while such studies by Bridgman[105] and Simon[105] indicated T_1 = 256K and 259K respectively. Crenshaw and

Ritter[106] reported the λ-transition to occur at 231K while Guillien[107] reported its occurence at $\sim$ 245K. Freymann[108] reported $T_1 \sim$ 239K in a cooling cycle and $T_1 \sim$ 268K in a heating cycle and no λ-transition. In X-irradiated samples which contained colour centres these transitions have been reported to occur at temperatures different from those in pure samples.

All these reports indicate that NH_4I lattice is very sensitive and due care must be taken while handling and interpreting any experimental data on this lattice. While the λ-transition has been found to occur rather rarely and to be too sluggish[110-112] the transition $\alpha \leftrightarrow \beta$ has been often reported to take place over a wide range of temperature[92,93,100,113] and the composition of the mixed phase (containing both α & β phases) largely depends on the thermal processing of the sample[92,93,100]. The structure of NH_4I has been studied extensively by Hovi et al[89,112,113,114] in all the three phases and the lattice parameters in the range 463K to 97K have been determined[112]. On the basis of these lattice parameters it has been found that the γ-phase is a slight tetragonal distortion of the cubic phase β-(CsCl).

REFERENCES

1. C.P. Poole, 'Electron Spin Resonance, A Comprehensive Treatise on Experimental Technique', Interscience Publishers, New York (1967).

2. T.H. Wilmshurst, 'Electron Spin Resonance Spectrometers', Hilger, London (1967).

3. H.A. Kramers, Proc. Amsterdam Acad. Sci. 33, 959 (1930).

4. H.A. Jahn and E. Teller, Proc. Royal. Soc. A161, 220 (1937); " " , ibid. A164, 117 (1938).

5. J.H. Van Vleck, J. Chem. Phys. 7, 72 (1939).

7. C.J. Ballhausen, 'Introduction to Ligand Field Theory', McGraw Hill, New York (1962).

8. L.D. Landau and E.M. Lifshitz, 'Quantum Mechanics', Pergamon Press (1959).

9. A. Abragam and B. Bleany, 'Electron Paramagnetic Resonance in Transition Ions', Clarendon, Oxford (1970).

10. J.W. Orton, 'Electron Paramagnetic Resonance', London Iliffe Book Ltd. (1968).

11. M.T. Hutchings, 'Solid State Physics', Vol. 16, edited by F. Scitz and D. Turnbull, Academic (1964) (p. 227).

12. C.P. Poole (Jr) and H.A. Farach, 'The Theory of Magnetic Resonance', Wiley-Interscience (1972).

13. G.E. Pake, 'Paramagnetic Resonance', Benjamin, New York (1962).

14. L.A. Sorin and M.V. Vlasova, 'Electron Spin Resonance of Paramagnetic Crystals': Translated from Russian by P. Gluck, Plenum, New York-London (1973).

15. K.W.H. Stevens, Proc. Phys. Soc. A65, 209 (1952).

16. R.J. Elliot and K.W.H. Stevens, ibid. A215, 437 (1952).

17. B. Bleany and K.W.H. Stevens, Rep. Progr. Phys. 16, 108 (1953).

38. A.M. Grekhov and A.B. Roitsin, Phys. Stat. Sol. B74, 323 (1976).

39. B. Carnaham, H.A. Luther and J.O. Wilkes, 'Applied Numerical Methods', Wiley Publishers, New York (1969).

40. J. Uhrin, Czech. J. Phys. B27, 595 (1977).

41. S.K. Misra and P. Vasilopoulos, J. Phys. C : Solid State Phys. 13, 1083 (1980).

42. H.W. de Wijn and R.F. Balderen, J. Chem. Phys. 46, 1381 (1967).

43. H.A. Buckmaster, R. Chatterjee, J.C. Dering, D.J.I. Fry, Y.H. Singh, J.D.S. Kirrow and B. Venkatesan, J. Magn. Reson. 4, 113 (1971).

44. M.R. Smith, H.A. Buckmaster and D.J.I. Fry, ibid. 23, 103 (1976).

45. D.G. McGavin, R.A. Palmer, W.A. Singers and W.C. Tennant, ibid. 40, 69 (1980).

46. S.K. Misra, ibid. 23, 403 (1976).

47. S.K. Misra, J. Phys. C : Solid St. Phys. 12, 5221 (1979).

48. R.M. Golding,'Applied Wave Mechanics', D. Van Nostrand Co. Ltd., London (1969).

49. A. Abragam and M.H.L. Pryce, Proc. Royal,Soc. (London) A205, 135 (1951).

50. B. Bleany, Phil. Mag. 42, 441 (1951).

51. T.E. Freeman, Ph.D. Thesis Monash University, Clayton, Victoria 3168 (1973) (p. 34).

52. G. Van Veen, J. Mag. Reson. 30, 91 (1978).

53. P.C. Taylor and P.S. Bray, ibid. 2, 305 (1970).

54. B. Bleany and D.J.E. Ingram, Proc. Roy. Soc. A205, 336 (1951).

55. B. Bleany and R.S. Rubins, Proc. Roy. Soc. 77, 103 (1961).

56. G.L. Bir, Soviet Phys. Solid State 5, 1628 (1964).

57. S.P. Burley, Australian J. Phys. 17, 537 (1964).

58. D.W. Posner, J. Mag. Reson. 9, 128 (1973).

59. G.C. Upreti, ibid. 13, 336 (1974).

60. V. Lupei, A. Lupei and I. Ursu, Phys. Rev. B6, 4125 (1972).

61. P. Mialhe, Phys. Stat. Sol. (b) 93, 189 (1979).

62. V. Lupei, A. Lupei and F. Domsa, J. Mag. Reson. 19, 337 (1975).

63. A. Lupei, V. Lupei, A. Stefanescu and F. Domsa, Rev. Roum. Phys. 20, 59 (1975).

64. P. Mialhe and A. Erbia, Phys. St. Sol. (b) 57, 509 (1973); J. Phys. C6, 1965 (1973); Phys. Rev. B7, 4061 (1973).

65. 'Magnetic Resonance of Phase Transitions', (Ed. by F.J.Owens, C.P. Poole Jr. and H.A. Farach), Academic Press (1979).

66. 'Structural Phase Transitions and Soft Modes', (Ed. by E.J. Samuelsen, E. Andersen and J. Feder, Universitets Forlaget, Oslo (1972).

67. C.N.R. Rao and K.J. Rao, 'Phase Transitions in Solids', McGraw Hill International Book Company (1978).

68. 'Topics in Current Physics' - Structural Phase Transitions I, (Ed. by K.A. Muller and H. Thomas, Springer-Verlag-Berlin Heidelberg-New York (1981).

69. F.J. Owens, Chem. Phys. Lett. 46, 380 (1977).

70. F.S. Stibbe and N.J. Trappeniers, Physica 9513, 81 (1978).

71. A. Kennewell, J.R. Pilbrow and J.H. Price, Phys. Lett. 27A, 228 (1968).

72. K.J. Standly and R.A. Voughan, 'Electron Spin Relaxation Phenomenon in Solids', Plenum, New York (1970).

73. C.P. Poole Jr. and H.A. Farach,, 'Relaxation in Magnetic Resonance', Academic Press, New York (1971).

74. J.A. Van Wyk, J. Mag. Reson. 18,235 (1975).

92. M. Couzi, J.B. Sokoloff and C.H. Perry, ibid., 58, 2965(1973).

93. A.R. Sharp and M.M. Pintar, Chem. Phys. 15, 431 (1976); J. Chem. Phys. 75, 2652 (1981).

94. J.A. Ketelaar, Nature 134, 250 (1934).

95. M. Stammler, J. Inorg. Nucl. Chem. 29, 2203 (1967).

96. T. Nagamiya, Proc. Math. Soc. Japan 24, 137 (1942); 25, 540 (1943); R.S. Seymour, Acta Cryst. A27, 348 (1971); A. Huller, Z. Phys. 254, 456 (1972) and 270, 343 (1974); V.G. Vaks and V.E. Schneider, Phys. Stat. Sol. (a) 35, 61 (1976); H.S. Guttowsky, G.E. Pake and R. Bersohn, J. Chem. Phys. 22, 643 (1954).

97. J.R. Hardy and A.M. Care, 'Lattice Dynamics', R.F. Wallis Ed. Pergamon Press Ltd., London (1963) (p. 195).

98. L. Pauling, Phys. Rev. 36, 430 (1930).

99. A.S. Sonin, Kristallg. 6, 137 (1961).

100. P.S. Goyal, B.A. Dasannacharya, J. Phys. C : Solid State Phys. 12, 209 (1979).

101. G. Stuhmer and E. Rieflin, ibid., 6; L324 (1973).

102. A. Smiths and G.J. Muller, Z. Phys. Chem. B36, 140 (1937).

103. H. Yamashita, J. Phys. Soc. Japan 29, 1391 (1970).

104. K. Kamayoshi, J. Chem. Phys. 24, 1265 (1956).

105. P.W. Bridgman, Proc. Amm. Acad. Arts Sci. 52, 89 (1916); C.V. Simon, Naturwiss. 38, 559 (1951).

106. J.L. Crenshaw and I. Ritter, Z. Phys. Chem. B16, 143 (1932).

107. R. Guillien, Compt. Rend. 208, 1561 (1939).

108. R. Freymann, ibid., 234, 279 (1952).

109. H. Ruchardt, Z. Physik 134, 554 (1453).

110. Z. Morlin, Acta. Phys. Acad. Sci. Hunga, 33, 377 (1973).

111. L. Niemela and E. Saini, Ann. Acad. Sci. Fenn. Series A205 (1966).

112. V. Hovi, K. Paavola and E. Nurmi, ibid., Series A328 (1969).

113. V. Hovi and M. Verteva, Low Temp. Phys. LT-9 Part B, 1184 (1965).

114. V. Hovi and J. Lainio, Ann. Acad. Sci. Fenn. Series A215 (1966).

115. F. Simon, C. Simon and M. Ruhemann. Z. Phys. Chem. 129, 321 (1927).

116. S.A. Zlunitzyn, J. Expt. Theoret. Phys. (USSR) 9, 72 (1939).

117. A. Arell and O. Alare, Phys. Kondens. Materie 2, 423 (1964).

118. F.E.C. Scheffer Akad. Wetenschappen 18, 446 (1915); 1498 (1916); Proc. Akad. Sci. Amsterdam 19, 798 (1917).

119. H.P. Klug and W.W. Johnson, J. Amm. Chem. Soc. 59, 2061 (1937).

120. A. Smits, J.A.A. Ketelaar and G.J. Muller, Z. Phys. Chem. A175, 359 (1936).

121. K. Kamiyoshi, Sci. Repts. A8, 252 (1956); J. Chem. Phys. 24, 1265 (1956); J. Meinnel, Bull. Soc. Sci. Bretagne 39, 31 (1964).

122. V.A. Grigorov, N.K. Kurmanov and E.F. Martynovich, Sov. Phys. Solid State 22, 509 (1980).

Possible B_l^m parameters for crystalline fields of different symmetry and ions and values of spin S.

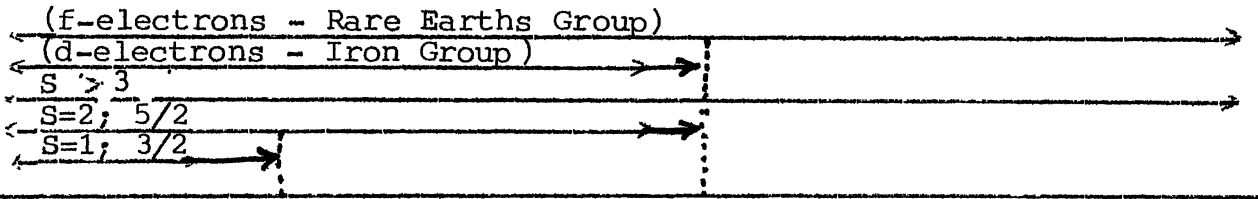

Symmetry	B_2^0	B_2^1	B_2^2	B_4^0	B_4^1	B_4^2	B_4^3	B_4^4	B_6^0	B_6^1	B_6^2	B_6^3	B_6^4	B_6^5	B_6^6
Cubic				+				+	+				+		
Trigonal	+			+			+		+			+			+
Tetragonal	+			+				+	+				+		
Rhombic Monoclinic	+		+	+		+		+	+				+		+
Monoclinic (C_s)	+	+	+	+		+	+	+	+		+	+	+	+	+
Triclinic (C_i)	+		+	+		+		+	+		+				+
Triclinic (C_1)	+	+	+	+	+	+	+	+	+	+	+	+	+	+	+
Pure axial*	+			+					+						

(*Symmetry under inversion, or under reflection of axes in a plane).

TABLE II.2

The Transformation Relations of Spin-Hamiltonian Parameters for Axis Systems S_1 , S_2 and S_3.

Primed SHP		Axis System S_1	Axis System S_2	Axis System S_3
$B_2^{o'}$	=	B_2^o	$-\frac{1}{2}(B_2^o+B_2^2)$	$\frac{1}{2}(B_2^2-B_2^o)$
$B_2^{2'}$	=	B_2^2	$\frac{1}{2}(3B_2^o-B_2^2)$	$-\frac{1}{2}(B_2^2+3B_2^o)$
$B_4^{o'}$	=	B_4^o	$\frac{1}{8}(3B_4^o+B_4^2+B_4^4)$	$\frac{1}{8}(3B_4^o-B_4^2+B_4^4)$
$B_4^{2'}$	=	B_4^2	$-\frac{1}{2}(5B_4^o+B_4^2-B_4^4)$	$\frac{1}{2}(5B_4^o-B_4^2-B_4^4)$
$B_4^{4'}$	=	B_4^4	$\frac{1}{8}(35B_4^o-7B_4^2+B_4^4)$	$\frac{1}{8}(35B_4^o+7B_4^2+B_4^4)$
$B_6^{o'}$	=	B_6^o	$-\frac{1}{16}(5B_6^o+B_6^2+B_6^4-B_6^6)$	$\frac{1}{16}(5B_6^o+B_6^2-B_6^4+B_6^6)$
$B_6^{2'}$	=	B_6^2	$\frac{1}{32}(105B_6^o+17B_6^2+5B_6^4+15B_6^6)$	$-\frac{1}{32}(105B_6^o-17B_6^2+5B_6^4+15B_6^6)$
$B_4^{4'}$	=	B_4^4	$\frac{1}{16}(-63B_6^o-3B_6^2+13B_6^4+3B_6^6)$	$\frac{1}{16}(-63B_6^o+3B_6^2+13B_6^4+3B_6^6)$
$B_6^{6'}$	=	B_6^6	$\frac{1}{32}(231B_6^o-33B_6^2+11B_6^4+B_6^6)$	$\frac{1}{32}(231B_6^o+33B_6^2+11B_6^4+B_6^6)$
g'_{11}	=	$g_z=g_{11}$	g_{22}	g_{33}
g'_{22}	=	$g_y=g_{22}$	g_{33}	g_{11}
g'_{33}	=	$g_x=g_{33}$	g_{11}	g_{22}

(i) For pure axial symmetry : $g_z=g_{11}=g_{||}$; $g_x=g_y=g_{22}=g_{33}=g_\perp$ and all $B_n^m = 0$ for $m > 0$.

(ii) For tetragonal symmetry : $B_n^4 \neq 0$ and other parameters are same as for pure axial symmetry.

TABLE II.3

Relations between units of measurements used in radiospectroscopy.

Unit	Erg	Hz	Cm^{-1}	G (Gauss)
Erg	x 1	x 1/h	x 1/hc	x $1/g\beta$
Hz	x hc	x 1	x 1/c	x $h/g\beta$
Cm^{-1}	x hc	x c	x 1	x $hc/g\beta$
Gauss	x $g\beta$	x $g\beta/h$	x $g\beta/hc$	x 1

Relative order of values in different units

	$10^{-4}Cm^{-1}$	KG	GHz
$10^{-4}Cm^{-1}$	1	1.07×10^{-3}	0.003
kG	933.5	1	2.8 (with g=2)
GHz	333	0.357 (with g=2)	1

Deriving relations and physical constants

$h(erg.S) \times \nu\ (S^{-1}) = g \times \beta\ (erg\text{-}G^{-1}) \times H(G)$

h = 6.62554 E-27 (erg S)

β = 9.27314 E-21 ($erg\ G^{-1}$)

c = 2.997925 E + 10 Cm S^{-1} $\simeq$ 3.0 E + 10 Cm S^{-1}

TABLE II.4

Formulae for ground state of d^3 in octahedral field with tetragonal distortion

(a) *Ground state* $|2^e\rangle$, *with twofold spin degeneracy.* The states $|\widetilde{+}\rangle$, $|\widetilde{-}\rangle$ are

$$|\widetilde{+}\rangle = |2^e, +\rangle - \frac{\lambda}{\Delta_0}|2^a, +\rangle - \frac{\lambda}{\sqrt{(2)}\Delta_1}|-1, -\rangle$$

$$|\widetilde{-}\rangle = |2^e, -\rangle + \frac{\lambda}{\Delta_0}|2^a, -\rangle + \frac{\lambda}{\sqrt{(2)}\Delta_1}|+1, +\rangle$$

$$g_\parallel = 2 - \frac{8\lambda}{\Delta_0}$$

$$g_\perp = 2 - \frac{2\lambda}{\Delta_1}$$

$$A = A_\parallel = 2g_n\beta\beta_n\langle r^{-3}\rangle\left\{-\kappa - \frac{4}{7} - \frac{6\lambda}{7\Delta_1} - \frac{8\lambda}{\Delta_0}\right\}$$

$$B = A_\perp = 2g_n\beta\beta_n\langle r^{-3}\rangle\left\{-\kappa + \frac{2}{7} - \frac{11\lambda}{7\Delta_1}\right\}$$

$$P_\parallel = -\frac{3e^2Q}{7I(2I-1)}\langle r_q^{-3}\rangle$$

The orbital states $|2^e\rangle$, $|2^a\rangle$, $|+1\rangle$, $|-1\rangle$, $|0\rangle$ are those shown in Fig. II.4 Δ_0 is the energy by which $|2^a\rangle$ lies above $|2^e\rangle$, and Δ_1 the energy by which the $|\pm 1\rangle$ states lie above $|2^e\rangle$.

(b) *Ground state* $|0\rangle$, *with twofold spin degeneracy.* The states $|\widetilde{+}\rangle$, $|\widetilde{-}\rangle$ are

$$|\widetilde{+}\rangle = |0, +\rangle - \sqrt{(\tfrac{3}{2})}\frac{\lambda}{\Delta_2}|+1, -\rangle$$

$$|\widetilde{-}\rangle = |0, -\rangle - \sqrt{(\tfrac{3}{2})}\frac{\lambda}{\Delta_2}|-1, +\rangle$$

$$g_\parallel = 2$$

$$g_\perp = 2 - \frac{6\lambda}{\Delta_2}$$

$$A = A_\parallel = 2g_n\beta\beta_n\langle r^{-3}\rangle\left\{-\kappa + \frac{4}{7} + \frac{6\lambda}{7\Delta_2}\right\}$$

$$B = A_\perp = 2g_n\beta\beta_n\langle r^{-3}\rangle\left\{-\kappa - \frac{2}{7} - \frac{45\lambda}{7\Delta_2}\right\}$$

$$P_\parallel = +\frac{3e^2Q}{7I(2I-1)}\langle r_q^{-3}\rangle$$

Δ_2 is the energy by which the $|\pm 1\rangle$ states lie above $|0\rangle$.

Lattice type	NaCl	CsCl	PH_4I(Tetragonal)	CsCl
NH_4^+ Orientation	Multiply Disordered	Doubly Disordered	Anti-parallel Ordering	Parallel Ordering
Space Group	$O_h^5(F_{m3m})$	$O_h^1(P_{m3m})$	$D_{4h}^7(P_{4/nmm})$	$T_d^1(P_{\bar{4}3m})$
Formula Units per unit cell	(Z = 4)	(Z = 1)	(Z = 2)	(Z = 1)

NH_4Cl: $\alpha \xleftrightarrow[\text{(I-order)}]{T_1 = 456K} \beta \xleftrightarrow{T_2 = 242K \quad (\lambda\text{-Transition})} \delta^*$

$a_o = 6.52$ (523K) $\qquad a_o = 3.8684$ (291K) $\qquad a_o = 3.82$ (88K

ND_4Cl: $\alpha \xleftrightarrow{T_1 = 448K} \beta \xleftrightarrow{T_2 = 249K} \delta$

$a_o = ??$ $\qquad a_o = 3.8682$ (291K) $\qquad a_o = 3.82$ (88K

NH_4Br: $\alpha \xrightarrow[\text{(I-Order)}]{T_1 = 411K} \beta \xleftrightarrow[\text{(}\lambda\text{-Transition)}]{T_2 = 235K} \gamma \xrightarrow[T_3 = 104K]{T_3 = 78K} \delta$

$a_o = 6.90$ (523K) $\qquad a_o = 4.059$(299K) $\qquad a_o = 4.026$, $c_o = 4.067$ (173K) $\qquad a_o = ??$

ND_4Br: $\alpha \xleftrightarrow{T_1 = 393K'} \beta \xleftrightarrow{T_2 = 215K} \gamma \xrightarrow[T_3 = 164K]{T_3 = 158K} \delta$

$a_o = 6.889$ (469K) $\qquad a_o = 4.084$(285K) $\qquad a_o = 4.047$, $c_o = 4.062$ (195K) $\qquad a_o = 4.016$(15

NH_4I: $\alpha \xleftrightarrow[\text{(I-Order)}]{T_1 = 257K} \beta \xleftrightarrow[\text{(}\lambda\text{-Transition)}]{T_2 = 231K} \gamma$

$a_o = 7.2613$(299K) $\qquad a_o = 4.37$(256K) $\qquad a_o = 4.321$, $c_o = 4.370$ (173K)

ND_4I: $\alpha \xleftrightarrow{T_1 = 254K} \beta \xleftrightarrow{T_2 = 224K} \gamma$

$a_o = 7.260$ (297K) $\qquad a_0 = 4.335$(253K) $\qquad a_o = 4.321$, $c_o = 4.341$ (173K)

*The δ phase of NH_4Cl is referred to as Phase III o
The lattice parameters a_o and c_o are in units of A

TABLE II.6

A selected summary of some reported transition temperatures of NH_4I

Transition Temp.	Physical Method	Remark	Reference
T_1=256K NaCl→CsCl	X-ray diffraction	The super cooling increases with decreasing particle size	95,112, 114
T_1=257K CsCl⇌NaCl T_2=231K Ttgl	Specific heat	NaCl phase could not be supercooled below 200K. No λ-transition occured	87
T_1=202K NaCl ⇢ CsCl	Cross relaxation time	The transition temperature depended on the thermal processing (rate of cooling/heating and number of repeated cycles	93
T_1=243K NaCl ⇢ CsCl T_1=278K CsCl ⇢ NaCl	Neutron scattering	The transition temp. T_1 depended on rate of cooling/heating. Mixed phase (NaCl+ CsCl) was evidenced on crossing the transition temp. both ways. No -transition was observed.	100
T_1 between 273 and 195K NaCl ⇠ CsCl	Dialatometric	It was necessary to keep sample at 195K for months to transform completely into CsCl phase.	102
No transition	UV reflectivity	NH_4I thin film on LiF substrate, no phase transition occured upto LNT	103
T_1=247K T_2=221K	Dielectric	Dielectric measurements on X-irradiated crystals	104
T_1=255.4K	Dialatometric	No λ-transition occured	105 (Bridgeman)

Contd

TABLE II.6 (Contd.)

Transition Temp.	Physical Method	Remark	Reference
T_λ =244K	Dielectric	A peak in dielectric constant around 244K was attributed to the λ-transition no other transition was observed	107
T_1=239K; T_1=268K I→II; I←II	Dielectric	No λ-transition was observed	108
T_1 between 273 and 257K NaCl⟷CsCl	Electrical conductivity	The phase transformation CsCl → Tetragonal developed rarely.	110
T_2 between 233 & 203K (CsCl⟷Tetragonal)			
T_1 between 255 and259K	X-ray(powder)	Coexistence of NaCl & CsCl phases was observed. Supercooling decreased with increasing particle size.	113
T_1=260.5K	Specific heat	No λ-transition occured	114
T_1=261K	Specific heat	No λ-transition was observed	115
T_1=260K	Specific heat	No λ-transition occured	116
T_1 between 255 & 261K	Lattice parameters		117
T_1=253K to 259K	Thermal analysis	Moisture affected the transition temperature	118
T_2=231K	Differential thermal analysis(DTA)	λ-transition Above T_λ, structure is regular and below tetragonal	120
$T_1 \sim$ 260K $T_2 \sim$ 229K	Dielectric	Two maxima in dielectric constant were observed at different cooling and heating measurements	121
T_2= 231K	DTA	λ-transition	119
T_1=256K T_2=115K	Tl-luminescence	No phase transition around 231K(λ-transition). At 115K a new phase transition is reported.	122
$T_1 \sim$256K NaCl⟷CsCl $T_2 \sim$231K CsCl⟷PH_4I(tetrg.)	Based on the literature survey	The most referred transition temps. are taken as T_1 and T_2.	84-86, 89,90

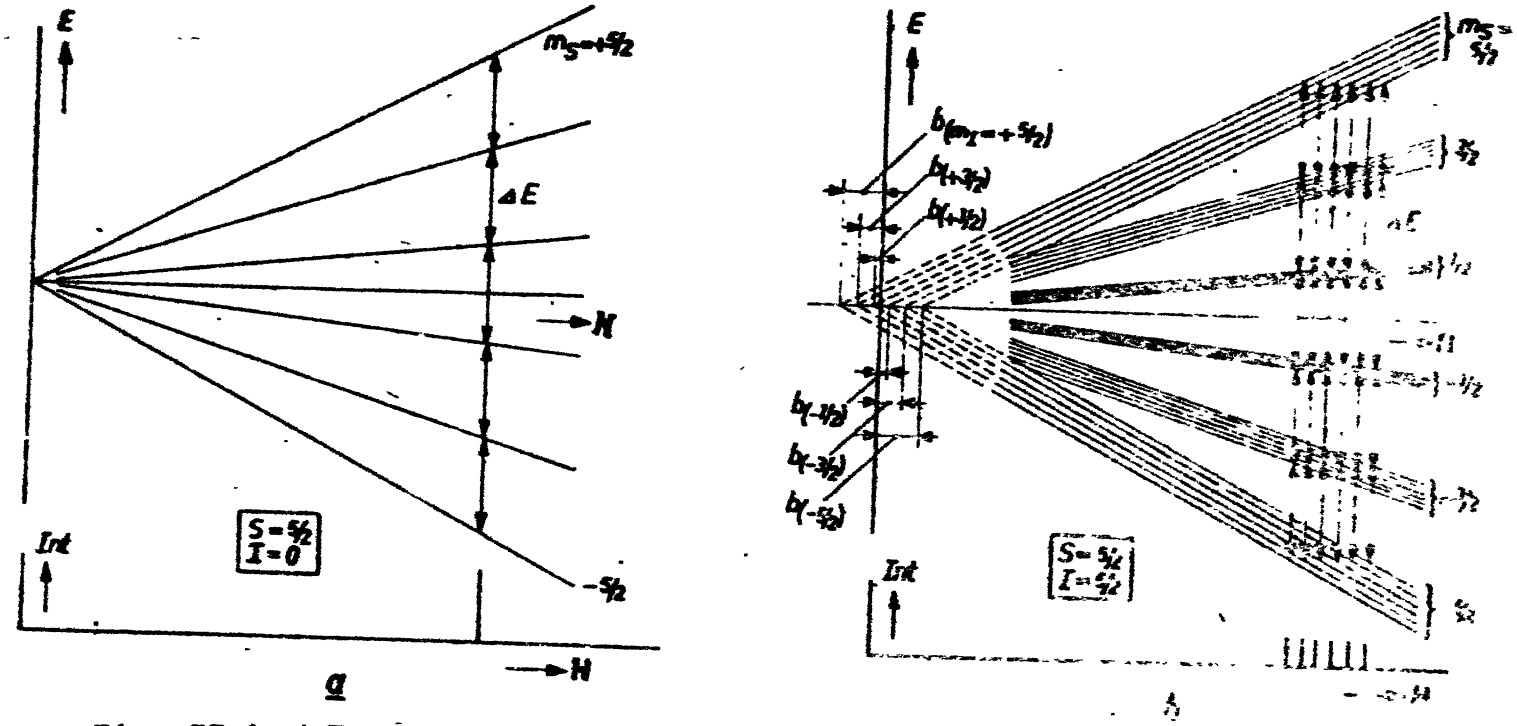

Fig. II.1 **a) Energy-level scheme of an ion with $S = \frac{5}{2}$ in a magnetic field H below, the resulting resonance spectrum (intensity *Int* as a function of H), which in this case consists of a single line.**

b) The same for an ion with $S = \frac{5}{2}$ which moreover has a nucleus of spin number $I = \frac{5}{2}$ (Mn^{3+}). Each of the levels of (a) is split into six sub-levels, corresponding to the six values of the field $H+b$. The 30 possible transitions give rise to six resonance peaks, as shown below.

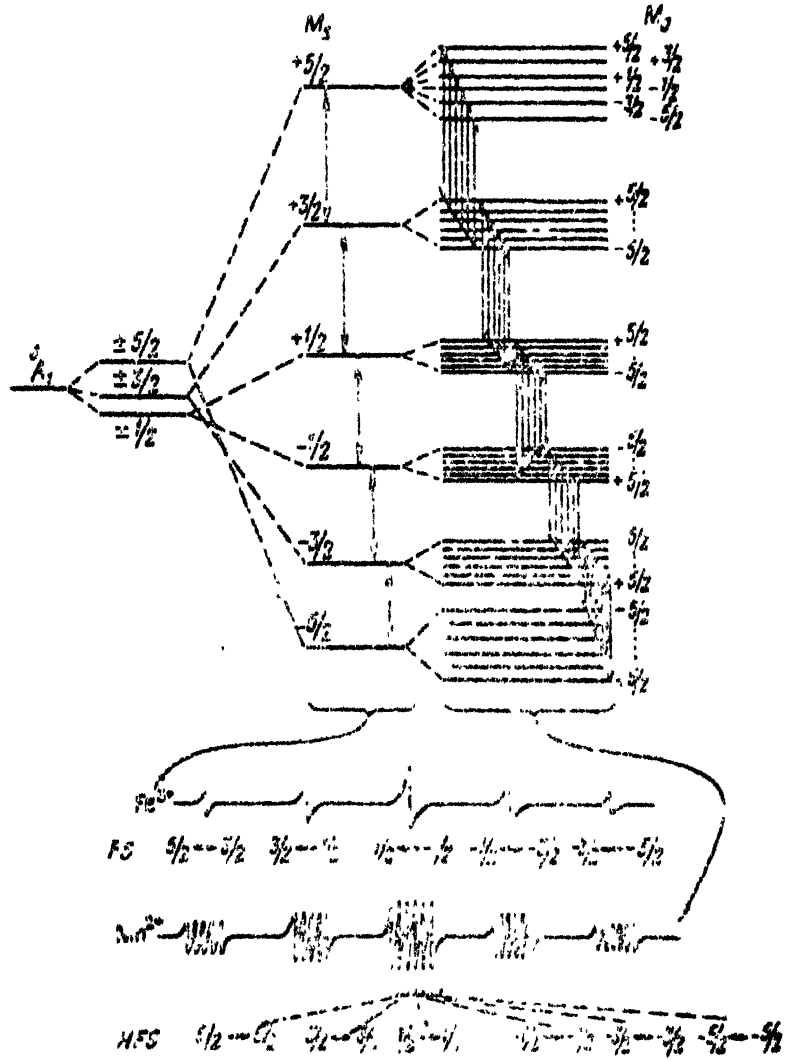

Fig. II.3 EPR spectra hyperfine structure for ions with spin $S=5/2$ and nuclear spin $I=3/2$. For the $M_S=\pm 1/2 \leftrightarrow (\pm 5/2)$ transition five fine structure lines of $M_S=\pm 1/2$ that yields no shfs, are shown. For $M_S=\pm 5/2$ each of one of the fine structure lines is split into six shfs lines, as shown.

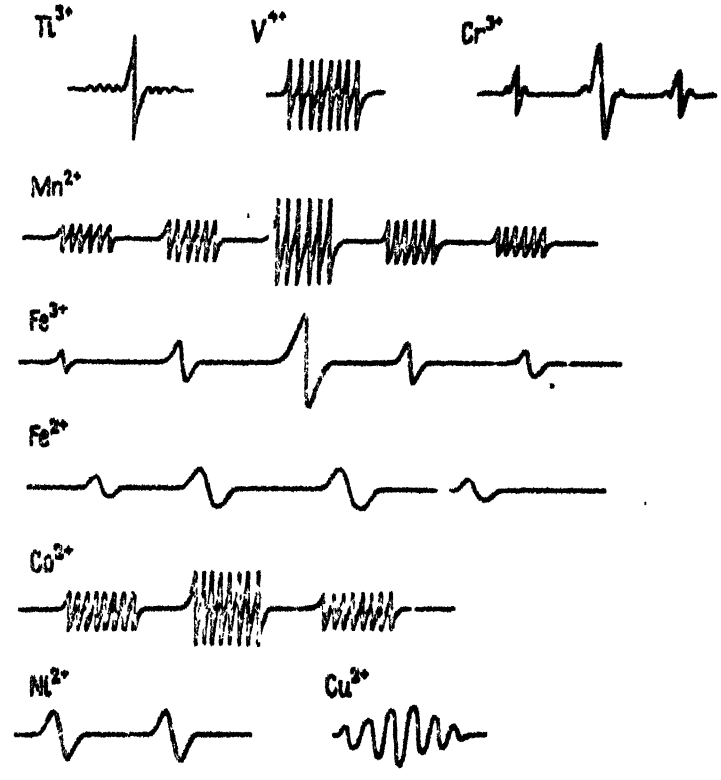

Fig. II.3 Patterns of the iron group ions EPR spectra.
Ti^{3+}: $S = 1/2; 2S = 1$—a single fine structure line (fs); Ti^{48}($I = 0$); Ti^{47} (7.75%) $I = 5/2$; Ti^{49}(5.5%) $I = 7/2$; V^{4+} (d^1): $S = 1/2$; V^{51} (100%) $I = 7/2$; $2I + 1 = 8$—eight lines of hyperfine structure (hfs). Cr^{3+} (d^3): $S = 3/2$; $2S = 3$—three fine structure lines (fs); Cr^{53} (9.5%) $I = 3/2$—apart from the even isotope central line each one of three fs-lines is split into four weak hfs lines, of which two are overlapped by the central line and two are seen in the form of weak satellites. Mn^{2+} (d^5): $S = 5/2$; $2S = 5$—five fs lines; Mn^{57} (100%) $I = 5/2$; $2I + 1 = 6$—six hfs lines. Fe^{3+} (d^5): $S = 5/2$; $2S = 5$—five fs lines, Fe^{2+} (d^6): $S = 2$; $2S = 4$—four fs lines. Co^{2+} (d^7): $S = 3/2$; $2S = 3$—three fs lines; Co^{59} (100%) $I = 7/2$—eight hfs lines. Ni^{2+} (d^8): $S = 1$; two fs lines. Cu^{2+} (d^9): $S = 1/2$—one fs line; Cu^{63} (68.9%) $I = 3/2$; Cu^{65} (31.3%) $I = 3/2$—two series with four partially overlapping hfs lines in each one of them

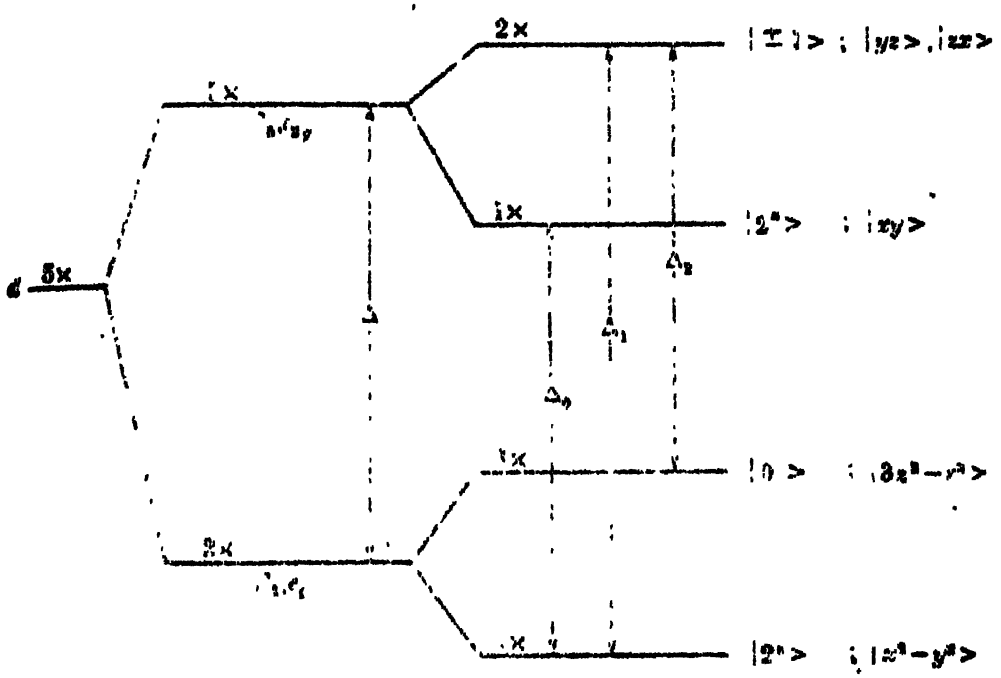

Fig. II.6 Orbital energy levels and states for a d^1 ion in a crystal field of octahedral symmetry with a tetragonal distortion.

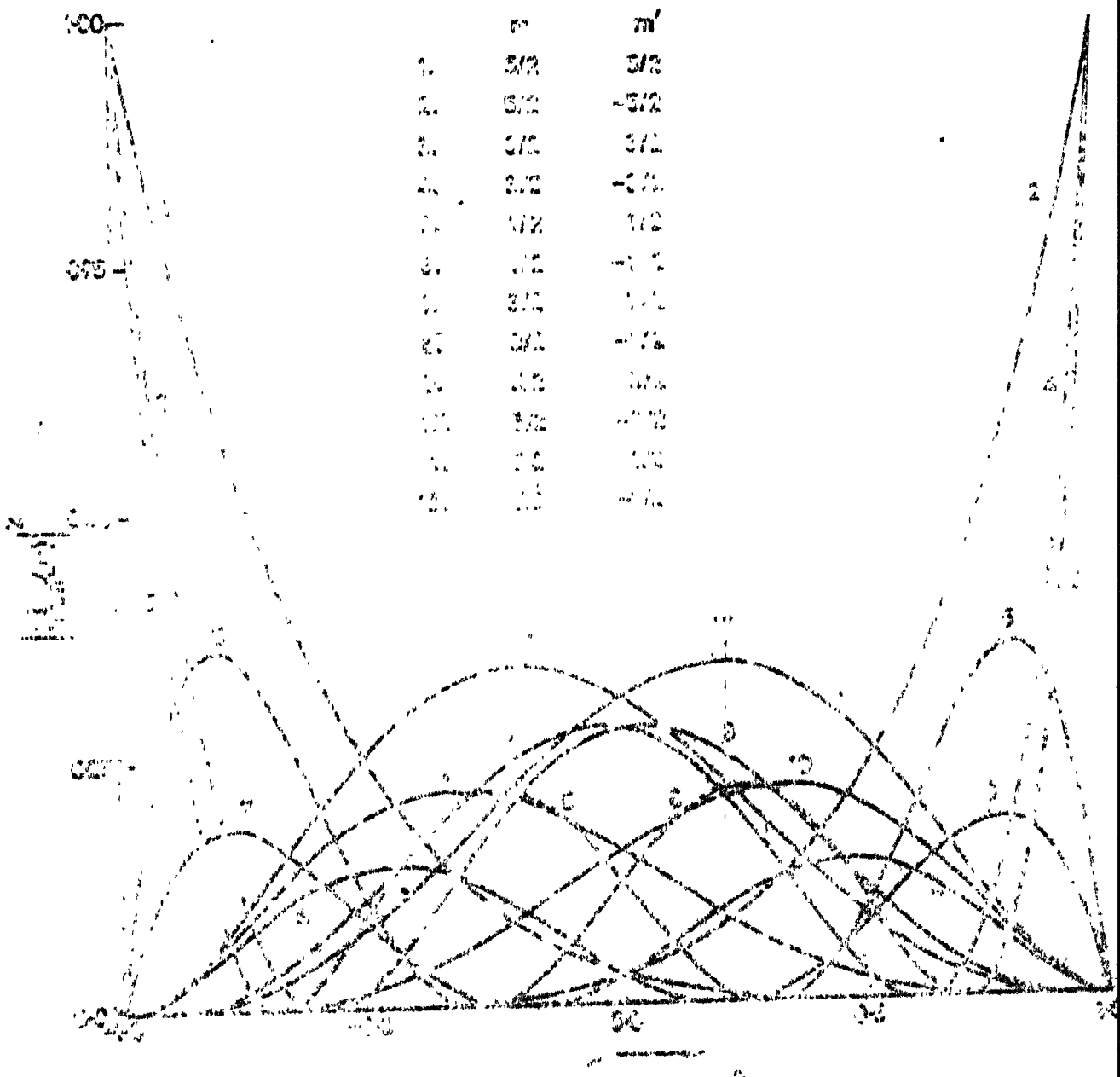
m
m'

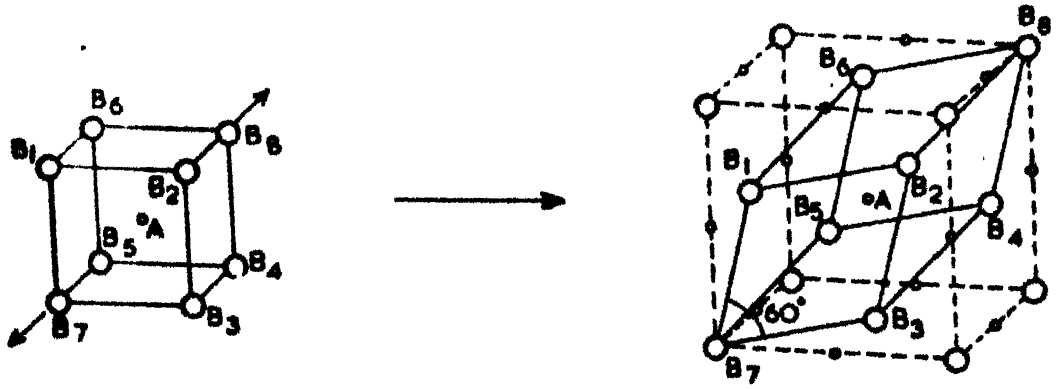

(a)

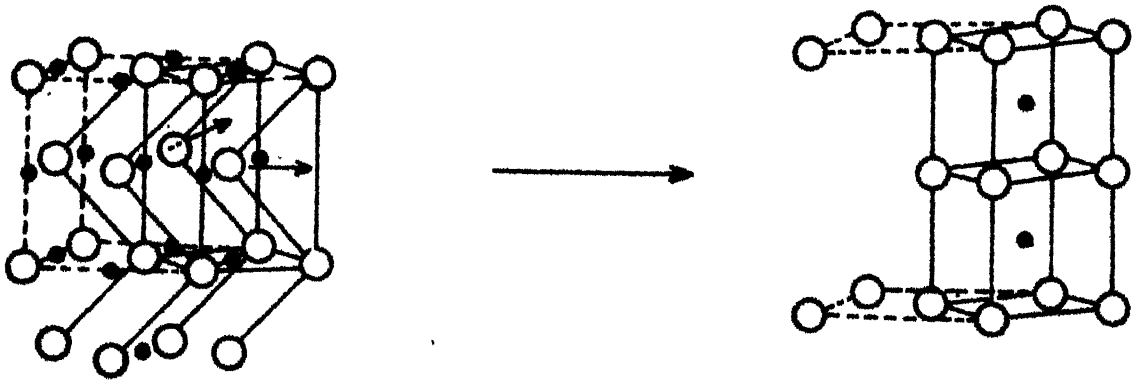

(b)

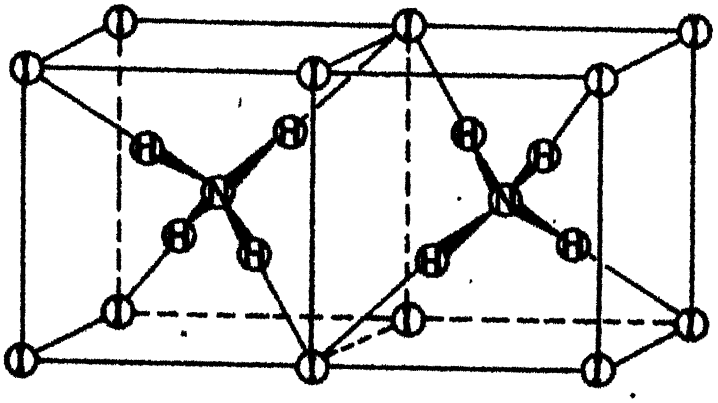

(c)

Fig. II.7 (a) Mechanism of a dilational transformation from CsCl to NaCl structure in an AB-type complex.
(b) Reshuffling of atomic positions in a transformation NaCl to CsCl structure in ammonium halides.
(c) Two possible orientations of NH_4^+ in phase II (β) of ammonium halides.

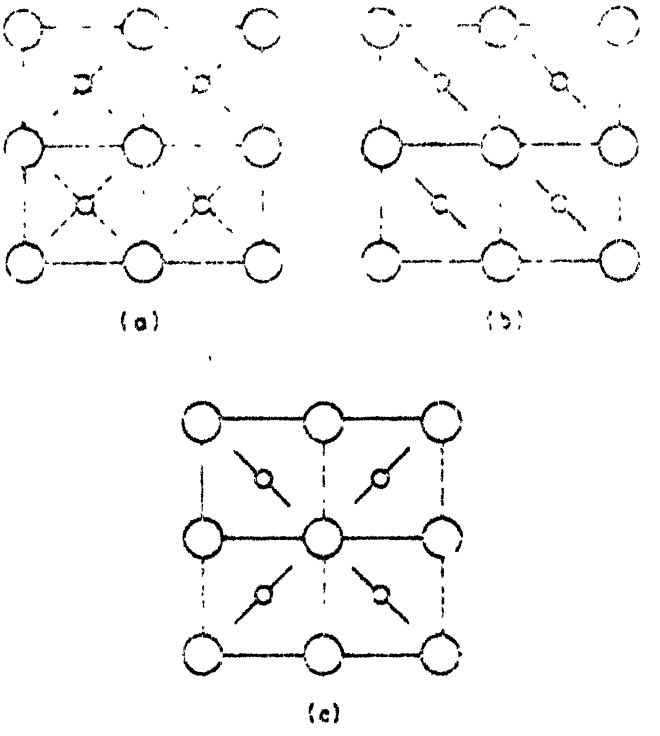

Fig. II.8 (a) A representation of the two energetically equivalent orientations of the ammonium tetrahedra in the disordered phases of the ammonium halides. One of the cubic axes is perpendicular to the page. Large circles represent the halogen ions and small circles represent the nitrogen of the ammonium ions. The nitrogen position is at the body centre of a cube of halogen ions. Lines drawn through the nitrogen represent the hydrogen–hydrogen vector for the hydrogen atoms above the plane of the nitrogen. Dotted lines indicate a dynamic disorder between the two equally probable orientations.

(b) A representation of the ferrodistortive order of the ammonium ions in the CsCl phase of NH_4Cl and ND_4Cl. The solid lines represent the energetically favoured orientation of the ammonium ion. One of the cube axes is perpendicular to the page.

(c) A representation of the anti-ferrodistortive order in the tetragonal phases of NH_4Br, ND_4Br, NH_4I and ND_4I. The tetragonal axis is perpendicular to the page, and the symbols are the same as those used in parts (a) and (b). All ammonium ions in the column parallel to the tetragonal axis have the same orientation as the ion of the column shown.

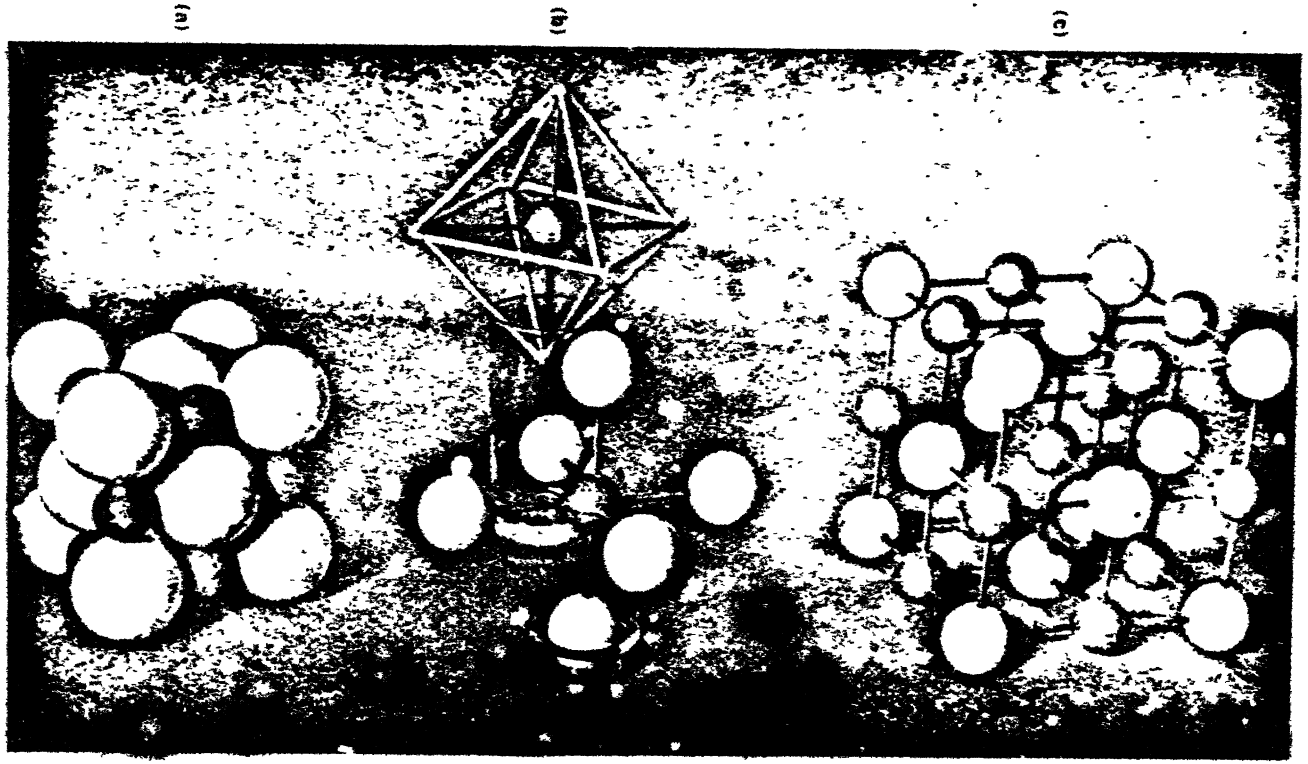

Fig. II.9 Packing (a) and lattice models (b) & (c) of NH_4I unit cell. The central small sphere in (b) & (c) representing NH_4^+ ion, has six an Iodide ions (big) arranged octahedrally about it.

CHAPTER III

EXPERIMENTAL

Abstract: A brief description of the experimental set up used in the EPR study - a Varian E-line X-band EPR spectrometer (Model E-109), a continuous flow cryostat, a variable temperature controller (Varian model E-257/WL-257), a two axis crystal rotating device and a Gaussmeter (Varian model E-500) - is presented. The techniques used for growing good quality single crystals of ammonium halides doped with paramagnetic impurities are described.

III.1 EPR SPECTROMETER[1]

EPR spectra were recorded on a Varian E-line Century Series spectrometer models E-109 and E-112*. The E-109 spectrometer operates at X-band frequency (8.8 - 9.3 GHz). The experiments on E-112 spectrometer were carried out at Q-band frequency ($\sim$ 35 GHz). All the EPR spectra have been recorded with 100 kHz field modulation. The maximum calibrated power available with these spectrometers is 200 mW and even higher power levels (uncalibrated) may be obtained if desired. The recording of EPR spectra both in absorption or dispersion modes is possible and the first or second derivative of absorption signal can be recorded. Through out this thesis the recorded spectra are the conventional first derivative of absorption signal. Various scan ranges (200 mG to 20 kG) with various scanning rates (1/2 minute to 16 hours) are available and can be used as the situation warrants. The modulation field amplitude depends on the type of cavity in use and ranges typically from 5 mG upto 40 mG with E-231 rectangular ($\sim$9 GHz - TE_{102}) and from 5 mG upto 15 G for E-266 (35 GHz-TE_{011}) cavity at 100 kHz field modulation. The E-266 cavity (unloaded Q = 7,000) is a cylindrical, tunable cavity which can be adjusted with the sample inserted allowing

*The experiments on E-112 EPR spectrometer at Q-band were carried out at RSIC, Indian Institute of Technology, Madras, India.

the operation at a fixed microwave frequency. This cavity permits sample tube sizes upto 3 mm outer-diameter and the angular variation study of the EPR spectra is possible by rotating the magnet about the axis of the cavity.

With E-109 EPR spectrometer a Varian rectangular cavity E-231 which operates in TE_{102} model with unloaded Q more than 7,000 and which permits sample-tube-sizes upto 11 mm outer-diameter has been used through-out in the experiments at X-band frequencies. The 11 mm sample access permits use of wide variety of accessories such as variable temperature equipment, liquid nitrogen dewar etc. and also allows the use of relatively bulky sample holders and samples in the cavity. The modulation amplitude usually has been kept small around $\frac{1}{2}$ Gauss (G) peak to peak (p-p). For most of the normal EPR recording a power level of $\sim$ 2 mW has usually been found adequate to give good signal height at normal gain levels of $1x10^3$. The field stability of these spectrometers after stabilization is of the order of 10 ppm with temperature coefficient of 2 ppm/C° between 3 KG and 15 KG. The S/N ratio with E-231 cavity at 100 kHz modulation is equal to 180 ($\sim 3.75x10^{10}$ x ΔH spins). The schematic diagram of the EPR spectrometer E-109 is shown in Fig. III-1.

III.2 FIELD CALIBRATION

Initially the magnetic field was calibrated with the help of a Varian model F-8A proton resonance fluxmeter and a Systronix model 701 Frequency Counter-timer. A small speck

of DPPH (g = 2.0036) glued to the samples was used to give a reference field marker. But later on the magnetic field was calibrated with more accurate Varian model E-500 Gauss-meter which became available afterwards. The E-500 NMR Gaussmeter provided an accurate, convenient and reliable method of field measurements with the help of a small in-cavity probe and a built-in display. The unit provides a choice of manual or automatic search for the magnetic field with continuous tracking in auto mode. A small accessory probe allows magnetic field measurements directly at the sample. A marker display cable can relay marker on the EPR spectrometer console recorder and can display the NMR resonance directly on the spectrometer's oscilloscope. The field measurement accuracy is (10 mG + 2 ppm) and the field marker accuracy is 1 part in 10^3.

III.3 SAMPLE HOLDER AND ANGULAR VARIATION

For initial studies with single crystals it is required to know the crystal field axes (X, Y, Z) as defined in the chapter II. For this purpose a two axis goniometer was designed and fabricated (Fig. III-2) which provides a possibility of rotation of the magnetic field in any desired plane of the crystal. The axes X, Y and Z were determined employing the following method. The crystal was rotated first independently about a horizontal and a vertical axis and a particular orientation was searched where the spread of the fine structure was maximum. Thus knowing

one direction of maximal spread in fine structure, the other two directions of extremum in fine structure spread were searched in a plane normal to the first direction of maximal spread. The directions are referred to as Z, Y and X in order of maximal spread (Chapter II).

Once the axes are known the crystal can be cut or the mounting end of the quartz sample holder can be cut to facilitate the angular rotation of the crystal about a desired direction. The Varian model E-229 Goniometer (Sample Rotator) permits an accurate rotation of samples in steps of $1/2^{o}$. The Goniometer E-229 is designed to be compatible with variable temperature accessory. The initial alignment of the crystals were made using the growth planes of the crystals and then it was possible to align the crystal quite accurately through the observation of the characteristic spectrum. For rotation of NH_4I and NH_4Br as-grown crystals about [110] as vertical axis a 45^{o} cut was made at the mounting end of quartz rod and the crystal was glued with one of the growth planes to the cut.

III.4 VARIABLE TEMPERATURE ACCESSORY

The Varian model E-257/WL-257 variable temperature accessory automatically controls the sample temperature within the range of 573K to 88K. The accessory provides a means to maintain the desired sample temperature for a sustained length of time with an accuracy of better than $1^{o}K$. The accessory consists of a dewar insert for the cavity heater

sensor assembly, electronic temperature control unit, transfer dewar, heat exchanger coil, liquid nitrogen storage dewar, associated mounting hardware and a source of dry nitrogen capable of supplying dry N_2 flow upto 40 cubic feet per hour. The schematic diagram of the assembly is given in Fig. III-3. For attaining the temperature of 77K a quartz dewar compatible with E-231 cavity, provided with a cold finger was used. In this arrangement liquid nitrogen cools a copper paddle whose tip is in thermal contact with the sample inside the cavity. The pumping of nitrogen vapours from the dewar permits the cooling of the sample down to 77K and some times even lower. The actual temperature at the sample was measured with the help of a potentiometer using a copper constantant thermocouple junction at the sample. The over all accuracy of the measured temperature is 0.5 K. Thc temperature stability at the sample was found to be within $\pm$ 0.5 K, after stabilization. The time required to accomplish a 100 K change in sample temperature was found to be about 15 minutes.

[II.5 CRYSTAL GROWTH

The crystals of NH_4I were grown from aqueous solution. The normal procedure of growing crystals from solution by natural evaporation at constant temperature failed in this case. It is well known that properly selected chemical additives aid in the growth of flawless crystals[2]. For ammonium halides some of such reported additives (some times called as habit modifier or flux) are chemicals[3] like urea, pectin, borax,

glycine, and ions[2] like Mn^{2+}, Cr^{3+}, Fe^{3+}, etc. Urea has been found to be a safe additive for NH_4Cl and NH_4Br[3-7], which very effectively prevents dendritic growth and results into nice crystals of cubic shape. Urea is also used to stimulate cubic growth of NH_4I crystals from aqueous solution but often only small crystals could be grown.

The suitable growth conditions for growing nice crystals with perfect faces suitable for EPR studies were obtained through judicious study of the effects of growth temperature, amount of additive, pH of mother liquor and evaporation rate. It was observed that if the mother liquor is kept at constant temperature but unprotected from light the subsequent evaporation of supersaturated solution does not yield good quality crystals. This was because, the liberated iodine due to photodecomposition of NH_4I turned the colour of the mother liquor to dark violet and prevented the growth of good quality crystals. It was found that protection of the mother liquor from exposure to light resulted in good quality crystals. Thus all the crystals were grown in complete darkness in a temperature controlled ($\pm$ .5 K) chamber. By adding urea ($\sim$10 percent by weight) and keeping the evaporation rate very slow, the above process successfully resulted in growth of excellent cubic crystals of good size (upto 1 cm^3) over a period of two months. The evaporation rate was controlled by placing a coverslip with adjustable exit hole and by placing the growth solution in a temperature controlled chamber over concentrated H_2SO_4. Large single crystals were grown by suspending a small seed crystal

in saturated mother liquor and by carefully controlled evaporation. The X-ray, IR and Raman analysis showed that urea did not contaminate the grown crystals.

For EPR experiments paramagnetic impurity doped crystals are required. We tried the incorporation of various ions viz. Co^{2+}, Ni^{2+}, Cu^{2+}, Mn^{2+}, VO^{2+}, Fe^{3+}, Cr^{3+} and Gd^{3+} by dissolving small amounts (.01 to 2 percent by weight.) of the corresponding halide in the mother liquor. Although growth of good quality crystals in all the cases was possible over a wide range of growth temperature (260 K to 350 K) but the incorporation of ions in the crystals was found to be selective and growth temperature dependent. The incorporation of ions was tested by observing EPR signal over the available temperature range in our laboratory (573 K to 77 K). The incorporation of Cu^{2+}, VO^{2+}, and Mn^{2+} was confirmed even at room temperature while no EPR signal could be observed from the crystals doped with the remaining impurity ions from room temperature down to LNT.

The trivalent Cr^{3+} ion has been found to be incorporated with difficulty in NH_4Cl[3]. It could be incorporated only at elevated growth temperatures ($\cap\cup$363 K) and by adding rather large quantity (upto 50% $CrCl_3$ by weight) of corresponding halide to the growth solution. We also tried the incorporation of Cr^{3+} in NH_4I by adding large amount of $CrCl_3.6H_2O$ (upto 50% by weight) to the growth solution and using different growth temperatures (upto 363 K). The process

resulted in nice cubic crystals even without urea as growth aid but no detectable traces of Cr^{3+} were found through EPR down to LNT. Although Cr^{3+} could not be incorporated but the results indicated use of Cr^{3+} ions as an alternative growth aid. Therefore, crystals containing Cu^{2+} were also grown from solutions to which $\sim$10% $CrCl_3.6H_2O$ was added as growth aid. The evaporation rate was kept very low such that it took about 3 months to grow sufficiently big crystals at 300 K. The presence of small quantity of $CrCl_3$ along with urea in growth solutions which contained $\cup$ 0.5% $CuCl_2.2H_2O$ by weight was found suitable for the homogeneous incorporation of Cu^{2+} in the crystals.

To incorporate VO^{2+} either $VOCl_2$ or $VOSO_4$ (hydrate) was added in small amount (1 to 0.5% by weight) while for Mn^{2+} incorporation, MnI_2 was added in proportions ranging from .01 to 1% by weight with urea as additive. The as-grown crystals showed development of perfect (100) faces of cubic crystal, irrespective of the ion being incorporated. All the crystals showed perfect cleavage planes parallel to (100) i.e. the faces of the as grown crystals. Therefore big crystals could easily be cut into small cubes to suit the requirement. The size of the crystals grown with Cu^{2+} was small ($\cup$3 mm^3) compared to the size of crystals grown with Mn^{2+} or VO^{2+} ($\cup$6 mm^3). The single crystals containing Mn^{2+} impurity were transparent and colourless, those with Cu^{2+} impurity were transparent but light blue in colour and those with VO^{2+}

impurity were transparent and light bluish green. The X-ray, IR and Raman analysis at room temperature showed that the incorporation of ions has not modified the lattice. The crystals recovered from growth solution were washed with carbon tetra-chloride, vacuum dried in dark, and were stored in dark descicator to avoid any possibility of photo-decomposition.

The crystals of NH_4Br doped with Mn^{2+} and VO^{2+} were grown from aqueous solution containing small amount of the corresponding bromide by slow evaporation at a temperature of 300 K and with urea ($\sim$ 10% by weight) as habit modifier. Small crystals ($\sim$ 3 mm^3) recovered from the solution were washed with carbon tetrachloride, vacuum dried and were stored in dark descicator. Crystals doped with Mn^{2+} were colourless while those doped with VO^{2+} were light brown to colourless. The faces of the as-grown crystals were identified to be (100) planes.

All the chemicals used were analytical grade reagents and were mostly obtained from Fisher Sci. Company, USA.

REFERENCE

1. 'EPR Spectrometer Manual for Model E-109', Publication No. 87-125-041, Varian Instruments Division, USA.
2. 'The Art and Science of Growing Crystals', Ed. J.J. Gilman, John Wiley & Sons, Inc. New York (1966).
3. F.S. Stibbe and N.J. Trappeniers, Physica 95B, 81 (1978).
4. S.H. Hagen and N.J. Trappeniers, Physica 47, 165 (1970).
5. J.R. Pilbrow & J.M. Spaeth, Phys. Stat. Sol. 20, 225 (1967).
6. M.D. Sastry and P. Venkateswarlu, Proc. Ind. Acad. Sci. 66, 208 (1967).
7. N.J. Trappeniers, F.S. Stibbe and J.L. Rao, J. Phys. Chem. Solids 42, 617 (1981).

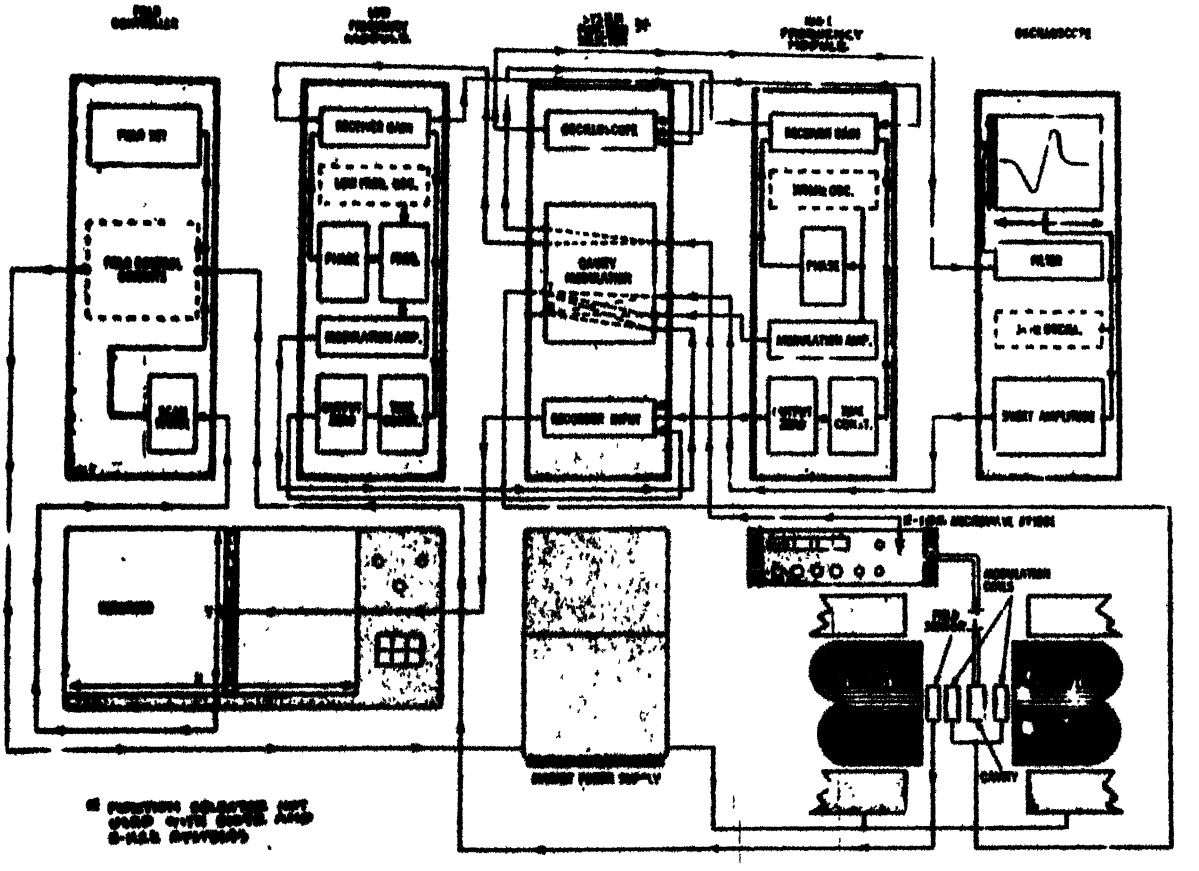

Fig. III.1 . Schematic diagram of EPR spectrometer - Varian Model E-109/E-112

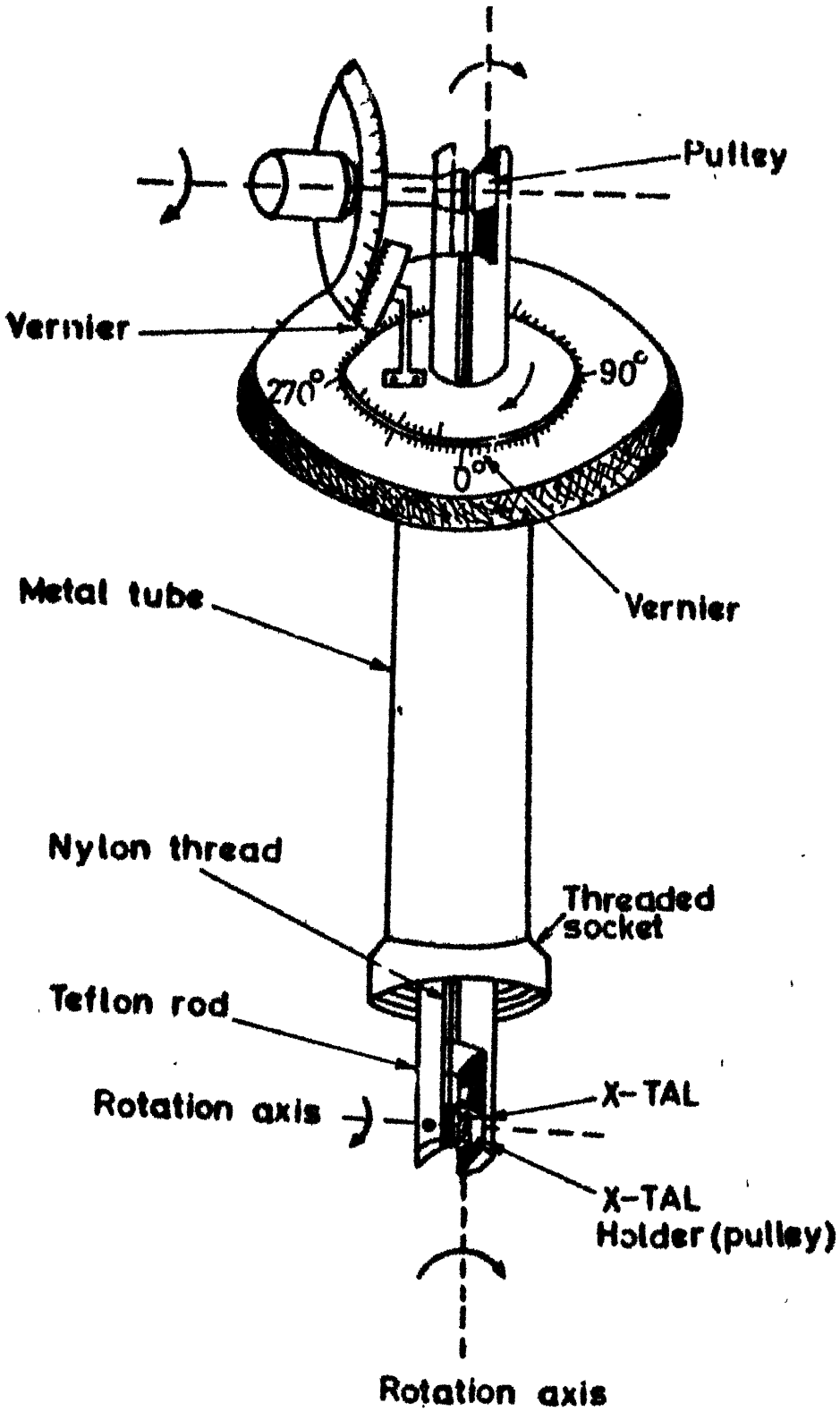

FIG. III-2 TWO AXIS GONIOMETER TO ROTATE THE CRYSTAL ABOUT AN ARBITRARY AXIS INSIDE THE MICROWAVE CAVITY.

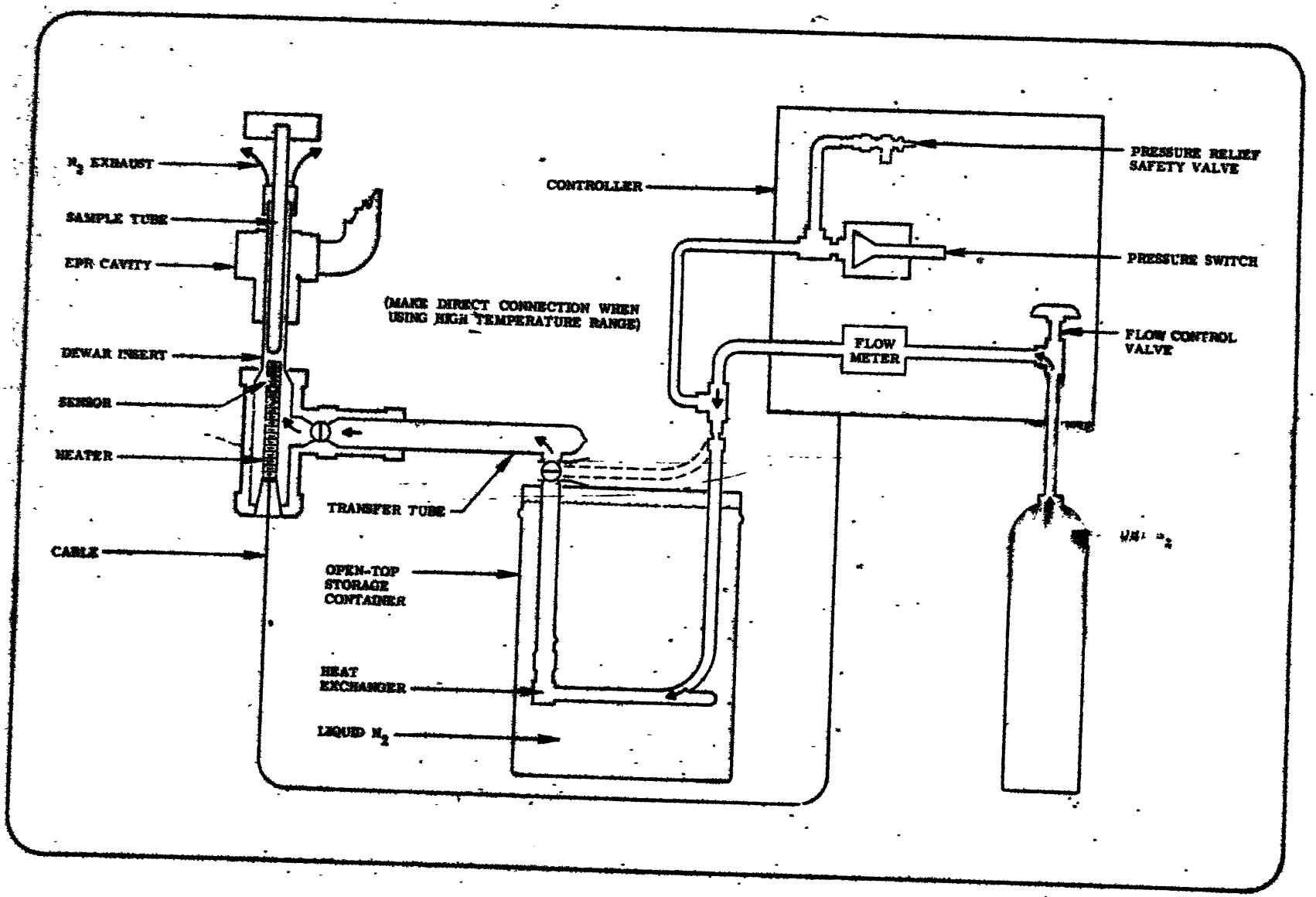

Fig. III.3 Temperature controller assembly - Varian Model E-257/WL-257

CHAPTER IV

EPR STUDY OF Mn^{2+} IONS DOPED IN NH_4I SINGLE CRYSTALS*

Abstract: Results of EPR study of Mn^{2+} doped in NH_4I single crystals are given in this chapter. The RT study at Q-band revealed only one type of Mn^{2+} centre with three distinct orientations of crystal field axes. The crystal field has an axial symmetry with very large tetragonal distortion. The D parameter is found to be very large ($|D|$ = 1612 G) and g-values are found to be close to free ion value. The $\tilde{g}$ and $\tilde{A}$ tensors are almost isotropic. Due to very large value of D-parameter the hyperfine structure was very anisotropic. The intensity of allowed and forbidden hf transitions of the central group ($\frac{1}{2} \leftrightarrow -\frac{1}{2}$) is explained using Bir-Lupei method. The EPR study at X-band was carried out over the temperature range 573 to 77K. Due to the very large value of D-parameter many unusual features were observed in the X-band spectra. At elevated temperatures ($\sim$ 473K) a single isotropic sextet is observed. Expulsion of Mn^{2+} impurity by NH_4I lattice took place at temperatures above 500K. The temperature variation of D-parameter showed an anomaly around $\sim$ 250K and is attributed to the structural phase transformation. The spectra at LNT indicated the presence of more than one type of Mn^{2+} centres. The g and A parameters were found to be almost temperature

---

*Part of the contents (RT-study) of this chapter has been accepted for publication in J. Chem. Phys. (in Press).

J. Chem. Phys. 78, 5930-5936 (1983)

independent. The temperature variation of line widths showed an anomalous behaviour around the transition temperature ($\sim$250K) The temperature variation of D-parameter and line widths was accompanied by a large hysteresis which depended on thermal processing of the samples. The cause of large thermal hysteresis is attributed to the hypothesis of coexisting phases below and above the phase transformation of NH_4I. The observed EPR spectra from polycrystalline samples at X- and Q- bands are also discussed.

IV.1 INTRODUCTION

It is well known that in alkali halides when divalent cation impurities are doped, the impurities substitute for monovalent cations and charge compensation takes place through various mechanisms. As an interesting extension of charge compensation studies in alkali halides, ammonium halides have also been doped with divalent impurities. But the EPR studies of doped ammonium halides have been confined mainly to NH_4Cl, NH_4Br and their deuterated analogues. The only other is NH_4F with Cu^{2+} as the impurity ion, studied by Parker[1]. The EPR of Mn^{2+} doped in NH_4Cl has been studied by a number of workers[2-11] but the site of Mn^{2+} incorporation has been rather controversial and the axial crystal field parameter b_2^o (=D) was found to be unusually large ($\sim$1605 Due to very large value of D, the EPR spectra at X-band were found to be unusual. The unpublished work of Sastry[12] on Mn^{2+} doped NH_4Br revealed that Mn^{2+} enters substitutionally for NH_4^+ with remote charge compensating sites at RT ($\sim$300K), resulting in an isotropic sextet. At liquid nitrogen temperature (LNT) they observed a spectrum comprising fine groups and have estimated a value of $|D| \sim 538$ G. Thus two ammonium halides viz. NH_4Cl and NH seem to behave differently for Mn^{2+} impurity. It was felt interesting, therefore, to observe through EPR, how Mn^{2+} doped in NH_4I behaves. To the best of our knowledge no EPR studies of Mn^{2+} in NH_4I and NH_4F have so far been reported in the literature. It i

well known that ammonium halides undergo several structural phase transitions with temperature.[13,14] We have therefore undertaken the EPR study of Mn^{2+} doped in NH_4I in the temperature range 573K to 77K at X-band frequency ($\sim$ 9.3 GHz) and at RT ($\sim$ 300K) at Q-band frequency ($\sim$ 35 GHz).

The X-band EPR study was carried out first and the analysi of the spectrum revealed that the D parameter is very large in th present system. We then carried out the study of Q-band frequencies and refined the parameters. We shall first discuss the Q-ba spectra and subsequently the X-band spectra.

IV.2 Q-BAND SPECTRA*

(i) Experimental

The crystal was fixed to the tuning rod of a cylindrical cavity in such a way that the magnetic field was rotated in one of the (100) planes by rotating the magnet. The observed angular variation of intensity and positions of the fine structure groups in the (001) plane revealed that there were three constituent spectra. One of the constituent spectra (Spectrum-I) did not sh angular variation in the (100) plane, while the other two (Spect II and III) were very anisotropic. Along [100] direction one of the constituent spectra (Spectrum-III) has a maximum spread in fine structure. The hyperfine structures of all the fine struct groups of Spectrum-III also show maxima in spreads along [100]. We shall call [100] the Z-axis of Spectrum-III. On rotating the magnetic field away from [100] towards [010], Spectra II and III start shrinking in spread and the hyperfine structure becomes

complex. There are many forbidden hyperfine transitions which are very anisotropic not only in position but also in intensity. There are orientations of the static magnetic field $\vec{H}$ for which the normal allowed hyperfine transitions almost disappear and the forbidden transitions are quite strong. Along [010] direction the positions of spectra-II and III get interchanged. Along the directions [010] and [100], one of the constituent Spectra-II or III coincides with Spectrum-I and the other one shows a maxima in spread. Therefore, the two spectra II and III are equivalent but are 90° out of phase in (001) plane. The Spectrum-I will be designated as X-Y Spectrum while the Spectra II and III will be designated as (X/Y)-Z spectra. All the crystal faces viz. (100), (010) (001) or equivalent are found identical so far as the angular behaviour of EPR spectra is concerned. The EPR spectrum shows a 4-fold symmetry in the above mentioned planes. Fig. IV.1 shows the spectrum at Q-band frequency (∿ 35.25 GHz) when $\vec{H}$ is oriented along any one of the cube edges. The groups marked as A, B, C, D and E are the sextets of the (X/Y)-Z spectrum for $\theta = 0^{\circ}$ i.e. $\vec{H}$ along the Z-axis. The groups have relative intensity in the ratio 5:8:9:8:5. The groups of sextet marked by F through J correspond to two identical spectra, exactly overlapping, one of which is the X-Y spectrum and the other is the 90° part of the (X/Y)-Z spectrum.

The lines are quite sharp (∿ 8 G peak to peak) even at RT. At RT no saturation behaviour was observed with 200 mW microwave power, and no superhyperfine structure was observed due to ligands. The spectra of the polycrystalline sample (fine crushed powder) were also recorded. Fig. IV.2 shows the spectrum of polycrystalli

sample at Q-band frequency ($\sim$34.99 GHz). Figs. IV.3 and IV.4 show the angular dependence of the allowed and forbidden hyperfine transitions of the central fine structure group ($M_s = \frac{1}{2} \leftrightarrow M_s = -\frac{1}{2}$) of the (X/Y)-Z spectrum.

Some of the crystals were heated at $\sim$ 430K for half an hour and were subsequently cooled down to RT by dry nitrogen gas flow over the annealed sample. Spectra recorded with the heat treated samples were found to be identical with the spectra of as-grown crystals. The crystals grown at growth temperatures ranging from 288K to 350K gave spectra identical to those for a crystal grown from neutral solution at RT.

(ii) Spin-Hamiltonian Analysis

The following conventional spin-Hamiltonian appropriate to Mn^{2+} ion in a crystalline field with axial symmetry was used for analysis of the spectra :

$$\mathcal{H} = \beta \vec{H}.\tilde{g}.\vec{S} + B_2^0 O_2^0 + B_4^0 O_4^0 + B_4^4 O_4^4 + \vec{S}.\tilde{A}.\vec{I} + \beta_N \vec{H}.\tilde{g}_N \vec{I} \quad .. \quad (IV.1)$$

For Mn^{2+}, S = I = 5/2 and the symbols have their usual meanings.

The fitting method discussed in Chapter II was used to obtain the Spin Hamiltonian parameters. The fitting was found to be insensitive to the last fine structure term viz. $\left(B_4^4 O_4^4 \right)$ which therefore was neglected subsequently. The spin-Hamiltonian (IV.1) may then be expressed as follows in terms of more common symbols[9] :

$$\mathcal{H} = \beta g_{\parallel} H_z S_z + \beta g_{\perp} (H_x S_x + H_y S_y) + \frac{1}{3} b_2^0 O_2^0 + \frac{1}{60} b_4^0 O_4^0 + A S_z I_z + B (S_x I_x + S_y I_y) + Q P_2^0 \quad .. \quad (IV.2)$$

The best fit parameters obtained are given in Table IV.1. The calculated and experimental field values of observed fine structure transitions are given in Table IV.2 and those of the hyperfine transitions of groups C and H are given in Table IV.3, for comparison. Fig. IV.5 shows the angular variation of the centres of hyperfine structure groups when $\vec{H}$ is varied in (001) plane. The solid lines are the theoretical curves obtained by exact numerical diagonalization of the spin-Hamiltonian matrix comprising only the fine structure terms on a computer and circles and triangles are the experimental points. The good agreement between the experimental points and the calculated curves justifies the adequacy of the spin-Hamiltonian used.

Normalizing the energy with $b_2^0(=D)$ and neglecting the hyperfine terms, the spin-Hamiltonian IV.2 may be written as :

$$\mathcal{H}/|D| = \beta g_{\parallel} \left(\frac{H}{|D|}\right) \mathrm{Cos}\theta\, S_z + \beta g_{\perp} \left(\frac{H}{|D|}\right) \left[\mathrm{Sin}\theta(\mathrm{Cos}\phi\, S_x + \mathrm{Sin}\phi\, S_y)\right] + \frac{1}{3}O_2^0 + \frac{1}{60}\frac{b_4^0 O_4^0}{|D|} \qquad \text{(IV.3)}$$

where the direction of the magnetic field $\vec{H}$ is expressed in spherical polar coordinates. The secular equation derived from the above Hamiltonian was solved numerically on a computer for Mn^{2+} with S = 5/2 and the energy diagrams ($E/|D| - H/|D|$ curve) so obtained are shown in Fig. IV.6 for $\vec{H} \parallel$ Z axis ($\theta = 0$) and $\vec{H} \perp$ Z axis ($\theta = 90^\circ$). The possible transition fields for allowed fine structure transitions are also shown for common X-band ($\sim$9 GHz), K-band ($\sim$23 GHz) and Q-band ($\sim$35 GHz) frequencies and are marked by X1 through X5 for X-band, by K1 through K5 for

K-band and by Q1 through Q5 for Q-band frequencies. The transition diagram ($\frac{h\nu_{MM'}}{|D|}$ - $\frac{H}{|D|}$ curves where $h\nu_{MM'} = |E_M - E_{M'}|$. are the matching microwave quanta) are shown in Fig. IV.7 for $\theta = 0^\circ$ and $\theta = 90^\circ$. In ordinary EPR experiments frequency of the microwave quanta is generally kept fixed and the intensity of the magnetic field is varied. So for the field swept EPR the transition-diagram provides the resonance fields, which may be obtained as the crossing points of a horizontal line $h\nu/|D| =$ constant, (appropriate to the fixed frequency of the microwave) with the curves of Fig. IV.6. Such transition-fields appropriate to the X-band, K-band and Q-band frequencies are also marked in the transition-diagrams (Fig. IV.6).

(iii) Ion-Vacancy Model

When Mn^{2+} substitutes for NH_4^+ lattice, a number of cation sites are available for creation of cation vacancy to maintain charge neutrality. As the concentration of Mn^{2+} ions is expected to be much greater than the equilibrium concentration of the intrinsic lattice defects at any temperature, one can assume equal number of Mn^{2+} ions and cation vacancies[15]. Because of the long range nature of the Coulombic interaction, one would expect an infinite number of possible Mn^{2+} - cation vacancy pair complexes (magnetic centres). We shall refer to the ion-vacancy complexes as M-V centres hereafter. Because of the screening arising from the polarization of the ionic atmosphere in the vicinity of a given charge, the effective interaction between Mn^{2+} and cation vacancy is, in reality, limited. Therefore a central charge (Mn^{2+}

will effectively interact only with a finite number of cation vacancy neighbours and only a limited number of M-V centres would be expected, which are favoured energetically also.

Based on the symmetry considerations various centres may be grouped according to their symmetry and their EPR spectra. There may be magnetically equivalent but differently oriented centres, while on the other hand there may be centres with the same orientation but magnetically inequivalent. The magnetically equivalent centres will have the same symmetry, will give identical spectra and can be described by a spin-Hamiltonian with the same parameters.

The observed tetragonal symmetry of the EPR spectra of Mn^{2+} in NH_4I, with its axis along [100] or equivalent directions is consistent with the following models for the M-V centres:

(I) Mn^{2+} substitutes for NH_4^+ and gets associated with a vacancy at the possible sites along [100], [010] and [001] directions. We will designate the complexes as M-V(200), M-V(400), etc. where the numbers in the parenthesis indicate the site of the vacancy with Mn^{2+} at the origin (Fig. IV.8). This is what has been the case for Mn^{2+} in various alkali halides with NaCl structure[16-19].

(II) Mn^{2+} substitutes for NH_4^+ while two iodines on either side of it (i.e. 5 and 6 in the MnI_6 octahedra shown in Fig. IV.8) along a cubic axis are substituted by OH^-. This results in an axial field with axis along the line joining the two OH^- ions i.e. along one of the crystallographic axes [100] or [010] or [001]. Such a model has been proposed for Mn^{2+} in NaCl[17]. Alternatively Mn^{2+}

substitutes for NH_4^+ while two iodines along two perpendicular axes, say [100] and [010], are replaced by OH^- ions. This will also result in an axial crystal field with axis along [001]. Such a model has been proposed for Mn^{2+} in LiF[20-22] and Mn^{2+} in NaF.[20,21] The overall charge compensation in both these cases may be achieved by having the vacancy away from the metal-ion.

Both the above models permit the existence of three axially symmetric magnetic centres which are magnetically equivalent but have different sets of axes. All equivalent distortions from normal cubic environment will occur with equal probability. Therefore one third of the total magnetic centres will have their tetragonal axes along [100], other one third along [010] while the remaining one third along [001]. As within experimental errors it was found that $g_{xx} = g_{yy} = g_\perp$, the X and Y axes are equivalent and thus indistinguishable. That is why, we have referred to the immobile (90°) spectrum as X-Y spectrum (being due to the centres for which magnetic field is oriented in their XY magnetic planes). The reason why we have referred to the angular dependent spectra-II and III as (X/Y)-Z is also now clear. These two spectra belong to the centres for which X and Y are indistinguishable and $\vec{H}$ rotates in their X-Z or Y-Z planes. When the magnetic field is rotated in (001) plane it rotates in the X-Y plane of one third of the centres while in the (X/Y)-Z plane of the remaining two thirds. Because of the equivalence of the X and Y axes the X-Y spectrum will obviously be immobile when $\vec{H}$ rotates in (001) or equivalent planes. When the magnetic field $\vec{H}$ coincides with [100] or [010] then the Z-axes of one third of the total centres become parallel to it

while the remaining two thirds of the centres will have their Z-axes perpendicular to H ($\theta=90^{\circ}$) i.e. their X/Y axes are parallel to $\vec{H}$. Therefore along this orientation of the magnetic field the (X-Y) spectrum becomes relatively more intense (theoretically twice that of (X/Y-Z) spectrum ($\theta=0^{\circ}$). Along [111] all these three types of centres will give identical, overlapping spectra resulting in a single spectrum. The observed symmetry of the over all spectrum in the (110) or equivalent planes is two fold, which is consistent with the above mentioned models.

(iv) Discussion

The observed unusually large value of D parameter clearly indicates that the axial distortion is very strong and warrants the presence of extra charge (required for charge neutrality) in the close proximity of the metal ion. In model (I) this would suggest a charge compensating vacancy at the next nearest neighbour cation site along an axis i.e. (M-V(200)) rather than at the far distant neighbours cation sites e.g. M-V400 etc.(Fig. IV.8). However, it has been found in the case of alkali halides that the centres associated with OH^- substitutional ligand impurity have large value of crystal field parameter D compared to its value for the centres associated with the pure ligand. This suggests the alternative model (II) for the centres. Because the crystals are grown from aqueous solution, the formation of $Mn(OH)_2$ is possible due to dissociation of H_2O molecules. In the most accepted model of the Mn^{2+} - vacancy centre in NH_4Cl and CsCl[6], the metal ion has H_2O molecules as ligand which makes the association

of OH^- with Mn^{2+} possible. The OH^- ligand seems to make large distortions in cubic environment possible. However, if OH^- is associated with the centres the spectrum should be affected by heat treatment of the crystals. Also it should be possible to confirm the association of OH^- impurity with the centres, by optical absorption spectra and other non-EPR studies[20-23]. The heat treated samples did not show any change in the intensity of the EPR spectra, and also the infrared spectra of the samples did not show the characteristic bands of water or OH^-. We therefore conclude that in the Mn^{2+} doped NH_4I single crystals the magnetic centre is M-V(200) i.e. metal ion substitutes for NH_4^+ cation

This also seems to be consistent with the fact that the RT structure of NH_4I is NaCl type[13,14] for which vacancy complex seems to be preferred in general[16-19].

Several mechanisms have been proposed in the past concerning the zero field splitting (ZFS) of the S-state ions[24-26]. Forman and van Wyk[6] have discussed for $NH_4Cl:Mn^{2+}$, various contributions to D and their signs. Zaripov and Chirkin[4] have estimated the sign and magnitude of D for different models and found that the point charge model estimates are in agreement with experimental values, if reasonable values of effective charges are assumed. However such calculations in $NaCl:Mn^{2+}$ for model (I) failed miserably[16] and were unable to give any agreement even in the orders of magnitude of D. The overlap and covalency effects seem to be dominant in this case giving large contributions to the zero field splitting. A list of some systems in which Mn^{2+} is subjected to very large zero field splitting[27-35] ($|D| \geq 1$ KG) is given in Table IV.

of OH^- with Mn^{2+} possible. The OH^- ligand seems to make large distortions in cubic environment possible. However, if OH^- is associated with the centres the spectrum should be affected by heat treatment of the crystals. Also it should be possible to confirm the association of OH^- impurity with the centres, by optical absorption spectra and other non-EPR studies[20-23]. The heat treated samples did not show any change in the intensity of the EPR spectra, and also the infrared spectra of the samples did not show the characteristic bands of water or OH^-. We therefore conclude that in the Mn^{2+} doped NH_4I single crystals the magnetic centre is M-V(200) i.e. metal ion substitutes for NH_4^+ cation

This also seems to be consistent with the fact that the RT structure of NH_4I is NaCl type[13,14] for which vacancy complex seems to be preferred in general[16-19].

Several mechanisms have been proposed in the past concerning the zero field splitting (ZFS) of the S-state ions[24-26]. Forman and van Wyk[6] have discussed for $NH_4Cl:Mn^{2+}$, various contributions to D and their signs. Zaripov and Chirkin[4] have estimated the sign and magnitude of D for different models and found that the point charge model estimates are in agreement with experimental values, if reasonable values of effective charges are assumed. However such calculations in $NaCl:Mn^{2+}$ for model (I) failed miserably[16] and were unable to give any agreement even in the orders of magnitude of D. The overlap and covalency effects seem to be dominant in this case giving large contributions to the zero field splitting. A list of some systems in which Mn^{2+} is subjected to very large zero field splitting[27-35] ($|D| \geq 1$ KG) is given in Table IV.

In the case of CsBr[29] crystal, Mn^{2+} is found to go substitutionally rather than interstitially in the lattice with cation vacancy at the next nearest neighbour cation site and does not involve any association with H_2O or (OH^-) as ligand. The reported D value in CsBr:Mn^{2+} case is equal to $\sim$4068 G, which is exceptionally large[29]. The value of D parameter in CsBr is larger by an order of magnitude than those in other alkali halides of NaCl-type structure. We can thus expect the observed large value of D in NH_4I:Mn^{2+} at RT with magnetic centre as M-V(200). Because of large discrepancies between values of D parameter calculated from point charge model and those observed experimentally, we will not attempt any such calculations in the present case.

The g values indicate that within the experimental errors, the g tensor is isotropic and has a value near to the free spin value (g_e = 2.0023), as is expected for an S-state ion. The hyperfine tensor is also almost isotropic. From the work of Van Wieringen[36] it is known that the magnitude of the hyperfine parameter A, depends on the amount of covalent bonding in the crystal. That is, the greater the covalent bonding, the smaller will be the hyperfine splitting. Matumura[37] has given a plot, where percent ionicity is plotted against the magnitude of A. Using the plot of Matumura we have estimated for Mn^{2+}:NH_4I, $\sim$ 95% ionicity or $\sim$5% covalent bonding. Covalent bonding is generally explained by the degree of overlap of the central paramagnetic ion-wave-functions with the wave functions of the ligand atoms. Depending on the strength of the covalent bonding, these ligands can be nearest neighbour atoms or even next nearest neighbour atoms.

The superhyperfine structure which may result from the interaction of the nonlocalized magnetic electrons of the metal ion (Mn^{2+}) with the nuclear spins of the ligands (I^- or OH^- or H^+) in our proposed models, if observed would have furnished some decisive information about the immediate surrounding of the central Mn^{2+} ion.

(v) Hyperfine Structure

The approximate techniques of calculating the EPR transition probabilities have been discussed in Chapter II, Section B. An excellent technique, the Bir-Lupei method[9,10,38] which has been found satisfactory to explain the observed angular behaviour of hf transitions (allowed and forbidden) in $NH_4Cl:Mn^{2+}$ system (which has almost the same SHP and same symmetry of the EPR spectra) has been applied in the present case of $Mn^{2+}:NH_4I$. The EPR spectrum of Mn^{2+} demonstrated a very peculiar aspect of the hyperfine structure angular dependence. There are many forbidden hyperfine transitions which are extremely anisotropic particularly in intensity. There are orientations where some of the normal transitions disappear completely and the forbidden hyperfine transitions are seen to be very strong in the same orientation. This unusual behaviour is certainly connected to the unusually large value of the fine structure parameter $b_2^o (= |D| \sim 1612$ G). A very powerful and simple tool for treating the intensity problem in the case of large fine structure parameter is the effective field method[39-41]. As discussed earlier in Chapter II, in this method the quantization axis of the nuclear spin is assumed to be determined by the

effective magnetic field at the nucleus created by the electrons. The hyperfine interaction is assumed as being equivalent to a Zeeman like interaction. The effective magnetic field is calculated by averaging the hyperfine interaction over the electron wave functions i.e. on eigenstates of the electronic Zeeman and fine structure terms in the Hamiltonian. Lupei et al[9,10] have evaluated the electronic eigenstates $|\phi_m\rangle$ by the perturbation theory, using strong field wave functions $|M_s\rangle$ as zeroth order functions and neglecting the fourth order fine structure parameters (b_4^m). The eigenfunctions of the system can be written as a product of pure 'electronic' eigenstates $|\phi_{M_s}\rangle$ and nuclear eigenstates $|m_I(M_s)\rangle$ which depend on M_s in the effective magnetic field, which, in its turn, depends on the quantum number M_s. The nuclear eigenstates $|m_I(M_s)\rangle$ and $|m_I'(M_s')\rangle$ determined by two effective fields, say, $\vec{H}^{M_s}$ and $\vec{H}^{M_s'}$ have the following linear relationship[39] :

$$|m_I(M_s)\rangle = \sum_{m_I'} d^{(I)}_{m_I m_I'}(w)\, |m'(M_s')\rangle \qquad .. \quad (IV.4)$$

where $d^{(I)}_{m_I m_I'}(w)$ is the matrix of the irreducible rotation group representation with weight I, and w is the rotation which converts the axis $\vec{H}^{M_s}$ to $\vec{H}^{M_s'}$. The intensity ratio of the various hyperfine transitions of the same fine group say $|M_s\rangle \leftrightarrow |M_s-1\rangle$ is given by:

$$\frac{I_{m_I \leftrightarrow m_I'}}{I_{m_I'' \leftrightarrow m_I'''}} = \frac{\left| d^{(I)}_{m_I m_I'}(w) \right|^2}{\left| d^{(I)}_{m_I'' m_I'''}(w) \right|^2} = \frac{P^{(I)}_{m_I m_I'}(\mathcal{M})}{P^{(I)}_{m_I'' m_I'''}(\mathcal{M})} \qquad .. \quad (IV.5)$$

where $\mu = \cos(\vec{H}^{M_s}, \vec{H}^{M'_s})$ and $P^{(I)}_{mm'}(\mu)$ are known functions[39] and have been given in Chapter II Section B. The angular dependence of $P^{(I)}_{m_I m'_I}(\mu)$ for $I = 5/2(Mn^{2+})$ is shown in Fig. II.5 of Chapter II. Since the most prominent anisotropy of intensity is observed in the central fine group $|\frac{1}{2}\rangle \longleftrightarrow |-\frac{1}{2}\rangle$, we will make use of the analytical expression for $\mu = (\cos(\vec{H}^{\frac{1}{2}}, \vec{H}^{-\frac{1}{2}})$ obtained by Lupei et al[9,10] and given below :

$$\mu = -\left[1 - 128T\left(\frac{H^2}{D^2}\right) + 7168T + 1088T\sin^4\theta + -T(3\cos^2\theta - 1)(608\sin^2\theta + 256) - 3072T\frac{(A^2 - B^2)}{K^2}\sin^2\theta\sin^2 2\theta\right] \quad \text{.. (IV.6)}$$

where $T = \frac{A^2B^2D^4}{K^4H^4}\sin^2 2\theta$; $K^2g^2 = A^2g_{||}^2\cos^2\theta + B^2g_{\perp}\sin^2\theta$

and $g^2 = g_{||}^2\cos^2\theta + g_{\perp}^2\sin^2\theta$.

where θ is the angle between Z-axis and static magnetic field $\vec{H}$ in the X-Z plane. Due to very large coefficients in front of each angular function in Equation (IV.6), has a strong dependence on θ. Besides, the functions $P^{(5/2)}_{mm'}(\mu)$ also have a strong dependence on μ. The intensity ratio of the various members of the central fine group thus becomes :

$$\frac{I_{m \leftrightarrow m'}}{I_{m'' \leftrightarrow m'''}} = \frac{\left| P^{(5/2)}_{mm'}(\mu) \right|^2}{\left| P^{(5/2)}_{m''m'''}(\mu) \right|^2} \qquad \ldots \text{(IV.7)}$$

and depends on the orientation through μ. Thus Equation (IV.7) can be used to check the validity of the theoretical expression for μ.

Fig. IV.3 and Fig. IV.4 show the angular behaviour of hyperfine components of the central group over the range of orientations $\theta = 0$ to $\theta = 20^{\circ}$. Due to superposition of the central fine group with other fine structure groups it was not possible to follow the spectra for the whole range of orientations and the observations have been limited only to the range of $\theta = 0^{\circ}$ to $\theta = 20^{\circ}$. We have compared theoretical value of μ with experimental value obtained by comparing the intensities of the different transitions with relations (IV.7) for different m_I'. In Table IV.5 some of the observed and computed values of μ are given. Mialhe[38] has compared the adequacy of the various approximate methods and their range of applicability which depends on the values of the crystal field splitting. He has found that for large fine structure parameter (D= -1605 G) for $NH_4Cl:Mn^{2+}$ the two approximate methods viz. the method of Bir-Lupei and the method of intensity operator give satisfactory explanation of the angular behaviour of line intensities. These methods have already been discussed in Chapter II Section B. We have computed the intensities for some transitions of the central fine group :

($m_I = m_I' = -\frac{1}{2}$; $m_I = m_I' = -\frac{5}{2}$, allowed hf transitions; $\left|m_I = -\frac{3}{2}\right\rangle \longrightarrow \left|m_I' = -\frac{5}{2}\right\rangle$; $\left|m_I = +\frac{1}{2}\right\rangle \longrightarrow \left|m_I' = -\frac{1}{2}\right\rangle$ and $\left|m_I = +\frac{1}{2}\right\rangle \rightarrow \left|m_I' = -\frac{3}{2}\right\rangle$, forbidden hf transitions) using intensity operator method[38] and Bir-Lupei method. The comparison with the experimental intensities is shown in Fig. IV.9. All the measurements were made relative to the intensity of $m_I = m_I' = -\frac{1}{2}$ line at $\theta = 0^o$, assuming it to be unity. The good fitting of the experimental data with the computed data using Bir-Lupei method indicates that for large D-value with $|D|/H_o$ within 0.1 and 0.15. Bir-Lupei method is more precise.

IV.3 X-BAND STUDY

(i) Experimental

As has been discussed earlier Mn^{2+} is believed to substitute for NH_4^+ ion in the NH_4I crystal lattice. Each metal ion is in a strong axial field caused by a vacancy created at neighbouring host cation sites for the purpose of charge compensation. The metal ion is in an environment with a four fold symmetry due to the cubic structure (NaCl) of the NH_4I lattice at RT. In fact we carried out the X-band study at RT initially, and analysed the spectra using the spin-Hamiltonian (IV.2) and the method mentioned earlier in Chapter II Section B. At RT the parameters obtained through the experimental data at Q-band are much more accurate compared to those from X-band data. However, since the temperatur

variation of EPR spectra has been studied only at X-band the X-band parameters at RT have been retained as such.

The same crystals were used for both X-band and Q-band studies. The room temperature EPR study of single crystals at X-band revealed several unexpected features in the spectrum. The reason for these unexpected features, of course, lies in the unusually large value of the parameter D($\sim$ 1612 G), such that the microwave quantum at X-band frequencies ($\sim$ 9.1 GHz) is almost equal to one pair of zero field levels.

The crystal was mounted on the crystal holder of a goniometer (Varian model E-229) fitted to the rectangular resonant cavity (Varian model E-231) operating in TE_{102} mode. By fixing the crystal to the horizontal plane of the mounting rod with one of its faces ((001) planes), it was possible to rotate the crystal about the vertical axis [001] such that $\vec{H}$ is rotated in (001) plane of the crystal. Planes (001), (010), and (001) and directions [100], [010], and [001] are indistinguishable here . The EPR spectrum along an arbitrary orientation in these planes was found to be complex and unusual for Mn^{2+} ions which usually show five sextets. The spread of the spectrum was found to be maximum when $\vec{H}$ was oriented along [100] or [010] i.e. along one of the cube edges (Fig. IV.10). The spectrum spreads over the complete 10 KG scan for this orientation. When $\vec{H}$ deviates from this position on either side the spread of the spectrum starts decreasing. The directions [100] and equivalent are thus identified to be Z-axes of the magnetic centres responsible for

the EPR spectra. The spectrum repeats itself after an interval of 90^{o} in the (100) plane or equivalent planes.

The groups marked as D, E, F, G, H, I in Fig. IV.10, do not show any angular variation when $\vec{H}$ is rotated from [100] to [010] in (001) plane. We will retain the same designation i.e. X-Y-spectrum, as at Q-band, for these immobile groups viz. D through I. The remaining groups of lines marked as A, B, C in Fig. IV.10 show unexpected angular dependence. These groups plus the mobile groups emerging from X-Y-spectrum positions when $\vec{H}$ is off Z-axis will be designated as (X/Y)-Z spectrum just like at Q-band frequencies. Some of the unusual features of the X-band spectra are :

(a) X-Y spectrum comprise six groups out of which only four seems to be comprising usual six hf lines while others show unusual relative intensity, position and structure.

(b) The Z-component ($\vec{H} \parallel Z$; $\theta = 0^{o}$) of the (X/Y)-Z spectrum seems only to comprise three sextets unlike the five sextets characteristic of the Mn^{2+} ion EPR spectra.

(c) When $\vec{H}$ moves away from Z-axis all the fine structure groups on either side of central fine structure group should normally move towards the central group to reduce the spread of the spectrum. However, in this case the highest field group A moves towards lower field side, whereas the next highest field group shows an unusual behaviour. This group B comprises eleven unusually spaced peaks with unsystematic relative intensity (Fig. IV.11). The lower field members (B') of this group B move towards lower field side, while the higher field members (B") first move towards higher field side, attain a maximum in position around 12^{o} from

Z-axis, then turn back towards the lower field side (Fig. IV.12).

(d) The fine group C (the central group of the Z-spectrum) comprises many more component lines than the usual sextet, the components having unusual relative intensities and spacings. The lower field members of this group (C') move towards lower field side while the higher field side members C" move towards higher field side when $\vec{H}$ deviates from Z-axis. The angular behaviour of these groups is more or less the same as shown by the members of group B (Fig.IV.12).

(e) The centres of the groups B and C are quite far from $H_o + 2|D|$ and H_o respectively where $H_o = \frac{h\nu}{g\beta}$.

When $\vec{H}$ is parallel to Z-axis the X-Y spectrum (groups D through I) has intensity almost twice the intensity of the Z-spectrum (groups A, B and C). The group of lines 'I' of the X-Y spectrum, centered around 1 KG has very weak relative intensity and consists more than usual six lines. When the magnetic field is slightly off the Z-axis, two more groups viz. J and K start showing up with weak relative intensity. These groups comprise six lines each and are situated around field values 3.4 KG and 4.3 KG respectively (Fig. IV.12). The intensity of these groups increases on moving away from the Z-axis. The positions of these groups show slight angular variation in the range 0^o to 30^o from the Z-axis in the (001) plane. On going away from the Z-axis various groups of the spectrum overlap with each other and the spectrum becomes very so complex that it is not possible to follow the various groups of lines over a wide range of angular variation. At RT no saturation of the lines was observed with 200 mW maximum power of the microwaves. The lines of the usual sextet groups have

widths (ΔH_{p-p}) $\sim$ 10 G. The lines of the other groups have widths which range from $\sim$ 10 G to $\sim$ 20 G. Little effect of the Mn^{2+} concentration (0.01 to 0.5 molar percent) was observed on the line widths. In the (110) plane the over all symmetry of the EPR spectrum was found to be two fold. Along the [111] direction the spectrum becomes very weak in intensity and comprises a large number of lines with the overall spread of $\sim$ 5 KG.

The spectrum from polycrystalline (crushed fine powder) samples has also been recorded. The RT spectrum from a powder sample is shown in Fig. IV.13. The line widths of powder spectrum are comparatively larger than the lines of the spectrum due to single crystals. The powder spectrum consists of all the corresponding groups of the single crystal spectrum (Fig. IV.10), except the highest field group A and in addition contains some groups J, K and L. The groups corresponding to these are not present in Fig. IV.10 but can be seen in Fig. IV.12. All the crystals grown at RT and above upto 60°C and from different pH of mother liquor from acidic to basic solutions gave identical spectra at all temperatures.

(ii) Spin Hamiltonian Analysis

The spin-Hamiltonian (IV.2) with axial symmetry was used for the analysis of the EPR spectrum. The SHP were calculated using the method of fitting as discussed in Chapter II. Because the Z-spectrum was unusual, the centres of the groups of X-Y spectrum (usual sextets) were taken as the transition fields, since these could be located accurately even for orientations away from

Z-axis such that they had least overlap with (X-Y)-Z spectrum. The parameters thus obtained were used and refined to obtain $g_{||}$ through an iterative procedure to get least squared residual sum (LSRS) :

$$(\text{LSRS}) = \left[\sum_k \left(|E_j - E_{j+1}| - \frac{h\nu}{\beta}\right)_k^2\right]_{\text{minimum}} \quad .. \text{ (IV.8)}$$

where summation is over the transitions considered and E_j and E_{j+1} are the energy levels involved in the transition k. The energy levels E_j are calculated by exact numerical computer diagonalization of the spin-Hamiltonian matrix neglecting hyperfine and nuclear terms. In calculating (LSRS) globally all the accurately known k transition fields of both X-Y and (X/Y)-Z spectra were taken into account. The same procedure was carried out for the computation of parameters at all temperatures. The best fit parameters thus obtained from analysis of X-band spectra at RT are given in Table IV.1. The signs of the parameters are relative assuming D to be negative. The values of A and B were calculated from the observed hf structure using perturbation expressions upto third order in D and A, appropriate to large D, which are mentioned in Chapter II.

(iii) Discussion of Results of X-band Spectra at RT

The observed angular variation of the intensities and positions of the fine structure in (001) plane is consistent with the existence of three distinct types of magnetically equivalent, axially symmetric centres with their tetragonal axes along [100], [010], and [001] directions as has been suggested earlier on the

basis of Q-band study. Looking at the energy diagrams (Fig.VI.6) and probable resonance fields for X-band microwave quantum we find that some of the states involved in resonance transitions are nearly degenerate for example transitions X_2 and X_3. Similar situation has been reported[5,6] for the cases of $NH_4Cl:Mn^{2+}$ and $CsCl:Mn^{2+}$. The X-band spectra of Mn^{2+} in NH_4I resemble closely with those of Mn^{2+} in NH_4Cl and CsCl. Apart from unusually large zero field splitting (ZFS) parameter D many more features are common in EPR of all these systems. For example, these exhibit the same features caused by the near degeneracies of the states involved in some of the transitions. It can be seen from Fig. IV.6 that the transitions B and C of Fig. IV.10 correspond to X_3 and X_2 respectively and are between nearly degenerate levels i.e. where the levels cross. When $\vec{H}$ is slightly off the Z-axis (small non zero θ) mixing of the states takes place by the magnetic field[5]. The mixing of the upper two states involved in the transition results in two states containing appreciable contributions from the states admixed. As a result two transitions become allowed between the admixed upper states and lower pure state. This will be the case with transition marked as in Fig. IV.6. Similarly the mixing of two upper and two lower states involved in the transition marked X_2 will result in four allowed transitions when $\vec{H}$ is off the Z-axis.

It has been mentioned earlier that the transitions B and C (Fig. IV.10) when $\theta = 0^\circ$ do not comprise usual six lines with systematic spacings. The group B comprise eleven peaks with

unsystematic spacings between adjacent peaks and with unsystematic relative intensities. This feature can be explained by taking into account the mixing of near degenerate levels by the term $B(S_xI_x + S_yI_y)$ of the SH (IV.2). The mixing of nearly degenerate terms can not be adequately described by using perturbation method[5]. However the positions of the peaks may be calculated by solving the quadratic equation for the mixing of nearly degenerate levels, to which perturbation corrections may then be added[5]. In general there should be twelve peaks in group B and twenty four peaks in group C. But because of the fact that the states $\left|\frac{1}{2}, -\frac{5}{2}\right\rangle$ $\left|3/2, -5/2\right\rangle$, and $\left|-1/2, -5/2\right\rangle$ can not be mixed through the term $B(S_xI_x + S_yI_y)$ with their corresponding nearby degenerate state, these states remain normal (unmixed). This is the reason why only eleven peaks are present in group B (Fig. IV.11). The hyperfine peaks of groups B and E along with the computed peak positions of group B are shown in Fig. IV.11. The normal peak is marked as N in Fig. IV.10 and Fig. IV.11. The computed and experimental peak positions have also been tabulated in Table IV.7. The six hyperfine peaks of group E of the X-Y spectrum can be clearly seen on going off the Z-axis, and are also shown in Fig. IV.11. A similar explanation holds for the group C which comprises twenty two peaks all of which are not resolved at RT due to overlap with the peaks of group F of X-Y spectrum. The sign of product DA is found to be positive from calculation of the peak position of the normal peak N. A negative sign of DA would result in an appreciable shift of this peak 'N' towards the

higher field side ($\sim$460 G). The relatively weak group I is due to electronically forbidden transition between levels $|-3/2\rangle$ and $|+1/2\rangle$ (Fig. IV.14) which has become allowed by mixing of two nearby levels by the term $B(S_xI_x + S_yI_y)$.

The observed spectrum from polycrystalline (crushed fine powder) samples can be explained in terms of the stationary resonance fields[42-44] of Fig. IV.14. The transitions having smaller angular dependence are expected to be more intense compared to the transitions with greater angular dependence. The transitions with very strong angular dependence will be smeared out in the powder spectrum because of the random orientations of the magnetic centres in powder. One would, therefore, expect that the intense transitions of powder spectrum (Fig. IV.13) correspond to the strong transitions of Fig. IV.14b, because these transitions do not show strong angular dependence. The transitions H, G and F are relatively more intense compared to E which is weaker because of its larger angular dependence near $\theta = 90^{\circ}$. The peak corresponding to the strong angular dependent transition are all missing as expected, while the peaks corresponding to B and C are relatively weak in intensity because of their appreciably large angular dependence. The peaks corresponding to forbidden transition I can also be clearly seen in the powder spectrum because of its weak angular dependence around $\theta = 90^{\circ}$.

IV.4 POWDER SPECTRA

An interesting feature of the X-band powder spectrum is the presence of additional groups of peaks marked as J, K and L in Fig. IV.13. These groups do not have any transitions in energy diagram (Fig. IV.14) to be correlated with. From energy diagram it is clear that the transition $|3/2\rangle \leftrightarrow |1/2\rangle$ is not possible at X-band frequencies when $\theta = 90^{\circ}$ because of the nonmatching energy separation. However, these levels approach each other as $\vec{H}$ is oriented off X/Y axis (i.e. $\theta \neq 90^{\circ}$) and at some angle this transition becomes possible as is evidenced by the presence of a group of peaks L in Fig. IV.12 when $\theta = 20^{\circ}$. We believe that group 'L' of powder spectrum belong to this transition. In Fig. IV.12 two more groups J and K appear when $\vec{H}$ is oriented off the Z-axis. These groups are weak in intensity but show scant angular dependence in the range $\theta = 0^{\circ}$ to $\theta = 30^{\circ}$ from Z-axis. We believe them to be the fine forbidden transitions which become allowed through the mixing of states when $\vec{H}$ is slightly off Z-axis as has been mentioned earlier. These two transitions correspond to the weak groups J and K of the powder spectrum in Fig. IV.13.

The presence of group of peaks 'D' at the lowest field (almost zero field transition) in all the spectra clearly indicates that the zero field splitting energy is being matched with the microwave quantum at X-band frequencies. This is also clear from the energy level diagrams of Fig. IV.14. Being an almost zero field transition it does not have appreciable angular dependence and consequently is present with quite large relative

intensity in the powder spectrum. Thus the observed features of the X-band spectra are found consistent with the model discussed earlier and all the salient features are explainable with the help of energy diagram obtained from the solution of energy matrix using the fitted parameters. A similar explanation is valid for the observed transitions in the powder spectrum at Q-band (Fig. IV.2). The groups G, H and I in Fig. IV.2 are relatively much more intense compared to other groups. These transitions can be explained in terms of the transitions shown in energy diagram (Fig. IV.6) for Q-band frequency. Because the transitions Q_1 , Q_2 , Q_3 , Q_4 , and Q_5 show large orientation dependence, therefore, transitions corresponding to them have almost vanished in the EPR spectrum of powdered sample. The strong transitions F, G, M, I and J correspond to the transitions Q_1' , Q_2' , Q_3' , Q_4' , and Q_5' shown in Fig. IV.6. The groups G, H, and I are very strong because of the small angular dependence of the corresponding transitions.

IV.5 TEMPERATURE VARIATION OF EPR SPECTRA (X-BAND STUDY)

(i) Experimental Results

It has been mentioned earlier in Chapter II Section D that NH_4I has two phase transitions around temperatures $T_1 \sim 231K$ and $T_2 \sim 257K$. Therefore the temperature variation of EPR spectra is expected to be interesting from the point of view of these phase transitions. The investigations were carried out at X-band frequencies in the temperature range 573K to 77K. The

parameters D, A, and B were obtained through computational method discussed earlier. The continuous gas flow cryostat mentioned earlier in Chapter III was used and the temperature dial was calibrated to better than 1K with the thermocouple placed in contact with the sample. Both single crystal as well as powder samples were studied in the above mentioned temperature range. The temperature variation study of line widths has also been carried out. The p-p line widths being $\sim$10 G to $\sim$20 G, their positions could be measured with an accuracy of$\sim$2 G.

As mentioned earlier the EPR spectrum is very well resolved along any one of the cubic axes, therefore most of the spectra at temperatures lower or higher than RT were taken along this orientation. As the temperature of the sample was lowered below RT, the line widths of the peaks of most of the groups increased. This trend of increase in the peak to peak line widths started $\sim$ 258K and was found to be most pronounced around 248K. Around this temperature most of the lines showed an almost discontinuous jump in broadening. Fig. IV.15 shows the behaviour of the line widths of representative lines from various groups of the EPR spectra along [100] i.e. Z-axis. It is noteworthy that the broadening trend is more pronounced in those lines which correspond the transitions between the states which are nearly degenerate e.g. transitions B and C in Fig. IV.14. Below 230K the lines again start showing a narrowing trend. The spectrum grew in intensity relative to RT intensity down to LNT. The line widths below 173K remained almost constant and in most of the

groups were of the order of 8 G. It is worth mentioning over here that the thermal process i.e. rate of cooling or heating affects drastically the results, at least in the temperature range 200K to 300K. For example, if one cools the sample at rates as fast as 15 K/hour or more the trend in line broadening was found to be flatter one and the discontinuities in broadening trend disappeared. Moreover a large thermal hysteresis was observed in the EPR spectra in a cooling and a heating cycle. The width of the thermal hysteresis was also found to be different for different rates of cooling and heating as well for repeated cycles. The faster was the rate of cooling and heating, the larger was the hysteresis. Repeated cycles also made the thermal hysteresis comparatively larger. A typical temperature variation of line width for both heating and cooling of the sample is shown in Fig. IV.15 which shows hysteresis. It may be mentioned here that to obtain a spectrum which did not change with time at a particular temperature below RT, it was found necessary to wait for a long time ($\sim$ 1/2 an hour at least in the temperature range from 253K to 223K) even after the set temperature got stabilized (which took less than 15 minutes in our case for a temperature change of $\sim$ 5K). The over all spread of the Z-axis spectrum increases on going down to LNT (Fig. IV.16). At LNT all the groups of lines showed some saturation with 200 mW microwave power. Some samples were also kept at LNT for long times (from 8 hours to one week). The spectra were recorded by heating samples slowly through the reported transition temperature

T_2 ($\sim$231K). In most of the cases no drastic changes were observed around T_2. Only in one such study where the sample was kept at LNT for one week and then the spectra were recorded by slowly heating up to 273K, an anomaly in intensity of the EPR spectra was observed. The changes were found reversible with that sample with considerable thermal hysteresis (Fig. IV.17).

The spectra from a polycrystalline sample were also recorded at low temperatures down to LNT and were found to show more or less similar trends in line widths and spread. The angular behaviour of the spectra at various temperatures down to LNT showed that the direction of Z-axis of the spectrum and the same tetragonal symmetry was preserved in the whole temperature range.

At temperatures higher than ambient one, the over all spread of the spectrum decreased and around 473K the fine structure got smeared out and an isotropic spectrum (sextet) superimposed on a single broad line was observed. This isotropic sextet showed many interesting features, for example, the line widths showed a m_I dependence. The isotropic spectrum (sextet) is characterized by the following parameter :

$$g = 2.0021(5); |A| = 84.5(5) \text{ Gauss}$$

Fig. IV.18 shows the conversion of anisotropic spectrum into an isotropic sextet. A sharp line ($\Delta H_{pp} \sim 5$ G) with g = 2.0033(1) can be seen to be present in all the spectra above this temperature. The broad line is $\sim$80 G (p-p) and has a g-value $\sim$ 2.004. When the sample was heated at temperatures higher than 500K some black material was expelled out from the crystal and it started

turning into powder at the outer surfaces. The change of axial spectrum into a cubic one $\sim$ 473K was found to be reversible if the sample was cooled down to RT. But heating of the sample at temperatures higher than 500K for $\sim$ 20 minutes turned the sample completely into a powder with some black material expelled out giving a single broad line and a sharp line. The black material though small in quantity was separated out and was found to give a sharp signal of width $\sim$ 5 G. The line width of this signal as well as the position (g = 2.0033(1) were found not to show any change with temperature within experimental errors.

The spectra from polycrystalline sample (fine powder) in the temperature range RT to 500K were found to show features similar to those mentioned above so far as spectral spread and line widths are concerned. In the case of powder sample the sample started turning its colour from white to brownish with some blackening of the inside surface of sample tube at a temperature above 500K. The intensity of the spectrum started diminishing and new signals around g $\sim$ 2.004 started showing up above 473K (Fig. IV.18). These signals grew at the expense of the normal powder spectrum. When the temperature was $\sim$ 480K a strong broad signal with a sextet superimposed on it was observed. The change was found to be reversible on cooling down the sample from 500K. However heating the sample above 500K resulted into an intense single broad line and the change was found to be

(ii) Discussion of Temperature Variation of EPR Spectra

(a) Low Temperature: The observed temperature variation of the parameters b_2^o(=D), A and B is shown in Fig. IV.19. The typical rate for cooling or heating is also mentioned. It can be seen that the hyperfine constants show little variation with temperature over the range indicated and no marked anomalies are observed around the two reported transition temperatures T_1 and T_2 shown by two vertical broken lines in the Fig. IV.19. However, the crystal field parameter b_2^o(=D) shows quite a large variation with temperature and also an anomaly around T_1 (NaCl $\leftrightarrow$CsCl) but no anomaly is observed in D around T_2 (CsCl $\leftrightarrow$ PH_4I) in cooling or heating cycle. The anomaly in the temperature dependence of D was found to be at 253K and 273K in a cooling and heating cycle respectively. Though the lattice parameters for Mn^2:NH_4I have not been measured, it may be assumed that the lattice parameter for both pure NH_4I and Mn^{2+}:NH_4I with low Mn^{2+} concentration will not be much different as was found to be the case with pure NH_4Cl and Cu^{2+}:NH_4Cl[45]. Hovi et al[46] have measured accurately the lattice parameters in all the three phases of NH_4I and have given polynomials for the temperature dependence of lattice parameters in all the three phases. The two phases II and III may be considered as one so far as the temperature variation of lattice parameters is concerned, because at the transition temperature T_2 (CsCl $\leftrightarrow$ PH_4I) the change in the lattice parameters is almost continuous as the distortion from cubic structure is very small. Around the transition temperature T_1 (NaCl $\leftrightarrow$ CsCl) the lattice

parameters show a discontinuous jump. Usually the D parameter is found to show an inverse cube dependence on lattice parameter in cubic crystals[4,7]. Because the other features of the EPR spectra of Mn^{2+} in NH_4I closely resemble with those of Mn^{2+} in NH_4Cl a similar dependence of D, on lattice parameter in $NH_4I:Mn^{2+}$ system is expected. As D is expected to be approximately proportional to the reciprocal of the cube of lattice parameter, consequently one would expect a discontinuous jump in D around T_1. Although there is an anomaly in D parameter around T_1 but no apparent discontinuity was observed. Moreover the anomaly was found over a considerable range of temperature rather than at a sharp temperature, as expected from the reported first order nature of the phase transition around T_1[14,47]. It may be noted that the cubic term b_4^o is almost negligible with respect to the axial term b_2^o(=D) and shows no measurable variation with temperature. The absolute sign of b_2^o could not be determined from the low temperature measurements since we could go only upto LNT.

The temperature dependence of line widths showed some anomaly around 253 K. These line width variations result from changes in relaxation times, which is probably brought about by the modulation of the crystal field interaction by the reorientational motion of the ammonium ions. Because of the complexities of relaxation calculations and difficulties in extraction of data from unresolved lines, it is not possible to get quantitative results, therefore only a qualitative discussion of line width is presented. The unresolved structure is expected due to SHF

interaction of the paramagnetic electrons with the ligand nuclei, and the lines are expected to be inhomogeneously broadened. The observation that the line width variations are larger for the transition where other fine energy levels are close to those involved in the transition, can be explained if the fine levels are coupled by a time dependent interaction. There are several ways that can be visualized in which the reorientational motion of the ammonium ions can cause time dependent distances of the nearest or next nearest neighbours of the metal ion. The time dependent distances of the neighbours may cause a time dependent crystal field which can then produce the required interaction. The time dependent part of the zero field interaction may be written as[8,48]:

$$\mathcal{H}(t) = \tfrac{1}{6}D_z^2(2S_z^2-S_x^2-S_y^2)+\tfrac{1}{2}D_{x^2-y^2}(S_x^2-S_y^2)+D_{xy}(S_xS_y+S_yS_x)+$$

$$+D_{yz}(S_yS_z+S_zS_y) = \sum_q D_q(t)S_q \qquad \text{..(IV.9)}$$

It can be shown that this interaction can induce transitions[8,49] between levels m_I and m'_I with transition probability :

$$P_{m_Im'_I} = \frac{1}{h^2}\sum_q \left|\langle m_I|S_q|m_I)\right|^2 \left\langle D_q^2(o)\right\rangle (2\tau_c/1+\tau_c^2w^2_{m_Im'_I}) \qquad \text{..(IV.10)}$$

where $\hbar w_{mm'} = (E_{m_I} - E_{m'_I})$ and τ_c is the correlation time associated with the fluctuations of the interaction. The maximum in the probability function occurs at $w_{m_Im'_I}\tau_c = 1$, its magnitude will be larger for smaller $(E_{m'} - E_m)$ when $w_{m_Im'_I}\tau_c \sim 1$, and will be

proportional τ_c when $w_{m_I m_I'} \tau_c \ll 1$. The condition $w_{m_I m_I'} \tau_c \sim 1$ will be fulfilled at temperatures ~235K for $(\omega_0/2\pi) = 9.5$ GHz, and subsequently $\tau_c = 1.67 \times 10^{-11}$S. For estimating this temperature the results of Niemela and Soini[50] for temperature dependence, of τ_c were used. It is noteworthy that almost all the lines selected for line width study in Fig. IV.15 showed some sort of maxima around 238K. The widths of the lines from group C (central group of Z-spectrum) showed the largest discontinuity around 248K. This transition (Fig. IV.14) occurs close to where two lower and two upper levels cross. The transition probability for any interaction coupling the levels which cross each other and which are coupled by electron spin operators should be relatively larger. The discontinuity in line widths may be attributed to the discontinuity in the relaxation time at the phase transition I <--> II (NaCl→CsCl)

The experimental observations reveal that the system NH_4I shows very strange behaviour so far as the phase transition is concerned. It has been discussed earlier in Section D of Chapter II that the transition temperatures based on results of various studies by different workers have been rather conflicting. Even the transition temperature reported by different workers has been quite different in many cases[50-55]. Dielectric study by Freymann[53] at 9.56 GHz showed that there is a jump in the dielectric constant at 239K in a cooling cycle and at 268K in a heating cycle. He attributed this anomaly, characterised by a jump in the dielectric constant, to the structural phase transformation in

NH_4I. It has also been reported that the crystals having colour centres have different transition temperatures compared to the pure crystals[54]. Morlin[55] has studied the kinetics of the low temperature phase transformations of NH_4I through specific electrical conductivity measurements of polycrystalline samples and according to his experiments the tetragonal modification (phase III) developed rather rarely and in most of the cases could not be observed even when the samples were kept at LNT for many hours. Hovi and Verteva[56] observed phase-I $\leftrightarrow$ phase-II transformation at different temperatures between 250K and 110K for four different particle sizes, using low temperature X-ray diffraction study and found that the observed super cooling increased with particle size of the samples. A large number of studies using optical, magnetic, relaxation and neutron scattering etc. methods have been undertaken in the past. Only some (for example, Goyal and Dasannacharya[57], Sharp and Pintar[58], and Couzi et al[59] have significantly taken care of the fact that a large hysteresis is observed for the trarsition phase-I $\leftrightarrow$ phase-II and the extent of supercooling, superheating and the exact nature of the structure at any temperature depends on the details of the thermal processing of the sample. Very recently Goyal and Dasannacharya[57] carried out neutron scattering experiments on NH_4I in the temperature range 213K - 300K. They have observed that both while cooling and heating, one finds phase (I) coexisting with low temperature phases II and III. They have very rightly pointed out that because of this hybrid nature of NH_4I crystal a great care is called for in interpreting the data of any study in this temperature range.

Our results of EPR study at low temperatures support the observation of Goyal and Dassannacharya[57] and Sharp and Pintar[58] where the two phases were found to coexist after the transformation I⟷II. The observation that sample had to be kept at a given temperature for very long times to obtain stable EPR spectra, supports the view of mixed phase, because the sample may require a comparatively longer time to stabilize in the mixed phase at a given temperature. Also the fact that the anomaly in parameter b_2^o and in line widths depends on the details of the thermal process (namely, rate of cooling or heating and number of repeated cycles, etc.) and are accompanied by large hysteresis, provides ample evidence in favour of the idea of mixed phase. The reason for a rather continuous anomaly in b_2^o seems to lie in the fact that the transformation I⟷II does not take place completely at the transition temperature and the process is rather sluggish. The absence of any marked changes around 231K, the most referred transition temperature T_2 (II⟷III), indicates that either this transformation does not take place at all or it is not reflected in the EPR spectra of Mn^{2+} since the transition involves a very small distortion in the structure. When the cooling rate is kept comparatively faster (>>10K per hour) phase I seems to get supercooled and thus the transformations I ⟶ II starts at a lower temperature, while reverse will be the case in a heating cycle. The structure of the mixed phase depends on the thermal processing is evidenced by the data typical of the processing particularly in the range 300 to 213K. Therefore we conclude on the basis of

results of EPR at temperatures below RT as supported by other studies[57,58] that in the system $NH_4I:Mn^{2+}$ the phase transformation I $\leftrightarrow$ II is not complete within a sharp temperature range. It occurs over a wide range of temperature and appears to be of mixed order due to the two coexisting phases. Within our experimental limitations we could not cool the samples at rates slower than those reported but we believe that there may be a certain rate of cooling to get a complete conversion of I $\rightarrow$ II within a sharp temperature range.

The spectrum along Z-axis at LNT (Fig. IV.16) shows that a large number of lines appear in groups B and C. The number of lines in B is found to be at least 28. This indicates the presence of two centres with Z-axis coinciding but having slightly different crystalline field which results in overlapping of the peaks from the two centres. As a result the group B will comprise (11 + 11) = 22 peaks due to -Z-spectrum and 6 peaks due to (X/Y) spectra, the total number being equal to 28 peaks. It was not possible to count accurately the number of peaks present. Some additional peaks (marked as a in Fig. IV.16) were observed near the highest field group also. These indicated the presence of some other centres with very low concentration. We have not attempted the analysis of these centres.

(b) High Temperature: The small line widths at higher temperatures which at temperatures above 373K become almost equal to the line widths at LNT indicates motional narrowing of the lines. The over all spread decreases due to the decrease in zero field

parameter D at higher temperatures. The conversion of axial spectrum into a cubic one around ~ 480K indicates that the ion is not bound with the vacancy and therefore the tetragonal distortion vansihes and the ion now experiences a cubic crystal field. On raising the temperature further the NH_4I lattice starts expelling the Mn^{2+} impurity, which on reaching the crystal surface forms some complex due to its oxidation, (most probably MnO), and turns the surfaces black. The black material scraped from the surfaces was found to give a narrow line and with g-valuue close to that of DPPH with almost constant line width in the temperature range LNT to 600K. Since DPPH, normally used as field marker at ~~temperatures~~ lower than ambient, is not stable above 373K, the black material expelled out from the NH_4I crystals could provide an alternative field marker in the temperature range LNT to 600K.

IV.6 ION VACANCY MODEL IN LIGHT OF TEMPERATURE VARIATION

The ion vacancy model M-V200 found consistent with angular behaviour of the EPR spectrum at RT (NaCl structure) preserves its symmetry even at lower temperatures where the lattice is believed to have CsCl arrangement. Therefore the position of the vacancy should be along the lines joining the central metal ion to the nearest cation sites. As there is a rearrangement of the nearest neighbours of cations and the coordination number changes from 6 to 8, the ion-vacancy pairs will also be rearranged in such a way that the symmetry of the crystalline field is preserved even after the rearrangement. Thus the possible ion-vacancy pair in the CsCl arrangement is Mn^{2+}

substituting at the body centred position in one cell while the cation vacancy is at any of the cation sites at the body centred position in the adjacent cells. Each NH_4^+ site has six nearest neighbour cation sites where a vacancy can be created for charge compensation. This model also allows the possibility of three types of magnetically equivalent centres but with different orientations. As no drastic changes have been observed in the EPR spectrum around the expected phase transformation (NaCl → CsCl) the nature of ion-vacancy pair seems to be the same in both the phases viz. I (NaCl) and II (CsCl) with a similar type of distortion in both the phases. This observation seems to indicate that in NH_4I the distortion of the crystalline field from cubic to tetragonal largely depends on the nature of ion-vacancy rather than on the coordination of the metal ion.

REFERENCES

1. I.H. Parker, J. Phys. C4, 2967 (1971).
2. H. Abe and H. Shirai, J. Phys. Soc. Japan. 15, 1711 (1960).
3. T.J. Seed, J. Chem. Phys. 41, 1486 (1964).
4. M.M. Zaripov and G.K. Chirkin, Soviet Phys. Solid State 7, 2391 (1966).
5. A. Forman and van Wyk, J. Chem. Phys. 44, 73 (1966).
6. A. Forman and van Wyk, Canad. J. Phys. 45, 3381 (1967).
7. J.A. Kennewell, J.R. Pilbrow and J.H. Price, Phys. Lett. A27, 228 (1968).
8. J.A. van Wyk, J. Mag. Reson. 18, 235 (1975).
9. A. Lupei, V. Lupei, A. Stefansscu and F. Domsa, Rev. Roum. Phys. 20, 59 (1975).
10. V. Lupei, A. Lupei and F. Domsa, J. Mag. Reson. 19, 337 (1975).
11. R. Bramley and S.J. Strach, Chem. Phys. Lett. 79, 183 (1981).
12. M.D. Sastry, Ph.D. Thesis, I.I.T. Kanpur, India (1967).
13. R.W.G. Wyckoff, 'Crystal Structures', Vol.1, Interscience (1968)
14. H.A. Levy and S.W.Peterson, J. Am. Chem. Soc. 75, 1536 (1953).
15. L.W. Barn and A.B. Lidiard, 'Physical Chemistry - An Advanced Treatise' Vol.10, Academic (1970) p.152.
16. G.D. Watkins, Phys. Rev. 113, 79 and 91 (1959).
17. K.N. Srivastava and P. Venkateswarlu, Proc. Ind. Acad. Sci. 63, 284 (1966); 67 (1969).
18. T. Iwasaki and H. Wakabayashi, J. Phys. Soc. Japan 40, 1359 (1976).
19. W.J. Veigele and W.H. Tantilla, J. Chem. Phys. 41, 274 (1964)
20. A. Bianchini, M. Martinelli, S. Santucci, P. Burge and C. Laj Phys. Letts. A29, 522 (1969).
21. C.G. Bousquet, A. Serra and M.G. Suore, J. Mag. Reson. 6, 117 (1972).

46. V. Hovi, K. Paavola and E. Nurmi, J. Ann. Acad. Sci. Fenn. A VI No. 328 (1969).

47. C.N.R. Rao and M. Natarajan, 'Crystal Structure Transformations in Binary Halides', a review, NSRDS, 41 (1972).

48. A. Carrington and G.R. Luckhurst, Mol. Phys. 8, 125 (1964).

49. C.P. Slichter, 'Principles of Magnetic Resonance', Harper and Row, New York (1963).

50. L. Niemela and E. Soini, Ann. Acad. Sci. Fenn. Sci. A No. 205 (1966).

51. P.W. Bridgemann, Proc. Am. Acad. Arts. Sci. 52, 89 (1916).

52. C.V. Simon Naturwiss. 38, 559 (1951).

53. R. Guillien, Compt. Rend. 208, 1561 (1939); R. Freymann, ibid. 234, 279 (1952).

54. K. Kamiyoshi, J. Chem. Phys. 24, 1265 (1956).

55. Z. Morlin, Acta. Phys. Acad. Sci. Hunga. 33, 377 (1973).

56. V. Hovi and M. Varteva, Phys. Kondens, Materie. 3, 305 (1965)

57. P.S. Goyal and B.A. Dassannacharya, J. Phys. C : Solid State Phys. 12, 209 (1979).

58. A.R. Sharp and M.M. Pintar, Chem. Phys. 15, 431 (1976); J. Chem. Phys. 75, 2652 (1981).

59. M. Couzi, J.B. Sokoloff and C.H. Perry, J. Chem. Phys. 58, 2965 (1973).

TABLE IV.1

SHP of Mn^{2+} Spectrum at RT (300K)

Parameter	From X-band Spectrum	From Q-band Spectrum
$g_{\|\|}$	2.0014(5)	2.00037(8)
$g_{\perp}$	2.0028(5)	2.00040(8)
$b_2^o(=D)$	-1611(2) G	-1612(1) G
b_4^o	6(2) G	3(1) G
$\|A\|$	90(1)	88.5(5) G
$\|B\|$	90(1)	89.5(5) G
Q	-	0.55(5) G

TABLE IV.2

Observed and calculated transition fields for allowed fine transitions at Q-band.

Transition	$\vec{H}$ parallel to Z axis ($\theta=0^\circ$)		$\vec{H}$ parallel to (X/Y) axis ($\theta=90^\circ$)	
$M_s \longleftrightarrow M'_s$	Observed (Gauss)	Calculated (Gauss)	Observed (Gauss)	Calculated (Gauss)
$\frac{5}{2} \longleftrightarrow \frac{3}{2}$	6061(1)	6060.5	15873(1)	15872.5
$\frac{3}{2} \longleftrightarrow \frac{1}{2}$	9260(1)	9259.3	13774(1)	13773.5
$\frac{1}{2} \longleftrightarrow -\frac{1}{2}$	12500(1)	12499.9	12104(1)	12103.8
$-\frac{1}{2} \longleftrightarrow -\frac{3}{2}$	15740(1)	15740.7	10722(1)	10721.0
$-\frac{3}{2} \longleftrightarrow -\frac{5}{2}$	18940(1)	18939.5	9550(1)	9551.7

TABLE IV.3

Observed and computed* transition fields for the hyperfine transitions ($\Delta m_I = 0$) of central fine structure groups C and H at Q-band.

m_I	Group C ($\theta = 0^o$)		Group H ($\theta = 90^o$)	
	Observed (Gauss)	Computed (Gauss)	Observed (Gauss)	Computed (Gauss)
+5/2	11904.0(5)	11904.52	12298.0(5)	12298.1
+3/2	11993.0(5)	11993.33	12386.0(5)	12386.2
+1/2	12082.0(5)	12082.15	12474.0(5)	12474.0
-1/2	12171.5(5)	12172.0	12562.5(5)	12562.8
-3/2	12261.5(5)	12262.25	12651.5(5)	12652.0
-5/2	12352.0(5)	12353.0	12741.0(5)	12742.0

*The transition fields were computed by diagonalization of complete SH matrix (36x36) on computer.

CsCl	1384 Gauss	6
CsBr	0.390 cm^{-1}	29
NH_4Cl	1605 Gauss 0.1498 cm^{-1}	9,10
$CdWO_4$	1430 Gauss	27
$Zn_2P_2O_7$	1298 Gauss	28
$Li_2O.4B_2O_3$	3.7 GHz	30
$Li_2O.4B_2O_2$	3.64 GHz	"
Lithium Borate glasses	4 GHz	"
$LiIO_3$	0.1308 cm^{-1}	32
*ACl_2	0.125 cm^{-1}	31
*BCl_2	0.140 cm^{-1}	"
*ABr_2	0.395 cm^{-1}	"
*BBr_2	0.395 cm^{-1}	"
*AI_2	0.975 cm^{-1}	"
*BI_2	0.975 cm^{-1}	"
*$MgTe_2$	0.860 cm^{-1}	35
ZnS_2	0.151 cm^{-1}	35

$Mn(Ph_3PO)_2Cl_2$	0.29 cm	"
$Mn(Ph_3AsO)_2Cl_2$	0.29 cm^{-1}	"
$(Ph_3PO)_2Br_2$	0.425 cm^{-1}	"
$(Ph_3AsO)_2Br_2$	0.425 cm^{-1}	"
$Mn(quin)_2Br_2$	0.485 cm^{-1}	"
$Mn(Ph_3PO)_2I_2$	0.81 cm^{-1}	"
$Mn(3\text{-Meisoquin})_2Br_2$	0.365 cm^{-1}	"
$(OPPh_3)_2ZnCl_2$	0.29 cm^{-1}	34
$(OPPh_3)_2ZnBr_2$	0.425 cm^{-1}	"
$(OPPh_3)_2ZnI_2$	0.81 cm^{-1}	"
$Mn(biet)_2Cl_2$	0.170 cm^{-1}	31
$Mn(biet)_2Br_2$	0.37 cm^{-1}	"
$Mn(biet)_2I_2$	0.68 cm^{-1}	"
Di-iodo tetrabis (pyrazole)	0.98 cm^{-1}	33
	0.16 to 0.87 cm^{-1}	

*Manganese complexes with heterocyclic ligands.

TABLE IV.5

Experimental and theoretical values of μ for several values of angle θ.

θ (degrees)	$\mu_{expt.}$	$\mu_{theo.}$
0	1.0	1.0
2	0.98	0.9889
4	0.95	0.9561
6	0.90	0.903
8	0.83	0.8332
10	0.74	0.7480
12	0.65	0.6534
14	0.55	0.5534
16	0.45	0.4531
18	0.35	0.3577
20	0.27	0.2723

TABLE IV.6

Observed and computed* transition fields of X-band EPR spectrum at RT.

Transition $M_s \leftrightarrow M'_s$	$\theta = 0^\circ$		$\theta = 90^\circ$	
	Observed (Gauss)	Computed (Gauss)	Observed (Gauss)	Computed (Gauss)
$-5/2 \leftrightarrow -3/2$	Not observed	Not possible	6671(2)	6672.49
$-3/2 \leftrightarrow -1/2$	Not observed	0.70	Not observed	Not possible
$-1/2 \leftrightarrow +1/2$	Not exactly known	3253.4	3000(2)	3001.3
$+1/2 \leftrightarrow +3/2$	Not exactly known	6506.22	1650(2)	1650.8
$+3/2 \leftrightarrow +5/2$	9675(2)	9675.01	1376(2)	1379.0

*The transition fields were calculated by exact numerical diagonalization of SH matrix (6x6) on a computer.

TABLE IV.7

Calculated and observed positions of 11 observed hyperfine peaks of group B (X-band spectrum $\theta = 0^{o}$).

Observed (Gauss)	Calculated (Gauss)
6055(2)	6065
6100(2)	6110
6174(2)	6179
6250(2)	6252
6275(2)	6285
6410(3)	6410
6410(3)	6419
6522(2)	6522
6618(2)	6618
6703(2)	6708
6765(2)	6765

TABLE IV.8

Values of parameter $|b_2^o|$ (=D) at several temperatures.

Temperature (K)	$\|b_2^o\|$ (Gauss)
473	1488
433	1525
393	1558
353	1583
300	1612
273	1620
233	1635
193	1645
163	1659
133	1668
93	1686
88	1690
77	1700

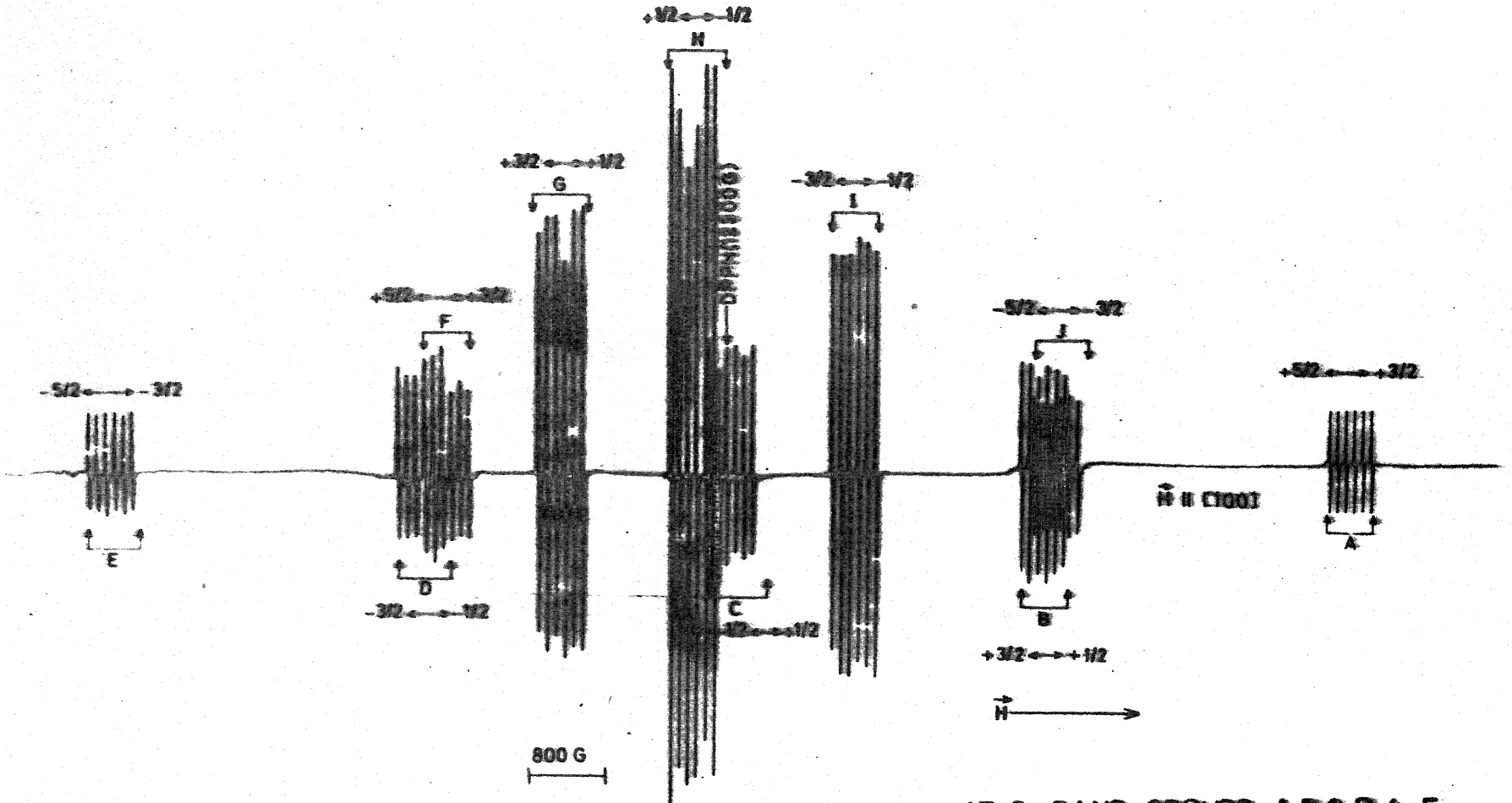

FIG. IV.1 : RT EPR SPECTRA OF Mn^{++} IN NH_4I SINGLE CRYSTAL AT Q-BAND GROUPS A,B,C,D & E BELONG (X/Y)-Z SPECTRUM(θ-0°) AND F,G,H & I TO X-Y-SPECTRUM(θ-90°)

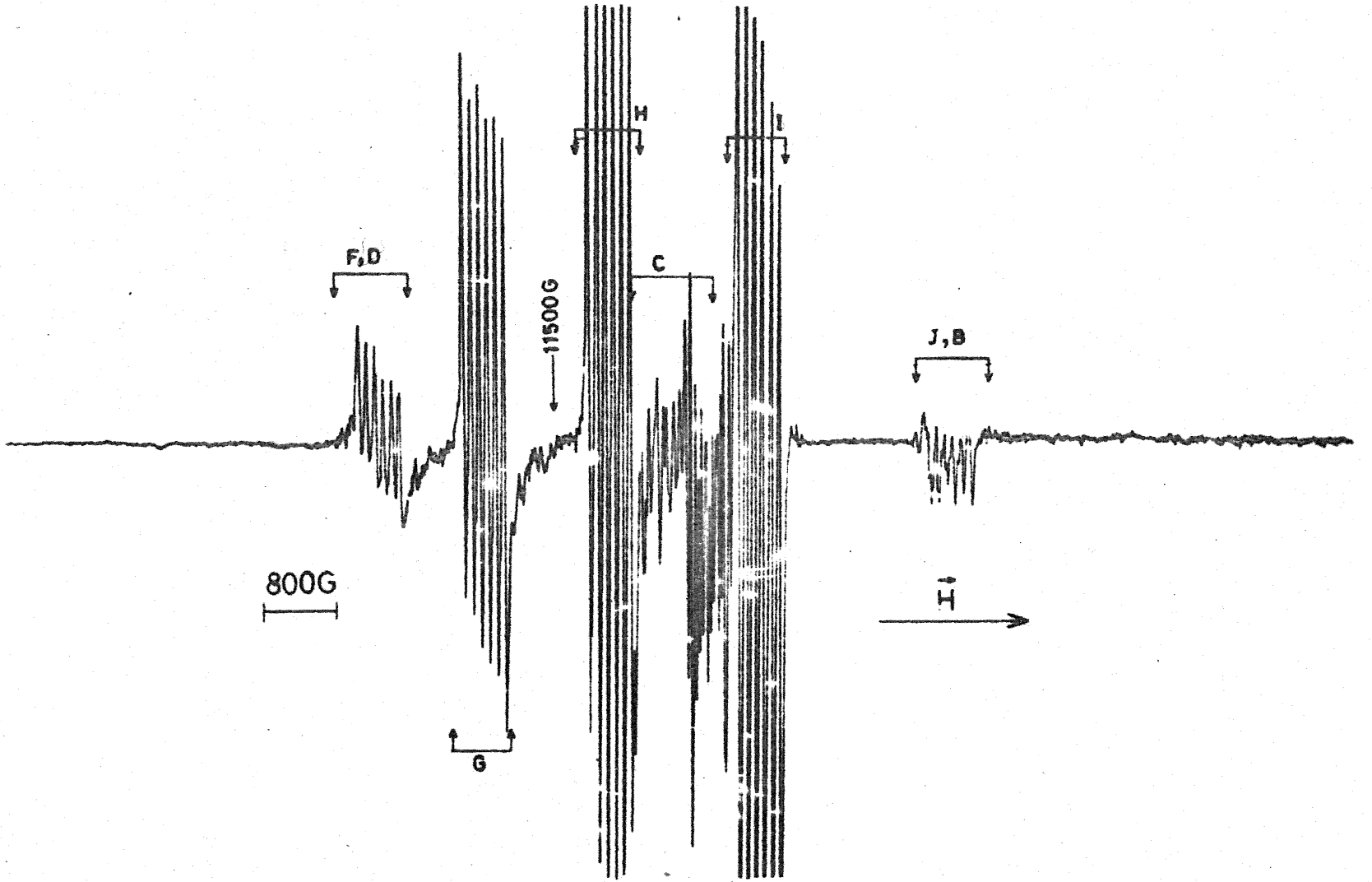

FIG. IV.2 : EPR SPECTRUM OF Mn^{++} IN POWDERED SAMPLE OF NH_4I AT Q-BAND AND RT.

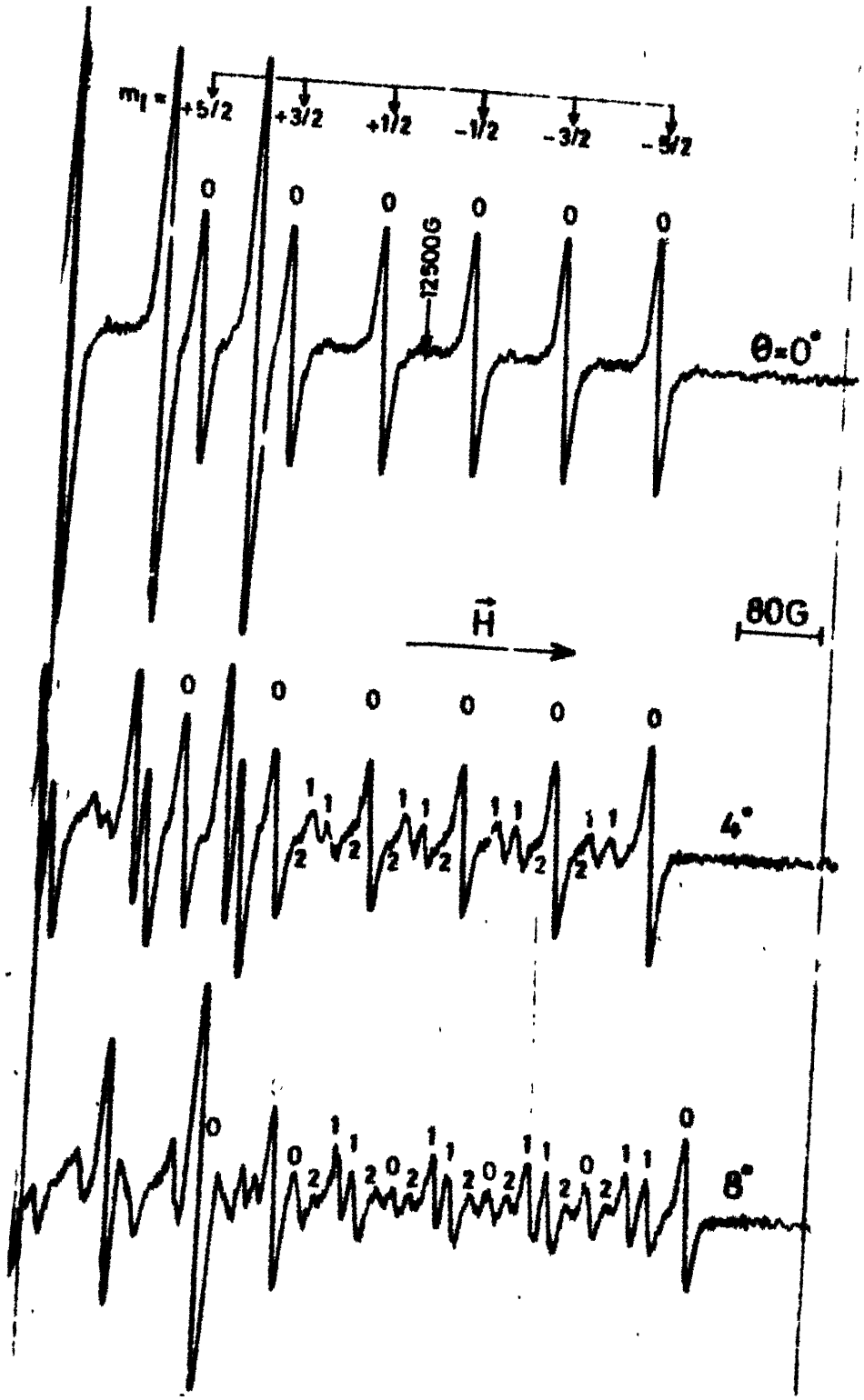
m_I =
+5/2
+3/2
+1/2
-1/2
-3/2
-5/2
12500G
θ=0°
$\vec{H}$
80G
4°
8°

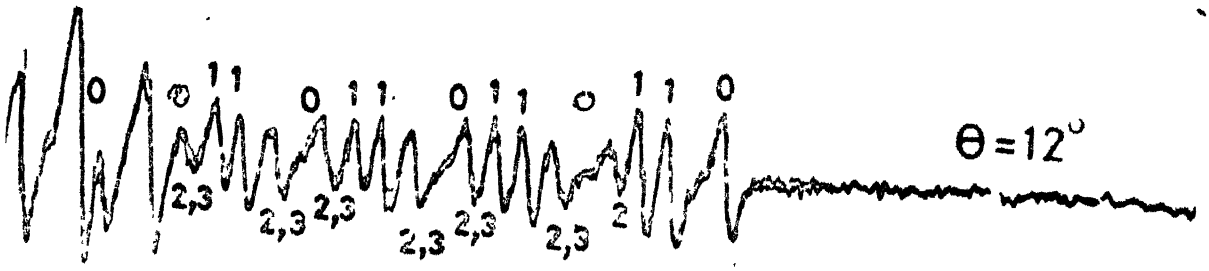

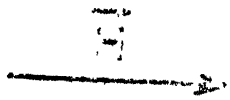

SOS

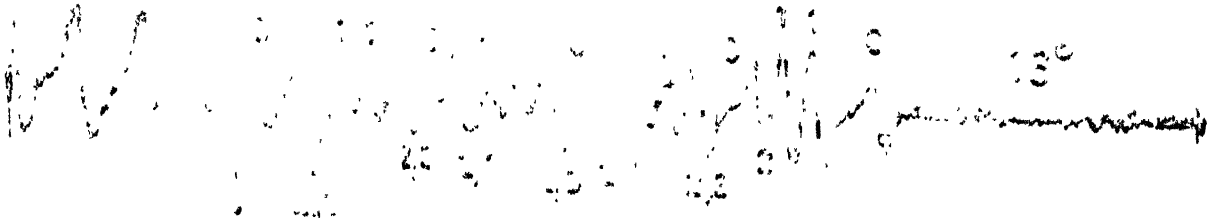

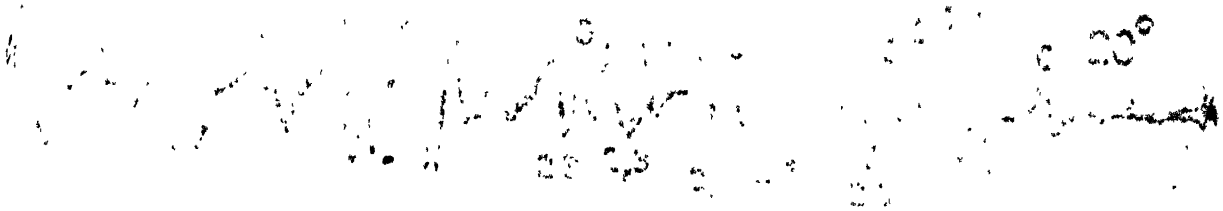

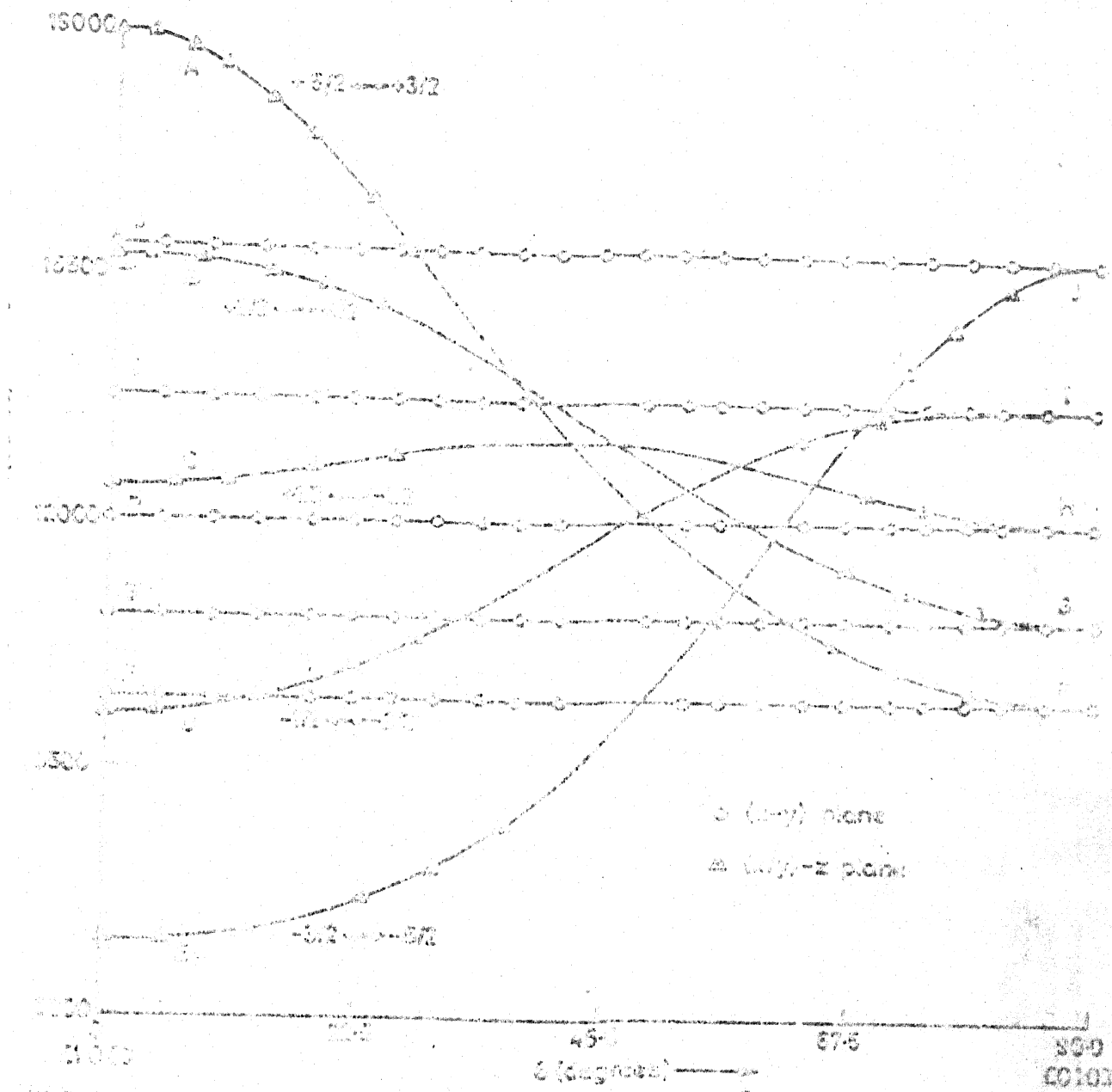

Angular variation of 3-band EPR spectrum of Mn^{2+} in Mn_2 single crystal in (001) plane at R.T. Solid lines are computed curves showing resonance fields and ○○Δ show experimental resonance fields for allowed fine transitions. Only one constituent of (xy)-z spectrum is shown in figure for clarity, the other constituent is only 30° out of phase.

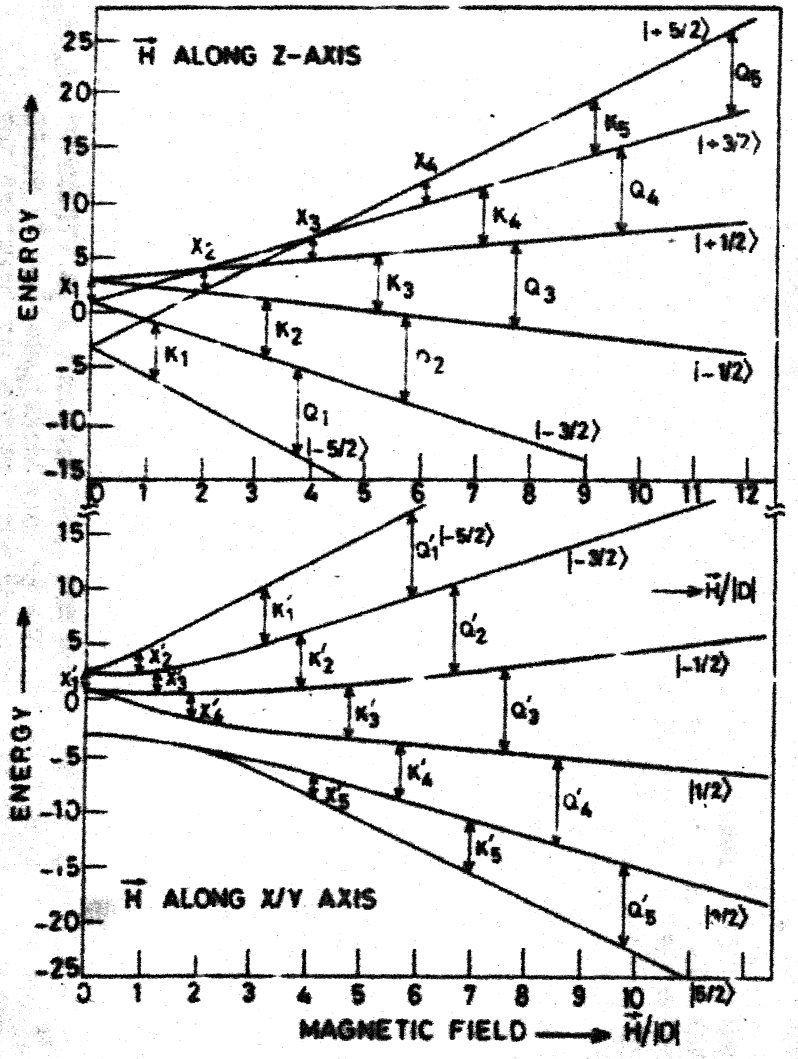

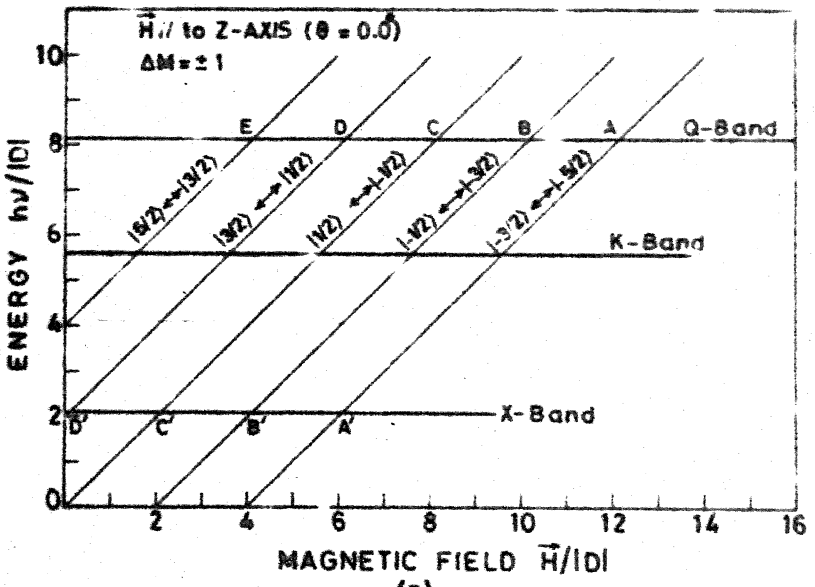

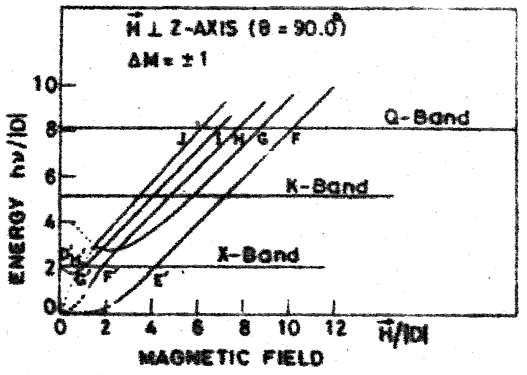

Fig. IV.6 ENERGY LEVEL DIAGRAMS FOR Mn^{2+}:NH_4I IN AN AXIAL CRYSTAL FIELD SHOWING ALLOWED TRANSITIONS AT X, K AND Q BAND FREQUENCIES.

Fig. IV.7 RESONANCE TRANSITION DIAGRAMS FOR Mn^{2+} IN NH_4I WITH AN AXIAL CRYSTAL FIELD (a) $\vec{H} \parallel Z$ (b) $\vec{H} \perp Z$

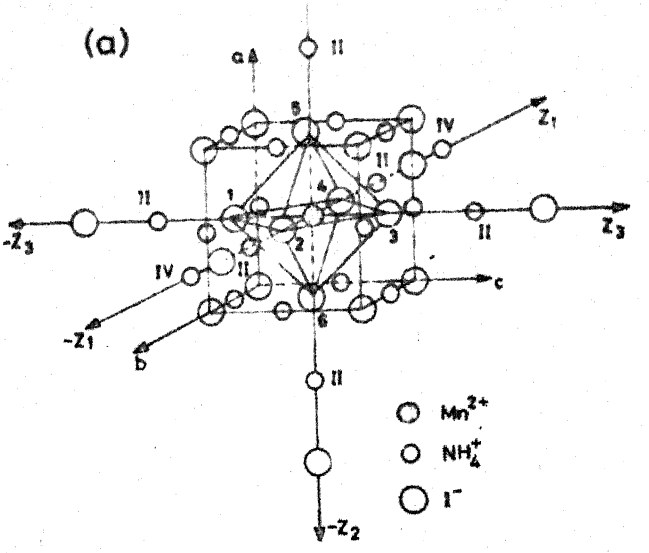

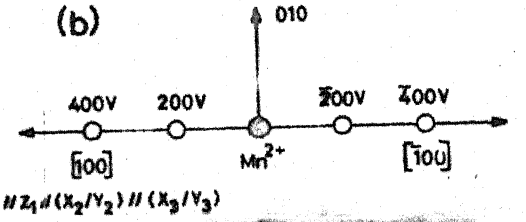

Fig. IV.8(a) THE ARRANGEMENT OF NH_4^+ AND I^- IONS IS SHOWN. THE NH_4^+ SITE AT $(\frac{1}{2}, \frac{1}{2}, 0)$ HAS BEEN SUBSTITUTED BY A DIPOSITIVE Mn^{2+} ION. ALL SIX SECOND-NEIGHBOUR CATIONS ARE MARKED II AND ONLY TWO OF THE SIX FOURTH-NEIGHBOUR CATIONS ARE SHOWN (MARKED IV) ALONG THE DIRECTION NAMED $-Z_1 Z_1$. THE IODINE OCTAHEDRON SURROUNDING THE Mn^{2+} ION IS SHOWN. Z_1, Z_2, Z_3 AND $-Z_1, -Z_2, -Z_3$ ARE THE POSSIBLE TETRAGONAL AXIS OF THE PARAMAGNETIC CENTRES. DIRECTIONS a, b and c ARE THE CUBE AXES.

(b) IT SHOWS THAT THE TWO Mn^{2+}-VACANCY PAIRS ARE MAGNETICALLY DEGENERATE (i) Mn^{2+} -200V & Mn^{2+} -200V (ii) Mn^{2+} -400V - Mn^{2+}-400V. DIRECTION [100] WHICH IS THE Z-AXIS FOR ONE POSSIBLE ION-VACANCY PAIR ALONG [010] & [010].

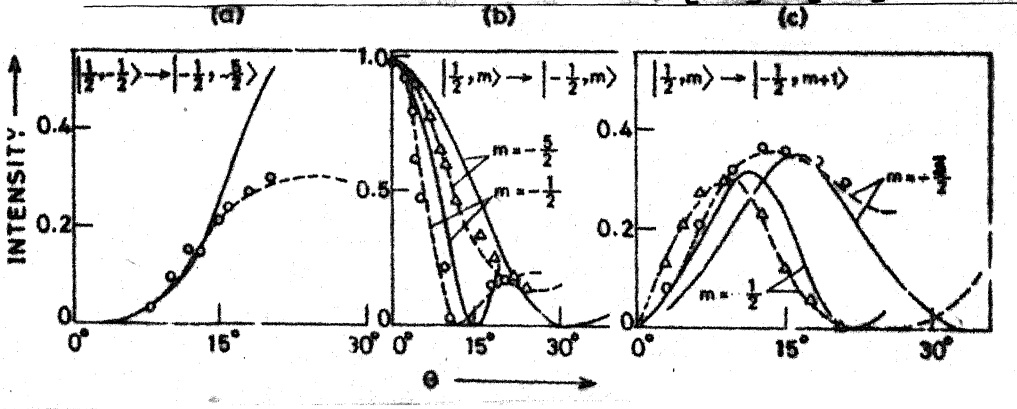

Fig. IV.9 INTENSITY AS A FUNCTION OF θ FOR HYPERFINE TRANSITIONS OF CENTRAL GROUP OF Mn^{2+}:NH_4I. VALUES OF m_I ARE SHOWN. CIRCLES AND DELTA ARE THE EXPERIMENTAL POINTS. THE RELATIVE INTENSITIES WERE MEASURED WITH RESPECT TO TRANSITION m_I=-1/2 → m_I=-1/2 AT θ=0. THE CURVES INDICATE CALCULATED VALUES. ——— INTENSITY OPERATOR. ------ BIR LUPEI METHOD.

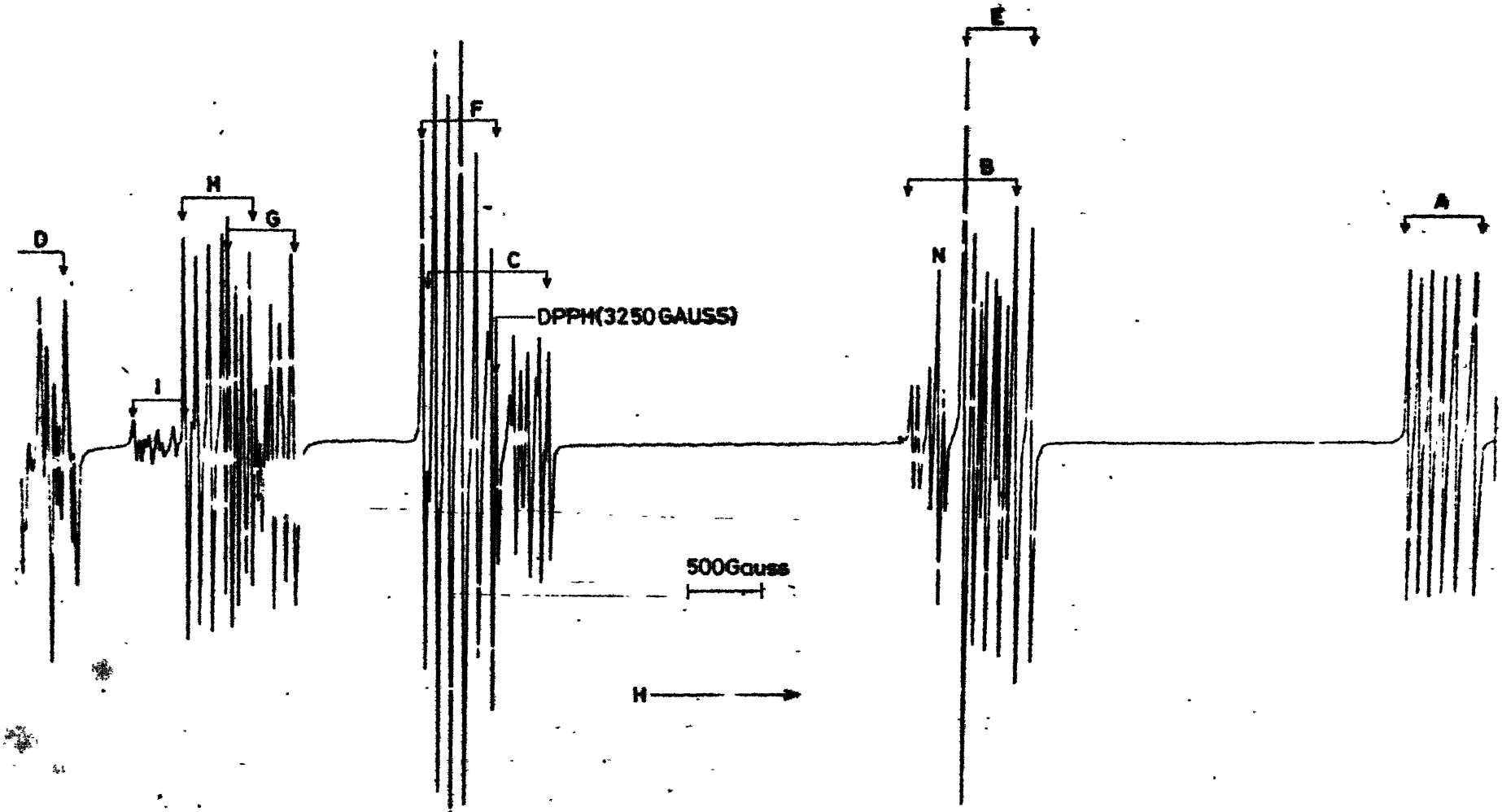

FIG.IV-9 EPR SPECTRUM OF Mn^{2+}:NH_4I AT RT WHEN H ∥ [100]. GROUPS A,B,C AND D BELONG TO θ=0° (XY-Z-SPECTRUM) AND GROUPS E,F,G,H AND D, TO θ=90° (XY-SPECTRUM). GROUP I IS THE FORBIDDEN TRANSITION OF θ=90°.

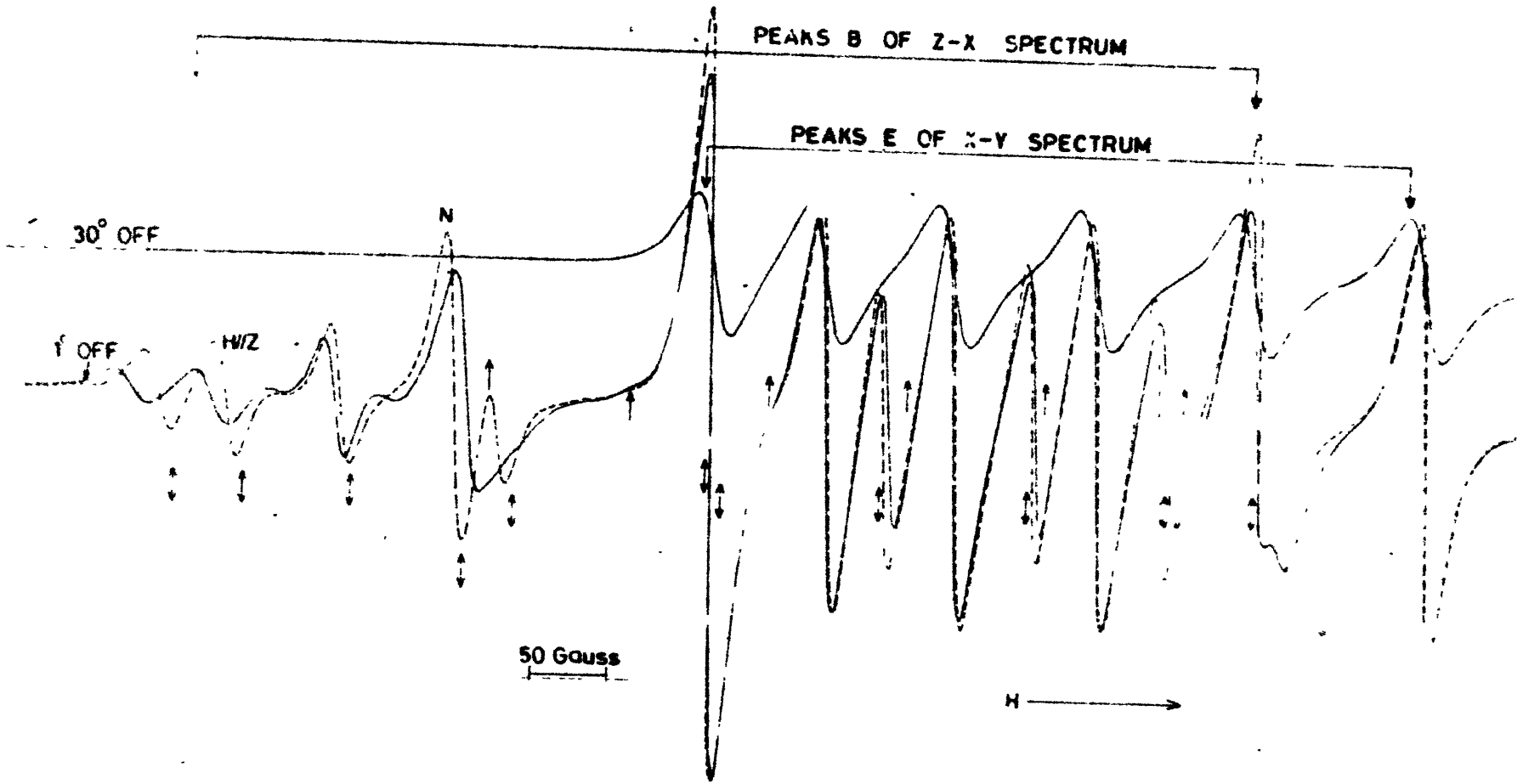

FIG.IV-11 EXPANDED RECORD OF FINE STRUCTUREGROUPS E AND B OF FIGIV-10 FOR THREE DIFFERENT ORIENTATIONS. THE LINE MARKED AS N IS THE NORMAL PEAK CORRESPONDING TO THE hf TRANSITION BETWEEN UNMIXED STATE $|3/2,-5/2\rangle$ AND $|1/2,-5/2\rangle$. THE POSITIONS MARKED BY SINGLE AND DOUBLE HEADED ARROWS ARE THE CALCULATED LINE POSITIONS OF hf GROUP B EXCLUDING AND INCLUDING THE TERM $(B\,S_x I_x + S_y I_y)$ RESPECTIVELY FOR $\vec{H} \parallel Z$.

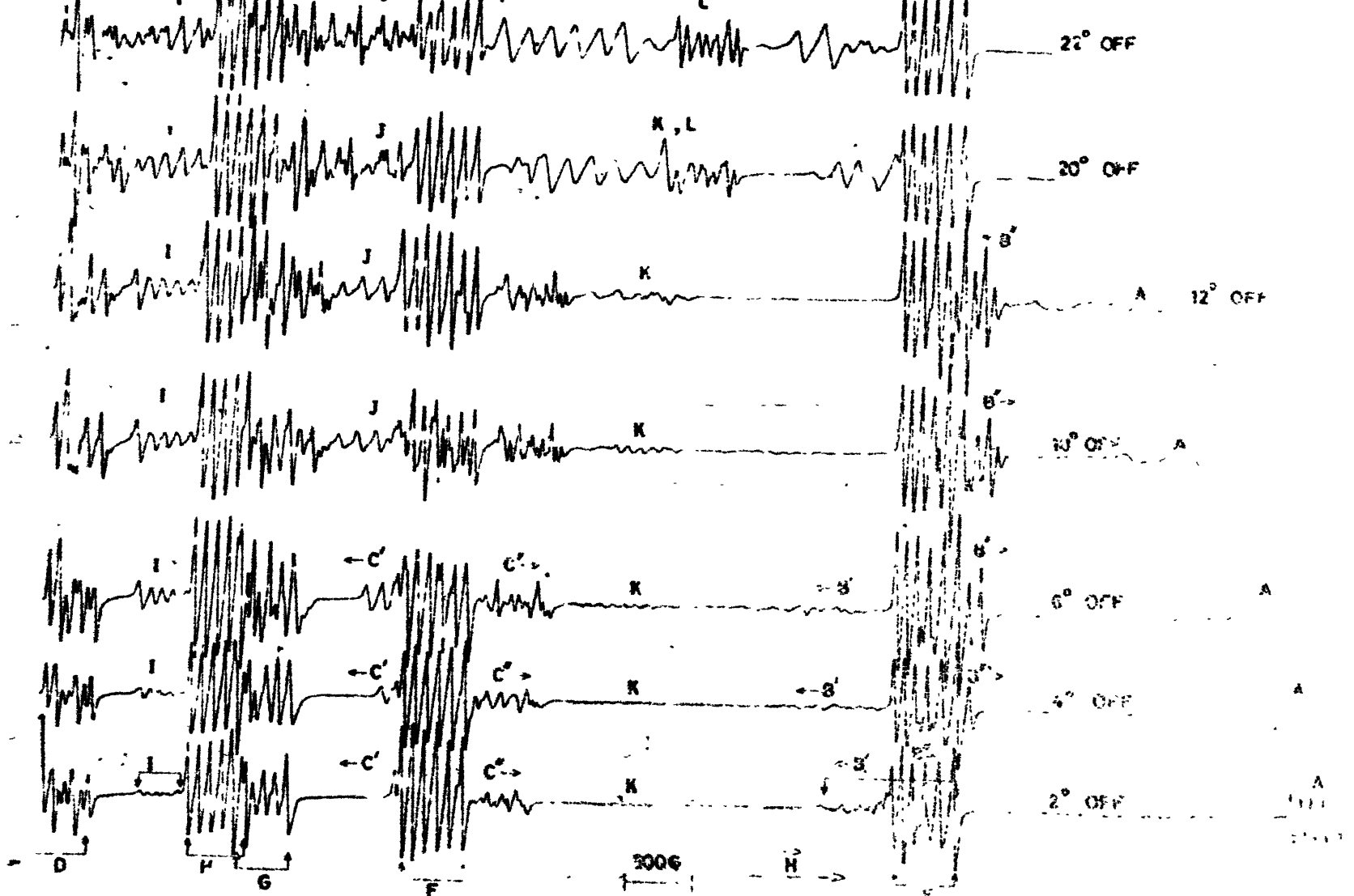

FIGURE 12 ANGULAR DEPENDENCE IN [001] PLANE OF [illegible]
GOING OFF θ=0° (I-AXIS) THE GROUPS [illegible]
ATTAIN MAXIMA IN POSITION AT θ=0°. THE [illegible]
J,K AND L ARE ALSO OBSERVED FOR θ OFF I-AXIS.

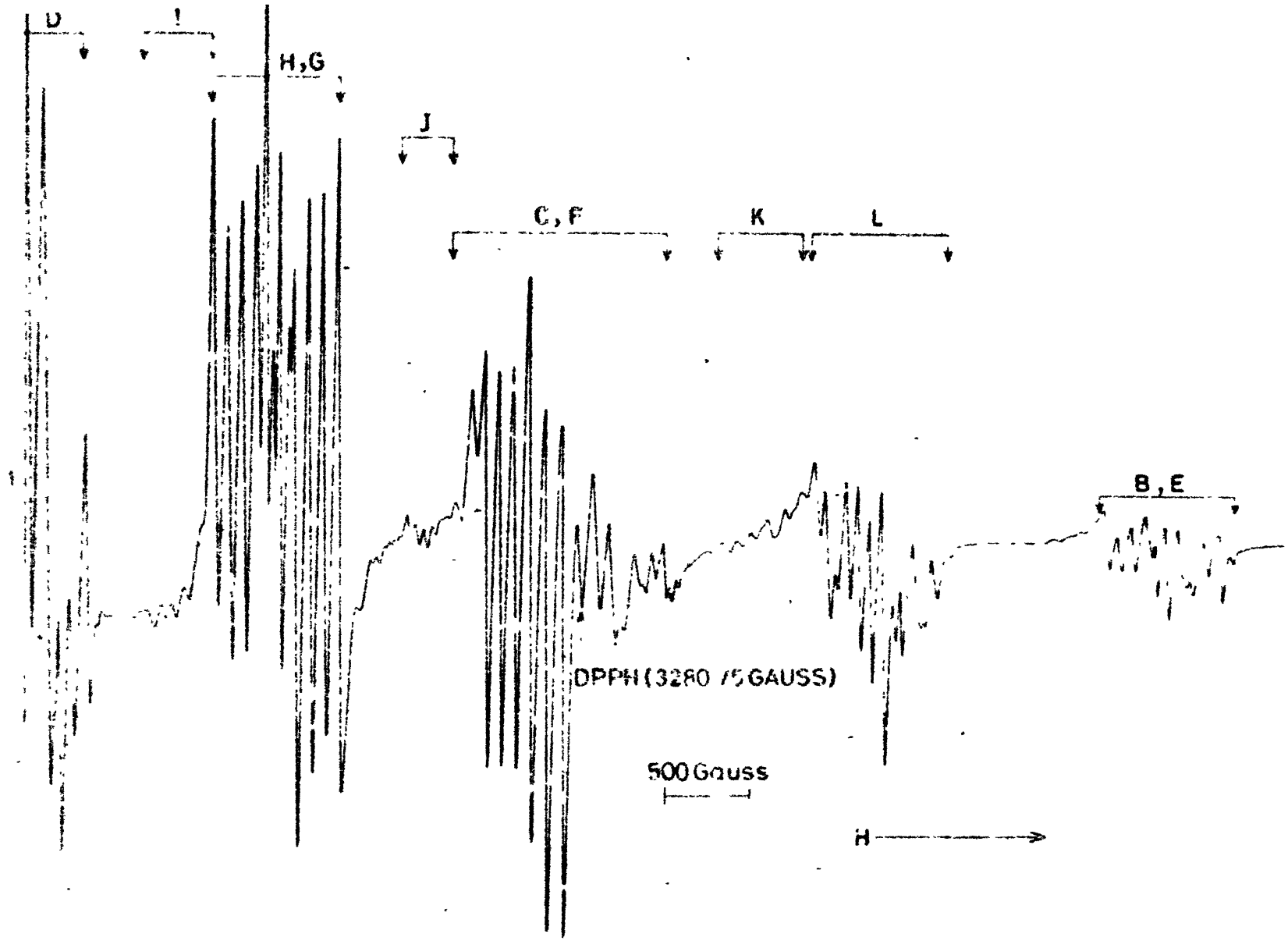

FIG. IV-13 THE EPR SPECTRUM OF A POWDERED SAMPLE OF Mn^{2+} DOPED NH_4I AT ROOM TEMPERATURE (~300K) AND AT X-BAND (9.3 GHz).

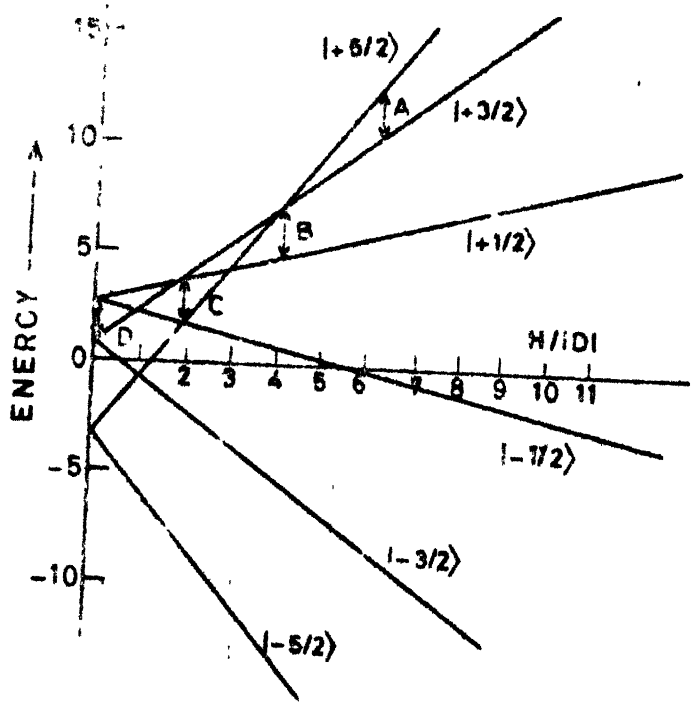

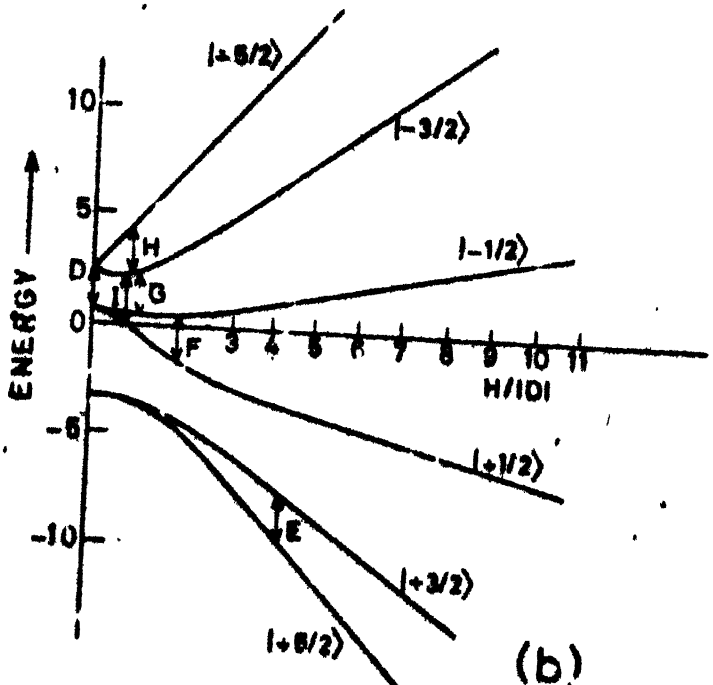

Fig. IV.14 ENERGY LEVEL DIAGRAMS AND OBSERVED FINE STRUCTURE TRANSITIONS AT X-BAND FOR Mn^{2+}:NH_4I (a) $\theta=0^\circ$ (b) $\theta=90^\circ$. CHOICE OF ZERO IN ENERGY IS ARBITRARY.

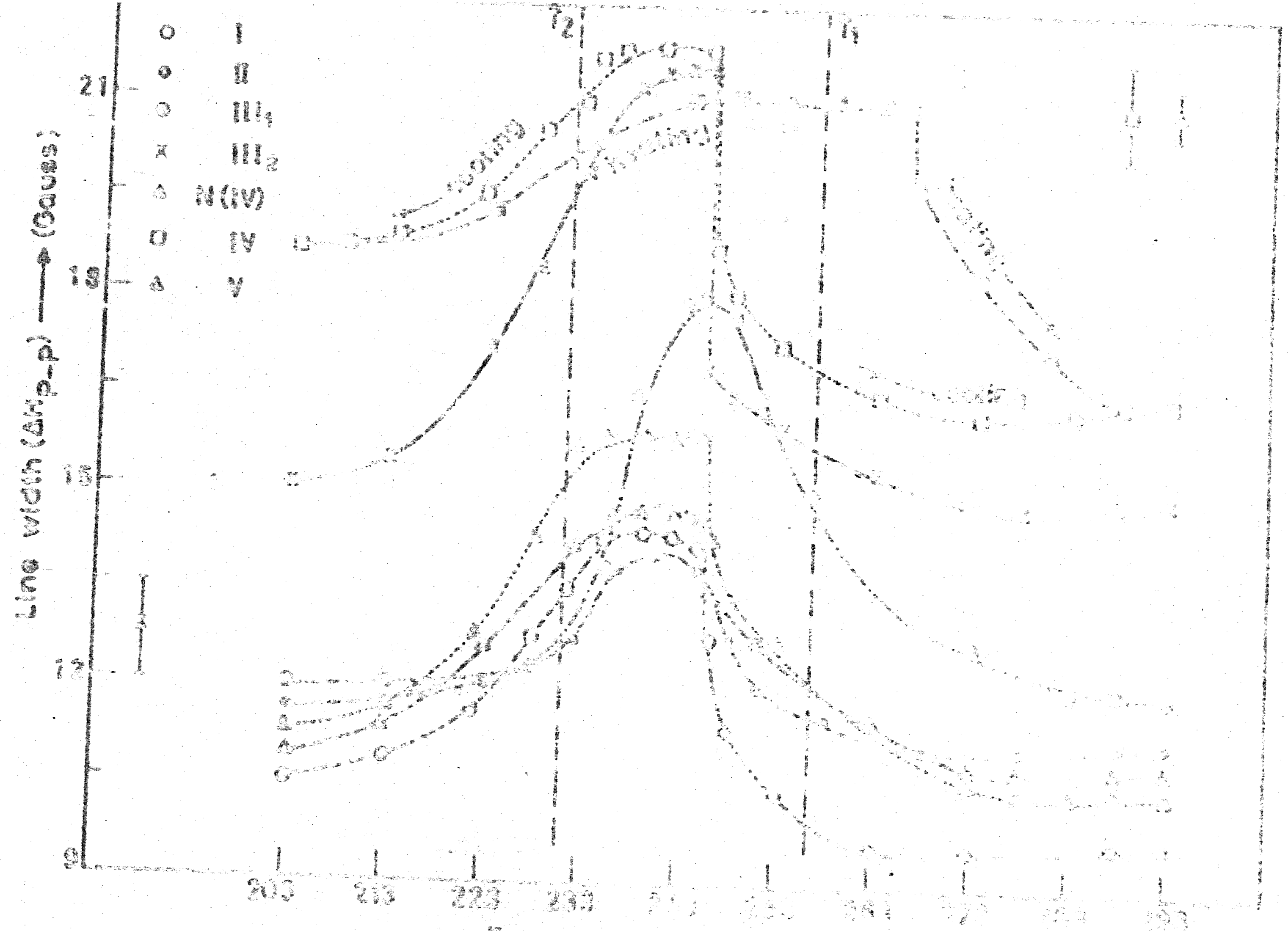

Fig. IV.15 TEMPERATURE DEPENDENCE OF LINE WIDTHS OF [illegible] HF TRANSITIONS AT X-BAND [illegible]. THE LINES SELECTED BELONGS TO DIFFERENT FINE GROUPS: I TO GROUP [illegible], II TO GROUP [illegible], III1 AND III2 [illegible] GROUP C, IV TO GROUP [illegible] AND V TO GROUP A OF FIG. [illegible] AND T2 THE TEMPERATURES AT WHICH PHASE TRANSITIONS OF [illegible] I ARE EXPECTED. A DISPERSION SHOWN BY LINE WIDTH IS ALSO DRAWN FOR ONE LINE.

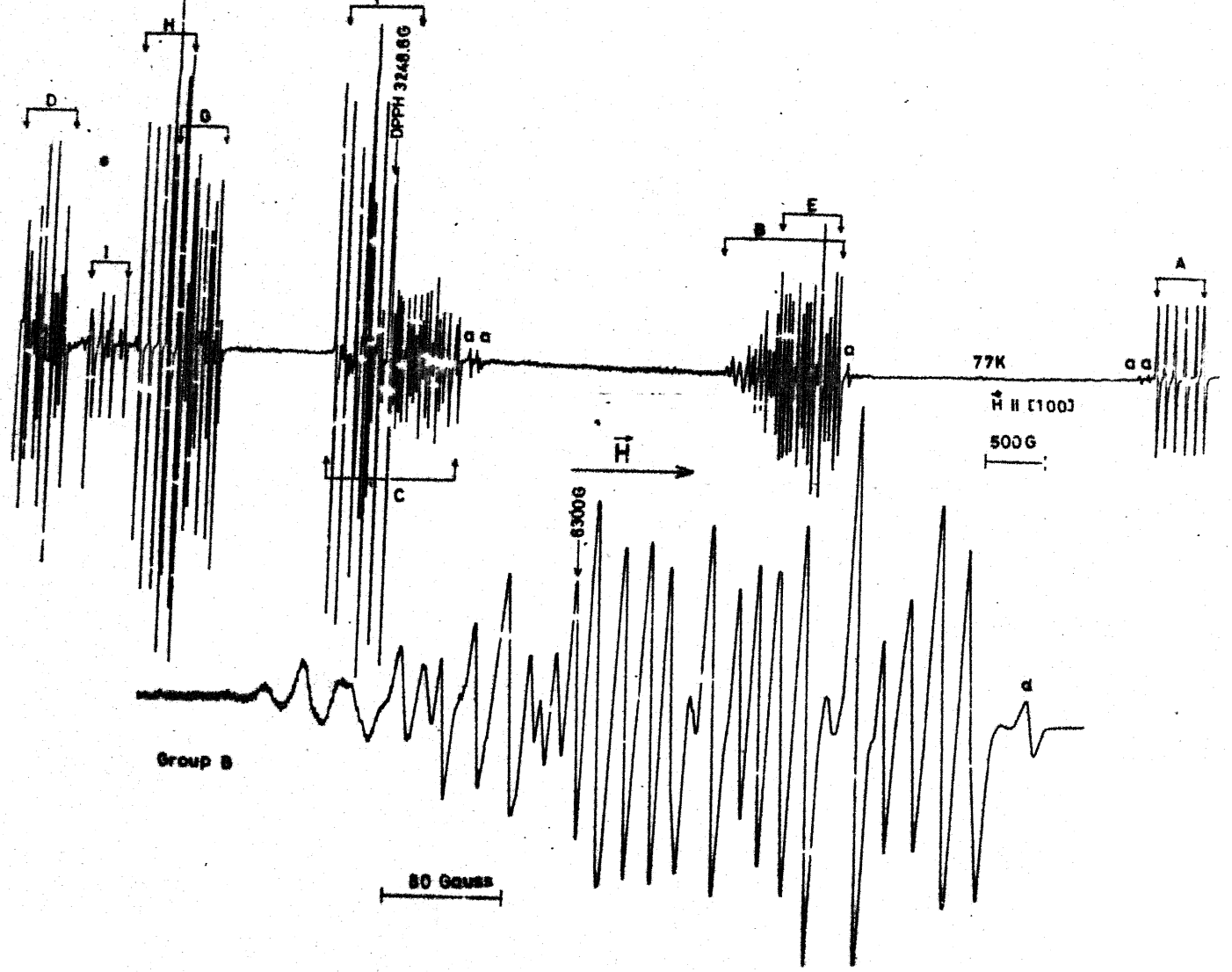

Fig. IV.16 X-BAND EPR SPECTRUM OF Fe^{3+} IN HgI_2 AT 77K. EXPANDED RECORD OF B IS SHOWN BELOW. PEAKS MARKED AS 'a' INDICATE THE PRESENCE OF A Fe^{3+} CENTRE WITH VERY WEAK RELATIVE INTENSITY.

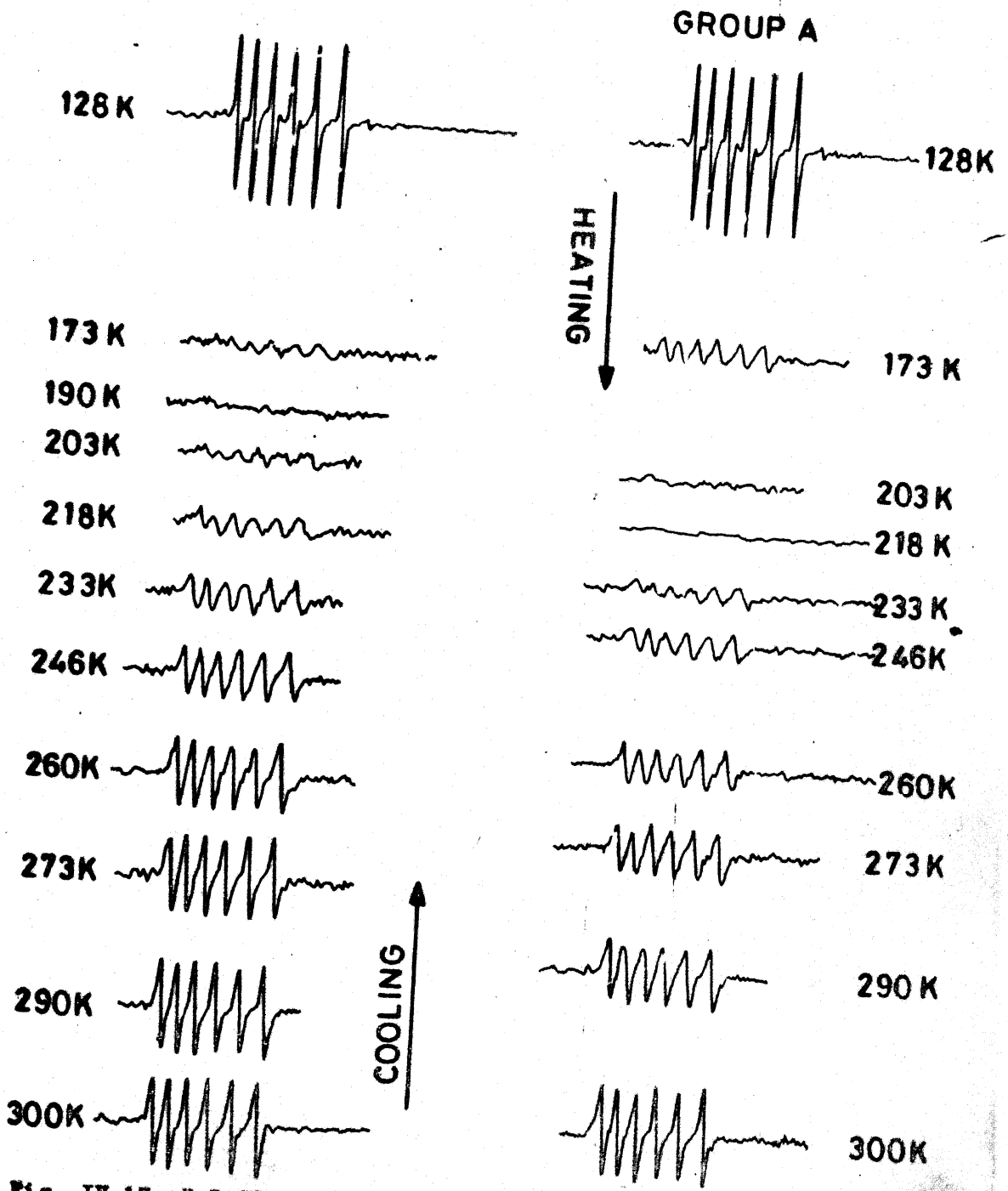

Fig. IV.17 X-BAND RECORDINGS OF THE HIGHEST FIELD TRANSITION 'A' OF $Mn^{2+}:NH_4I$, IN A HEATING AND A COOLING CYCLE WHEN $\vec{H}//\vec{z}$. THE CRYSTAL WAS PRECOOLED AT LNT FOR A WEEK. AN INTENSITY ANOMALY AND HYSTERESIS CAN BE CLEARLY SEEN.

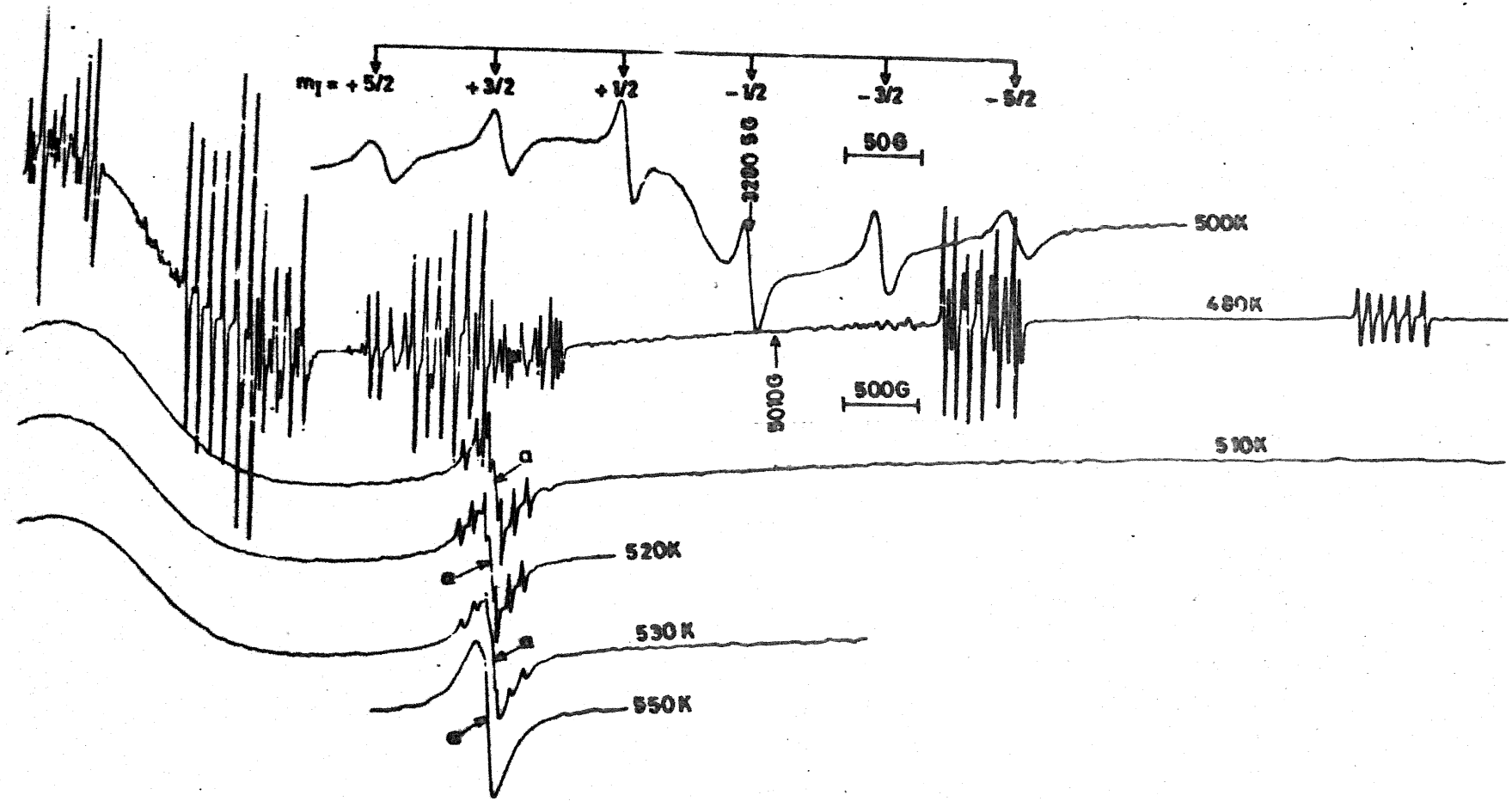

FIG.IV-48 TRANSFORMATION OF ANISOTROPIC SPECTRUM OF Mn^{2+} IN NH_4I INTO AN ISOTROPIC SEXTET SPECTRUM AT 500K. THE ISOTROPIC SEXTET IS SUPERIMPOSED ON A BROAD LINE. A VERY SHARP LINE MARKED 'a' CAN BE SEEN IN THE SEXTET SPECTRUM AND INDICATES EXPELLING OF Mn^{2+} IMPURITY. THE TOP SPECTRUM IS THE EXPANDED ISOTROPIC SEXTET SPECTRUM.

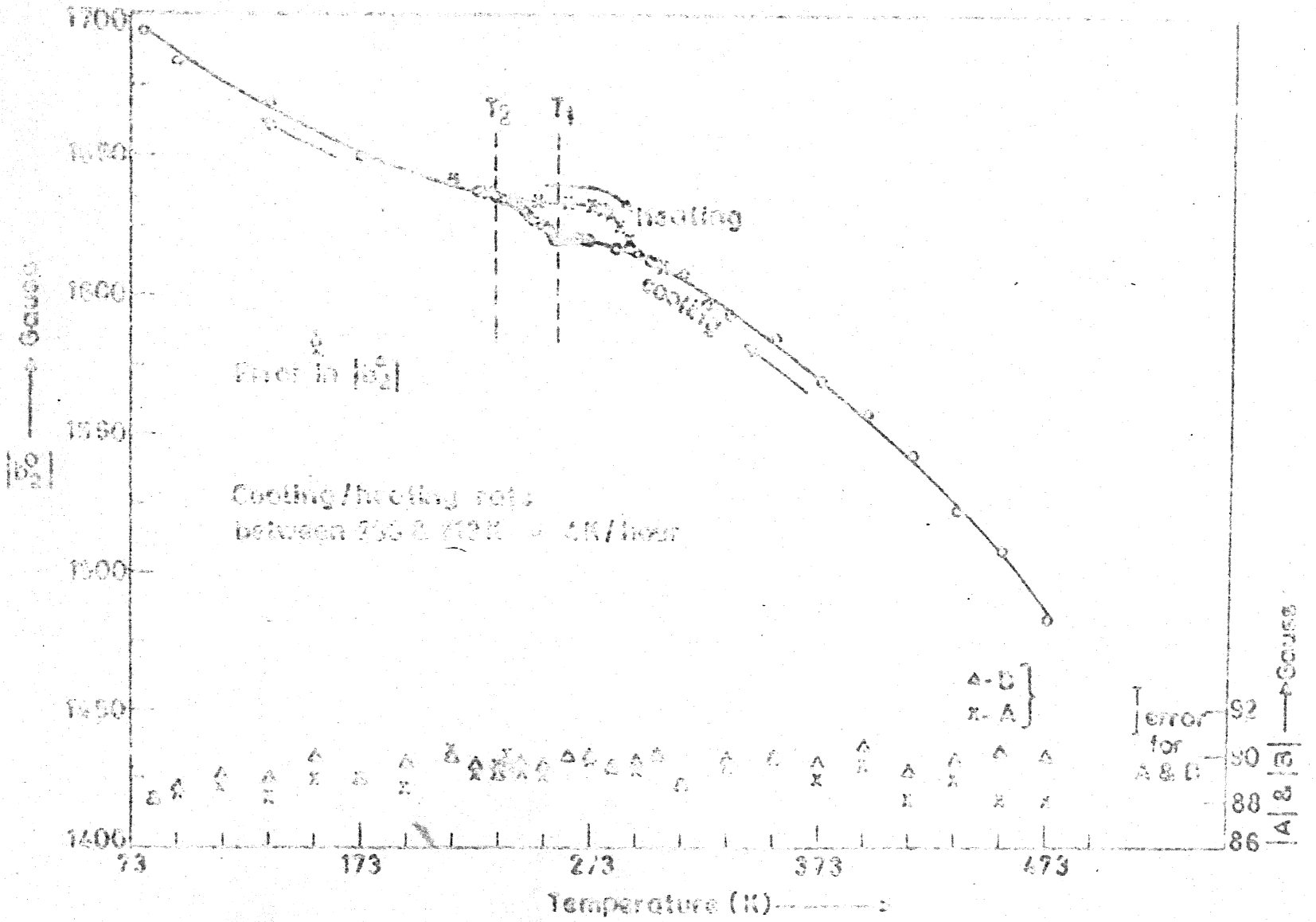

Fig. IV.19 TEMPERATURE DEPENDENCE OF D, A & B PARAMETERS OF Mn^{2+}:NH_4I. THE A & B PARAMETERS ARE ALMOST TEMPERATURE INDEPENDENT. D PARAMETER SHOWS A LARGE TEMPERATURE DEPENDENCE. AN ANOMALY IN D PARAMETER IS ALSO SEEN AND SHOWS A LARGE HYSTERESIS IN A HEATING AND A COOLING CYCLE. T_1 & T_2 ARE THE EXPECTED TRANSITION TEMPERATURES OF NH_4I.

CHAPTER V

EPR STUDY OF Cu^{2+} IONS DOPED IN NH_4I SINGLE CRYSTAL*

Abstract: EPR study of Cu^{2+} ions in NH_4I lattices in all the three phases viz. NaCl, CsCl and PH_4I-tetragonal has been carried out. Three distinct species of Cu^{2+} centres were identified in NH_4I crystals grown under different conditions. Specific Cu^{2+} centre can be selectively produced by judicious control of growth conditions. The results of EPR study in temperature range 573 to 77K are presented in this chapter.

The angular variation of the EPR spectra shows that all the three types of Cu^{2+} centres show tetragonal symmetry of the crystalline field with [100] or equivalent directions as tetragonal axis. The temperature variation of EPR spectra and SHP show distinct anomalies around 250K and $\sim$ 230K which are attributed to the structural phase transition of NH_4I around these temperatures.

The $\tilde{g}$ and $\tilde{A}$ tensors are highly anisotropic and temperature dependent. On the basis of observed fact that $g_{\perp} > g_{\parallel} > 2$, a predominantly dz^2 ground state for Cu^{2+} ion is assumed. At elevated temperatures Cu^{2+} impurity is expelled out from NH_4I crystals at $\sim$500K. The spectra due to all the three types of Cu^{2+} centers get smeared out around 500K. The spin Hamiltonian analysis, discussion on SHP their temperature dependence and tentative models for Cu^{2+} centres are presented. The hypothesis of coexisting NaCl and CsCl phases below phase transition also reviewed in the light of the temperature behaviour of EPR spectra.

---

*Part of the contents (RT X-band study) of this chapter has been published in Chem. Phys. Lett. 88, 309 (1982)

V.1 INTRODUCTION

The ammonium halides have attracted a large number of workers for last many years. The reasons have been two fold. Firstly they offer an opportunity to study charge compensation mechanism when doped with divalent impurities as a simple extension of such studies in isostructural alkali halides. Secondly their various polymorphic modifications at different temperatures and the effect of various factors like pressure, impurity etc., on the nature and transition temperatures of phase transformations have been of great interest in the recent past. Both of the above mentioned studies can be carried out by EPR studies in single crystals doped with transition metal ions. In the recent past such studies have been carried out for divalent copper doped in NH_4F[1], NH_4Br[2-4] and NH_4Cl[5-11]. No EPR study of copper in the remaining ammonium halide viz. NH_4I has so far been reported, except our RT results[12]. Further, NH_4I is of particular interest because its room temperature (RT) structure (NaCl-type) is different from the RT structure (CsCl-type) of NH_4Br and NH_4Cl[13-15]. We have carried out a detailed EPR study of copper doped in NH_4I in the temperature range 550K to 77K.

V.2 EXPERIMENTAL RESULTS

The EPR spectrum of Cu^{2+} doped in NH_4I single crystal for an arbitrary orientation of magnetic field $\vec{H}$ in (001) planes is found to be complex. The nature of the EPR spectra and their angular variation show the presence of three types of magnetically

nonequivalent paramagnetic centres henceforth designated to be as I_2 , II_4 and III (Fig. V.1). The relative concentrations of these three distinct types of centres were found to be different in crystals grown under different conditions. For example crystals grown from mother liquor containing urea as habit modifier, mainly two types of centres (I_2 and II_4) were present, the third type if at all present must be too small in number to give an observable EPR spectrum at RT. But in crystals grown without urea from solutions which contained Cr^{3+} ions as growth aid the third type of centres were sufficient in number to give an observable spectrum. It was also observed that the crystals grown around 340K contain only centres I_2 (Fig. V.2). By growing the crystals ~293K or even lower temperatures, mainly II_4 type of centres were found to be present. The remaining type of centres were found in high relative concentration in crystals grown with Cr^{3+} ion as habit modifier (Fig. V.3). The crystals grown from mother liquors to which either few drops of NH_3 solution or few drops of concentrated HI were added, gave spectra identical to those from crystals grown at the corresponding growth temperature without the addition of acid or NH_3-solution. Thus unlike NH_4Cl (salammoniac) where the pH of the growth solution affects the type of centre incorporated[6,7] in NH_4I,pH seems to have no effect on the type of magnetic centre incorporated in the crystal lattice We shall now present the experimental results for these types of centres separately.

(A) Centre I_2 : It has been mentioned earlier that, crystals grown above 350K contained only one type of centre (I_2). The angular dependence of the line positions and intensities of the resonance lines revealed that the spectrum due to centre I_2 is a combination of three types of spectra. In case when $\vec{H}$ is oriented in planes parallel to crystal faces i.e. (100) or equivalent planes there are three components of the spectrum one of which is angular independent in positions but shows angular dependence in intensity due to overlapping of other components over it. This spectrum will be referred to as (X-Y)-spectrum for reasons discussed in Chapter IV in the case of Mn^{2+}:NH_4I because the symmetry of EPR spectrum is same. This component of the complex spectrum is due to those centres whose magnetic X/Y axis lie in the plane under consideration and is their X-Y plane. For axial symmetry X and Y axes are indistinguishable and may rather more conveniently be referred to as $\perp$ axes. Thus the (X-Y)-spectrum is some times referred to as $\perp$ -spectrum. The (II) second and (III) third components are identical but are out of phase by 90° from each other. For example when static magnetic field $\vec{H}$ is oriented say along [100] in (001) plane then one of the components exactly overlap with the $\perp$ part and the second show a maximum g-value position with maximal spread in hyperfine structure. The latter will be referred to as Z-spectrum or $\parallel$-spectrum while the former as (X/Y)-Z spectrum. When $\vec{H}$ is rotated away from [100] towards [010] these two components move towards each other, cross over and interchange their respective positions when $\vec{H}$ orients exactly

along [010]. This behaviour clearly indicates that there are three types of magnetically equivalent but differently oriented magnetic centres. The Z-axes of the internal electric crystal fields acting on the Cu^{2+} ions are directed along the edges of the cubic cell. The X/Y axis of the crystalline field also coincides with the crystallographic axis. Therefore in an orientation of $\vec{H}$ || to one of the crystallographic axes, $\vec{H}$ will be simultaneously || and ⊥ the Z-axes of the differently oriented but otherwise equivalent centres. In Fig. V.2 the RT spectra due to I_2 type of centres are shown. In (110) plane the over all symmetry of the spectrum is two fold and along the direction [111] all the complexes belonging to species I_2 become equivalent and only four lines are observed. In general, the line width in the Z-component of EPR spectrum is of the order of 35 G while higher concentrations of doping (0.1% by weight) resulted in larger line widths. The ⊥ part comprises only a single strong line with a width ~ 95 G, Neither resolved hfs due to the isotopes of copper nor the shfs due to ligand Iodines would be observed.

(B) Centre II_4: The salient features of spectrum II_4 are identical to the spectrum due to centres I_2 with the difference that in the former the hyperfine structure is well resolved for both the || and the ⊥ parts each of which comprises four hyperfine lines. This spectrum is also a super position of three individual spectra which will be designated just as for centres I_2. In this case also no copper isotopic resolution and no shfs due to ligands were observed. The line widths in this case were found to be slightly smaller (~ 30 G). To obtain well resolved spectra low

copper concentrations (~.05% by weight) were found suitable.

In crystals which contain both I_2 and II_4 centres the spectra due to both types of centres overlap and some of the lines overlap exactly giving larger peak to peak height and larger line width. Fig. V.3 shows spectra at RT due to different samples grown under different growth conditions. The growth temperatures lower than ambient were found favourable for the creation of II_4 type of centres. It is to be noted that in crystals grown at ~290K by carefully controlled evaporation and with Cr^{3+} ions as growth modifier the centres I_2 are completely absent. In crystals grown from solutions containing both Cr^{3+} ions and urea additives and kept at ~300K and from solutions containing only urea and kept at ~318K, all the three types of centres are present with enough concentrations to give the EPR spectra.

(c) Centres III : The spectra due to centres of type III are given in Fig. V.4. It may be mentioned here that the crystallographic axes coincide with the crystal field axes for this centre also like the other two centres I_2 and II_4. The characteristic features (viz. symmetry, number of component spectra, line widths etc.) of the EPR spectra of centre III are similar to those of I_2 and II_4. The important difference, however, are as follows :

(i) The //- component i.e. Z-spectrum of centre III at RT is not well resolved unlike the Z-spectrum of centres I_2 and II_4. The parallel component of centre III comprises a single line with a width of ~50 G.

(ii) Unlike the ⊥ spectrum of centre I_2, the ⊥-component of centre III spectrum is well resolved like ⊥ spectrum of centre II_4, and mostly overlaps with it.

V.3 SPIN HAMILTONIAN ANALYSIS

General methods for determining $\tilde{g}$ and $\tilde{A}$ tensors have already been discussed in Chapter II. As mentioned above all the three types of identified centres give EPR spectra revealing axial symmetry. The usual spin-Hamiltonian with axial symmetry[16,17] :

$$\mathcal{H} = g_{\parallel}\beta H_z S_z + g_{\perp}\beta(H_x S_x + H_y S_y) + A I_z S_z + B(S_x I_x + S_y I_y) + Q' [I_z^2 - \tfrac{1}{3} I(I+1)] \quad .. \text{(V.1)}$$

with $S = \frac{1}{2}$ and $I = \frac{3}{2}$ and with the notations $g_{\parallel} = g_z$, $g_{\perp} = g_x = g_y$, $A = A_z$, and $B = A_x = A_y$, has been used to describe the main features of the observed EPR spectra for the three types of centres. The above spin-Hamiltonian has been solved by Bleany[18] and discussed extensively by Low[17] and Abragam and Bleany[16] carrying perturbation theory to second order. The resonance values of transition fields for two simpler cases $\theta = 0^\circ$ i.e. $\vec{H} \parallel$ Z-axis and $\theta = 90^\circ$ i.e. $\vec{H} \perp$ Z-axis are readily available in literature.[17-19]

Initial estimates of the spin-Hamiltonian parameters were made by solving the eight expressions for resonance fields as simultaneous equations by a least squares programme available in the computer library of dec system-10 computers. These parameters were then used for a computer diagonalization of the complete (8 x 8) matrix using a computer programme based on the standard

Jacobi method. The parameters were next refined by an iterative computer programme to give a minimum least squared deviation (LSD) in the computed and experimental resonance fields at suitable intermediate angles. The angular variation of the resonance fields was computed by a complete diagonalization of the (8 x 8) spin-Hamiltonian matrix on computer and matching the corresponding energy levels with the microwave quantum i.e. $|E_1-E_2| - \frac{h\nu}{\beta} \leq \delta$ where δ is the tolerance limit for energy mismatch. The observed spectra were analysed using the method mentioned above and the best fit parameters thus obtained from the analysis of RT spectra for the three types of centres are given in Table V.1. The angular dependence of resonable fields at RT in (100) plane is shown in Fig. V.5 for all the type of centres. The very good fit of the experimental points with the computed curves justifies the adequacy of the spin-Hamiltonian (V.1) used for the description of the EPR spectra for Cu^{2+} in NH_4I crystals.

V.4 MODEL FOR MAGNETIC CENTRES

Earlier work on alkali halides[20-23] and ammonium halides[1-11] has shown that the divalent impurity ions could individually go in substitutionally, interstitially, in clusters or as precipitates. The vacancy created to maintain the charge neutrality of the crystal could be a close neighbour of the divalent impurity giving rise to associated vacancy-ion pairs or it could be far away from the divalent impurity. The symmetry of the observed spectra helps in identifying the type and structure of the centre.

The observed symmetry of the spectra in the present case of Cu^{2+} doped NH_4I can be explained by the following models for charge compensation (Fig. V.6) :

(i) The Cu^{2+} goes substitutionally for NH_4^+ and gets associated with a cation vacancy at one of the second neighbour sites, which corresponds to centre I_2 and will be designated as Cu^{2+}-V200

(ii) The Cu^{2+} goes substitutionally for NH_4^+ and gets associated with a vacancy at one of the fourth neighbour cation sites which corresponds to centre II_4 and will be designated as Cu^{2+}-V400.

(iii) The Cu^{2+} goes substitutionally for NH_4^+ and two adjacent axial ligands (Iodine ions) from the surrounding octahedron (i.e. any two adjacent Iodines marked from 1 through 4 in Fig. V.6) are replaced by some negative impurity like OH^- anions or two apical (5 and 6 in Fig. V.6) Iodines are replaced by OH^- anions. The overall charge compensation may be achieved by NH_4^+ vacancy far away from the complex. Presumably this may correspond to our centre III.

All the three models proposed above tentatively, permit the existence of three axially symmetric magnetic centres which are otherwise equivalent but have different orientation relative to each other. All the three axially symmetric magnetic centres are further magnetically doubly degenerate as has been mentioned earlier for Mn^{2+}:NH_4I in Chapter IV. There are thus six axial centres. Fig. V.6(b) shows that the complex pairs like Cu^{2+}-V200 and Cu^{2+}-$\bar{V}$200 or Cu^{2+}-V400 and Cu^{2+}-$\bar{V}$400 are magnetically degenerate due to their indistinguishability from EPR spectra. Thus

in each model there are three equally probable magnetically non-generate centres with one of the cubic axes as the Z-axis and the remaining two cubic axes as X and Y axes (the last two being indistinguishable here). Therefore when the magnetic field is oriented || to [100] direction it is || to the Z-axis of one third of the centres and ⊥ to X/Y axis of the remaining two thirds of the centres. This explains the observation of a || and a ⊥ part of the spectrum when $\vec{H}$ is oriented along a cube edge and the fact that the ⊥ part is more intense (theoretically twice). In Fig. V.7 it has been shown that if Z_1-Z_2 , Z_2-Z_3 and Z_3-Z_1 planes represent the planes parallel to the cube faces, then for an orientation $(H, \theta, 90^\circ)$ in Z_3-Z_1 plane there shall be three different characteristic spectra corresponding to three orientations of $\vec{H}$ with respect to three sets of axes viz. (X_1 , Y_1 , Z_1), (X_2 , Y_2 , Z_2) and (X_3 , Y_3 , Z_3) out of which two will coincide with each other for either $\theta = 0^\circ$ or $\theta = 90^\circ$, while in an orientation of $\vec{H}$ || [111] direction all the three characteristic spectra will be exactly identical and will in general comprise four hf peaks. This is consistent with the experimental observation.

The centres associated with second or fourth neighbour vacancy are consistent with our models for I_2 and II_4 and also have earlier been characterized for Mn^{2+} in alkali halides with NaCl structure[21-25], while models similar to our model for center III have been proposed for Mn^{2+} in LiF and NaF[26-28]. Our tentative models are based only on EPR results and need confirmation through other studies. For example the association of OH^-

impurity with the centres can probably be explored by optical absorption spectra and other non-EPR studies[26-29].

V.5 DISCUSSION ON THE SHP

The $\tilde{g}$ tensor and the hyperfine tensor are found to be anisotropic as can be seen from Table V.1. The hyperfine tensor is highly anisotropic for centres I_2 and III. It is expected that the proximity of the cation vacancy to the dipositive ion or association of comparatively smaller size OH^- with the dipositive ion will cause large tetragonal distortion. The extent of tetragonal distortion is probably reflected in the extent of anisotropy in the hyperfine tensor i.e. $\Delta A(=(A-B))$. Therefore, in our models assigned to centre I_2 and II_4 since the associated vacancy is respectively at the second and fourth distant cation sites along cubic axes, the anisotropy in hyperfine parameter for centre I_2 is expected to be larger than for II_4. The calculated values of A and B for both I_2 and II_4 thus support our models (Table V.1). Similarly the anisotropy in hyperfine tensor for centre III is also expected to be large which is consistent with the calculated values of the parameters A and B for this centre. It is rather surprising that ion-vacancy pairs associated with vacancies at sites farther away by factors $2^{1/2}$ and $2^{3/2}$ compared to the nearest available sites for centres I_2 and II_4 respectively are favoured. But the study of Mn^{2+} in NaF[22] has revealed the presence of above type of centres and the centres associated with a fourth distant vacancy was found to be more favourable and stable. Our experiments with crystals grown at different temperatures reveal that

reasonable values for P, however, for the choice A/B > 0, the value of -PK has a sign opposite to that for free Cu^{2+} and for most of the other copper complexes. The possibility of $k < 0$ can not be ruled out since detailed calculations on the free ions show that the contributions to k from 1s, 2s, 3s, and 4s electrons are about the same in magnitude but different in sign[38]. A similar sign-change has been reported for centre I for Cu^{2+} in NH_4Cl by Hagen and Trappeniers[6,7]. They have discussed the role of admixture from 4s orbitals and covalency and have justified that for the d_{z^2} ground state the admixture from 4s orbitals can produce such large changes in k - that a change of sign of (-PK) from that in other Cu^{2+} complexes with ground state $d_{x^2-y^2}$ is possible. For a $d_{x^2-y^2}$ ground state d-s admixture is ruled out in the first order.

A comparison of P, -PK and $\langle r^{-3} \rangle$ values obtained for these centres with their respective free ion values shows that the choice A/B > 0 for centre II_4 does not yield reasonable value of P, PK and $\langle r^{-3} \rangle$. For centre III both the choices $A/B \lesssim 0$, at RT give reasonable values of parameters. The values of $\langle r^{-3} \rangle$ at RT are rather low compared to the estimated free ion value thus indicate that there is a diminution in $\langle r^{-3} \rangle$ in the solid state, which is often attributed to the bonding effects[16,39]. As has already been mentioned that the observation $g_{\parallel} > 2$ for all the three centres indicates some admixture of $d_{x^2-y^2}$ into the predominantly d_{z^2} ground state. For a rigorous analysis, the admixture and the detailed interaction of the Cu^{2+} ion with the

ligands, should be accounted for. A wave function of the form :

$$(\psi) = c_1|d_{z^2}\rangle + c_2|4s\rangle + c_3(\sum(\psi_{ligands}) \quad .. \quad (V.2)$$

for the ground state should be used for calculation of SH parameters. For want of optical data for Cu^{2+} in NH_4I, no analysis of the so called "vibronic-admixture" is possible in the present case. Strong bonding along the Z-axis can be promoted through d-s mixing[40]. As the strong d-s mixing is expected for centre I_2 due to -PK > 0, a strong bonding between the Cu^{2+} ion and one NH_4^+ along ion-vacancy line is expected. The unresolved (super-hyperfine structure) from iodine and unresolved hfs from Cu^{63} and Cu^{65} isotopes and perhaps the rotation of NH_4^+ in the NaCl structure of NH_4I are the chief causes for the observed large line widths.

V.6 TEMPERATURE DEPENDENCE OF THE EPR SPECTRA

The temperature dependence of the EPR spectra from I_2 , II_4 and III centre over the temperature range 573 to 77K, the spin Hamiltonian analysis and the consistency of the models will be presented in this section. The results in the two ranges viz. (i) 300 to 500K (High temperature study) and (ii) 300K to 77K (Low temperature study) will be discussed separately.

(A) High Temperature Study

Fig. V.8 shows the temperature dependence of EPR spectra for $\vec{H}$ parallel to one of the crystal edges i.e. [100] from a crystal which contained all the three types of centres with

different relative concentration. A relatively weaker spectrum due to I_2 indicates that this type of centres are much less in the sample under study. The intensity of the spectra is found to vary with temperature. The line widths for all the three types of centres have been found to increase with temperature. This observation is contrary to the observation of decrease in line widths at high temperatures for Mn^{2+} in NH_4I (Chapter IV). The g, A, and B parameters also show a temperature dependence (Table V.1). The line width for centre III $\perp$-spectrum is $\sim$40 G at RT (300K) and it becomes $\sim$ 10 G around 433K. The line widths for centres I_2 and II_4 $\parallel$-spectrum also increased from $\sim$35 G at RT to 45 G around 433K. It is noteworthy that the spectrum due to centre III starts diminishing in intensity much faster than the spectra due to I_2 and II_4 and around 443K the spectrum due to III almost vanishes (Fig. V.8). At temperatures around 473K spectrum due to II_4 also disappears completely and only very weak traces of the spectrum due to I_2 remain. At 500K no EPR spectrum is seen due to any of the three types of centres. On cooling from 500K back to RT the changes are found to be reversible. But if the sample is heated over and above 500K it begins to lose its bluish colour and starts turning into a powder. Therefore on cooling back the observed spectrum contains an additional part due to a small part of the crystal turning into polycrystalline form. The clear part of the heated sample, at RT, gives spectrum identical to an unheated sample. It is also observed that if the samples are heated at 500K for a long time, some of the copper

impurity is expelled out from the volume of the crystal. Due to this expulsion of impurity over to the surface, the crystal loses its transparency which can be restored by polishing the crystal surfaces. Due to the expulsion of impurity a broad signal due to cluster or aggregation of expelled copper impurity is superimposed on the normal spectra and is observable when samples heated for a long time at 500K are cooled back to RT.

When samples containing mainly centre I_2 were heated above RT it was observed that this centre is more stable compared to II_4 and III. The spectra due to I_2 could be observed clearly even up to 473K. The whole sample was destroyed irrerversibly on heating around 523K.

(B) Low Temperature Study

For low temperature study different samples viz. those containing only I_2 centres, those containing mainly II_4 and III centres or those containing all the three centres in comparable concentrations, were selected. Most of the spectra were analysed for $\vec{H}$ along Z-axis i.e. $\vec{H}$ oriented parallel to one of the crystal edges. It was observed that the temperature dependence of the spectrum was different for different thermal processes depending on the rates of cooling or heating, number of repeated cycles and on the direction (heating or cooling) in which the temperature was changed prior to the recording. The important results of the temperature dependence of the EPR spectra below RT will now be described for the three types of centres separately :

(i) Centre I_2 : The intensity and line widths of the || -part at RT show slight m_I dependence. As the temperature is lowered below RT there is a slight variation in the over all spread of the || - and the ⊥ -part of the spectrum. The intensity of the peaks also increases with the lowering of the temperature of the sample. At a temperature around 248K, which is found to be very sensitive to the thermal history and rates of temperature variation the spectra show drastic changes. At this temperature both the parts || as well as ⊥ show sudden increase in their spreads. Afterwards the rate of increase in the spread is quite large. Over a temperature range ($\sim$248 to $\sim$ 220K) and then becomes slow down to LNT. The line widths of || -part are m_I dependent at LNT, but the lines are narrower by $\sim$5 G at LNT compared to those at RT. At LNT the highest field line of the || -part is asymmetrical and shows some under-resolved structure on it (Fig. V.9).

The temperature at which drastic changes start in a cooling experiment has been found to vary from 254K to 243K depending upon the rate of cooling and the previous history of thermal processing. Cooling at rates much faster than 5K/hour lowers the transition temperature drastically. Both during the heating and the cooling cycles for rates much faster than 5K/hour there is no abrupt change in the spread or position of || or ⊥ part of the spectrum as we pass through the reported transition temperature T_1 ($\sim$256K). The abrupt change occurs at temperatures different from 256K typically around 260K in a heating cycle and around 243K in a cooling cycle. The temperature dependence of the EPR spectrum of centre I_2 is

very sensitive to thermal process and is accompanied by a thermal hysteresis which is also sensitive to the width of thermal cycle, the rates of cooling and heating and, the number of repeated cycles. The hysteresis is found to increase with increasing number of repeated cycles through transition temperature. Below transition temperature the $\perp$ part show much more drastic changes and the single broad line gets resolved into four. The line widths of the $\perp$-part are $\sim$30 G. The temperature dependence of g, A and B are shown in Fig. V.10 and V.11.

Usually no drastic changes were observed on passing through the reported transition temperature T_2 ($\sim$232K). In some cases when the sample was precooled at LNT for long time (upto 2 or 3 days) and the sample was warmed carefully at sufficiently slow rate, marked changes occured around 230K in the width of the spectrum. After passing through this temperature, subsequent cooling did not show similar changes around 230K. In most of the experiments, the changes in the spread of the spectrum and positions of the peaks were much more pronounced between 263K and 223K. Below 173K and above 263K the changes were relatively slower. Due to various constraints we could not perform repeated experiments with the same samples at rates slower than or equal to $\sim$5K/hour. However, it has been observed that at rates of $\sim$4K/hour for a thermal cycle between RT and 223K, by carefully, maintaining a one way change reduced the width of the thermal hysteresis in the values of $|A|$ and $|B|$ by considerable amount - $\sim$ 5K for a typical cycle shown in Figs. V.12 and V.13. In Fig. V.14a the temperature

dependence of a part of the $\perp$-spectrum is shown both for a heating and a cooling experiment. In Fig. V.14b $\perp$-part of spectrum is shown partly at some temperatures on a warming experiment with a sample precooled for two days at LNT. The marked changes at 229.5K can be seen clearly. The SHP at LNT are tabulated along with SHP at room temperature and higher temperatures (Table V.1). The over all symmetry and axes of the spectra were consistent with their RT counter parts. The angular variation of the spectrum at LNT is shown in Fig. V.15.

(ii) Centre II_4 and III : It has been mentioned earlier that no crystal could be grown incorporating only II_4 centres independently. The temperature variation of this type of centre was studied in samples containing mainly centres II_4 and partly centres III. The results of temperature dependence for these two types of centres are therefore presented together in what follows. The dependence of the EPR spectra on thermal processing and the paths followed in a cooling and heating experiment are more or less the same as mentioned earlier for centres I_2. The spectra from centres II_4 and III also showed drastic changes around 250K and this is so called transition temperature depended on the path followed (i.e. cooling or heating), rate of cooling and previous history of thermal processing. Noticeable changes in the spectra from centres II_4 and III were observed $\sim$231K (near the so called λ-transition). The changes around 231K were clear for centre III when a sample precooled for 8 hours at LNT and was cautiously warmed up through 231K undirectionally.

An anomaly is clear around 231K in the hyperfine constant A of centre III as shown in Fig. V.16. The observed temperature dependence of the SHP for II_4 and III in typical experiment are shown in Figs. V.16 through 19 and the spectra due to them at LNT are shown in Fig. V.4. The important features of the spectra from centres II_4 and III observed on lowering the temperature of the samples are as follows :

(a) The || -part of spectrum due to centres III, which comprise a single line ($\sim$50 G p-p) due to unresolved hf structure at RT gets resolved into four hf lines below $\sim$ 250K, which depends on the thermal process to some extent. The line widths of the resolved hf structure in ||-part of III are of the order of 15 G at LNT. The line width of $\perp$ -part of III at RT is $\sim$30 G and increases as the transition temperature ($\sim$ 253K) is approached. Consequently derivative heights also decrease. But as the transition temperature is crossed over, the trend in the change in line widths and derivative heights reverse and line widths become 2 5 G p-p at LNT. The spread and position of || -part and $\perp$-part of the spectrum due to centre III also show a temperature dependence with some anomaly around $\sim$ 250K.

(b) For spectrum due to centre II_4 the line widths are practically same from RT down to LNT. The $\perp$-part did not show any drastic temperature dependence while the || -part was observed to show a rather large temperature dependence, with clear cut anomalies in position (g - value) and spread (A value) around the two reported transition temperatures (Fig. V.18 and Fig. V.19). The changes

around 231K develop rather occasionally and the changes around 250K are highly sensitive to thermal processing and are accompanied by large thermal hysteresis.

In the temperature range 500 to 77K the over all symmetry of the spectra from all three centres are found to be the same i.e. tetragonal within the experimental errors. Thus the angular behaviour at LNT (Fig. V.15) is similar to that described earlier for RT. The temperature dependence of EPR spectrum in (110) plane is also shown in Fig. V.20 and it can be seen that there are definite changes in the EPR spectrum around 250K. The spectrum due to polycrystalline samples (crushed powder) also have been recorded in the temperature range 500 to 77K. The powder spectra were not well resolved even at LNT and no useful or additional information could be gathered from the temperature dependence of these spectra.

V.7 SH ANALYSIS AND DISCUSSION

The SHP were calculated by using the spin-Hamiltonian (V 1) and the spectra for $\vec{H} \parallel [100]$ or equivalent directions. At LNT the SHP were refined for best fit of angular dependence as mentioned earlier. The SHP at some temperatures above RT, at RT and at LNT where they were found to be independent of thermal processing are tabulated in Table V.1. A typical temperature dependence of EPR spectra below RT is shown in Fig. V.21.

The temperature dependence reveals definite anomalies in SHP at temperature around the reported transition temperatures $T_1 \sim$ 256K (NaCl$\leftrightarrow$CsCl) and $T_2 \sim$ 231K (CsCl$\leftrightarrow$tetragonal). These anomalies in the temperature dependence of SHP clearly indicate the occurrence of structural phase transformations around these temperatures. These are also supported by observation of anomalies in line widths and in some cases in the derivative heights. A structural phase transformation starts taking place around 253K if the samples are cooled undirectionally at a rate of $\sim$4K/hour. The dependence of the transition temperature on thermal processing and previous history throws some light on the nature of the phase transition taking place from disordered NaCl-type of disordered CsCl-type. The following points may be mentioned about the nature of phase transitions revealed by the observed temperature dependence.

(i) The NaCl phase may be supercooled below the transition temperature T_1 ($\sim$256K) at least down to 243K and the degree of supercooling depends on the thermal process.

(ii) The anomaly in SHP as well as changes in the EPR spectrum reveals that this transformation is rather sluggish if temperature is varied very fast, though in most of the literature this transformation has been reported to be of first order. However, if the transformation was of first order it should have been reflected in the EPR spectra through large anomalies at the transition temperature. But the observed behaviour of the temperature dependence shows anomalous behaviour over a rather

wide range of temperatures indicating that this transformation is rather sluggish. The transformation is not completed just around the temperature where it actually starts. This behaviour indicates that below the transition temperature the crystal is in a mixed phase containing regions of NaCl as well CsCl phases. This view is also consistent with the observation of large thermal hysteresis accompanied by this transformation. On reversing the cooling process the CsCl phase can be superheated above the transition temperature and the process of establishment of an statistical equilibrium at a certain temperature makes this transformation also sluggish. This is supported by the observation that to get the changes completely stabilized at a particular temperature especially between $\sim$253K and $\sim$193K rather long times ($\sim$1 hour) are required (Fig. V.9).

(iii) The second transformation CsCl to tetragonal (PH_4I) does not readily develop. In a cooling cycle from RT down to LNT it is never observed, most probably due to coexisting NaCl and CsCl phases and the domain structure may prevent the transformation CsCl to tetragonal. No large anomalies are observed around this temperature as has been revealed by warming experiments on samples precooled at LNT for longer times long enough that the tetragonal phase get stabilized in dominant proportion even if the domain structure exists down to LNT. The small changes observed around the transformation CsCl to tetragonal are expected because the tetragonal phase is nearly CsCl-type and has a very small distortion from the latter. Therefore in

observing this transformation in a cooling experiment from RT to LNT the changes seem to be masked due to the coexistence of the upper two phases (NaCl and CsCl).

(iv) The centres I_2 and III are found to be more sensitive to the structural phase transformations. The marked changes in EPR spectra especially the $\perp$-part of centre I_2 and $\parallel$-part of centre III clearly indicate the onset of the structural phase transformation. This again supports the view that the centres I_2 and III are associated with larger tetragonal distortions and therefore changes in crystalline field environment are better reflected in their EPR spectra.

(v) The transition temperatures which in our case are defined as the temperatures around which appearance of marked changes in EPR spectra are noticed most often in cooling or heating experiments performed by us with the slowest possible rates (4K/hour) are found to be lower by 2 to 5K than those reported by others. This lowering of transition temperatures is often observed when defects are present in a pure lattice. Thus the presence of Cu^{2+} and ion vacancies may affect the transition temperatures to some extent.

The above mentioned points may be reviewed in the light of other reports on phase transitions in NH_4I made by several workers and have earlier been mentioned in Chapter II Section D. Of special mention are those by Kamiyoshi[41] (dielectric) and references cited therein, Grigorov et al[42] (NH_4I:Tl, Luminescence), Sharp and Pintar[43] (Relaxation), Cauzi et al[44] (Raman) and Goyal and Dasannacharya[45] (Neutron scattering). The results of

Kamiyoshi[41] give an idea as to how conflicting the reported transitions temperatures are. The transition temperatures reported on the basis of dielectric studies by Kamiyoshi[41] are T_1 = 259.5K and T_2 = 229K while those reported by others are[41] : Simon T_1 = 258.5K, Bridgman T_1 = 255.4K, Guillen T_2 = 294.5K, Freymann T_1 = 239K (cooling) and 268K (warming). For X-irradiated crystals the transition temperatures were found[41] to be T_1= 247K and T_2 = 221K. Out of large number of workers only Couzi et al[44], Sharp and Pintar[43] and Goyal and Dasannacharya[45] have specifically taken account of the fact that the transition (NaCl$\leftrightarrow$CsCl) around 256K shows a large hysteresis and depends on the thermal history. Since NH_4I lattice is very sensitive to thermal history, especially in the temperature range 213K to 300K, great care must be taken in interpreting any data on NH_4I in this temperature range. The conflicting reports on transition temperatures may be a result of overlooking this point. In their recent study of neutron scattering on NH_4I in NaCl phase and CsCl phase, Goyal and and Dasannacharya[45] have unambigously shown coexistence of the two phases on passing through the transition temperatures in both cooling and heating cycles. Their data did show some evidence that the sample takes several hours to attain an equilibrium mixed structure. The typical cooling and heating rates are not explicitly mentioned by Goyal and Dasannacharya but they do mention that these rates were faster than 5K/hour. In a typical thermal cycle an abrupt change in intensity or width of diffraction peaks was observed by them at 243K and 278K in a cooling and

in a warming cycle respectively. They also observed any marked changes in the diffraction pattern on passing through the transition temperature T_2 (~ 232K). Since the tetragonal distortion in phase III is reported to be very small it may very nearly be CsCl type and many experiments might not be able to distinguish in between the phases CsCl and tetragonal. It may be because of this that elastic neutron diffraction experiments of Goyal and Dasannacharya did not indicate the existence of phase III.

Very recently Sharp and Pintar[43] made spin lattice relaxation measurements on ammonium halides. In NH_4I they have found a direct evidence for the existence of domains of both ordered and disordered type even below the order-disorder (NaCl + CsCl) $\longrightarrow$ (PH_4I) transition. From the non-exponential recovery of the proton magnetization between 203K and 163K for NH_4I they have concluded that NaCl phase supercools and one obtains a mixed phase (NaCl + CsCl) below 203K. The existence of domain structure and the change in the domain size with temperature were found strongly dependent on temperature and on the direction in which the phase transition was traversed. The authors found this to be responsible for the observed hysteresis.

Our results of EPR study are thus consistent with the hypothesis of coexisting phases and with the extreme sensitiveness of the NH_4I lattice to the thermal history. The defects in small numbers have been found to lower the transition temperatures[41,42] and are some times when in large numbers, reported to induce unknown additional structural transformation[42].

V.8 CONSISTENCY OF MODELS FOR CENTRES I_2 , II_4 AND III AT LOW AND HIGH TEMPERATURES

As mentioned earlier the EPR spectra from the three types of complexes preserve their symmetry and angular behaviour through out the temperature range of the present study. At temperatures above RT no structural phase transformation is observed so the models proposed for I_2 , II_4 and III consistent with their angular dependence are valid. As the spectra disappear at some typical temperatures above RT, a dissociation of ion-vacancy pairs is expected and the magnetic centres are expected to be in rapid thermal motion (jumping between equivalent sites) which results in a smearing out of the spectra. On the basis of the observed behaviour centre I_2 is found to be relatively more stable which is expected due to the proximity of vacancy and therefore a relatively stronger binding between the ion and the vacancy pair. In II_4 and III the latter seems to be more easily dissociated compared to the former. This behaviour seems to be consistent with the proposed model for centre III, since it is easier to dissociate OH^- groups associated with the metal ion as compared to the associated vacancies. There seems to be an inherent tendency of NH_4I lattice to expel impurity (at least paramagnetic ions) at elevated temperatures (below decomposition)as discussed earlier in the case of Mn^{2+} doped NH_4I in Chapter IV.

Below RT NH_4I undergoes two structural phase transformations viz. NaCl $\longleftrightarrow$ CsCl and CsCl $\longleftrightarrow$ PH_4I tetragonal). Now we will discuss how the ion vacancy-pair for each centre reshuffles

itself to retain the tetragonal symmetry of the crystalline field. The important reshuffling will take place on the transformation NaCl$\leftrightarrow$ CsCl. In the NaCl phase the substitutional sites are in octahedral co-ordination while in CsCl phase they are in 8-fold co-ordination. In Fig. II.7b of Chapter II the reshuffling scheme of the ions in a NaCl $\leftrightarrow$ CsCl structure transformation is shown. Two possible models for a reshuffled ion vacancy pair are possible. According to one of the arragnements the Cu^{2+} ions reshuffles to the body centred sites of CsCl structure and the pairing cation vacancy is either in the adjacent cells at the equivalent sites or in the next adjacent cells at the similar sites. With this proposal of substitutional cation sites for Cu^{2+} the observed [100]-tetragonal symmetry is expected and the existence of three pairs of magnetically equivalent centres with different tetragonal axes is also possible due to the availability of 6 possible sites for pairing-vacancy to each substitutional site. The predominent crystalline field, however, will then be 8-fold cubic and hence the ground state for Cu^{2+} ions will be either a d_{xy} state or the degenerate pair[10] of states d_{zx} and d_{xy}. For d_{xy} state as ground state it has been shown[10] that $g_{\parallel} > g_{\perp} > 2$ and $(g_{\parallel} - 2) \simeq 4(g_{\perp} - 2)$. However the observed g-values ($g_{\perp} > g_{\parallel}$) do not support the assumption that d_{xy} state is the ground state. The calculations with d_{xz} and d_{yz} pair as ground state only yield a weak $\Delta M_s = 2$ transition[10] at $g \sim 4$. Hence neither of these states accounts for the observed g-values and therefore contradicts the above substitutional reshuffling.

Alternative to the above model is the interstitial reshuffling of the Cu^{2+} ions i.e. Cu^{2+} ion occupies an off centre place in the plane spanned by four ligands with two NH_4^+ vacancies either at nearest neighbour or second nearest neighbour positions along the [100] direction. No definite conclusions can be made about the positions of the vacancies associated. However if the observed anisotropy in $\tilde{g}$ and $\tilde{A}$ i.e. $\Delta g = |(g_{||} - g_{\perp})|$ and $\Delta A = (A-B)$ (Table V.1) is taken as a possible index of the extent of tetragonal distortion, the distortion seems to be more for centre I_2 and II_4 at LNT compared to at RT and suggests the proximity of vacancy to the Cu^{2+} ion. Therefore the vacancies associated with Cu^{2+} ion are expected to be at nearest neighbour sites in CsCl structure. The value of ΔA at LNT for centre III suggests that for this type of centre the tetragonal distortion may reduce in CsCl structure compared to that in NaCl structure, and therefore distant sites for the vacancies may be expected.

The analysis of the SHP obtained from low temperature spectra at LNT and high temperatures above 400K (Table V.1) reveals that the ground state for Cu^{2+} for all the three different species of copper centres remains predominently d_{z^2}. Also the observation of $g_{\perp} > g_{||} > 2$ indicates some admixture of higher orbitals by vibrational modes as described by O'Brien[37]. The fact that the difference $\Delta g_{||} = (g_{||} - 2)$ is comparatively small at LNT and larger at higher temperatures indicates that the influence of this admixture is comparatively small at LNT and increases with temperature. The small variations in g-factors,

however, indicate that the vibrational admixture may be ignored for a first order analysis of hyperfine interaction along with its temperature dependence to be discussed in the following paragraphs.

The analysis of hyperfine parameters ignoring the vibronic admixture (Table V.2) at different temperatures and based on similar analysis by Hagen and Trappeniers[6,7] for copper centres in NH_4Cl, ND_4Cl and CsCl lattices, shows that the choice, $A/B > 0$ for centre I_2 is more reasonable, while the choice, $A/B < 0$ seems to be more reasonable for centres II_4 and III. However, the sign of PK for centre I_2 with the choice $A/B > 0$ is opposite to the sign of PK for the free ion and also for many other complexes with the $d_{x^2-y^2}$ ground state. A similar change of sign of PK for Cu^{2+} ion in NH_4Cl lattice has been reported by Hagen and Trappeniers[6,7]. The authors[6,7] have given an explanation for this change of sign in the case of a d_{z^2} ground state taking into account the s-d and ligand admixtures. We have no alternative explanation and give a brief preview of their explanation in the following paragraph.

In an improved analysis of the ground state and the SHP, detailed interaction of Cu^{2+}-ion with the ligands should also be taken into account by constructing molecular orbitals consisting of linear combination of atomic orbitals of the central ion and the ligands, consistent with the relevant point group. The ground state wave function then takes the form (V.2). The positive sign of PK in copper complexes with $d_{x^2-y^2}$ lowest state and in free ion[39] is attributed to exchange polarization which gives a

dominant interaction of 's-spins' antiparallel to the spin of the d-electrons with the nucleus[38,46,47]. The admixture of 4s orbitals which is possible in a d_{z^2} ground state but is ruled out for $d_{x^2-y^2}$ ground state in first order[31], however, introduces a larger spin density at the nucleus of spins aligned || to the spin of d-electrons, thus reducing the effect of the spin polarization of the core electrons. The admixture of the 4s is of-course influenced by changes in the environment of the ion. The Fermi contact interaction (-PK) for the 4s-orbitals ($=1970\times10^{4}cm^{-1}$) is rather high and opposite in sign to that for d-orbitals.[7] Therefore small admixtures from 4s can produce rather large change in PK and with considerable extent of admixture a change in sign of (-PK) from conventional one is thus possible.

Tables V.1 and V.2 show that there is a large temperature dependence of hyperfine parameters of centres I_2, II_4 and III and the Fermi contact interaction (-PK) has some temperature dependence. However, it can be seen from the analytical expressions[7] for A and B that the difference A-B ($= \Delta A$) should be independent of Fermi contact interaction. The difference ΔA is also temperature dependent. Similar temperature dependence of ΔA has been reported for $Cu^{2+}:NH_4Cl$ and $Cu^{2+}:CsCl$ by Trappeniers and Hagen[7]. The main part of the change with temperature of the hyperfine parameters of centre I_2 seems to be caused by a change in the Fermi contact term. In the foregoing discussion we have mentioned that for centre I_2 there is an important admixture of the 4s-orbitals, which even changes the sign of the Fermi-contact

interaction term. The observed dimunition of Fermi-contact interaction with increasing temperature could mean that either the spin polarization increases or that the extent of admixture from 4s-orbitals reduces. However, the g-factors show small variation with temperature and the change in the strength of crystal field with temperature does not seem to be drastic and therefore can not be expected to cause large changes in d-s-admixture. Pilbrow and Spaeth[10] explained the change in the hyperfine parameters, arising from a change in the spin polarization due to an expanding radial wave function of the d_{z^2} orbital. The very large temperature dependence of hf parameters observed for these centres in NH_4I lattice are comparable to a similar dependence for Cu^{2+} in NH_4Cl[7] and is a rather rare phenomenon.

REFERENCES

1. I.H. Parker, J. Phys. C4, 2967 (1971).

2. M.D. Sastry and P. Venkateswarlu, Proc. Ind. Acad. Sci. 66, 208 (1967); M.D.Sastry & P.A.Narayana, J.Chem.Phys.357, 3266 (1972).

3. M.V. Sorokin and G.K. Chirkin, Sovt. Phys. Solid State 21, 169; 1720 (1979).

4. N.J. Trappeniers, F.S. Stibbe and J.L. Rao, J. Phys. Chem. Solids 42, 616 (1981).

5. M.M. Zaripov and G.K. Chirkin, Sovt. Phys. Solid State 6, 1290 (1964); 7, 74 (1965); 7, 2391 (1966).

6. S.H. Hagen, Ph.D. Thesis, University of Amsterdam (1966).

7. N.J. Trappeniers and S.H. Hagen, Physica 31, 122, 251 (1965); 47, 165 (1970); 66, 166 (1973).

8. K. Watnabe and H. Abe, J. Phys. Soc. Japan 38, 755 (1975); Phys. Lett. 51A, 415 (1975).

9. T.E. Freeman and J.R. Pilbrow, J. Phys. C7, 2365 (1974).

10. J.R. Pilbrow and J.M. Spaeth, Phys. Stat. Solidi 20, 225, 237 (1967).

11. N. Kuroda and A. Kawamori, J. Phys. Chem. Solids 32, 1233 (1971).

12. Prem Chand and G.C. Upreti, Chem. Phys. Lett. 88, 309 (1982).

13. R.W.G. Wyckoff, 'Crystal Structures', Vol.1, Interscience, New York, (1968).

14. H.A. Levy and S.W. Peterson, J. Amm. Chem. Soc. 75, 1536 (1953).

15. C.N.R. Rao and M. Natrajan, A Review of Crystal Structure Transformations in Binary Halides; NSRSDS 41 (1972).

16. A. Abragam and B. Bleany, 'Electron Paramagnetic Resonance of Transition Metal Ions', Clarendon, Oxford (1970).

17. W. Low, 'Paramagnetic Resonance in Solids', Academic, New York (1960).

18. B. Bleany, Phil. Mag. 41, 441 (1951).

19. R.M. Golding, 'Applied Wave Mechanics', D. Van Nostrand Co. Ltd., London (1969).

20. R. Botcher, W. Windsch and W. Ludke, Phys. Stat. Sol. 20, 121 (1967).

21. G.D. Watkins, Phys. Rev. 113, 79, 91 (1959).

22. K.N. Srivastava and P. Venkateswarlu, Proc. Ind. Acad. Sci. 53A, 284 (1966).

23. A.V. Jagannadham and P. Venkateswarlu, ibid. 69A, 67 (1969).

24. T. Iwasaki and H. Wakabayashi, J. Phys. Soc. Japan, 40, 1359 (1976).

25. W.J. Veigele and W.H. Tantila, J. Chem. Phys. 41, 274 (1964).

26. A. Bianchini, M. Martinelli, S. Santucci, P. Berge and C. Laj, Phys. Lett., A29, 522 (1969).

27. C.G. Bousquet, A. Serra and M.G. Sucre, J. Mag. Reson. 6, 117 (1972).

28. B. Fritz, F. Luty and J. Anger, Z. Phys. 158, 595 (1960).

29. T.G. Stoebe, J. Phys. Chem. Solid 28, 1375 (1967).

30. B. Bleany, K.D. Bowers, and M.H.L. Pryce, Proc. Roy. Soc. A228, 166 (1955).

31. J.S. Griffith, 'The Theory of Transition Metal Ions', Cambridge University Press (1961).

32. K.V.S. Rao and M.D. Sastry, J. Chem. Phys. 57, 3266 (1972); 58, 769 (1973).

33. V.G. Krishnan, S.G. Sathyanarayan and G.S. Sastry, J. Chem. Phys. 66, 1715 (1972).

34. W. Hayes and J. Wilkens, Proc. Roy. Soc. A281, 340 (1964).

35. Z. Skoubek and K. Zdansky, J. Chem. Phys. 44, 3078 (1966).

36. R.H. Dunhill, J.R. Pilbrow, and T.D. Smith, J. Chem. Phys. 45, 1474 (1966).

37. M.C.M. O'Brien, Proc. Roy. Soc. A281, 323 (1964).

38. V. Heine, Phys. Rev. 107, 1002 (1967).

39. A. Abragam, J. Horowitz and M.H.L. Pryce, Proc. Roy. Soc. A228, 166 (1955).

40. L.E. Orgel, 'An Introduction to Transition-metal Chemistry: Ligand Field Theory', Methuen and Co. Ltd., London(1960) p.66.

41. K. Kamiyoshi, J. Chem. Phys. 24, 1265 (1956) and references cited therein.

42. V.A. Grigorov, M.K. Kurmanov and E.F. Martynovich, Soviet Phys. Sol. St. 22, 509 (1980).

43. A.R. Sharp and M.M. Pintar, Chemical Phys. 15, 431 (1976); J. Chem. Phys. 75, 2652 (1981).

44. M. Couzi, J.B. Sokoloff and C.H. Perry, J. Chem. Phys. 58, 2965 (1973).

45. P.S. Goyal and B.A. Dasannacharya, J. Phys. C : Solid State 12, 209 (1979).

46. J.H. Wood and G.W. Pratt (Jr.), Phys. Rev. 107, 995 (1957).

47. R.E. Watson and A.J. Freeman, ibid. 120, 1125 (1960).

TABLE V.1

Spin-Hamiltonian Parameters of Cu^{2+} centres I_2 , II_4 and III in NH_4I single crystals.

Centre	Temp. (K)	$g_{\parallel}$	$g_{\perp}$	|A| Gauss	|B| Gauss	Q' Gauss	$\Delta g = (g_{\perp} - g_{\parallel})$	$\Delta A = (\|A\| + \|B\|)$ Gauss
	300	2.011(1)	2.216(1)	190(1)	30(2)	-	0.205	160
I_2	77	2.0051(5)	2.2385(5)	250.0(5)	65.5(5)	-	0.2334	184.5
	500	2.013(1)	2.214(1)	175(2)	25(2)	-	0.201	150
	300	2.019(1)	2.222(1)	80(1)	56(1)	7(1)	0.203	24
II_4	77	2.0189(5)	2.2290(5)	128.5(5)	63.5(5)	8(1)	0.2101	65
	433	2.021(1)	2.220(1)	75(2)	48(2)	-	0.199	27
	300	2.0390(5)	2.249(1)	15(2)	70(1)	-	0.210	-55
III	77	2.0280(5)	2.2501(5)	43.5(5)	60.5(5)	-	0.2221	-17
	433	2.0394(5)	2.248(1)	18(1)	58(1)	-	0.2086	-40

Centre	Temperature	A/B > 0				A/B < 0				Free ion Values
		P (Gauss)	-PK (Gauss)	$\langle r^{-3} \rangle$ (au)	Q (barn)	P (Gauss)	-PK (Gauss)	$\langle r^{-3} \rangle$ (au)	Q (barn)	
I_2	300K	267.7	+45.2	5.2	-	368	-9.11	7.1	-	P=385 G $=360\times10^{+4}cm^{-1}$
	77K	324.2	+75.8	6.3	-	556.8	-49.2	10.7	-	
	500K	251.4	+39.2	4.9	-	339.3	-8.25	6.6	-	
II_4	300K	40.3	+58.2	0.8	0.03	230.1	-44.5	4.4	0.159	PK=105.5 G $=108\times10^{-4}cm^{-1}$
	77K	112.3	+68.5	2.2	0.288	333.3	-50.55	6.4	0.183	
	433K	45.7	+50.3	0.9	-	215	-11.1	4.2	-	$\langle r^{-3} \rangle_{free}$ =7.5 a.u.
III	300K	100.0	-68.7	2.0	-	153.0	-67	3.0	-	
	77K	23.8	-56.80	0.45	-	147.0	-34.75	2.8	-	
	433K	71.9	-56.6	1.4	-	136.7	-55.2	2.6	-	

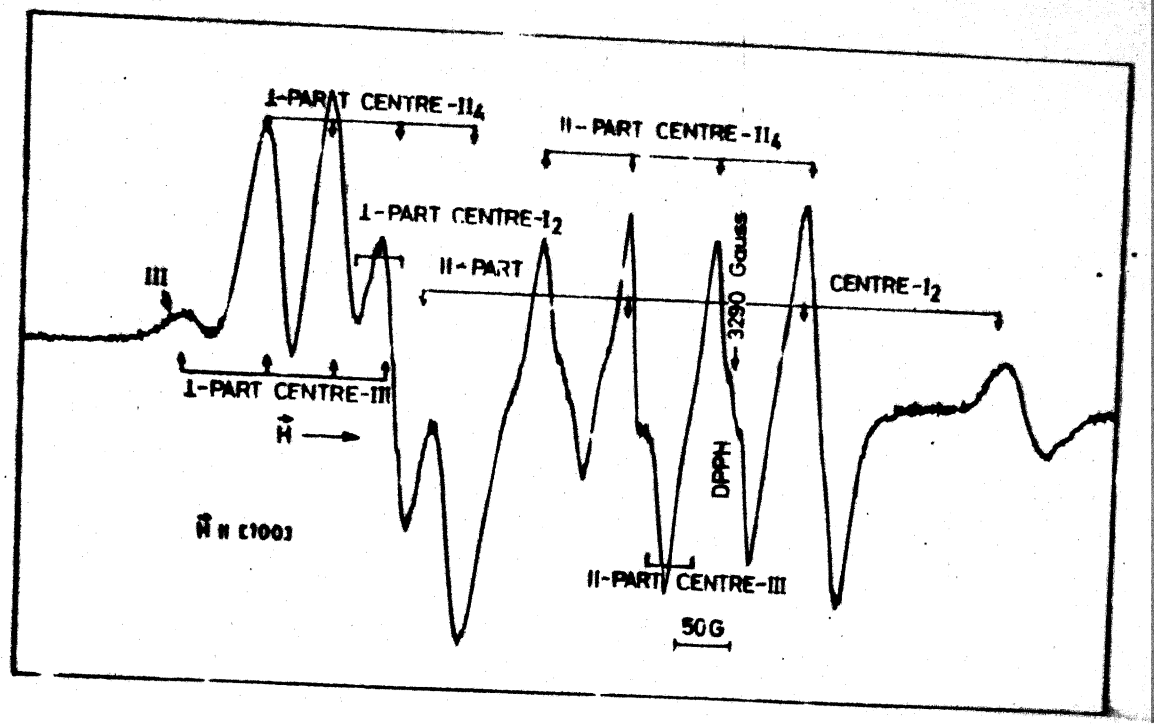

Fig.V.1 EPR SPECTRUM AT RT FROM A CRYSTAL OF NH_4I GROWN AT 300K AND DOPED WITH Cu^{2+}. ALL THE THREE COPPER CENTRES VIZ. I_2, II_4 & III ARE PRESENT AND SPECTRA DUE TO THEM ARE MARKED.

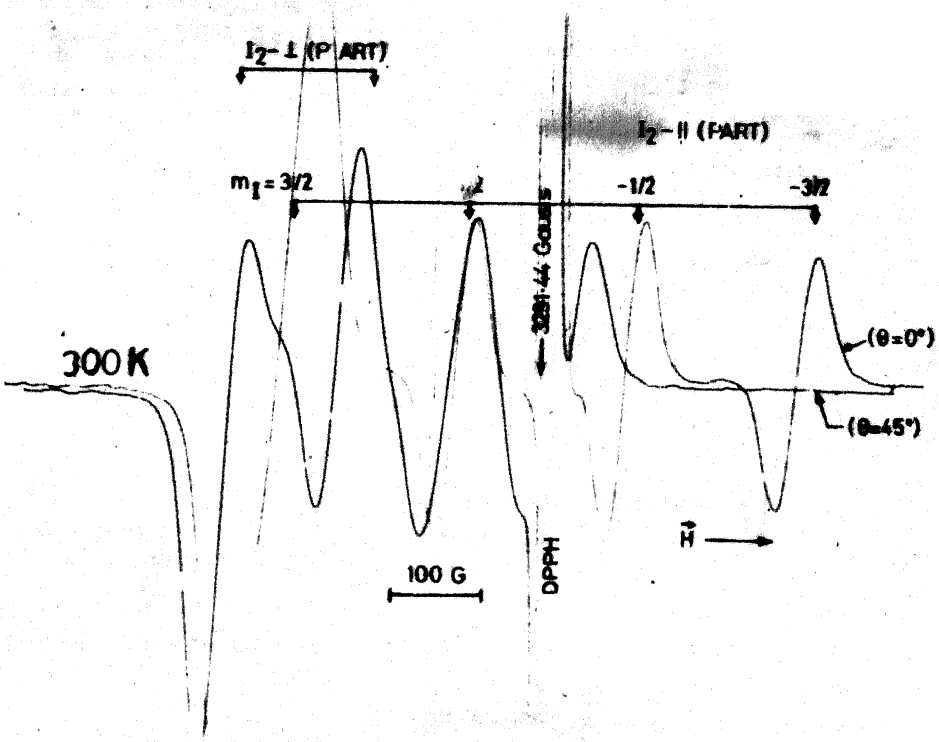

Fig.V.2 EPR SPECTRA OF Cu^{2+} CENTRE-II_4 IN NH_4I CRYSTAL GROWN AT 340K WITH UREA AS GROWTH AID. θ=0 MEANS $\vec{H}$ // [100] AND θ=45° MEANS $\vec{H}$ // [110].

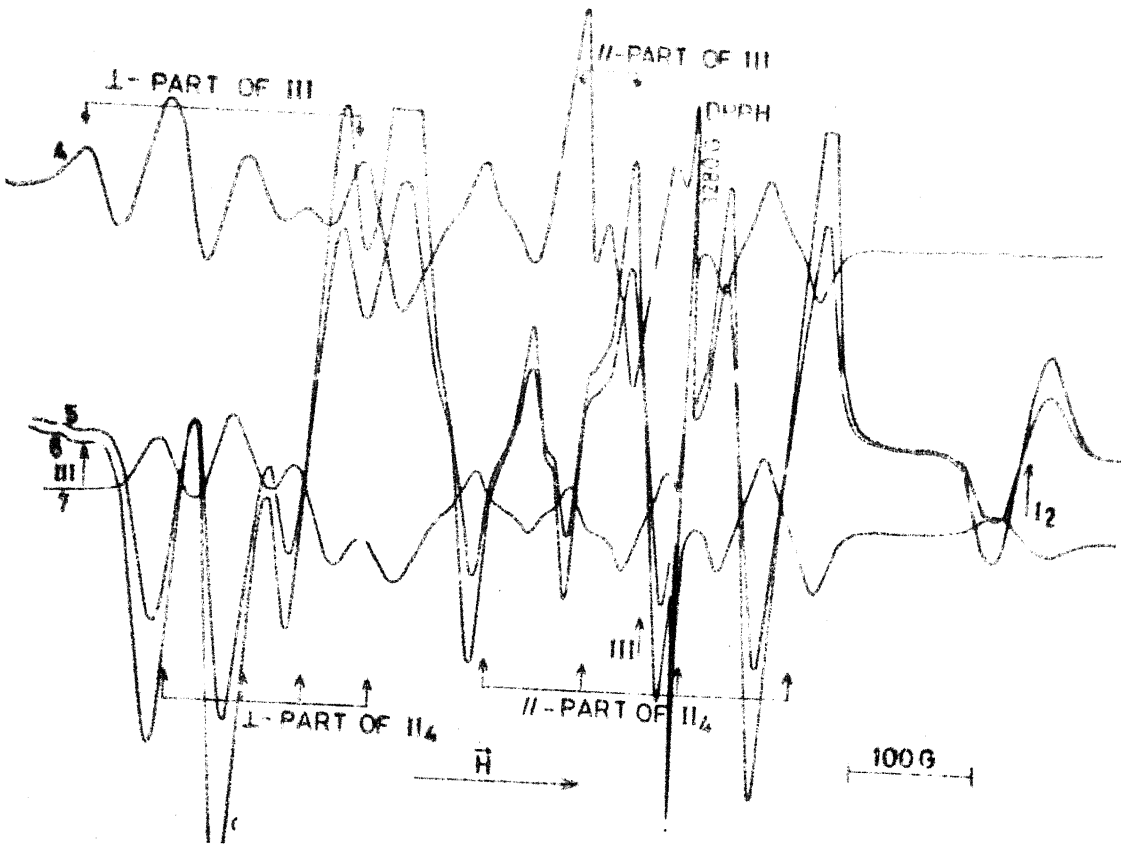

Fig.V.3 THE EFFECT OF GROWTH CONDITIONS ON Cu^{2+} CENTRES INCORPORATED IN NH_4I CRYSTALS. SPECTRUM MARKED AS 4 IS FROM CRYSTAL GROWN WITH Cr^{3+} IONS AS FLUX AT 280K AND CONTAINS ONLY CENTRE-II_4 AND CENTRE-III. SPECTRUM MARKED AS 7 IS FROM CRYSTAL GROWN AT 298 WITH UREA AS FLUX AND CONTAINS ONLY CENTRE-I_2 AND CENTRE-II_4. SPECTRA MARKED AS 5 AND 6 ARE FROM CRYSTALS GROWN AT 318K AND 300K RESPECTIVELY WITH (Cr^{3+} IONS+UREA).

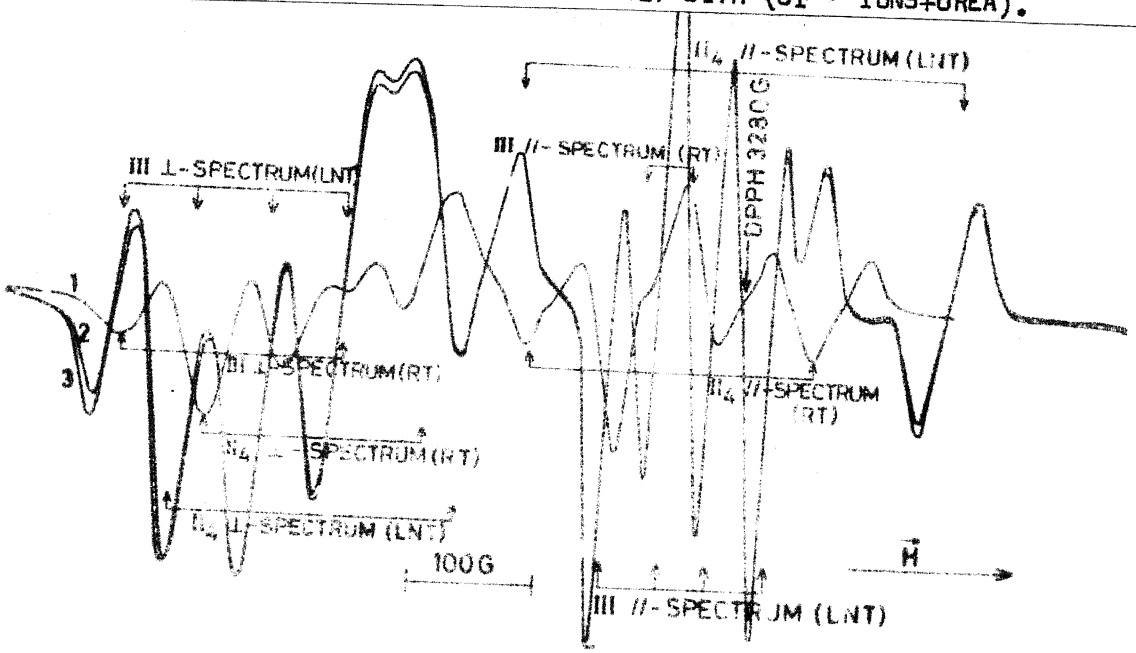

Fig.V.4 EPR SPECTRA OF Cu^{2+} CENTRES II_4 AND III IN A CRYSTAL OF NH_4I GROWN WITH Cr^{3+} IONS AS FLUX AT RT AND AT LNT. THE //-PART OF THE III SPECTRUM GETS RESOLVED INTO FOUR hf LINES. THE SPECTRA DUE TO CENTRE II_4 AND III ARE ALSO MARKED AT LNT AND RT. THE SPECTRA MARKED 2 AND 3 WERE RECORDED AT LNT WITH THE SAME GAIN BUT 3 AFTER 1/2 HOUR OF 2.

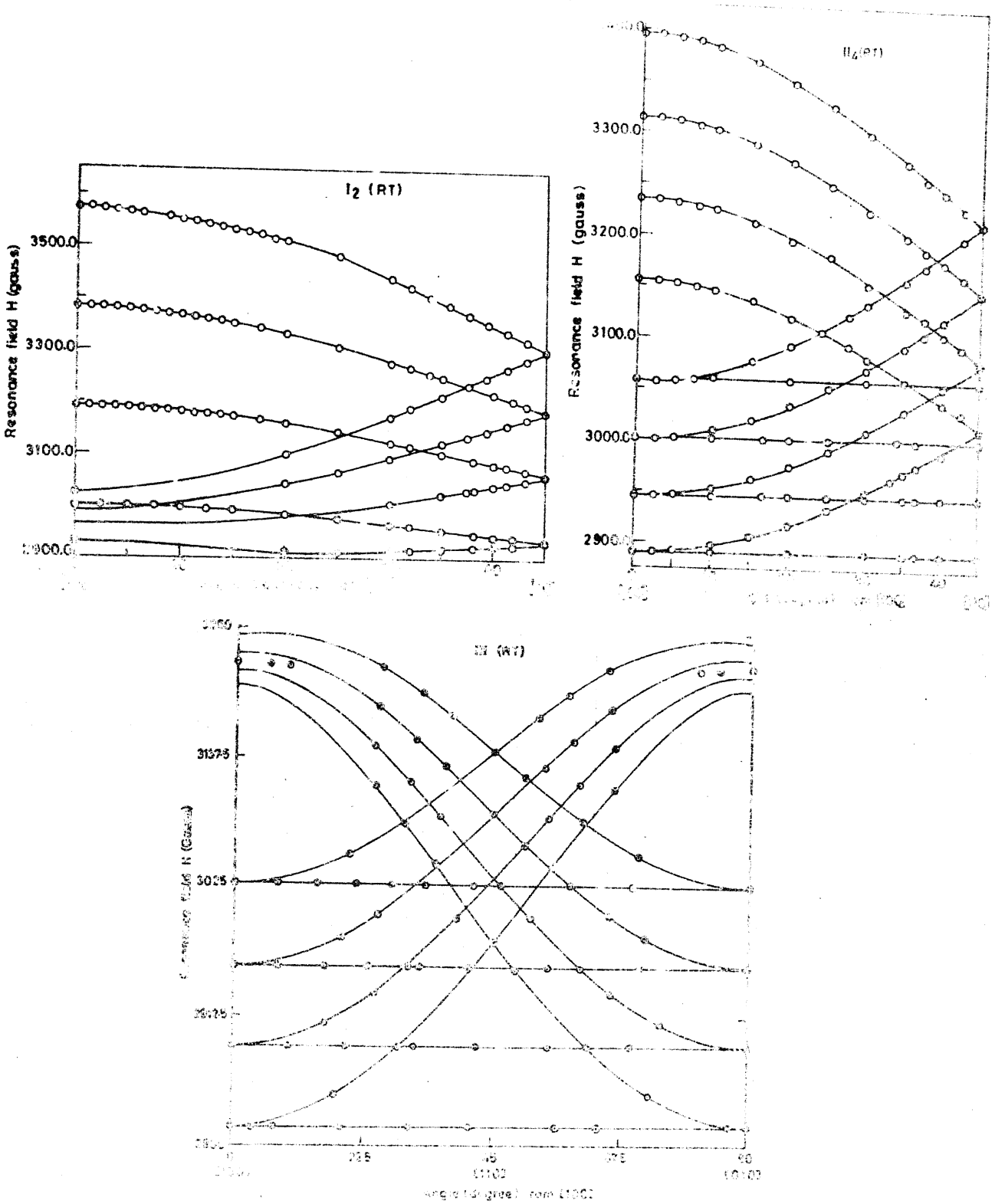

Fig.V.5 ANGULAR VARIATION OF EPR SPECTRA OF Cu^{2+} CENTRES I_2, II_4 & III IN NH_4I LATTICE AT RT. THE SOLID LINES ARE COMPUTED CURVES AND CIRCLES DENOTE OBSERVED RESONANCE FIELDS.

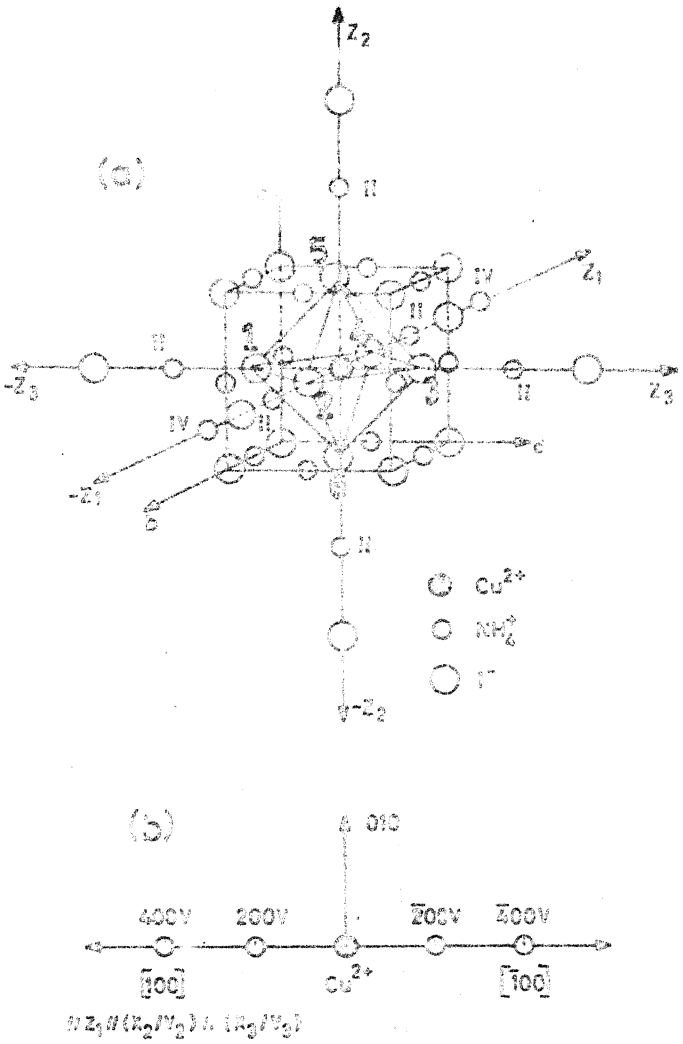

FIG. 6. (a) The arrangement of NH_4^+ and I^- ions is shown. The NH_4^+ site at $(\frac{1}{2}, \frac{1}{2}, 0)$ has been substituted by a diposi-tive copper ion. All six second-neighbour cations are marked II and only two of the six fourth-neighbour cations are shown (marked IV) along the direction marked $-z_1 z_1$. The iodine octahedron surrounding the Cu^{2+} ion is shown. z_1, z_2, z_3 and $-z_1$, $-z_2$, $-z_3$ are possible tetragonal axes of the magnetic centres. Directions a, b and c are the cube axes. (b) It shows that the two Cu^{2+}–vacancy pairs are magnetically degenerate (i) $Cu^{2+}-200V$ and $Cu^{2+}-\bar{2}00V$ for centre I_2 (ii) $Cu^{2+}-400V$ and $Cu^{2+}-\bar{4}00V$ for centre II_4. Direction [100] which is the z axis for one possible ion–vacancy pair is also the x/y axis of the two other possible ion–vacancy pairs along [010] and [001].

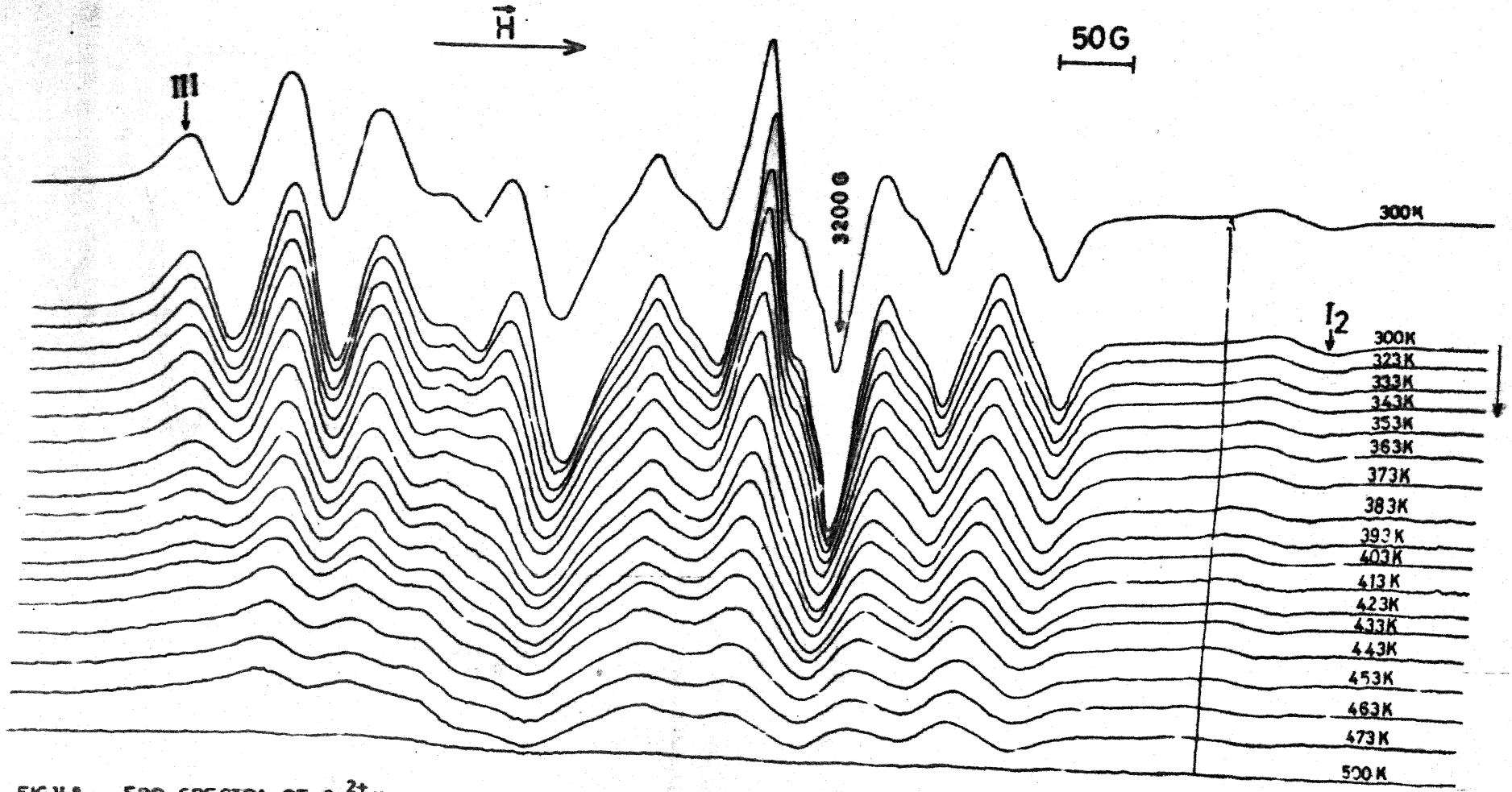

FIG.V-8 EPR SPECTRA OF Cu^{2+} IN NH_4I RECORDED AT DIFFERENT TEMPERATURES WITH THE SAME GAIN AND $\vec{H} \parallel [100]$. THE DOWNWARD ARROWS INDICATE HEATING WHILE THE UPWARD ARROWS INDICATE COOLING. AT 500 K NO SIGNAL IS OBSERVED. BUT SUBSEQUENT COOLING TO 300 K RECOVERS THE NORMAL EPR SPECTRUM. THE PEAKS MARKED AS I_2 AND III INDICATE THE PRESENCE OF CENTRES I_2 AND III RESPECTIVELY.

Fig. V.9 EPR SPECTRA OF Cu^{2+} centre-I_2 IN NH_4I AT RT AND AT LNT WITH $\vec{H}$ // [100]. THE BROKEN CURVE SHOWS THE RT SPECTRUM. AT LNT THE CURVES (a) AND (b) SHOW THE RESOLVED hfs IN ⊥ -PART OF THE SPECTRUM WHICH WAS UNRESOLVED AT RT. SPECTRUM (a) WAS RECORDED HALF AN HOUR AFTER (b) WITH THE SAME GAIN AT LNT. THE hf PEAK MARKED AS C IN //-PART OF SPECTRUM AT LNT IS

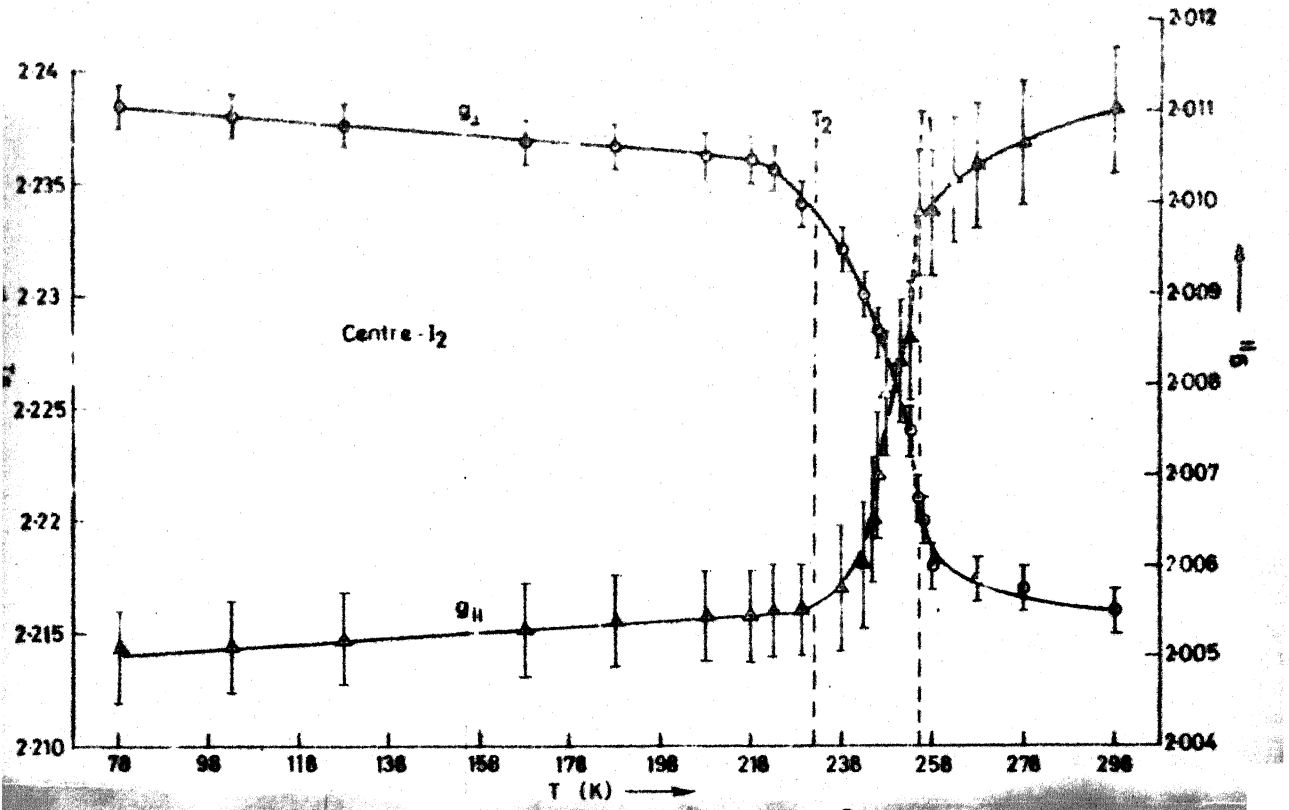

Fig.V.10 TEMPERATURE VARIATION OF g-PARAMETER OF Cu^{2+} CENTRE-I_2 IN NH_4I. THE VERTICAL LINES MARKED BY T_1 & T_2 SHOW EXPECTED TRANSITION TEMPERATURES OF NH_4I.

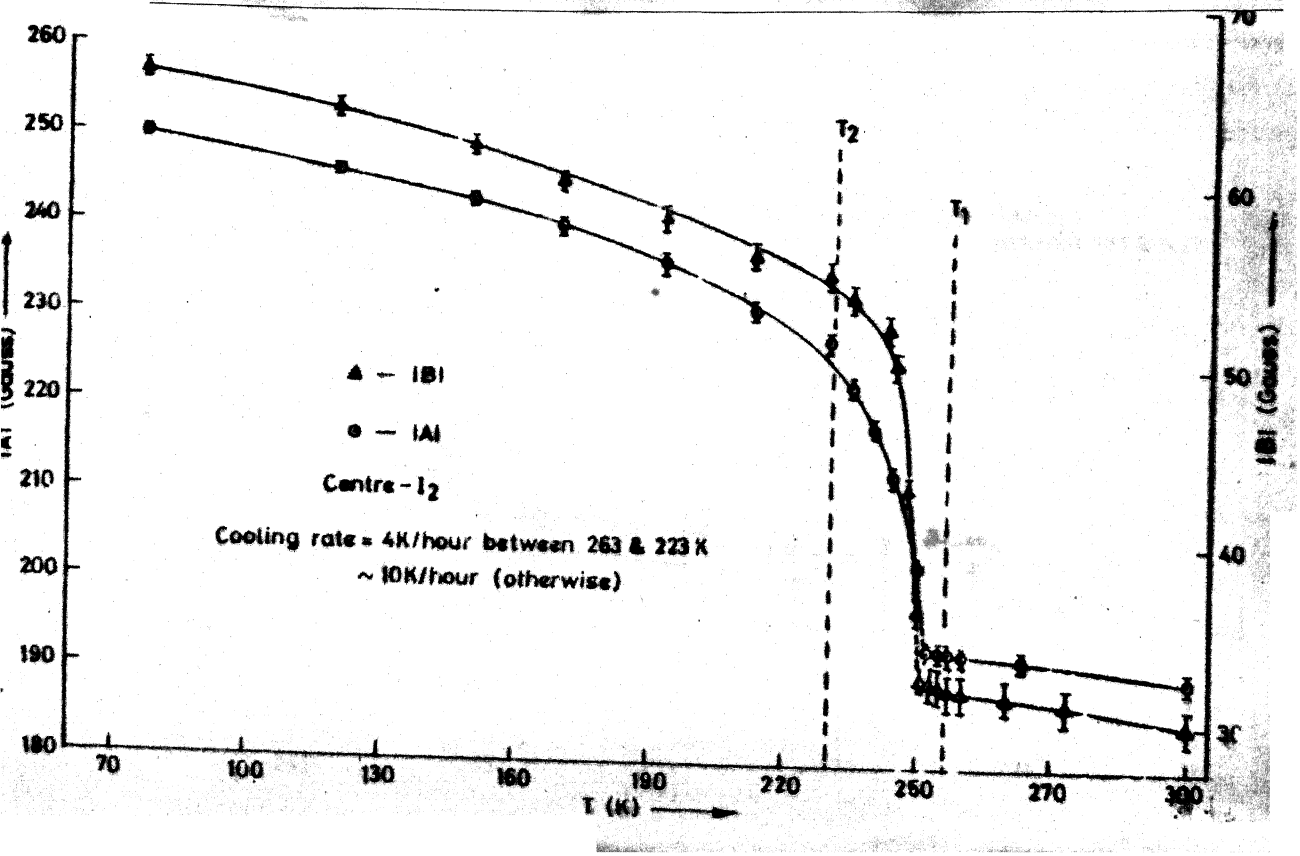

g.V.11 TEMPERATURE VARIATION OF |A| & B OF Cu^{2+} CENTRE-I_2 IN NH_4I. VERTICAL LINES MARKED BY T_1 & T_2 SHOW EXPECTED TRANSITION TEMPERATURES OF NH_4I.

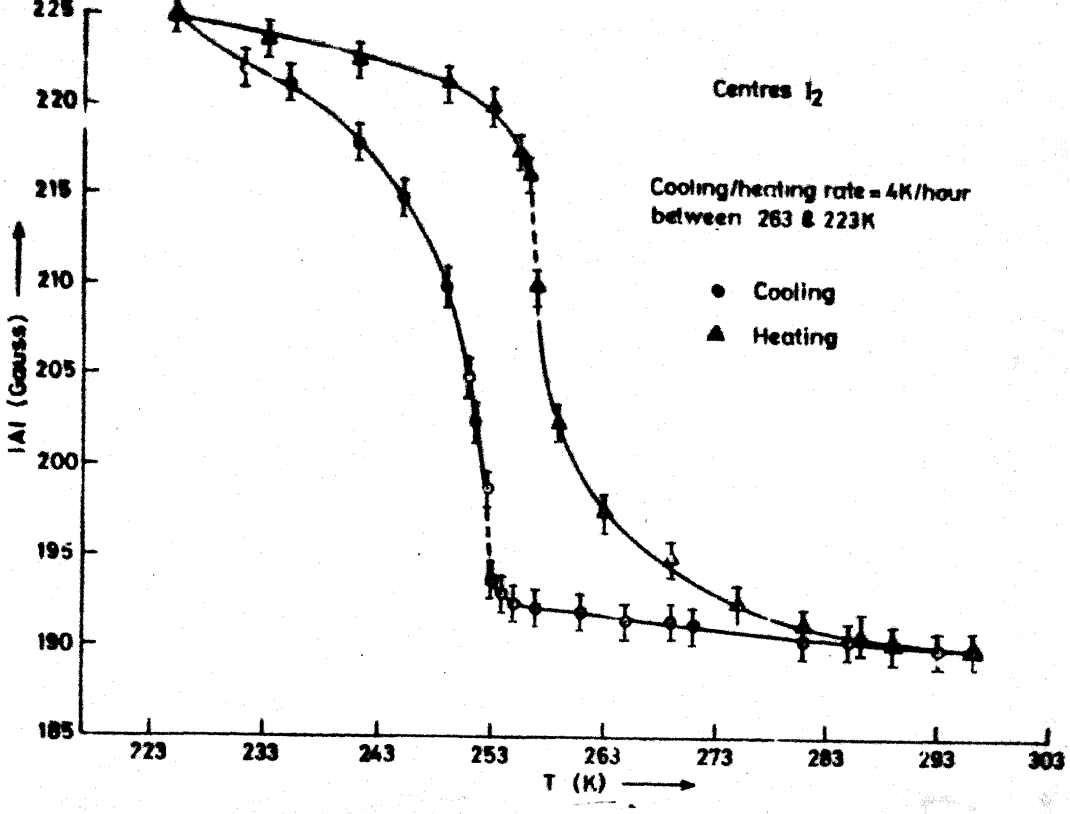

Fig.V.12 THERMAL HYSTERESIS IN A-PARAMETER OF Cu^{2+} CENTRE-I_2 IN NH_4I IN A TYPICAL COOLING AND HEATING CYCLE.

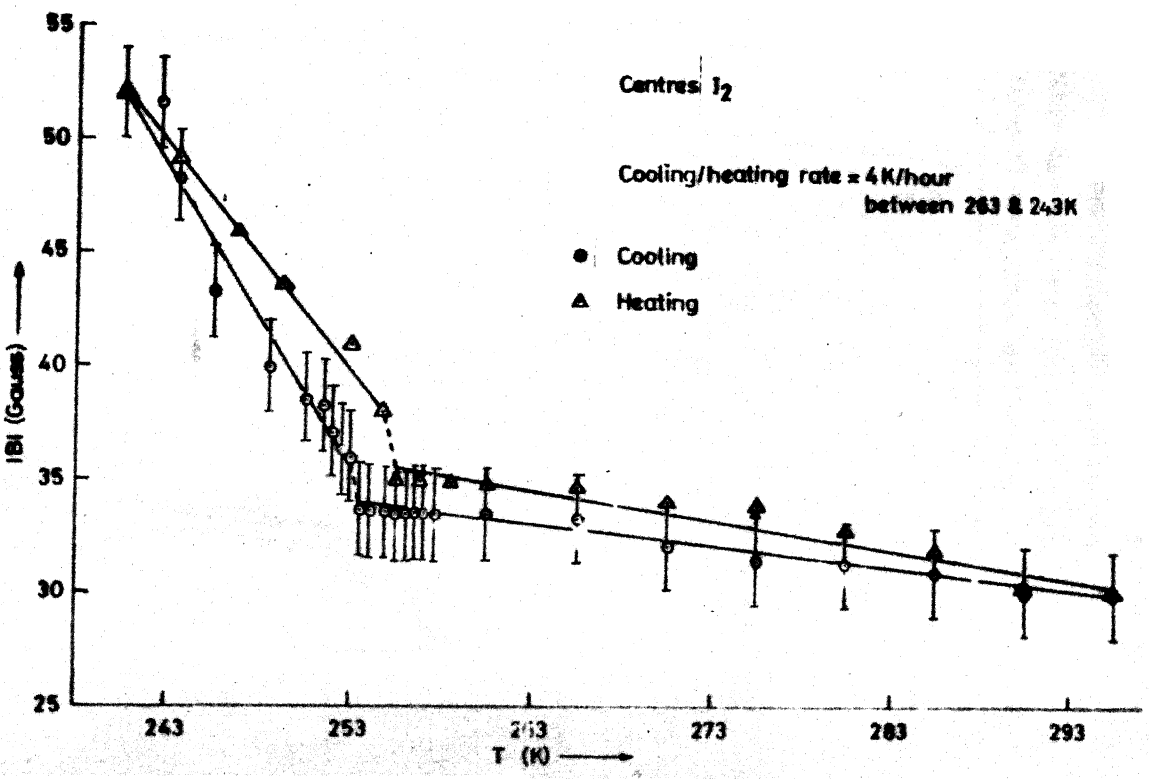

Fig.V.13 THERMAL HYSTERESIS IN B-PARAMETER OF Cu^{2+} CENTRE-I_2 IN NH_4I IN A TYPICAL COOLING AND HEATING CYCLE.

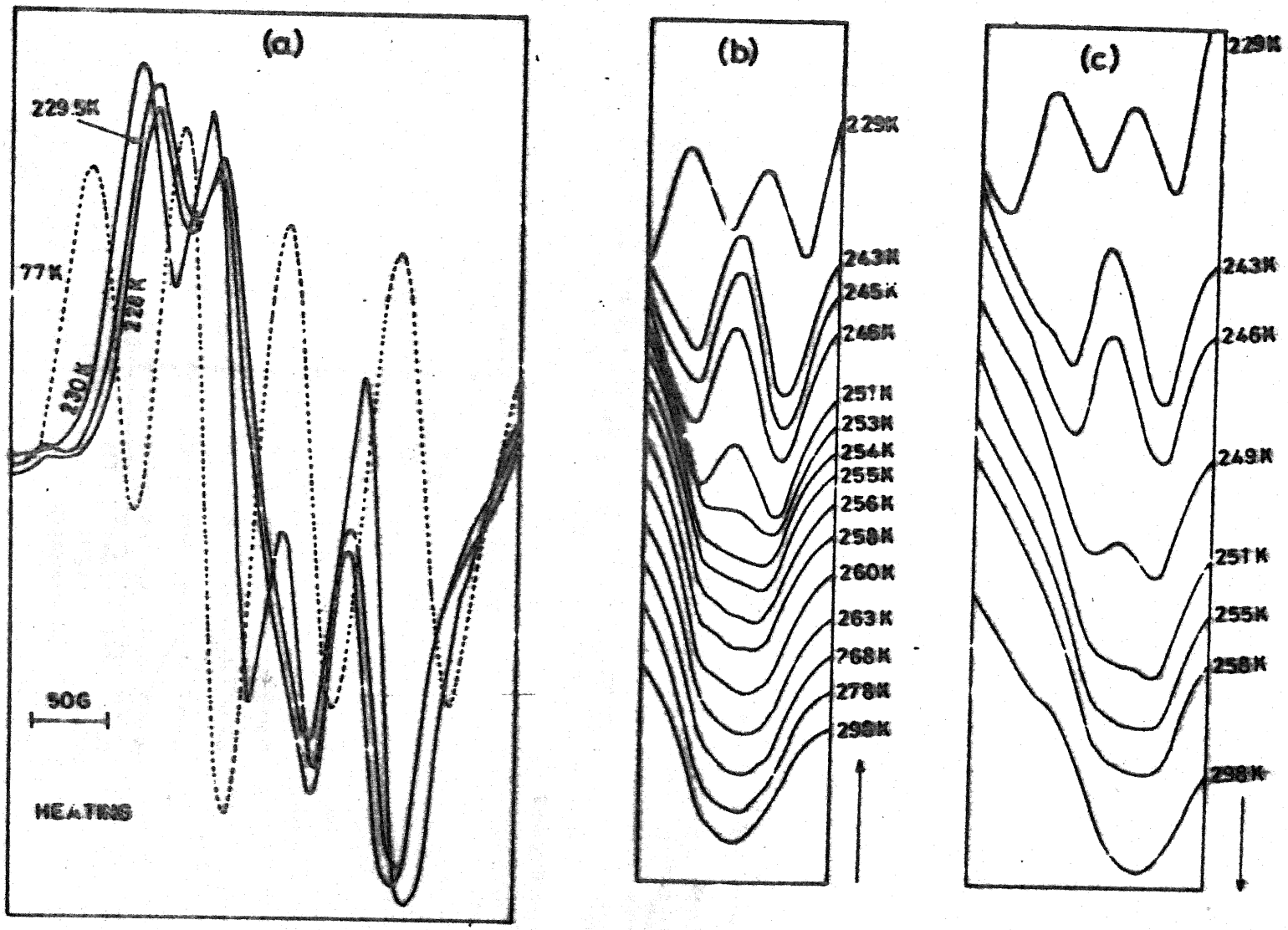

FIG. V-14 (a) A PART OF EPR SPECTRUM (⊥-PART) OF CENTRE I_2 IS SHOWN RECORDED AT DIFFERENT TEMPERATURES. AT 229·5 K MARKED CHANGES ARE OBSERVED IN THE SPECTRUM. THE SPECTRA WERE RECORDED IN A HEATING CYCLE WITH PRECOOLED SAMPLE.

(b) & (c) A PART OF THE EPR SPECTRUM OF Cu^{2+} CENTRES I_2 RECORDED IN A HEATING AND A COOLING CYCLE SHOWS CONSIDERABLE HYSTERESIS.

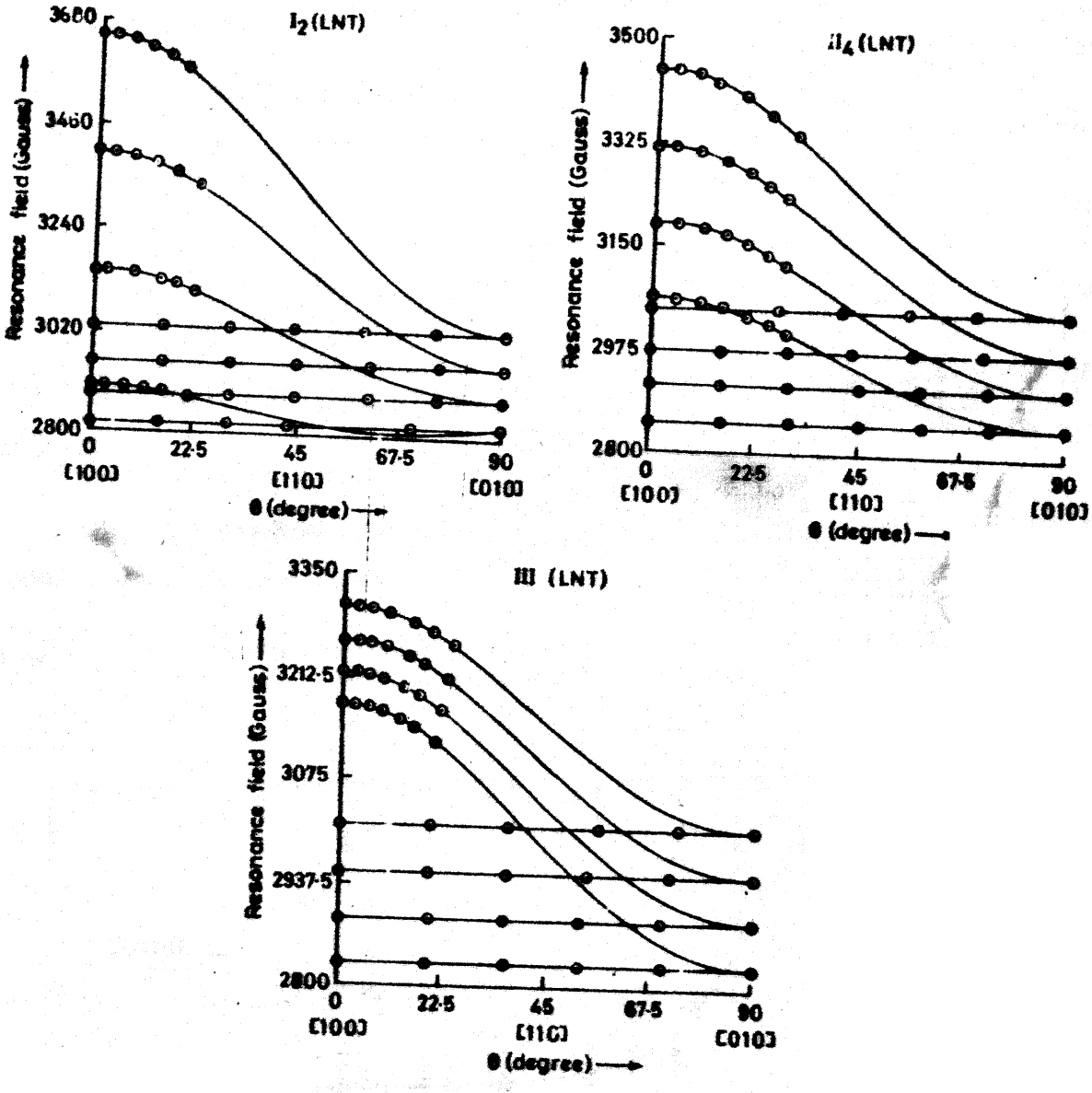

V.15 THE ANGULAR VARIATION OF EPR SPECTRA OF Cu^{2+} CENTRES I_2, II_4 & III IN NH_4I LATTICE AT LNT. THE SOLID CURVES ARE COMPUTED ONES AND CIRCLES DENOTE OBSERVED RESONANCE FIELDS. FOR CLARITY ONLY TWO COMPONENTS OF THE COMPOSITE EPR SPECTRUM ARE SHOWN.

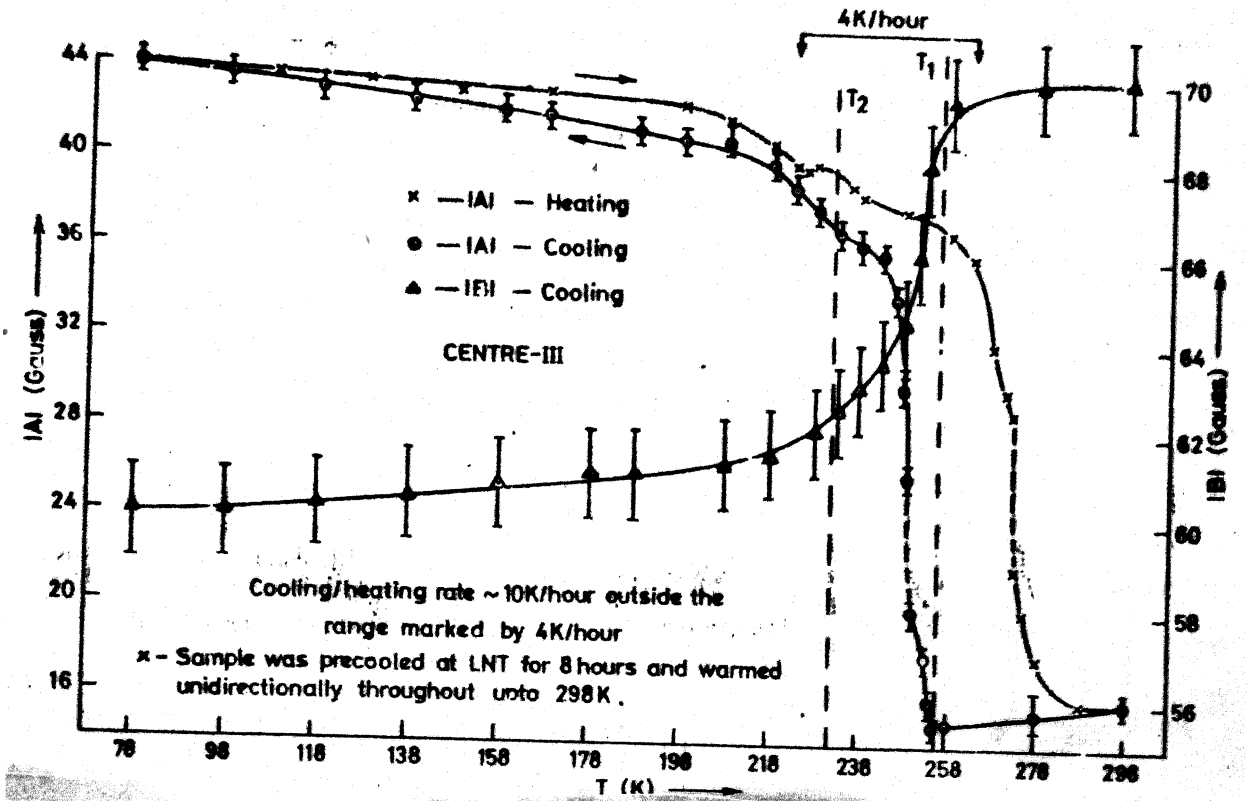

Fig.V.16 TEMPERATURE VARIATION OF |A| & |B| OF Cu^{2+} CENTRE III IN NH_4I CRYSTAL. THE VERTICAL LINES MARKED BY T_1 & T_2 SHOW THE EXPECTED TRANSITION TEMPERATURES OF NH_4I.

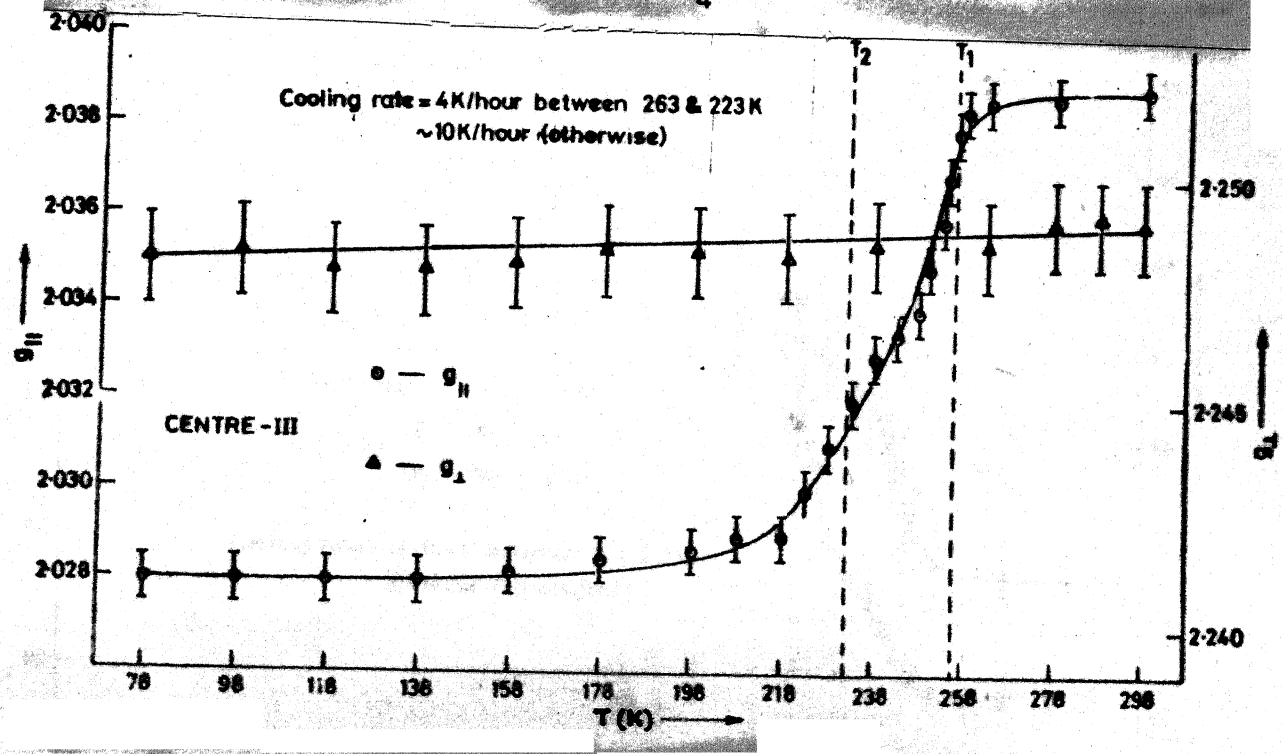

Fig.V.17 TEMPERATURE VARIATION OF g-PARAMETER OF Cu^{2+} CENTRE-III IN NH_4I. THE TWO VERTICAL LINES MARKED BY T_1 & T_2 SHOW EXPECTED TRANSITION TEMPERATURES OF NH_4I.

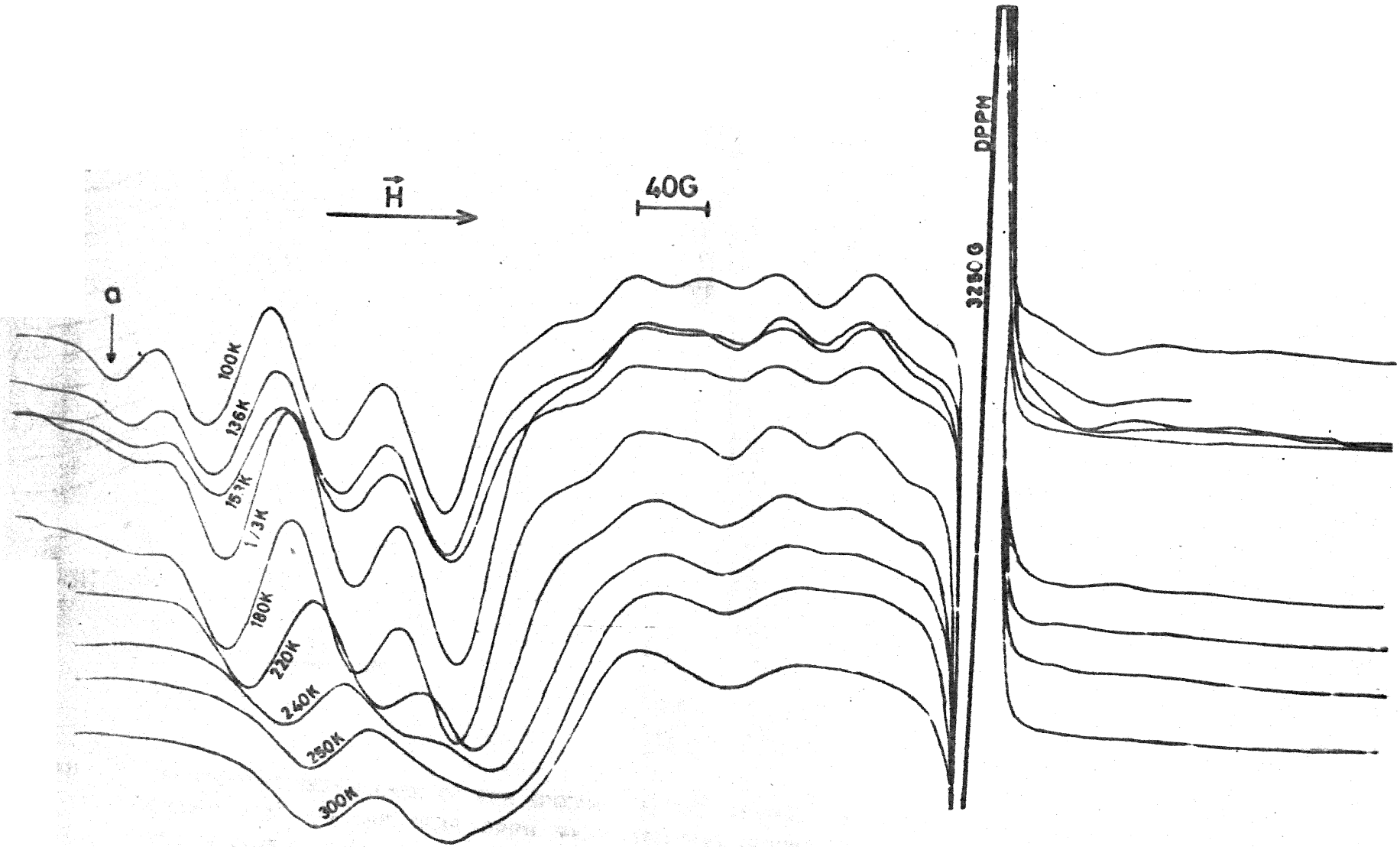

FIG.V-20 EPR SPECTRUM WHEN $\vec{H} \parallel [111]$ RECORDED AT DIFFERENT TEMPERATURES IN A COOLING EXPERIMENT. THE CRYSTAL CONTAINED ALL THE THREE CENTRES I_2,II_4 AND III IN RELATIVE PROPORTION AND THUS AT LOW TEMPERATURES MANY PEAKS ARE OBSERVED AROUND 240 K. MARKED CHANGES CAN BE SEEN IN THE SPECTRUM.

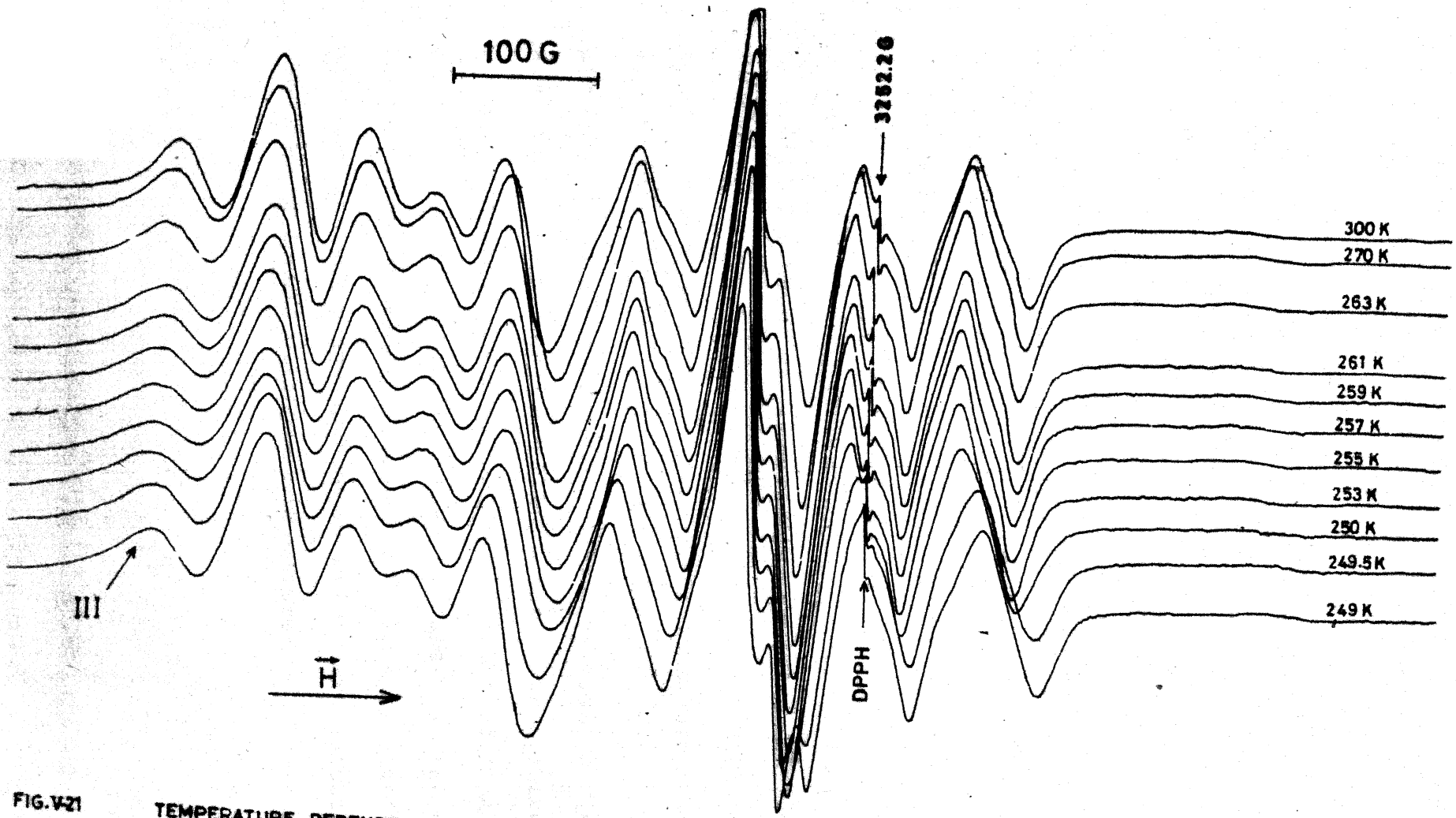

FIG.V-21 TEMPERATURE DEPENDENCE OF EPR SPECTRA OF Cu^{2+} CENTRES IN A NH_4I CRYSTAL GROWN WITH (UREA+Cr^{3+}) AS GROWTH AID. THE LINE NEAR DPPH SHOWS SPLITTING AROUND 250 K. AN ABRUPT CHANGE IN SPECTRA IS OBSERVED AT 249·5 K. THE LINE MARK III SHOWS ANOMALY IN LINE WIDTH AROUND THIS TEMPERATURE. THE CRYSTAL CONTAINS II AND III Cu^{2+} CENTRES IN COMPARABLE NUMBER WHILE I_2 CENTRES ARE RELATIVELY A FEW.

CHAPTER VI

EPR STUDY OF $NH_4I:VO^{2+}$

Abstract: Results of the EPR study of VO^{2+} doped in NH_4I single crystals in the temperature range 373K to 77K are reported. The observed spectra suggest a liquid like behaviour of VO^{2+} in ammonium iodide crystal. A single eight line isotropic spectrum with $g_o = 1.970 \pm 0.001$ and $A_o = -110 \pm 2$ Gauss was observed in the temperature range from 373K to $\cap$ 245K. No spectrum was observed in the temperature range from $\cap$ 245 to $\cap$ 173K. In the temperature range from $\cap$ 173K to 77K a spectrum with two sets of eight isotropic lines with $g_{||} = 1.948 \pm 0.001$, $g_{\perp} = 1.980 \pm 0.001$, $|A| = 190 \pm 1$ Gauss and $|B| = 68 \pm 1$ Gauss was observed. The m_I dependence and the temperature variation of line widths are discussed. The low temperature phase spectra confirm that the free tumbling motion of VO^{2+} ions is effectively hindered in this phase and these motions are effectively quenched at liquid nitrogen temperature.

I.1 INTRODUCTION

Since the first report by Sastry and Venkateswarlu[1] of liquid like behaviour of molecular vanadyl ion VO^{2+} in ammonium chloride lattice, a number of workers have reported similar behavior of VO^{2+} in many other lattices[2-6]. Host lattices where vanadyl ion undergoes rapid tumbling motion are summarised in Table VII.2 of Chapter VII. To investigate the behavior of molecular VO^{2+} ion in other ammonium halides we have, undertaken the EPR study of the system VO^{2+}:NH_4I. This system is also interesting because of the various structural phase transitions it undergoes at different temperatures below room temperature (RT)[7-9]. The EPR technique provides a sensitive probe[10] for the structural phase transitions to be observed or confirmed in case these have been observed or predicted from other studies. With these two points in mind we have carried out a detailed EPR study of VO^{2+} doped in NH_4I single crystals in the temperature range 373K to 77K at X-band.

I.2 THEORY AND SPIN-HAMILTONIAN ANALYSIS

Vanadium (Z = 23), a member of the first series transition metal group has the electron configuration $(Ar)^{18}3d^3 4s^2$. It is found to react readily to form a number of oxycations. The simplest and most stable oxycation is VO^{2+} (vanadyl ion), which may be

supposed to consist of a tetravalent vanadium ion $V^{4+}([Ar]^{18}3d^1)$ and a closed cell O^{2-} ion $([Ne]^{10})$. In this formulation the molecular VO^{2+} ion has a single unpaired d electron attached to the tetravalent vanadium ion and is similar to the other ions with d^1 configuration. However the binding with the oxygen is highly covalent and a better description involves a $(V\equiv O)^{3+}$ molecular core with a partial covalent triple bond character, to which a single unpaired electron is added in a $^2\Delta$ non-bonding orbital. The non-bonding orbital which lies in the plane perpendicular to the V-O bond, is centred on the vanadium ion. The description of the molecular ion VO^{2+}, based on an LCAO-MO calculation of the complex $(VO(H_2O)_5)^{2+}$ by Ballhausen and Gray[11], has shown that the d^1 electron occupies a non-bonding orbital of b_2 symmetry, and the resulting ground state is an orbital singlet. Thus for a single unpaired electron (S = 1/2) interacting with a single vanadium nucleous (^{51}V, I = 7/2, 99.8 percent abundant) the EPR spectrum may be described by the following Hamiltonian[12], neglecting the quadrupole and nuclear-zeeman interaction:

$$\mathcal{H} = \beta \vec{H}.\tilde{g}.\vec{S} + \vec{S}.\tilde{A}.\vec{I} \qquad \ldots \quad \text{VII.1}$$

with S = 1/2 and I = 7/2 and the other symbols having their usual meaning. The resonance field values of the above Hamiltonian, under the assumption that the principal axes of $\tilde{g}$ and $\tilde{A}$ coincide, have been calculated by Abragam and Bleany[12] and by Bleany[13]. For the case of axial symmetry the resonance field values are given by the following relations :

$$H_{m_I} = H_o - Km_I - \left[\left(\frac{63}{4} - m_I^2\right)\right] \frac{B^2(A + K^2)}{4H_oK^2} +$$

$$- \frac{(A^2 - B^2)g_{\parallel}^2 g_{\perp}^2}{8H_oK^2g^4} \sin^2 2\theta \qquad \ldots \quad (VI.2)$$

where

$$H_o = \frac{h\nu}{g\beta}$$

$$g^2 = g_{\parallel}^2 \cos^2\theta + g_{\perp}^2 \sin^2\theta$$

$$K^2g^2 = A^2g_{\parallel}^2 \cos^2\theta + B^2g_{\perp}^2 \cdot \sin^2\theta$$

and θ is the angle between the symmetry axis i.e. the Z-axis and the Z static magnetic field $\vec{H}$. The parameters K, A and B are in units of gauss.

For a tumbling molecular ion averaging out all orientations results in an isotropic spectrum with effective g and A values given as[14-16]:

$$g_{eff} = g_o = \frac{1}{3}\sum_{i=1}^{3} g_{ii} = \frac{1}{3}(g_{\parallel} + 2g_{\perp}) \qquad \ldots \quad (VI.3)$$

$$A_{eff} = A_o = \frac{1}{3}\sum_{i=1}^{3} A_{ii} = \frac{1}{3}(A + 2B)$$

The resonance field values for this isotropic spectrum are given by:

$$H_{m_I} = H_o - A_om_I - \frac{A_o^2}{8H_o}\left(\frac{63}{4} - 4m_I^2\right) \qquad \ldots \quad (VI.4)$$

where $H_o\left(= \frac{h\nu}{g_o\beta}\right)$ and A_o are in units of gauss.

I.3 EXPERIMENTAL RESULTS

The EPR spectra of vanadyl ion doped in NH_4I single crystal at different temperatures are shown in Fig. VII.1. The RT spectrum consists of eight hyperfine lines with unequal spacings. This spectrum will be designated as spectrum-I, hereafter. The line widths and peak heights of the lines of spectrum-I were found to depend upon the nuclear magnetic quantum number m_I. This spectrum was found to be independent of the crystal orientation relative to the static magnetic field. The spectra from crystals doped with $VOCl_2$ or $VOSO_4.6H_2O$ were identical. To rule out the possibility of inclusion of $VOCl_2$ or $VOSO_4$ solution in the crystals, the crystals were annealed at $\sim 130^{\circ}C$ for three hours and then cooled quickly to RT or were quenched by dropping into liquid nitrogen. The EPR of the heat treated crystals were found to be identical with those from as-grown crystals, thus ruling out the possibility of inclusion of $VOCl_2$ or $VOSO_4$ solution in the crystals. All the crystals grown at RT or higher temperatures (upto 333K) from acidic, basic or neutral mother solutions gave identical spectra.

As the temperature was raised above RT though the linewidths decreased, the over all intensity of the spectrum started diminishing. At $\sim$ 340K the spectrum almost vanished. The linewidth measurements could be carried out satisfactorily only upto 325K. Similar behavior was observed for $VO^{2+}:NH_4Cl$ by Rao and Sastry[1].

On lowering the temperature below RT the lines showed a broadening trend. Due to the broadening of the lines the derivative heights were reduced. The broadening trend became faster at about 255K and spectrum-I disappeared completely at $\sim$ 245K. For spectrum-I, Fig. VI.2 shows the m_I dependence of linewidths and temperature dependence of linewidth for the $m_I = -1/2$ line.

On further lowering the temperature below 245K no spectrum appeared upto $\sim$ 173K. Below this temperature some weak structure started showing up slowly with decreasing temperature. This low temperature spectrum will be designated as spectrum-II. To get the changes stabilized at each temperature we waited quite long ($\sim$1 hour). The weak structure appearing below 173K became quite strong in intensity as liquid nitrogen temperature (LNT) was approached. At LNT spectrum-II became quite strong. The samples were kept at LNT for about three hours and the spectra were observed at different orientations of the crystal relative to the static magnetic field. Spectrum-II was found to be completely isotropic. As can be seen in Fig. VII.1, spectrum-II at LNT comprises two sets of hyperfine groups of eight lines each, overlapping with each other in the middle part of the spectrum. The two parts of the spectrum are designated as parallel-spectrum and perpendicular-spectrum. The parallel-spectrum has a larger spread compared to the perpendicular-spectrum. On reversing the process of cooling i.e. heating the crystal from LNT upwards the changes in the spectrum were found to be reversible. The temperature at which spectrum-I reappears or disappears depends on the rate of heating or cooling respectively. The faster the cooling and heating rate in a cycle, the

larger is the hysteresis width. On returning to RT the eight line isotropic spectrum was recovered.

The spin-Hamiltonian parameters (SHP) for spectrum-II at LNT were calculated using field expressions (VI.2) and setting $\theta = 0^{o}$ for parallel-spectrum and $\theta = 90^{o}$ for perpendicular-spectrum respectively. The SHP for spectrum-I were obtained using expression (VI.4). The parameters thus obtained were next varied in a narrow range to obtain the least squared deviation in the experimental fields and those calculated by the exact numerical diagonalization of the 16x16 spin-Hamiltonian matrix on a computer. The parameters thus obtained are given in Table VI.1.

I.4 DISCUSSION

The observed spectrum I and II of VO^{2+} in NH_4I are very similar to the spectra of vanadyl ion in liquids of low and high viscosity[16-19] respectively. Similar spectra were reported by O'Reilly[16] and Roberts et al[17] of vanadyl etioporphyrin II (VEPI) in benzene (low viscosity) and in castor oil (high viscosity) at 293K and in solid asphaltenes containing vanadium porphirins. These similarities help in the understanding of the EPR spectra of vanadyl ion in NH_4I. Spectra similar to our spectrum-II have been reported in polycrystalline samples[20-22] containing VO^{2+} ions with preferred V-O bond orientation and in amorphous glass[23]. The observation that spectrum-I in VO^{2+} doped NH_4I is recovered on returning back to RT from LNT rules out the possibility of the V-O orientation becoming preferential and at the same time the sample becoming polycrystalline. We thus conclude that at RT VO^{2+} ions

in NH_4I lattice are subjected to hindered motions in a manner similar to VO^{2+} ions in liquids of low viscosity where they are rapidly tumbling so that all the anisotropy in g and A is averaged out. Drastic changes in the EPR spectrum can occur when the paramagnetic entity is immobilized compared with the spectrum when the paramagnetic entity is tumbling rapidly in solution. The reason for these changes lies, of course, in the fact that the anisotropic contributions to the g-factor and hyperfine splittings are averaged out in the latter case and because only angular distributions contribute in the former case. This is the reason why VO^{2+} in castor oil, which hinders the V-O tumbling almost completely due to its high viscosity, gives a solid like spectrum showing g and A anisotropies. Thus, we believe that the low temperature phases of NH_4I - CsCl type and PH_4I type-hinder the freely tumbling motion of VO^{2+} ions and near LNT these motions are effectively quenched just like in a liquid of very high viscosity. Therefore, at LNT the V-O orientation is random and its tumbling motion is slow enough that the anisotropic interactions also contribute to the spectrum. If the rotational correlation time for the magnetic entity is sufficiently long compared to the reciprocal of the spread of the spectrum in time, the spin-Hamiltonian (VI.1) remains anisotropic and it may be used with a suitable average of allowed transitions over all orientations. The isotropy of spectrum-II is explained on the basis of the statistical distribution of the V-O axis orientation in the host lattice, just like in powders, which makes the spectrum angular independent. The similarity of spectrum-II with those of powder spectra of samples

containing a preferred V-O axis is thus obvious. The powder spectrum also arises from a statistical distribution of the randomly oriented VO^{2+} ions in the crystal lattice[12,24,25]. The extreme positions of the lines in a powder spectrum correspond to two turning points i.e. to parallel (//) and perpendicular ($\perp$) orientations. In a statistical distribution the number of V-O axes parallel to the static magnetic field will be one-half that of the number of V-O axes perpendicular to the static magnetic field. Thus, the intensity due to magnetic centres with the V-O bond perpendicular to the magnetic field will be twice that due to the centres with V-O bond parallel to the magnetic field. Figure VI.1 shows spectrum-II at LNT where the parallel and perpendicular spectra have been marked on the basis of their expected relative intensities. O'Reilly[16] has obtained the eigen values of the spin-Hamiltonian (VI.1) by perturbation theory and the resulting line shapes for each value of m_I for $g\beta H \gg A,B$. As for the isotropic spectrum-I, $g_o = \frac{1}{3}(g_{//} + 2g_{\perp})$ and $A_o = \frac{1}{3}(A + 2B)$ are expected on the basis of rapidly tumbling V-O axis; the values of g_o and A_o obtained from the SHP of spectrum-II are in agreement with the values obtained directly from the spin-Hamiltonian analysis of spectrum-I (see Table VI.1).

Due to the isotropy of spectrum-I it is difficult to decide about the type of magnetic entity and the associated lattice defects in VO^{2+} doped NH_4I crystals. However the crystalline field or the motions of the NH_4^+ ions seem to affect the tumbling motion of VO^{2+} ions. Consequently the line widths of the spectrum-I change drastically near the structural phase transformations - NaCl structure $\longleftrightarrow$ CsCl structure.

The present study clearly indicates that VO^{2+} in NH_4I exhibits a behaviour like that in liquids, so far as the paramagnetic resonance and relaxation are concerned. The line widths of the EPR spectrum-I are found to show m_I dependence. It was felt interesting, therefore, to carry out a systematic study of line widths to test the applicability of Kivelson's theory[26] of paramagnetic relaxation in liquids to the present case.

A detailed discussion of the relaxation mechanisms has been given by Kivelson and others,[26-29] and the resulting expression for line widths is :

$$(\Delta H)_{m_I} = \left(\frac{1}{T_2}\right)_{m_I} = A_1 + A_2 m_I + A_3 m_I^2 + A_4 m_I^3 + A_5 m_I^4 \quad \ldots \text{(VI-5)}$$

Since the fourth and fifth terms in (VI-5) are usually found to be small we will neglect these. In the limit of rapid tumbling the coefficients A_i are related to the SHP by the following relations[30]:

$$A_1 = \frac{1}{T_{20}} + \frac{2}{15}(\Delta g)^2 \left(\frac{H_o}{\hbar}\right)^2 \tau_c + \frac{1}{20}(\Delta a)^2 I(I+1)\tau_c$$

$$A_2 = -\frac{4}{15}\left(\frac{H_o}{\hbar}\right)(\Delta g \Delta a)\tau_c \qquad \ldots \text{(VI-6)}$$

$$A_3 = \frac{1}{12}(\Delta a)^2 \tau_c$$

where $\frac{1}{T_{20}}$ is the line width from other interactions non-sensitive to nuclear orientations m_I, $H_o = \frac{h\nu}{g\beta}$, $(\Delta a)^2 = \sum_{i=1}^{3}(A_{ii} - A_o)^2$, $(\Delta g \Delta a) = \sum_{i=1}^{3}(A_{ii} - A_o)(g_{ii} - g_o)$ and τ_c is the rotational correlation time.

The experimental line widths of spectrum-I at RT were determined by using the relation $h_{m_I} \times (\Delta H_{m_I})^2 = \text{constant}$, where h_{m_I} is the derivative height and ΔH_{m_I} the peak-to-peak (p-p) line width. The p-p line width for the narrowest line ($m_I = -1/2$) was measured directly and the p-p widths of other lines were computed by using the above relation. Fig. VI-2 shows the observed m_I dependence of line width. By fitting the experimental data to equation VI-5 after setting $A_4 = A_5 = 0$ and using a least square method, the following values of the A 's were obtained :

$A_1 = 19.037$ Gausss, $A_2 = 1.999$ Gauss, $A_3 = 1.93$ Gauss.

Making use of the value of A_3 and the spin-Hamiltonian parameters of spectrum-II, τ_c and the ratio A_2/A_3 were estimated through relations (VI-6) and were found to be $\sim 10^{-11}$ sec. and 8.6 respectively. The estimated ratio (A_2/A_3) was found to be in disagreement with that obtained from the experimental values of A_i. A similar disagreement was also found fromsuch an analysis by Kivelson[26] for the data of O'Reilly[16] for VEPI in low and high viscosity solutions and by other workers[1-4]. We have estimated the ratio A_2/A_3 for different systems through relation (VI-7) and making use of the reported spin-Hamiltonian parameters[1-4] and these are given in Table VI-2 for comparison. As the low temperature g and A values are found to satisfy relations (VI-3) at room temperature, the g and A parameters are not expected to have an appreciable temperature dependence and the disagreement in the ratio, A_2/A_3 may be due to factors other than the temperature

dependence of g and A. The ratio A_2/A_3 is fairly constant over the temperature range over which liquid like behaviour is observed.

O'Reilly[16] and Kivelson[26] estimated τ_c for vanadyl complex in benzene solution to be of the order of 6×10^{-11} sec. The typical value of τ_c for liquids is found to vary from 2×10^{-11} sec. to 8×10^{-11} sec. The estimated value $\sim 1\times10^{-11}$ sec. of τ_c in the present case of VO^{2+} in NH_4I supports the assumption that vanadyl ion in NH_4I exhibits a behaviour like that in liquids. Therefore, the theory of line widths in liquids appears adequate to explain the observed effects in VO^{2+} doped NH_4I crystal. At low temperatures the tumbling of the molecular ion VO^{2+} gets hindered indicating that the viscosity of NH_4I for vanadyl ions becomes very high at low temperatures compared to that at room temperature.

To get some qualitative idea of the temperature dependence of the correlation time τ_c the temperature dependence of $\Delta H_{-\frac{1}{2}}$ has been studied. Fig. VI-2 shows this temperature dependence in the temperature range for which satisfactory measurements of p-p line width could be made. As is clear from Fig. VI-2 the line width increases on lowering the temperature. The increase may be assumed to be largely due to an increase in the rotational correlation time τ_c because the dominant relaxation process in viscous media is attributable to the modulation of anisotropic magnetic interactions by the rotational motion of the ions. It has been observed that the line broadening trend shows a little discontinuity around 256K, which incidently is the transition temperature between phase I and phase II. Thus the discontinuity appearing in τ_c may be attributed to the structural phase transition at

$\sim$256K. Since no discernible spectrum was observed around the transition temperature between phase II (CsCl) and phase III (tetragonal) this transition could not be studied.

Recently Goyal and Dasanacharya[31] carried out neutron scattering experiments on NH_4I and found that both on cooling and heating phase I coexists with the low temperature phases II and III. Their results are supported by the observation of large thermal hysteresis[32,33] for the transition 256K both while cooling and while heating. The existence of mixed phases calls for great care in interpreting any data on NH_4I in the temperature range 200K to 300K. Their estimated concentrations of NaCl and CsCl phases were respectively found to be 61% and 39% at 240K and 35% and 65% at 220K in a typical cooling experiment. Their data have shown that the sample takes several hours to stabilize in the mixed phase which depends on the rates of cooling and heating. We have also observed a hysteresis in the temperatures at which spectrum-I disappears and reappears on cooling and heating respectively. This is consistent with the hypothesis of coexisting phases. Also, our observation that it takes a long time to achieve the maximum intensity of the spectra at temperatures below $\sim$256K on cooling and at temperatures above $\sim$173K on heating supports the view that the equilibrium between the mixed phases is achieved after a long time.

REFERENCE

1. M.D. Sastry and P. Venkateswarlu, Mol. Phys. 13, 161 (1967); K.V.S. Rao and M.D. Sastry, Chem. Phys. Lett. 2, 20 (1968).
2. A.V. Jagannadham and P. Venkateswarlu, Proc. Ind. Acad. Sci. 69A, 307 (1969).
3. K.V.S. Rao, M.D. Sastry and P. Venkateswarlu, J. Chem. Phys. 49, 1714 (1968), J. Chem. Phys. 52, 4035 (1970).
4. S. Radhakrishna, B.V.R. Chowdari and A. Kasiviswanath, J. Phys. Soc. Japan 41, 1530 (1976).
5. M.V. Krishnamurthy, J. Phys. Chem. Solids 33, 1645 (1972).
6. Y. Tomkiewicz, S. Saito and M. Fujimoto, J. Magn. Reson. 8, 188 (1972).
7. R.W.G. Wycoff, 'Crystal Structure', Vol. 1, Inter Science Publishers (1968).
8. H.A. Levey and S.W. Peterson, J. Am. Chem. Soc. 75, 1536 (1953)
9. C.N.R. Rao and M. Natarajan, Crystal Structure Transformation in Binary Halides, NSRDS-NBS 41 (1972).
10. F.J. Owens, C.P. Poole (Jr) and H.A. Farac, 'Magnetic Resonance of Phase Transitions', Academic Press (1979).
11. C.J. Ballhausen and B.H. Gray, Inorg. Chem. 1, 111 (1962).
12. A. Abragam and B. Bleany, 'Electron Paramagnetic Resonance of Transition Ions', Oxford University Press (1970).
13. B. Bleany, Phil. Mag. 42, 447 (1951).
14. H.M. McConnel, J. Chem. Phys. 25, 709 (1956).
15. R.M. Golding, 'Applied Wave Mechanics', D. Van Nostrand Co. Ltd., (1969).
16. D.E. O'Reilly, J. Chem. Phys. 29, 1188 (1958).
17. E.M. Roberts, W.S. Koski and W.S. Caughey, J. Chem. Phys. 34, 591 (1961).
18. R.N. Rogers and G.E. Pake, J. Chem. Phys. 33, 1107 (1960).

19. P.W.D. Boyd, T.D. Smith, J.H. Price and J.R. Pilbrow, J. Chem. Phys. 56, 1253 (1972).

20. R. Borcherts and C. Kikuchi, J. Chem. Phys. 40, 2270 (1964).

21. Keh-Chang Chu, J. Magn. Reson. 21, 151 (1976).

22. R.S. Saraswat and G.C. Upreti, J. Phys. Soc. Japan, 44, 1142 (1978).

23. G. Hochstrasser, Phys. Chem. Glasses, 7, 178 (1966).

24. R.H. Sands, Phys. Rev. 99, 1222 (1955).

25. F.K. Kneubuhl, J. Chem. Phys. 33, 1074 (1960).

26. D. Kivelson, J. Chem. Phys. 27, 1087 (1957); J. Chem. Phys. 33, 1044 (1960); J. Chem. Phys. 45, 1324 (1966).

27. R. Wilson and D. Kivelson, J. Chem. Phys. 44, 154, 4440 (1966); P.W. Atkins and D. Kivelson, J. Chem. Phys. 44, 169 (1966).

28. R.N. Rogers and G.E. Pake, J. Chem. Phys. 33, 1107.

29. McConnell, J. Chem. Phys. 25, 709 (1956).

30. C.P. Poole (Jr) and H.A. Farach, 'Relaxation in Magnetic Resonance', Academic Press (1971).

31. P.S. Goyal and B.A. Dasannacharya, J. Phys. C : Solid Sta. Phys. 12, 209 (1979).

32. A.R. Sharp and M.M. Pintar, Chem. Phys. 15, 431 (1976).

33. M. Couzi, J.B. Sokoloff and C.H. Perry, J. Chem. Phys. 58, 2965 (1973).

TABLE VI.1

Spin-Hamiltonian Parameters of VO^{2+} in NH_4I obtained from analysis of spectrum-I and spectrum-II

	Spin-Hamiltonian Parameters	
Spectrum-I (RT)	$g_o = 1.970(1)$	$\|A_o\| = 110(2)$ Gauss
Spectrum-II (LNT)	$g_{\parallel} = 1.948(1)$	$g_{\perp} = 1.980(1)$
	$\|A\| = 190(1)$ Gauss	$\|B\| = 68(1)$ Gauss
Calculated from Spin-Hamiltonian Parameters of Spectrum-II	$g_o = 1.969$	$\|A_o\| = 108.7$ Gauss
	$g_o = \frac{1}{3}(g_{\parallel} + g_{\perp})$	$A_o = \frac{1}{3}(\|A\| + \|B\|)$

TABLE VI.2

Ratio (A_2/A_3) calculated $(A_2/A_3)_{Cal.}$ from analytical expressions and $(A_2/A_3)_{LW}$ from line widths analysis of EPR spectrum-I of VO^{2+}.

System	$(A_2/A_3)_{LW}$	$(A_2/A_3)_{Cal.}$	Reference
NH_4I	1.7	8.6	Present work
NH_4Br	1.5	14.0	Present work (Chap.VII)
NH_4Cl	1.5	15.2	1
NaCl	1.9	19.5	2
KCl	2.4	14.8	2
RbCl	2.3	7.2	2
KNO_3	2.0	10.5	3
$CsNO_3$	2.8	14.3	3
$NaNO_3$	3.4	6.0	3
NH_4NO_3	2.2	8.6	3
$Ba(NO_3)_2$	1.3	17.8	3
$UO_2(NO_3)_2.6H_2O$	2.5	9.5	5
$BaCl_2.2H_2O$	1.8	21.6	4
$BaBr_2.2H_2O$	1.9	7.9	4

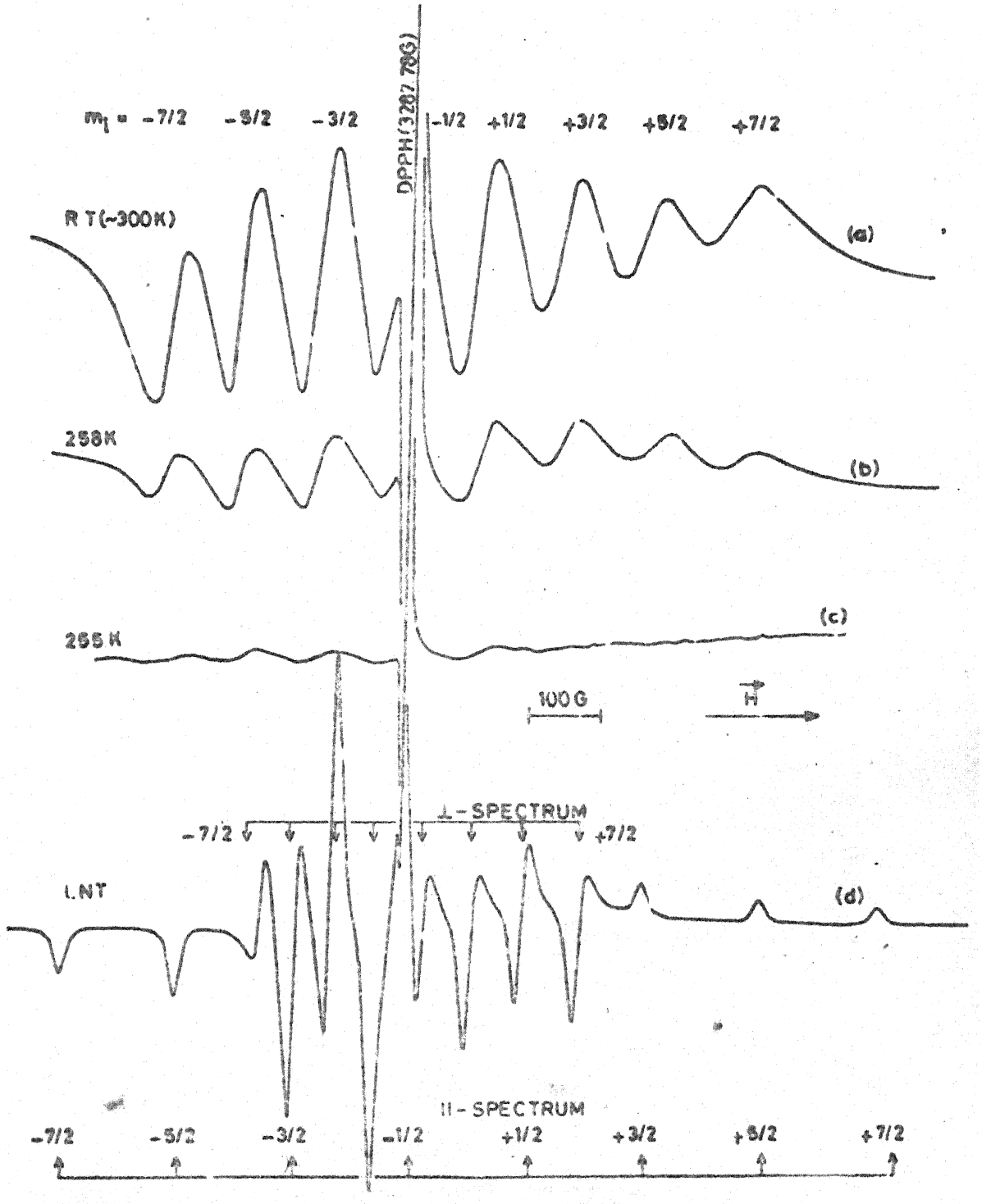

Fig. VI.1 THE X-BAND EPR SPECTRA OF VO^{2+} DOPED IN NH_4I SINGLE CRYSTALS AT DIFFERENT TEMPERATURES.

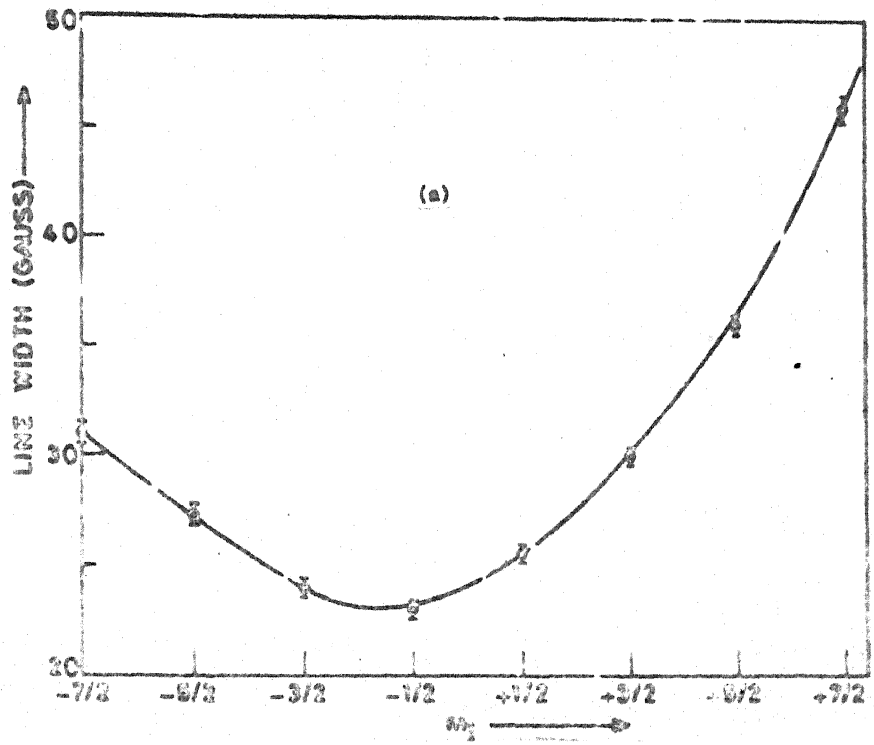

Fig. VI.2a THE m_I DEPENDENCE OF THE WIDTHS OF VO^{2+} RESONANCE LINES IN NH_4I SINGLE CRYSTAL AT 300K. THE EXPERIMENTAL POINTS ARE MARKED BY OPEN CIRCLES. THE SOLID LINE IS A SMOOTH CURVE DRAWN THROUGH THE EXPERIMENTAL POINTS.

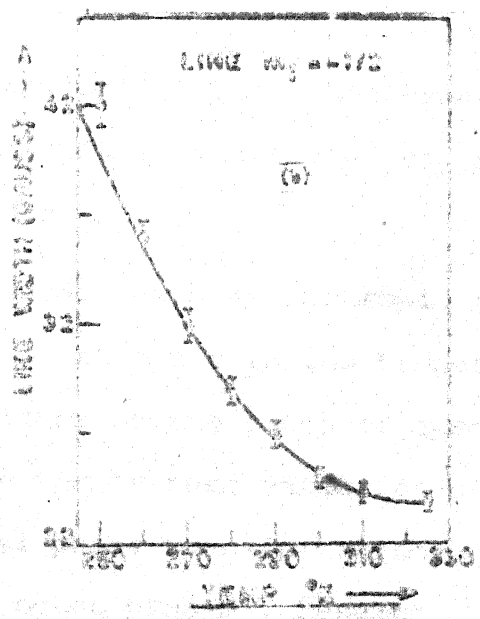

Fig. VI.2b THE TEMPERATURE DEPENDENCE OF THE WIDTH OF THE m_I= -1/2 RESONANCE LINE OF VO^{2+} IN NH_4I SINGLE CRYSTAL. THE EXPERIMENTAL POINTS ARE MARKED BY OPEN CIRCLES. THE SOLID LINE IS A SMOOTH CURVE DRAWN THROUGH THE EXPERIMENTAL POINTS.

CHAPTER VII

EPR STUDY OF $NH_4Br:Mn^{2+}$ AND $NH_4Br:VO^{2+}$

Abstract: The results of EPR study of Mn^{2+} and VO^{2+} ions doped in single crystals of NH_4Br in the temperature range 77 to 500K are presented. At RT an isotropic spectrum (spectrum-I) comprising a sextet superimposed on a broad line is observed from crystals doped with Mn^{2+}. On heating the crystal around 400K the single sextet disappears due to expulsion of Mn^{2+} impurity from crystal. On lowering the temperature of the crystal below RT, the isotropic spectrum-I disappears around 230K and a new spectrum (spectrum-II) appears below this temperature. The spectrum-II is very anisotropic and unusual. Spectrum-I is attributed to the Mn^{2+} ions substituting for NH_4^+, with the charge compensating NH_4^+ vacancies far away from Mn^{2+}. The transformation of spectrum-I to spectrum-II around 230K is attributed to a structural phase transformation of NH_4Br.

VO^{2+} doped crystals gave an isotropic spectrum (spectrum-I) comprising an octet in the temperature range 430K to 230K. The widths of the lines of spectrum-I show a m_I dependence. The temperature variation of line width reveals two structural phase transformations at 408K and 230K. The isotropic octet probably results from a rapid tumbling motion of VO^{2+} ions. The low temperature phase of NH_4Br appears to hinder the tumbling motion of VO^{2+} and as a result a new isotropic (spectrum-II) comprising two octets is observed.

VII.1 INTRODUCTION

The detailed EPR studies of Mn^{2+}, Cu^{2+} and VO^{2+} in NH_4I (presented in Chapters IV, V and VI respectively in this thesis) and in NH_4Cl (reported by a number of workers[1-15]) also of Cu^{2+} in NH_4Br[15,16] have yielded enough information regarding the behaviour of these ions. It may be concluded that these ions showed more or less similar behaviour in the two members viz. NH_4Cl and NH_4I while in NH_4Br only Cu^{2+} ion has so far been studied[15,16] and showed a behaviour similar to that in NH_4Cl and NH_4I. No report of EPR of Mn^{2+} in NH_4Br is made till date except for the unpublished work of Sastry[17]. It was, therefore, felt interesting to carry out the EPR study of Mn^{2+} and VO^{2+} in NH_4Br on a complementary basis. It has been reported that Mn^{2+} in CsCl showed a large zero field splitting[4] and Mn^{2+} in CsBr showed exceptionally large zero-field splitting[18] ($D \sim 4$ kG) which apparently is in violation to the spectrochemical series ($Cl^- > Br^- > I^-$). We note that for Mn^{2+} in both NH_4Cl and NH_4I the value of zerofield splitting parameter D is almost equal ($D \sim 1605$ G in NH_4Cl[7] at 300 K and $D \sim 1612$ G in NH_4I at 300 K). In the unpublished work of Sastry[17] it has been mentioned that for Mn^{2+} in NH_4Br $D \sim 538$ G at LNT. It was somewhat surprising that while in Cs-hallides zerofield splitting increased from Cl to Br being

exceptionally large for CsBr, why NH_4Br behaved differently as compared to other ammonium hallides. Therefore a systematic EPR study of Mn^{2+}:NH_4Br was carried out in the temperature range of 573K to 77K. To complete the study of VO^{2+} in ammonium halides, VO^{2+} doped in NH_4Br has also been studied systematically by EPR in the temperature range mentioned above. The EPR studies of Mn^{2+} and VO^{2+} in NH_4Br single crystals will be presented separately in the following.

SECTION A : EPR OF Mn^{2+} IN NH_4Br

EXPERIMENTAL RESULTS

The EPR spectra were recorded on X-band EPR spectrometer E-109 described in Chapter III. Crystals grown under different conditions were studied and it was observed that the temperature or pH of the mother liquor had no effect on the type of magnetic centres incorporated in NH_4Br crystals. However the line widths were comparatively larger in crystals either grown at relatively higher temperature ($\sim$350K) or grown from solution containing higher amount of $MnBr_2$ ($\sim$3% by weight). The incorporation of Mn^{2+} ions in NH_4Br was found to be much less than in NH_4Cl and NH_4I, grown under similar conditions.

At RT ($\sim$300K) the EPR spectrum comprises a sextet (referred to as spectrum-I) which is found to be isotropic superimposed on a broad line (Fig. VII.1). When the temperature of the sample was raised above RT the line width of the members of this sextet decreased slightly and around 400K the intensity of

the sextet decreased suddenly. On keeping the sample at 400K for longer time the sextet-structure disappeared leaving behind a sharp single line, similar to the one observed for Mn^{2+} in NH_4I at elevated temperatures. On physical examination it was found that though the crystal was still intact its surfaces were blackened due to the expulsion of Mn^{2+} impurity. This black material was found to give an EPR signal with line width and g-value similar to that from the material expelled from Mn^{2+} doped NH_4I lattice at higher temperatures. The heated crystal after cleaning its black surfaces did not give any discernible spectrum upto LNT.

On lowering the sample temperature below RT the peak to peak height of the sextet structure decreased and around 230K the sextet disappeared completely. The temperature dependence of p-p signal height is shown in Fig. VII.2. Around 223K a new spectrum (referred to as spectrum-II), highly anisotropic in nature and somewhat abnormal in structure (not showing the characteristic five hyperfine groups) started showing up. The intensity of this spectrum increased with the lowering of the temperature of the sample and at LNT it was quite intense. The transformation of the isotropic spectrum-I into the anisotropic spectrum-II was found to be reversible. The observed angular behaviour of the spectrum-II was same in the temperature range 223K to 77K. The angular dependence at LNT of the EPR spectra in (100) plane is shown in Fig. VII.3. The angular dependence in other planes was found to be more complicated. It can be seen clearly that two

sextets marked A and B are angular independent in this plane while the other sextets are extremely angular dependent both in their intensity and position. The overall symmetry of the EPR spectrum was observed to be 4-fold with $\vec{H}$ rotating in (100) plane and 2-fold with $\vec{H}$ rotating in (110) plane. It has not been possible to find out the crystal field axes (X,Y,Z) explicitly in this case because of the complexity of the EPR spectrum at X-band, but it seems reasonable to assume (100) as the tetragonal axis of the crystalline field. The Q-band studies at low temperatures were not possible due to nonavailability of the facility. However such study would give more and unambiguous information regarding the speculation of large ZFS and tetragonal symmetry derived from X-band observation.

2 DISCUSSION

The crystal structure of NH_4Br in the four phases may be summarized as follows:

Phase I (NaCl-disordered) $\xleftarrow{410\ K}$ Phase II (CsCl-disordered) $\xleftarrow{235\ K}$ λ-Transition Phase III (PH_4I) (Tetragonal)

Phase III (PH_4I) (Tetragonal) $\xrightarrow{78\ K}$ Phase IV (CsCl-ordered)

Phase III (PH_4I) (Tetragonal) $\xleftarrow{108\ K}$ Phase IV (CsCl-ordered)

When doped, Mn^{2+} ions can enter the NH_4Br lattice in several ways - it can substitute for NH_4^+ just like Mn^{2+} in CsCl[18] or it can enter at interstitial site coplanar with four Br^- ions just like Cu^{2+} and Mn^{2+} in NH_4Cl[2,4,7,11] and Cu^{2+} in NH_4Br[14] or it can be present in small clusters. In cases of both substitutional or

interstitial incorporation of Mn^{2+} in NH_4Br lattice creation of cation vacancies is necessary for overall charge compensation. If the vacancies are close to the metal ion they become bound and form ion-vacancy pairs. In such cases normally the cubic crystalline field becomes tetragonally distorted[2-4] and if this distortion is not exceptionally large to cause a large zerofield splitting, Mn^{2+} should show a characteristic 30 line spectrum even at X-band frequencies. In the present case of NH_4Br with CsCl structure at RT three distinguishable tetragonal axes viz. [100], [010] and [001] are possible if the paired off vacancies lie along these directions. Thus as in the case of Mn^{2+} in NH_4I (Chapter IV) when $\vec{H}$ is aligned parallel to Z-axis i.e. $\theta = 0$ there should be one 30 line spectrum corresponding to centres for which $\theta = 0$ and simultaneously another 30 line spectrum corresponding to centres for which $\theta = 90^{\circ}$. When $\vec{H}$ is rotated from $\theta = 0$ to $\theta = 90^{\circ}$ in (100) $\vec{H}$ would be always at $\theta = 90^{\circ}$ for one set of centres while it will make angles θ and $(90-\theta)$ with the tetragonal axes of the other two sets of centres. Therefore, there should be an angular independent 30 line spectrum and two other spectra which should interchange their positions on going from $\theta = 0$ to $\theta = 90^{\circ}$. If the zerofield splitting is very large ($\gg g\beta H$) then the normal picture of 30 line spectra will not be valid (for example for Mn^{2+} in NH_4I at X-band (Chapter IV) and for Mn^{2+} in CsBr even at Q-band[18]).

When the vacancy is quite remote from the metal ion then the metal ion does not feel its presence and feels essentially the undistorted local crystalline field as reflected in the EPR spectra. In such cases of moderate crystalline field the S state of Mn^{2+}

will be subjected to quite small zero field splittings and the fine structure may not be resolved, thus giving rise to an isotropic sextet. Therefore the single sextet observed at RT in the present case indicates that the Mn^{2+} goes substitutionally and the charge compensating sites are quite remote from the substitutional sites. The incorporation of ion clusters will give a broad EPR signal due to dipolar broadening which is indicated by the presence of a broad background signal on which the isotropic sextet is superimposed (Fig. VII.1).

The isotropic spectrum comprising a sextet is analysed using the following expression for resonant fields:

$$H_{m_I} = H_o - A_o m_I - \frac{A_o^2}{8H_o}(35 - 4m_I^2) \qquad (7\text{-}1)$$

where $H_o = \frac{h\nu}{g_o\beta}$ and $m_I = -5/2, -3/2, \ldots 5/2$ and g_o is the isotropic g-factor and A_o is the isotropic hyperfine interaction parameter expressed in gauss. The calculated parameters are as follows:

$$g_o = 2.0056\ (6) \text{ and } |A_o| = 95\ (1)\ G$$

As mentioned earlier NH_4Br undergoes three structural phase transitions around 410K, 235K and 78K respectively. It was not possible to study the transition at 410K in the present case as the EPR spectrum vanished well before this temperature because of the expulsion of Mn^{2+} impurity from the NH_4Br lattice. The phase III after a transition at 235K is reported to be a tetragonal distortion of CsCl-structure resulting from an antiferrodistortive

ordering of NH_4^+ ions in the lattice. The temperature variation of the EPR spectra reveals a structural phase transformation taking place around 230K which is reflected in the transformation of the isotropic spectrum into an anisotropic spectrum at 230K. However, the transition temperature is lowered by $\sim$5K from its reported value. Such lowering of transition temperature of NH_4Br has earlier been reported by Sastry and Venkateswarlu[14] and Trappeniers et al[15] and has been attributed to the presence of impurity ions in the crystal. As has been mentioned earlier no changes in the EPR spectra were observed around 78K and therefore the transformation phase III$\leftrightarrow$phase IV was not reflected in the present EPR study.

It is worth mentioning here that in the unpublished work of Sastry[17] it has been mentioned that the transformation of the EPR spectra at 223K is from a sextet to an isotropic spectrum comprising five sets of sextets. Our observations are completely different and the spectrum II is not only anisotropic but also does not comprise the usual five sextets. We have compared our spectra with theirs and found that there is some mistake in their assignment of the sextets observed at LNT. In a particular orientation of $\vec{H}$ their assigned spectrum resembles to a part of the EPR spectrum observed by us. Therefore their analysis of the spectrum seems to be erroneous and the value of $|D| \sim 536$ G obtained by them is not reliable and compatible with the observation. However, their observations in the temperature range of 300K (RT) to 223K are similar to our observations.

It is rather impossible from only X-band EPR spectra to obtain a quantitative information about the crystalline field in the present case, albeit, one can get some qualitative information from the observed low temperature spectra II. For example one can see that the angular behaviour is consistent to a tetragonal field with the tetragonal distortions coinciding with crystallographic axes. This is supported by the presence of two sextets 'A' and 'B' which do not show any angular variation in (100) planes and correspond to the centres for which $\vec{H}$ is at $\theta = 90^{\circ}$, throughout in these planes. Secondly observation of only two sextets corresponding to $\theta = 0^{\circ}$ indicates that the zerofield splittings of Mn^{2+} ground state in the tetragonal phase III of NH_4Br is very large (much larger than in NH_4I or NH_4Cl). The absence of normal five groups of sextet for other orientation of $\vec{H}$ and the extremely large anisotropy in position and intensity of various sextets is also consistent with the assumption of a large zerofield splitting.

Nicklin et al[13] have computed the g-factor of Mn^{2+} for the case $|D| \gg \beta gH$ by assuming that for a pair of energy levels the Spin-Hamiltonian may be written in terms of an effective spin $S_{eff} = 1/2$ and equating its Hamiltonian matrix to that of the Zeeman-Hamiltonian with $S = 5/2$ for the pair of levels under consideration. It is clear that for large axial crystalline field a transition at $g_{eff} \approx 6$ should be observed for orientations of $\vec{H}$ at $\theta = 90^{\circ}$. Similar conclusion has been drawn by Dousing and Gibson[20] and Castener et al[21]. It is noteworthy that in the present case for $\vec{H}$ at $\theta = 90^{\circ}$ a group of peaks (A) is observed at $g_{eff} \sim 6$. We may thus conclude that the complexity of the EPR

spectra at LNT is a consequence of very large zerofield splitting in the NH_4Br lattice which is expected for an Mn^{2+} - vacancy pair just like in other ammonium and cesium halides. It is rather surprising that vacancies which are remote in the upper phase become dramatically bound on phase transition to lower temperature phase and vice versa. The values of hyperfine constants determined from the low temperature spectrum are:

$$|A| = |B| = 92 \text{ G}$$

SECTION B : EPR STUDY OF VO^{2+} IN NH_4Br

EXPERIMENTAL RESULTS

At RT ($\sim$300K) the spectrum was found to be isotropic. The peak to peak derivative height and linewidths showed a m_I dependence. As the temperature was raised above RT upto $\sim$ 406K, the derivative heights increased and the p-p line widths decreased. Above $\sim$ 406K the line widths demonstrated an anomaly and above 410K the trend reversed. On further increasing the temperature it was observed that around 433K the background signal (single broad line structure) started increasing, indicating some physical changes occuring in the sample. On physical examination it was found that the crystal surfaces had decayed into a powder and heating the crystal above $\sim$ 433K for some time turned it completely into a powder. This powder gave only a single broad EPR signal. It was found safe to heat the samples only upto 430K and the changes in line widths around 408K were found to be reversible indicating a structural phase transition around 408K. In Fig. VII.4 EPR spectra comprising isotropic octet are shown at different temperatures and

in Fig. VII.5 the temperature dependence of line width of the line $m_I = -1/2$ is shown. It was noticed that above 380K the lines started showing saturation with 200 mW microwave power. At temperatures around 400K the saturation behaviour was much more pronounced. Therefore the power level was kept sufficiently low ($\sim$2 mW) to avoid any possibility of saturational line broadening. At RT and below, the lines did not show saturation behaviour even when using 200 mW microwave power for getting the EPR spectra. Fig. VII.6 shows at 388K for various lines the graph between derivative height and square root of microwave power used.

On lowering the temperature below RT the derivative heights decreased and the line widths increased and around 233K the octet structure disappeared completely leaving behind a broad background signal which increased in intensity compared to its RT intensity. Below 223K a new structure started showing up which gained intensity with further lowering of the temperature. This spectrum was also found to be completely isotropic and comprised two sets of octets. One set was relatively stronger in intensity but compressed in spread compared to the other set. This spectrum observed below 223K did not show temperature variation in position down to LNT. The line widths of the octets at LNT were found to be large compared to those for VO^{2+} in NH_4I at LNT. The isotropic single octet observed above 233K will be referred to as spectrum-I (Fig. VII.4) while the low temperature spectrum comprising two sets of isotropic octets will be referred to as spectrum-II (Fig. VII.4). It may be mentioned here that the change from spectrum-I $\leftrightarrow$II was found to be reversible. The crystals did not show any

signs of damage on repeated cooling and heating between 300K and LNT. At LNT the lines of the spectrum did not show any saturation with 200 mW microwave power.

3.2 DISCUSSION

The salient features of spectra-I and II are similar to those of the corresponding spectra of VO^{2+} in NH_4Cl[16] and NH_4I (Chapter VI). Therefore most of the arguments given for VO^{2+}:NH_4I are also applicable to the present case of VO^{2+}:NH_4Br. In the following the results of the SH analysis and line width analysis will be presented and discussed in brief. The additional features of the EPR spectra of VO^{2+} in NH_4Br will also be discussed in what follows.

The spectra I and II at various temperatures were analysed by the methods used for VO^{2+} in NH_4I. It was observed that the SHP of spectra I and II are almost constant within experimental errors over the respective temperature ranges studied. Therefore the SHP obtained from analysis of spectrum I at 400K and of spectrum II at 77K are presented in the Table VII.1.

The spectrum-I is attributed to vanadyl ion undergoing rapid tumbling motions in NH_4Br lattice and the reorientation rate is fast enough to average out the anisotropy in g and A tensors. At low temperatures the rapid motions of the vanadyl ion become hindered progressively and at sufficiently low temperatures (around LNT) these are almost quenched, and as a consequence the anisotropic interactions also contribute to the EPR spectrum. However it has been observed that the spectrum II is also independent of

crystal orientation with respect to static magnetic field, which can be explained on the basis of a random distribution of V-O bond in the host lattice at low temperatures. The spectrum-II is similar to that of VO^{2+} in polycrystalline samples. Therefore, a random distribution of V-O bond in the NH_4Br lattice at low temperatures results in lines corresponding to $\vec{H}$ parallel and $\vec{H}$ perpendicular to V-O bond. From a statistical distribution it is also expected that the intensity of lines corresponding to perpendicular orientation will be twice that of lines corresponding to parallel orientation. In Fig. VII.4a lines marked by 'a' represent the parallel-spectrum and those marked by 'b' represent the perpendicular-spectrum. It is, therefore, believed that while in the upper two phases I (NaCl) and II (CsCl-disordered) the molecular ion is tumbling very fast, in phase III (CsCl-ordered) the motions get effectively quenched.

B.3 LINE WIDTH

The observed m_I dependence of line width is also believed to be a consequence of rapid tumbling motion of vanadyl ions even in the solid state lattice in the present case. Kivelson's theory of line width for rapidly tumbling paramagnetic complex has already been described in Chapter VI for $VO^{2+}:NH_4I$. The expressions given there were used for the line width analysis in the present case and the obtained parameters are listed along with the SHP in Table VII.1. In Fig. VII.5 the m_I dependence of line width for spectrum I is shown. It was found that the ratio (A_2/A_3) obtained from the line width analysis does not show a temperature dependence

and is found to be around 1.5 in the present case. It is also possible to obtain this ratio from the analytical expressions given in Chapter VI by making use of the SHP obtained from the analysis of spectrum-II. It is found that like in the case of VO^{2+}:NH_4I and other lattices (see Table VI.2) the two ratios viz. $(A_2/A_3)_{LW}$ and $(A_2/A_3)_{Cal}$ are not in good agreement. This disagreement has already been discussed in Chapter VI.

Using the analytical expression for A_3 given in Chapter VI it was possible to estimate the correlation time τ_c at various temperatures describing the reorientational processes and was found to be of the order of 10^{-11} sec. Such values of correlation time are typical of the vanadyl ion in liquids of low viscosity (e.g. VO^{2+} in benzene)[22,23]. Therefore the assumption that vanadyl ion in solid lattice of NH_4Br behaves like in a liquid, so far as the relaxation in EPR are concerned, seems to be justified. In Table VII.2 the various solid state lattices, in which VO^{2+} ion is believed to behave like in a liquid showing rapid tumbling behaviour, are summarised.

Due to the isotropy of both spectra I and II it is almost impossible to decide about the type of magnetic centre (vanadyl complex) in the present case also. However the crystalline field or the motions of the NH_4^+ ions seem to affect the line width of spectrum-I. The observed anomalies around 408K and around 230K clearly indicate the structural phase transitions around these temperatures. The former phase transition is of first order and the latter of second order in nature. In the ordered CsCl

structure phase III there are no rotations of NH_4^+ ions and the structure seems to favour quenching of the tumbling motion of vanadyl ions just like in the case of NH_4I. In the high temperature phase (NaCl-disordered) the NH_4^+ ions are multiply disordered in orientation and undergo complex motions and the relaxation mechanism seems to be affected differently in NaCl and CsCl (disordered) structures. No significant changes in line width were noticed around the third reported phase transition temperature (78K). Therefore either this transition did not take place in the present case or did not affect the line positions and widths.

REFERENCES

1. H. Abe and H. Shirai, J. Phys. Soc. Japan 15, 1711 (1960).
2. T.J. Seed, J. Chem. Phys. 41, 1486 (1964).
3. M.M. Zaripov and G.K. Chirkin, Soviet Phys. Solid State 6, 1290 (1964); 7, 74 (1965), 7, 2391 (1966).
4. A. Forman and J.A. Van Wyk, J. Chem. Phys. 44, 73 (1966); Canad. J. Phys. 45, 3381 (1967).
5. J.A. Van Wyk, J. Mag. Reson. 18, 235 (1975).
6. J.A. Kennewell, J.R. Pilbrow and J.H. Price, Phys. Lett. A27, 228 (1968).
7. A. Lupei, V. Lupei, A. Stefanscu and F. Domsa, Rev. Roum. Phys. 20, 59 (1975).
8. V. Lupei, A. Lupei and F. Domsa, J. Mag. Reson. 19, 337 (1975).
9. R. Bramby and S.J. Strach, Chem. Phys. Lett. 79, 183 (1981).
10. J.R. Pilbrow and J.M. Spaeth, Phys. Stat. Solidi20, 225 and 237 (1967).
11. N.J. Trappeniers and S.H. Hagen, Physica 31, 122 and 251 (1965); 47, 165 (1970); 66, 166 (1973).
12. N. Kuroda and A . Kawamori, J. Phys. Chem. Solids 32, 1233 (1971).
13. H. Abe, K. Ono, I. Hyashi, J. Shimada and K. Iwanaga, J. Phys. Soc. Japan 9, 814 (1952).
14. M.D. Sastry and P. Venkateswarlu, Proc. Ind. Acad. Sci. 66, 208 (1967).
15. N.J. Trappeniers, F.S. Stibbe and J.L. Rao, J. Phys. Chem. Solids 42, 617 (1981).
16. M.D. Sastry and P. Venkateswarlu, Mol. Phys. 13, 161 (1967); K.V.S. Rao and M.D. Sastry, Chem. Phys. Lett. 2, 20 (1968).
17. M.D. Sastry, Ph.D. Thesis, I.I.T. Kanpur (1967) (Unpublished).

18. T. Iri and G. Kuwabara, J. Phys. Soc. Japan, 23, 536 (1967).

19. R.C. Nicklin, C.P. Poole Jr. and H.A. Farach, J. Chem. Phys. 58, 2579 (1973).

20. R.D. Dowsing and J.F. Gibson, ibid. 50, 294 (1969).

21. Th. Castner, G.S. Newell, W.C. Holton and C.P. Slichter, ibid. 32, 608 (1960).

22. D.E. O'Reilly, J. Chem. Phys. 29, 1188 (1958).

23. D.J. Kivelson, ibid. 33, 1094 (1960).

24. A.V. Jagannadham and P. Venkateswarlu, Proc. Indi. Acad. Sci. 69, 307 (1969).

25. S. Radhakrishna, B.V.R. Chowdhari and A. Kasi Viswanath, J. Phys. Soc. Japan 41, 1530 (1976).

26. K.V.S. Rao, M.D. Sastry and P. Venkateswarlu, J. Chem. Phys. 49, 1714 (1968).

27. K.V.S. Rao, M.D. Sastry and P. Venkateswarlu, ibid. 52, 4035 (1970).

28. M.V. Krishnamurthy, J. Phys. Chem. Solids 33, 1645 (1972).

29. Y. Tomkiewicz, S. Saito and D. Fujimoto, J. Mag. Reson. 8, 188 (1972).

TABLE VII.1

SHP of spectrum-I and spectrum-II at given temperatures of VO^{2+} in NH_4Br single crystal.

Spectrum	Spin-Hamiltonian Parameters
spectrum-I (400K)	$g_o = 1.974(1)$ $\lvert A_o \rvert = 112(1)$ Gauss
spectrum-II (77K)	$g_{\parallel} = 1.938(2)$ $\quad g_{\perp} = 1.991(2)$ $\lvert A \rvert = 200(2)$ Gauss $\quad \lvert B \rvert = 70(2)$ Gauss $g_{eff} = (g_{\parallel} + 2g_{\perp})/3 = 1.9733$ $A_{eff} = (\lvert A \rvert + \lvert 2B \rvert)/3 = 113.3$ Gauss

Line Width Analysis Parameters
$A_1 = 13.0$ Gauss $\quad A_2 = 1.5$ Gauss $\quad A_3 = 1.0$ Gauss
$(A_2/A_3)_{LW} = 1.5$ $\quad (A_2/A_3)_{Cal} = 14.$

TABLE VII.2

Lattices in which VO^{2+} exhibits rapid tumbling motion: studied from EPR.

Host	SHP of Spectrum-I		SHP of Spectrum-II				Ref.
	g_o	$\|A_o\|$ (G)	$g_{\|\|}$	$g_\perp$	$\|A_\|\|$ (G)	$\|B\|$ (G)	
NH_4Cl	1.966	103.9*	1.925	1.977	174	67.8*	(16)
NH_4Br	1.974	112	1.938	1.991	200	70	Chapt. VI present thesis
NH_4I	1.970	110	1.948	1.980	190	68	Chapt. VI present thesis
NaCl	1.971	104*	1.925	1.996	176.8*	64.2*	(24)
KCl	1.969	106.8*	1.932	1.988	186.8*	70.4*	(24)
RbCl	1.967	106*	1.939	1.968	188.7*	63.9*	(24)
$BaCl_2.2H_2O$	1.966	106.4*	1.930	1.977	177.2*	74.4*	(25)
$BaBr_2.2H_2O$	1.963	107*	1.928	1.979	182.9*	73.4*	(25)
KNO_3	1.966	116	1.935	1.974	199	78	(26)
$CsNO_3$	1.964	115	1.919	1.984	218	67	(26)
$NaNO_3$	1.965	115	1.947	1.974	218	67	(27)
NH_4NO_3	1.963	116	1.939	1.975	206	67	(27)
$Ba(NO_3)_2$	1.964	116	1.919	1.984	199	78	(27)
$UO_2(NO_3)_2$	1.964	116	1.930	1.981	198	77	(28)
Dimethyl alanine crystals	-	95	-	-	195	45	(29)

*Values are in 10^{-4} cm^{-1}.

Fig VII-1

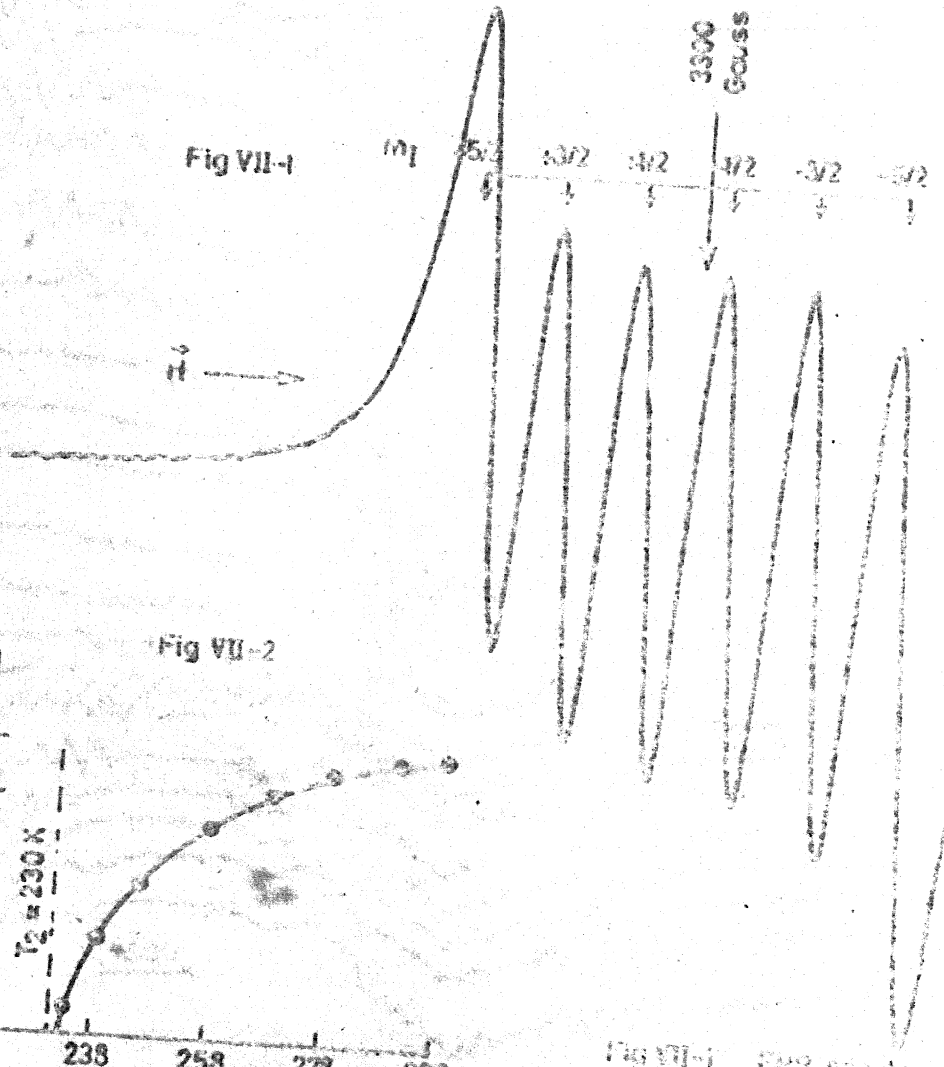

Fig VII-2

Fig VII-2 Temperature dependence of P-P signal height of isotropic sextet of EPR spectrum-I.

Fig VII-1 EPR spectrum of Mn^{2+} doped ZnS single crystal at R.T. The isotropic sextet is superimposed over a broad background signal due to Mn^{2+} clusters in the crystal.

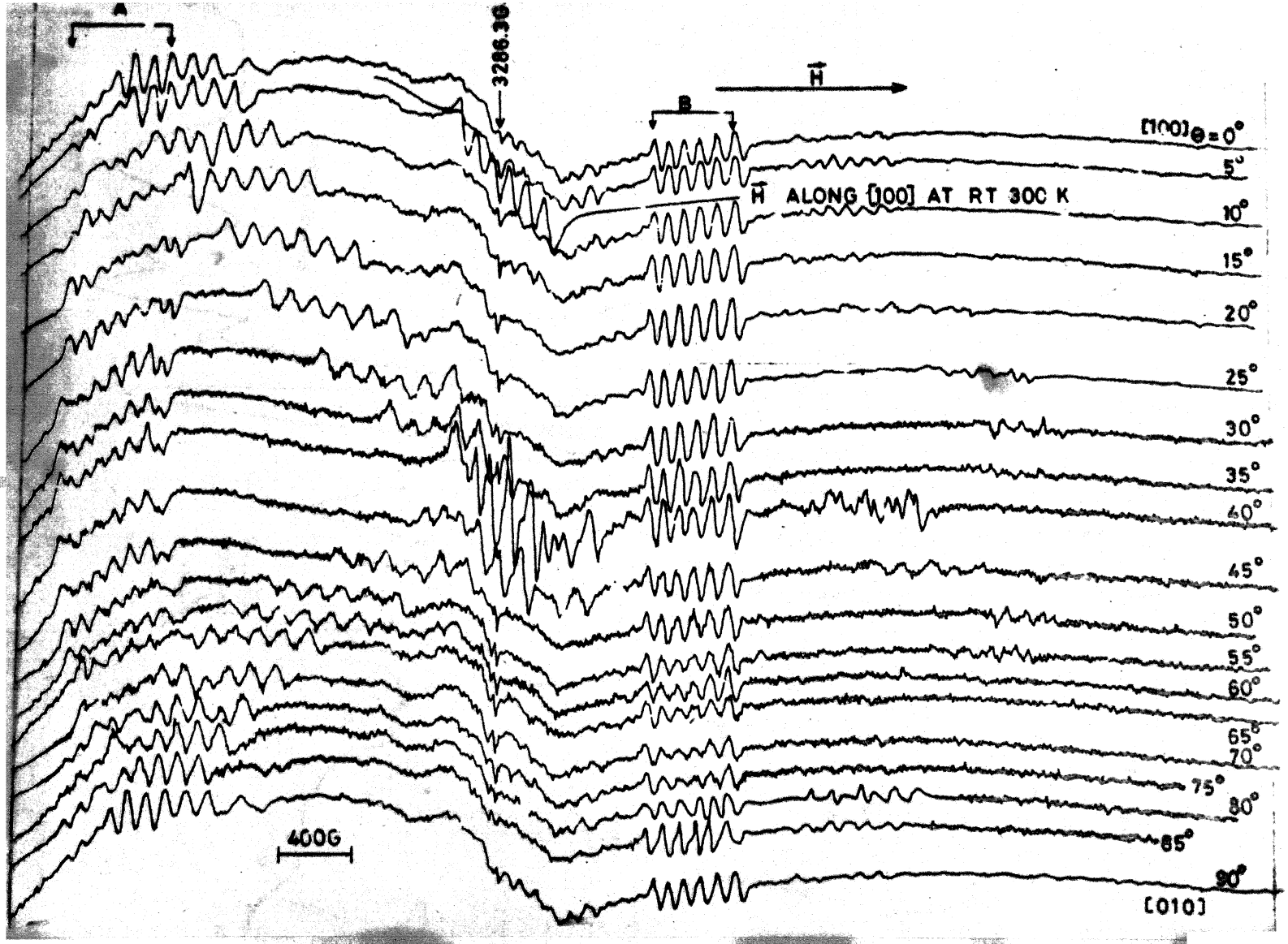

Fig. VII.3 EPR SPECTRA RECORDED AT VARIOUS ANGLES IN (001)-PLANE OF NH_4Br CRYSTAL DOPED WITH Mn^{2+} AT LNT. SEXTETS MARKED AS A AND B ARE ANGLE INDEPENDENT IN THEIR POSITION. THE ISOTROPIC SEXTET-SPECTRUM AT RT IS ALSO SHOWN.

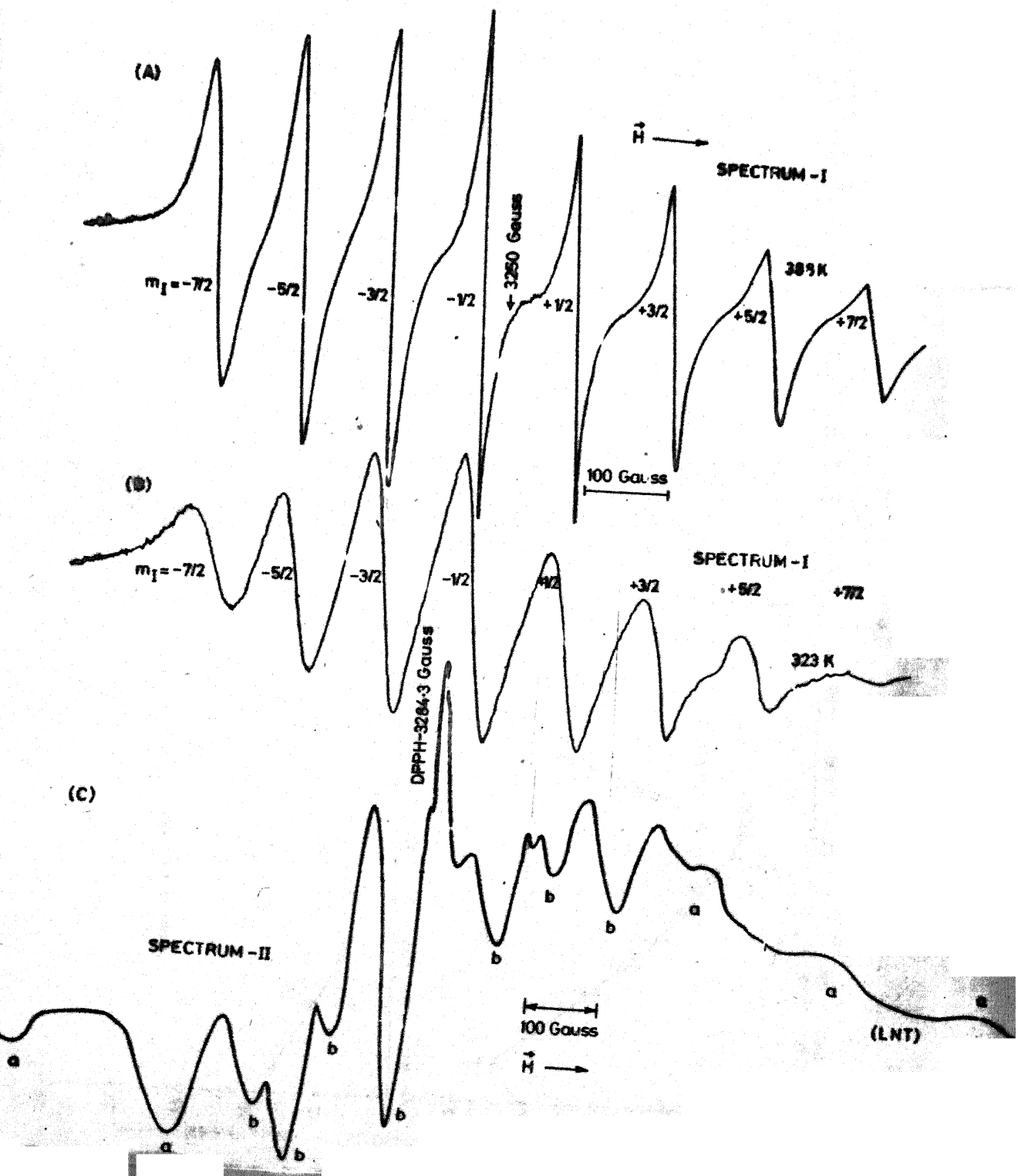

Fig.VII.4 EPR SPECTRA OF VO^{2+} IN NH_4Br AT VARIOUS TEMPERATURES. (A) ISOTROPIC OCTET AT 388K (SPECTRUM-I), (B) ISOTROPIC OCTET AT 323K AND (C) ISOTROPIC SPECTRUM-II AT LNT. THE LINES MARKED BY 'a' BELONG TO V-O BOND // TO H AND THOSE MARKED BY 'b' BELONG TO V-O BOND ⊥ TO H.

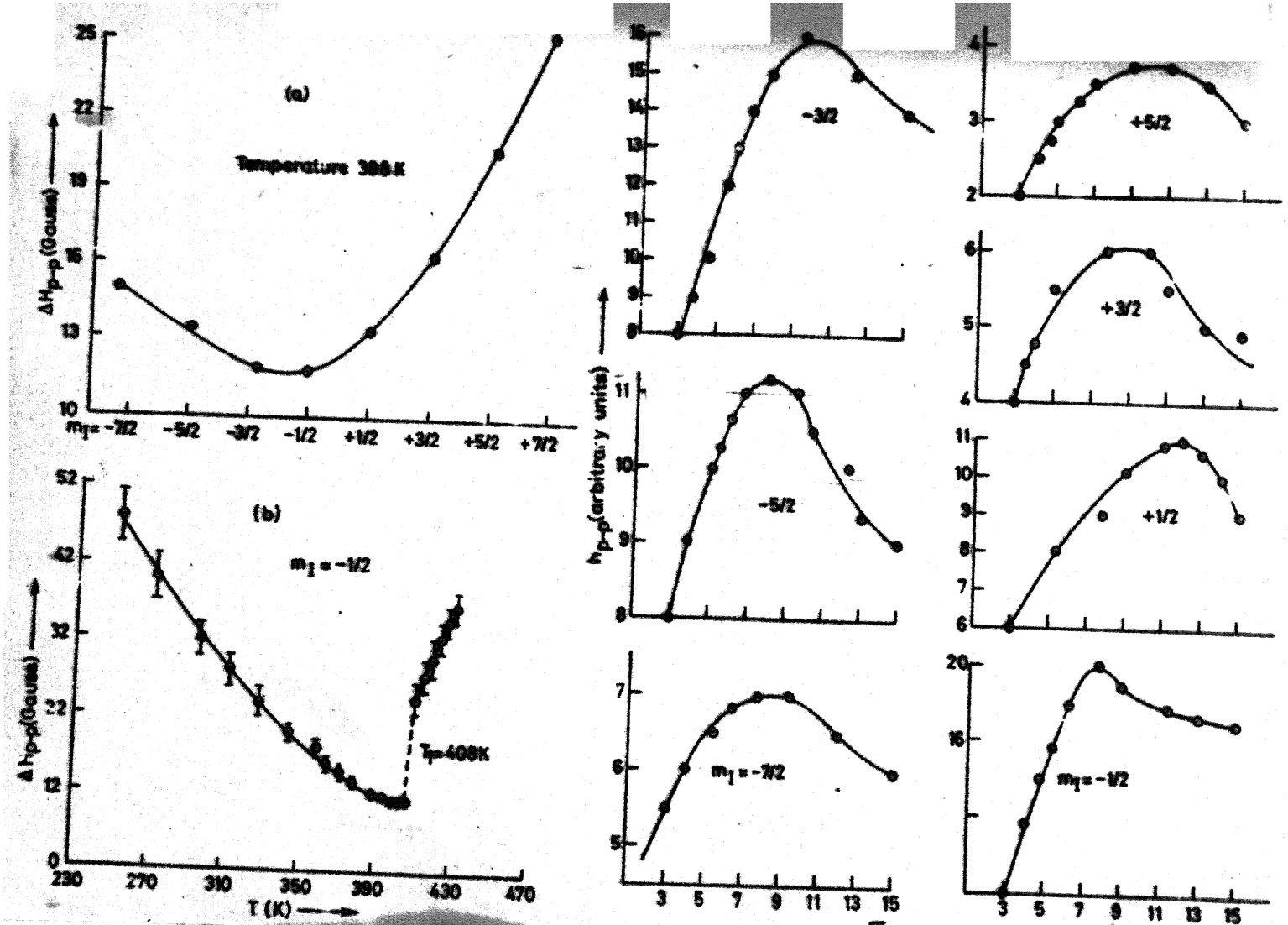

Fig.VII.5 (a) m_I-DEPENDENCE OF PEAK TO PEAK LINE WIDTH (ΔH_{pp}) OF EPR SPECTRUM-I OF VO^{2+} IN NH_4Br. THE CONTINUOUS CURVE IS A SMOOTH CURVE THROUGH THE EXPERIMENTAL POINTS.

Fig.VII.5 (b) TEMPERATURE DEPENDENCE OF ΔH_{p-p} OF

Fig.VII.6 PEAK-TO-PEAK HEIGHT, h_{p-p} , OF FIRST DERIVATIVES OF TRANSITION OF SPECTRUM-I OF VO^{2+} IN NH_4Br PLOTTED AGAINST THE SQUARE ROOT OF MICROWAVE POWER (mW) AT 388K.

CHAPTER VIII

CONCLUSIONS

In this chapter we give a comparative discussion on the EPR studies of Mn^{2+}, Cu^{2+} and VO^{2+} in NH_4Cl, NH_4Br and NH_4I carried out by us and by other workers. At the end of the chapter is given the scope for further studies on these systems that may help in further understanding these systems and substantiating the conclusions drawn from the studies till now.

(i) Mn^{2+} IN NH_4Cl, NH_4I AND NH_4Br

The RT EPR results of Mn^{2+} in NH_4Cl and NH_4I are similar and are characterized by a large zero field splitting with tetragonal symmetry. In NH_4Br, however, the RT spectrum is different and suggests no distortion in cubic crystal field - the charge compensating vacancy seems to be far away from the metal ion.

No results are available for studies at temperatures higher than RT for NH_4Cl. However, in NH_4I on raising the temperature above RT first the spread of the axial spectrum decreases, then $\sim$ 480K only a six line spectrum remains, which above 500K finally gives a broad band with a sharp line superimposed on it. The changesare reversible upto $\sim$ 500K. But on heating above $\sim$ 500K Mn^{2+} gets expelled from the lattice and the crystal turns into a powder.

In NH_4Br the expulsion of Mn^{2+} impurity starts around 400K. This was revealed by the disappearance of isotropic single sextet $\sim$ 400K and appearance of some black material (MnO) on the crystal surfaces on prolonged heating.

On lowering the temperature below RT the parameter D and peak-to-peak line widths show similar behaviour in NH_4Cl and NH_4I. The phase transitions are reflected by an anomalous behaviour in D and line widths. In the case of NH_4Br there is a drastic change in the spectrum at the phase transition temperature ($\sim$ 230K). The RT spectrum disappears around the phase transition temperature and several groups of sextets are observed below this temperature. This presumably is due to a large tetragonal distortion taking place after the phase transition. The D value appears to be much larger than that in NH_4Cl and NH_4I, although no quantitative information about D parameter was possible from the complex EPR spectrum of Mn^{2+} in NH_4Br at low temperatures.

(ii) Cu^{2+} IN NH_4Cl, NH_4Br AND NH_4I

The behaviour of Cu^{2+} is similar in all the three hosts. Three types of Cu^{2+} centres are observed which could be selectively produced by proper choice of crystal growth conditions. The SH parameters in the three hosts are given in the Table VIII.1 for comparison. The temperature variation studies in all three hosts show drastic changes in the hyperfine parameters around the phase transition temperatures.

(iii) VO^{2+} IN NH_4Cl, NH_4Br AND NH_4I

At RT and above VO^{2+} in all three hosts shows a similar behaviour like that of VO^{2+} in liquids giving rise to an isotropic eight line spectrum resulting from a rapid tumbling motion. On lowering the temperature the tumbling motion in all three hosts

gets hindered below their respective phase transition temperatures leading to two isotropic octets.

(iv) SCOPE FOR FURTHER STUDIES

It would be interesting to study Mn^{2+}:NH_4Cl system at temperatures above RT and to compare the results with those in NH_4Br and NH_4I, particularly the expulsion of Mn^{2+} from the lattice at higher temperatures.

In the case of Mn^{2+}:NH_4Br the low temperature spectra if studied at Q-band could give more and unambiguous information about the presumably large tetragonal distortion.

In Cu^{2+}:NH_4I and Cu^{2+}:NH_4Br, studies with deuterated samples and with enriched isotope of copper will give sharper lines. This will help in the observation of shfs due to ligands which could give definite information.regarding Cu^{2+} ion site and its coordination. Further, sharper lines could also allow the observation of hf forbidden transition from which accurate quadrupole parameters can be obtained.

Lastly EPR studies in solid solutions of ammonium halides may be helpful in understanding the correlation, if any, of the D-parameter with the halogen ligands. The nature and transition temperatures in solid solutions may be helpful in understanding the role of halogens in the phase transitions.

TABLE VIII.1

SHP of some of the Cu^{2+} centres in NH_4Cl, NH_4Br and NH_4I hosts.

Host	Centre	Temp.	$g_{\|\|}$	$g_{\perp}$	$\|A\|$ Gauss	$\|B\|$ Gauss	Refr.
NH_4Cl	I	RT	2.0232	2.2896	41.9*	61.8*	(1)
		LNT	2.045	2.254	11*	75*	
	II	LNT	2.0003	2.2191	233.9*	67.2*	
	III	LNT	2.009	-	118*	-	
NH_4Br	I	RT	2.0036	2.217	182.6	0	(2)
		143K	2.032	2.032	164.0	-	
	II_2	RT	2.301	2.15	46	49	
	III_1	143K	2.367	2.152	70	68.4	
NH_4I	I_2	RT	2.011	2.216	190	30	Present thesis
		LNT	2.0051	2.2385	250	65.5	
	II_4	RT	2.019	2.222	80	56	
		LNT	2.0189	2.229	128.5	63.5	
	III	RT	2.039	2.249	15	70	
		LNT	2.0280	2.250	43	60	

*Values are in units of $10^{-4}cm^{-1}$

(1) S.H. Hagen and N.J. Trappeniers, Physica 47, 165 (1970).

(2) M.D. Sastry and P. Venkateswarlu, Proc. Ind. Acad. Sci. 66, 208 (1967).

APPENDIX A

Literature Survey of Magnetic Resonance and Relaxation Studies on Ammonium Halides.

System	Physical Method	Remark*	Ref.
$NH_4I:Mn^{2+}$	EPR	Very large D parameter, Q-band & X-band study at RT.	1
$NH_4I:Cu^{2+}$	EPR	Three types of copper center at RT, SHP analysis.	2
$NH_4Cl:Mn^{2+}$	ZF-EPR	Improved SHP, EPR at zero mag. field.	3
$NH_4Cl_{1-x}Br:Cu^{2+}$	EPR	100 to 290K, Temperature dependence of SHP, Effect on SPT, Tricritical points.	4
NH_4(Cl,Br,I)	NMR	Cross relaxation dispersion, temp. dependence.	5
$NH_4Cl:Rh$	EPR	γ-irrad, stabilization, EPR investigation of Rh^0 and Rh(II) centres.	6
NH_4Cl	NQR	Electric-field gradient at Cl nucleus, quantum mechanical, atomic orbital and STO-Calc. NQR frequency.	7
$NH_4Cl:Ni^{2+}$	EPR	EPR spectrum, spin Hamiltonian, zero field splitting effects.	8
$ND_4Br:Cu^{2+}$	EPR	Pseudo-Jahn-Teller effect, manifestation in EPR.	9
NH_4(Cl,Br)	Relaxn.	Anisotropy of T_1D, T_1	10
NH_4Br	PMR	Proton spin-lattice relaxation, temp. dependence.	11
NH_4(Br,I)	NMR	^{14}N, NMR observation, relaxation to struc. transition.	12
NH_4Cl	PMR	Free induction decay shape and moments.	13
$NH_4Cl:Cr^{3+}$	EPR	EPR of Cr^{3+} centres, room temp.	14

*Information under the column Remark are given in abbreviated form for the point of space-economy.

Contd.

System	Physical Method	Remarks	Ref.
$NH_4(Cl,Br,I)$	NMR	NMR under high pressure	15
$NH_4Br:Cu^{2+}$	NMR EPR	NMR under high pressure EPR & Optical absorption of copper centres.	16
$NH_4Cl:MoO^{3+}$	EPR	Molybdenyl centres in NH_4Cl single crystal.	17
NH_4Cl	NMR	Cl, ^{15}N, NMR Chem. Shift references evaluation.	18
NH_4Cl	PMR	NH_4Cl in RbCl (KCl), NH_4 motion, PMR, proton-spin lattice relaxation time, temperature dependence.	19
$ND_4Cl:Cu^{2+}$	EPR	High pressure EPR, order-disorder transitions.	20
NH_4I	NMR	Tortional spectroscopy by NMR in rotating frame.	21
$NH_4Cl:Pd$	EPR	Pd complex, γ-irrad.	22
NH_4Cl	NMR	Order-disorder transition.	23
$NH_4Br:MoO^{3+}$	EPR	Hyperfine interaction.	24
$NH_4I:SnF_2$	Mossbauer	Mossbauer data for various phases.	25
$NH_4Cl:Cu^{2+}$	EPR	4.2K to 400K effect of motion of ligands.	26
$NH_4Cl:Mn^{2+}$	EPR	Forbidden hyperfine transitions.	27
$NH_4Cl:Cu^{2+}$	EPR	EPR on centre I of Cu^{2+}	28
$NH_4Cl:MoOCl_5^{2-}$	EPR	EPR study at RT and LNT.	29
$NH_4Cl:Mn^{2+}$	EPR	Position, intensity of hyperfine line calculation.	30
$NH_4Cl:Mn^{2+}$	EPR	Line width temp. dependence, order-disorder transformation & molecular reorientation.	31
$NH_4Cl:Cu^{2+}$	EPR	Pressure effect on EPR near T_λ	32
$NH_4Cl:Cr^{3+}$	EPR	Single crystal, SHP Temp. depend.	33

System	Physical Method	Remarks	262
NH_4 Cl	NMR	Cl^{35} spin-lattice relaxation due to critical effects.	34
ND_4Cl	NMR	^{14}N and Cl^{35} spin-lattice relaxation near order-disorder transition.	35
NH_4(Cl,Br)	NMR	Cl^{35} spin-lattice relaxation observation near critical effects.	36
NH_4Cl	NMR	^1H spin-lattice relaxation, reorientation of NH_4^+.	37
NH_4Cl	NMR	^1H spin-lattice relaxation, experimental results near λ-transition.	38
NH_4Cl	NMR	^1H spin-lattice relaxation, calculation for 4-spin system	39
NH_4Cl	NMR	^1H spin-lattice relaxation, exptl. results outside λ-transition.	40
NH_4Cl	PMR	Anisotropy in proton spin-lattice relax. time in rotating frame.	41
$NH_4Cl:Cu^{2+}$	EPR & ENDOR	ENDOR and EPR investigation at 4.2K	42
$NH_4Cl:Cu^{2+}$	EPR & ENDOR	ENDOR investigation of superhyperfine interaction theoretical analysis.	43
NH_4Br	NMR	Spin-lattice relaxation time of nuclear dipolar energy.	44
NH_4I	NMR	Spin-lattice relaxation time of nuclear dipolar energy	45
NH_4Cl	NMR	Free induction decay means; zero time resolution pulsed NMR method.	46
$NH_4(^{35}Cl,^{81}Br)$	NMR	High pressure order-disorder trans.	47
NH_4Br	NMR	Order parameter determination for order-disorder transition ^{81}Br NMR	48
NH_4Cl	NMR	N & Cl spin-lattice relaxation nearer λ-transition.	49
$NH_4Cl:Cu^{2+}$	EPR	Optical and crystal parameter.	50
NH_4Cl and $ND_4Cl:Cu$	EPR	Cu complexes, temperature dependent	51

Contd.

System	Physical Method	Remarks	Ref.
NH_4Cl	SLR	Spin-lattice relaxation & molecular reorientation near T_c	52
$NH_4Cl:Pd^+$	EPR	reorientation of NH_4^+. Investigation of Pd^+ Pd^+ centres, SHP calculations.	53
$NH_4(Cl,Br,I)$	PMR	PMR line shape of NH_4^+ ions with tunneling influence.	54
NH_4Br	NMR	Investigation of order-disorder phase transition.	55
$NH_4Br:Cu^{2+}$	EPR	EPR spectral interpretation and SHP calculation.	56
NH_4Br	NMR	Time dependent spectra at 4.2K.	57
$NH_4(Br,I)$	PMR	Study of tunneling of NH_4 ions.	58
NH_4Cl	NMR	Nuclear mag. relax. induced by random molecular reorientation.	59
NH_4Cl	PMR	Proton spin-lattice relax. and order-disorder trans. low temp. spin relaxation of hindered ions.	60
NH_4Cl		Low temp. spin relax. of hindered ions.	61
NH_4Cl	SLR	Spin-lattice relax. time of nuclear dipolar energy temp. and orientation dependent.	62
$NH_4Br:Cu^{2+}$	EPR	EPR covalency, core polarization.	63
NH_4I	PMR	PMR intensity, nuclear spin value.	64
$NH_4Cl:Cu^{2+}$	EPR	Effects of order-disorder transition in EPR and Optical spectra.	65
$NH_4Cl(ND_4Cl):Cu^{2+}$	EPR	off-centre position, EPR observation at 6K.	66
NH_4Cl	NMR	Enhancement of N^{15} resonance by nuclear overhauser effect.	67
NH_4Cl	PMR	Proton spin lattice relax. times.	68
NH_4Br	PMR	Proton spin lattice relax. times., SPT.	69

Contd.

System	Physical Method	Remarks	Ref.
NH_4F	EPR	EPR of Cu^{2+}, tetrahedral,site, calculation of SHP.	70
$NH_4Cl:Fe^{3+}$	EPR	Zero field energy level determination.	71
$NH_4Cl:Cr^{3+}$	EPR	77-330K-temperature dependence.	72
$NH_4Cl:Co^{2+}$	EPR	Relaxation 4.2K, saturation.	73
NH_4Cl	Relaxn.	Solid, spin rotational relaxation.	74
$NH_4Cl:Ni^{2+}$	EPR	Single crystal.	75
NH_4Cl ND_4Cl	EPR	Irradiated, $N_2H_4^+$	75a
$NH_4Cl:Co^{2+}, Ni^{2+}, VO^{2+}$	EPR	X-irradiated, F-centres observation.	76
NH_4Cl	EPR	EPR of radiation induced paramagnetic centres.	77
NH_4Cl	NMR	Internal motions, NMR use of relaxation function.	78
$NH_4Cl:Cu^{2+}$	ESR	λ-type phase transition Cu^{2+} impurity effects.	79
NH_4I	NMR	Polycrystalline, NMR study of hindered rotation.	80
$NH_4(Cl,Br)$	EPR	Radiation-induced paramagnetic NH_3Cl colour centre.	81
NH_4Cl	NMR	Effect of impurities on spin-lattice relaxation.	82
$NH_4Cl:Mn^{2+}$	EPR	Temperature dependence.	83
$NH_4Cl:VO^{2+}$	EPR	Line widths.	84
NH_4I	NMR	Cubic & tetragonal magnetization coexistence proton spin-lattice relaxation determination.	85
NH_4I	PMR	Hindered rotation of NH_4^+ ions.	86
$NH_4Cl:Mn^{2+}$	EPR	EPR spectrum of Mn^{2+}, SHP calcul.	87

Contd.

System	Physical Method	Remarks	Ref.
$NH_4Cl:VO^{2+}$	ESR	ESR studies of VO^{2+}, Tumbling motion of VO^{2+}.	88
$NH_4Cl:Cu^{2+}$	ESR	Temp. depen. of Cu^{2+}, 4.2K to 453K, SPT, G.S. calculation.	89
NH_4Cl	NMR	NMR of Cl^{35}, Temp. & Press. depend.	90
NH_4Cl	NMR	H^1 & D^2 spin-lattice relaxation, temperature variation observation.	91
ND_4Cl	NMR	D^2 and N^{14} NMR spectrum.	92
NH_4Br	NMR	λ-trans. detection by proton spin-lattice relaxation.	93
$NH_4Br:Cu^{2+}$	EPR	EPR of Cu^{2+} centres.	94
ND_4Br	NMR	Spin-lattice relaxation and phase transition.	95
$NH_4Br:Cu^{2+}$	EPR	EPR of Cu^{2+}.	96
$NH_4Cl:Mn^{2+}$	EPR	EMPR of Mn^{2+}.	97
$NH_4Cl:Cu^{2+},Mn^{2+}$	EPR	EPR of Cu^{2+}, Mn^{2+} temp. variation.	98
NH_4Cl	ESR	Related to phase transitions of second order.	99
NH_4Cl	NMR	Relaxation at high pressure.	100
$ND_4(Cl,Br)$	NMR	d mag. resonance	101
ND_4Cl, NH_4Br	NMR	Deuteron mag.resonance in single crystal.	102
NH_4Br	ESR	V_k centre, Br_2^- ESR observation.	103
NH_4I		Spin-lattice relaxation times for protons & Iodine nuclei, different phases.	104
NH_4I	NMR	Nuclear Spin-lattice relaxation of protons and I nuclei.	105
$NH_4Cl:Cu^{2+}$	EPR	λ-point effect.	106
$NH_4Cl:Cu^{2+}$	EPR	77^oK to 295K, SPT.	107

Contd.

System	Physical Method	Remarks	Ref.
NH_4Cl:Fe	EPR	EPR spectra, with Fe group ions.	108
ND_4Cl	NMR	Rotation of NH_4^+	109
$NH_4Cl:Cu^{2+}$	ESR	ESR spectrum.	110
NH_4Cl	ESR	Electron deficiency centres.	111
NH_4Cl	ESR	NH_4Cl-$MnCl_2$-H_2O solid solution, EPR of Mn^{2+}	112
ND_4(Cl,Br)	DMR	DMR line width transtions observation.	113
NH_4(Cl,Br)	PMR	Proton mag. resonance in single crystal.	114
NH_4(Cl,Br,I)	NMR	NMR of halogen.	115
NH_4I	PMR	Proton resonance, motional narrowing and line shape.	116
$NH_4Cl:Mn^{2+}$	ESR	Very large D parameter at RT.	117
ND_4Br	Relaxation	Spin lattice relaxation and phase transition.	118

REFERENCES

1. Prem Chand and G.C. Upreti, J. Chem. Phys. (~~in press~~). 78, 5930 J. Chem. Phys. (in press)-(1984)
2. Prem Chand and G.C. Upreti, Chem. Phys. Lett. 88, 309 (1982).
3. R. Bramley and S.J. Strach, ibid., 79, 183 (1981).
4. B. Aruna, Y.V.S. Ramakrishana and P.A. Narayana, Phys. Status Solidi, B105, 347 (1981).
5. A.R. Sharp and M.M. Pintar, J. Chem. Phys. 75, 2652 (1981).
6. M.D. Sastry, K. Savitri and B.D. Joshi, J. Chem. Phys. 73, 556 (1980).
7. M.C. Montabonel and M. Snard, Mol. Phys. 40, 1503 (1980).
8. V.A. Galushko, V.I. Kurochkin, S.N. Lukin and G.A. Tsintsadze, Phys. Status Solidi, B100, K73 (1980).
9. M.V. Sorokin and G.K. Chirkin, Soviet Phys. Solid State 21, 169 and 1720 (1979).
10. K. Morimoto, K. Shimomura and M. Yoshida, J. Phys. Soc. Jap. 46, 627 (1979).
11. F. Koksal and S. Bahceli, J. Chem. Soc. Faraday Trans. (II) 74, 1844 (1978).
12. R. Blinc, M. Burgar and V. Rutar, Solid State Commun. 27, 1021 (1978).
13. M. Bogdan, Rev. Roum. Phys. 23, 197 (1978).
14. F.S. Stibbe and N.J. Trappeniers, Physica B & C 95, 81 (1978).
15. K.V. Ramanathan and R.Srinivasan, J. Phys. Chem. Solids 39, 891 (1978).
16. N.J. Trappeniers, F.S. Stibbe and J.L. Rao, Chem. Phys. Lett. 56, 10 (1978).
17. S. Radhakrishna, B.V.R. Chowdari and A.K. Viswanath, J. Chem. Phys. 66, 3938 (1977).
18. P.R. Srinivasan and R.L. Lichter, J. Magn. Reson. 28, 227 (1977
19. Z.M. El Saffar and J. Erhard, J. Chem. Phys. 67, 5335 (1977).
20. P.J. Van der Valk and N.J.Trappeniers, Chem.Phys.Lett.52, 225 (1977).
21. R.S. Hallsworth, D.W. Nicoll, J. Peterneli and M.M. Pinter, Phys. Rev. Lett. 39, 1493 (1977).
22. M.D. Sastry, J. Chem. Phys. 64, 3957 (1976).
23. K.H. Michel, Proc. Int. School of Phys. (Enrico Fermi Course) LIX local properties of phase transition, Verenna, Italy 9-21 July (1973)(Amsterdam, Netherlands, North Holland 1976), p.392.
24. S. Radhakrishna, B.V.R. Chowdari and A. Kasi Viswanath, Chem. Phys. Lett. 42, 319 (1976).

25. J.D. Donaldson and J. Silver, J. Solid State Chem. 18,117(197
26. K. Watanabe and H. Abe, Phys. Status Solidi B72, 275 (1975).
27. V. Leupei, A. Lupei and F. Domsa, J. Magn. Reson. 19, 337(197
28. K. Watanabe and H. Abe, J. Phys. Soc. Jap. 38, 785 (1975).
29. S. Radhakrishna, B.V.R. Chowdari and A.K. Viswanath, Chem. Phys. Lett. 30, 231 (1975).
30. A. Lupei, V. Lupei, A. Stefanescu and F. Domsa, Rev. Roum. Phys. 20, 59 (1975).
31. J.A. Van Wyk, J. Magn. Reson. 18, 235 (1975).
32. K. Watanabe and H. Abe, Phys. Lett. A51, 415 (1975).
33. F.S. Stibbe and N.J. Trappeniers, Proceeding of the 18th Ampere Congress on Magn. Reson. and Related Phenomena, Vol.I, Notingham, England 9-14 Sept. 1974 (Amsterdam, North-Holland, 1975) p-137.
34. M.J.R. Hoch, S.P. McAlister and M.I. Gordon, ibid.,Vol.II,p.30
35. D.F. Cooke and K.R. Jeffrey, J. Magn. Reson. 18, 455 (1975).
36. M.J.R. Hoch, S.P. McAlister and M.I. Gordon, J. Phys. C8, 53 (1975).
37. W. Mandema and N.J. Trappeniers, Physica 76, 85 (1974).
38. ibid., 76, 123 (1974).
39. ibid., 76, 73 (1974).
40. ibid., 76, 102 (1974).
41. K. Shimomura, R. Sugimoto and H. Negita, J. Sci. Hiroshima Univ. (Jap.) 38, 71 (1974).
42. F. Boettcher and J.M. Spaeth, Phys. Status Solidi B61,465(1974
43. ibid., B62, 65 (1974).
44. M. Punkkinen, J. Nonmet 2, 79 (1974).
45. M. Punkkinen and P. Ingman, Phys. Fenn (Finland) 9, 57 (1974).
46. I.J. Lowe, K.W. Volmers and M. Punkkinen, Proc. of the 1st Specialized Ampere Colloquium on Pulsed NMR and Spin Dynamics in Solids, Knakow, Poland, 28 Aug.-1 Sept. (1973), p.70.
48. K.R. Jeffrey, A.G. Brown and R.L. Armstrong, Phys. Rev. B8, 3071 (1973).
47. S. Veda, Mem. Fac. Technol Kanazawa Univ. (Jap.) 7, 167 (1973).
49. P.A. Spight and K.R. Jeffrey, J. Magn. Reson. 10, 195 (1973).
50. S.V. J. Lakshman and J. Lakshmana Rao, Physica 68, 123 (1973).
51. S.H. Hagen and N.J. Trappniers, Physica, 66, 166 (1973).
52. K.H. Michel, J. Chem. Phys. 58, 142 (1973).
53. M.D. Sastry, NPSSP, Bangalore, India, 27-31, Dec. (1973).

54. A. Walton and H.E. Petch. Phys. Rev. B7, 12 (1973).

55. A.G. Brown, R.L. Armstrong and K.R. Jeffrey, Phys. Can. 29, 46 (1973).

56. P.A. Narayana and K.V.L.N. Sastry, J. Chem. Phys. 58,769(1973).

57. Z.T. Lalowicz and J.W. Hennel, Acta Phys. Pol. A44, 637 (1973).

58. R. Ikeda and C.A. McDowell, Mol. Phys. 25, 1217 (1973).

59. F.I. Bashirov, Yu. L. Popov, K.S. Saikin and R.A. Dautov, Soviet Phys. JEPT 35, 937 (1972).

60. T. Kodama, J. Magn. Reson. 7, 137 (1972).

61. A.R. Sharp, J. Peterneli, D.W. Nicol and M.M. Pintar, 17th Congress Ampere Nuclear Magn. Reson. and Related Phenomena, Turku, Finland, 21-26 Aug. 1972, p.19. (Turku Finland : Wihuri Physical Laboratory 1972).

62. M. Punkkinen, ibid., p.20.

63. P.A. Narayana and K.V.L.N. Sastry, J. Chem. Phys. 57, 3266 (1972).

64. J.W. Hennel and Z.T. Lalowicz,(17th Congress Ampere Nuclear Magn. Reson. and Related Phenomena, Turku, Finland, 21-26 Aug. 1972, p.18.

65. N. Kuroda and A. Kawamori, J. Phys. and Chem. Solid 32, 1233 (1971).

66. B. Bechtle, F. Boettcher and J.M. Spath, Phys. Status Solidi 43, K169 (1971).

67. R.L. Lichter and J.D. Roberts, J. Am. Chem. Soc. 93, 3200 (1971).

68. K. Shimomura; T. Kodama and H. Negita, J. Phys. Soc. Jap. 31, 1291 (1971).

69. A.R. Sharp, S. Vrscaj and M.M. Pintar, Conf. on Magn. Reson. and Related Phenomena, Bucharest, Romania, 1-5 Sept. 1970 (Bucharest, Romania: Inst. Atomic Phys. 1971) p.22.

70. I.H. Parker , J. Phys. C4, 2967 (1971).

71. K.V.S. Rao and K.V.L.N. Sastry, Chem. Phys. Lett. 6, 485(1970).

72. I.H. Parker, J. Phys. C3, 298 (1970).

73. P.A. Narayana and K.V.L.N. Sastry, Phys. Status Solidi 41, K9 (1970).

74. A.R. Sharp and M.M. Pintar, J. Chem. Phys. 53, 2428 (1970).

75. P.A. Narayana and P. Venkateswarlu, ibid. 52, 5159 (1970).

75a. M.H. Reilly and C.L. Marguardt, ibid. 53, 3248 (1970).

76. W.C. Lin, C.A. McDowell and M.D. Sastry, Chem. Phys. Lett. 3, 244 (1969).

77. C.L. Marguardt and F.W. Patten, Solid State Commun. 7, 393 (1969).

78. E.M. Roberts and C.W. Merideth, Phys. Rev. 179, 381 (1969).

79. N. Kuroda, A. Kawamori and E. Mito, J. Phys. Soc. Jap. 26, 868 (1969).

80. L. Niemala and E. Yeinen, Ann- Acad. Sci. Fennicaea AVI 307, 7 (1969).

81. F.W. Patten, Phys. Rev. 175, 1216 (1968).

82. D.E. Woessner and B.S. Snowden, Jr., J. Phys. Chem. 72, 1139 (1968).

83. J.A. Kennewell, J.R. Pibrow and J.H. Price, Phys. Lett. 07A, 228 (1968).

84. K.V. Rao and M.D. Sastry, Chem. Phys. Lett. 2, 20 (1968).

85. M. Pintar, A.R. Sharp and S. rscai, Phys. Lett. 27A, 169 (1968).

86. T. Tsang, T.C. Farrar and J.J. Rush, J. Chem. Phys. 49, 4403 (1968).

87. A. Forman and J.A. Van Wyk, Canad. J. Phys. 45, 3381 (1967).

8. M.D. Sastry and P. Venkateswarlu, Mol. Phys. 13, 161 (1967).

89. J.R. Pilbrow and J.M. Spaeth, Phys. Status Solidi 20, 225 and 237 (1967).

90. S. Veda and J. Itoh, J. Phys. Soc. Jap. 22, 927 (1967).

91. D.E. Woessner and B.S. Snowden, Jr., J. Phys. Chem. 71, 952 (1967).

92. M. Linzer and R.A. Forman, J. Chem. Phys. 46, 4690 (1967).

93. D.E. Woessner and B.S. Snowden, Jr., J. Chem. Phys. 47, 378 (1967).

94. G.M. Larin, I.V. Miroshinichenko and G.K. Chirkin, Soviet Phys. Solid State 9(2) (1967).

95. D.E. Woessner and B.S. Snowden, Jr., J. Chem. Phys. 47, 2361 (1967).

96. M.D. Sastry and P. Venkateswarlu, Proc. Ind. Acad. Sci. A66, 208 (1967).

97. D.H. Goode, J. Chem. Phys. 45, 1366 (1966); A. Forman and J.A. Van Wyk, ibid., 44, 73 (1966).

98. M.M. Zaripov and G.K. Chirkin, Soviet Phys. Solid State 7, 2391 (1966).

99. ibid., 7, 2744 (1966).

100. N.J. Trappeniers and W. Mandema, Physica 32, 1170 (1966).

101. V. Hovi and P. Pyykko, Phys. Kondens Materie 5, 1 (1966).

102. V. Hovi and P. Pyykko, Second Nordic Solid State Conf. Tylosand (1968) (Goteborg Chalmers Univ. of Tech. 1966) CC5.

103. F.W. Patten and M.J. Marrone, Phys. Rev. 142, 513 (1966).

104. L. Niemela and E. Soini, Ann. Acad. Sci. Fennica AVI205, 12 (1966).

105. L. Niemela and E. Soini, Second Nordic Solid State Conf. Tylosand (1968) (Goteborg Chalmers Univ. of Tech. 1966) CC5.

106. N.J. Trappeniers and S.H. Hagen, Physica 31, 251 (1965).

107. ibid., 31, 122 (1965).

108. M.M. Zaripov and G.K. Chirkin, Soviet Phys. Solid State 7, 74 (1965).

109. S.W. Rabideau and P. Waldstein, J. Chem. Phys. 42, 3822 (1965).

110. M.M. Zaripov and G.K. Chirkin, Soviet Phys. Solid State 6, 1290 (1964).

111. H.R. Zeller, L. Vannotti and W. Kanzig, Phys. Kondens Materic (Germany) 2, 133 (1964).

112. T.J. Seed, J. Chem. Phys. 41, 1486 (1964).

113. V. Hovi and Pyykko, Proc. 9th Int. Conf. Low Temp. Phys. Columbus 1964, New York, Plenum Press (1965), Pt. B, pp.1175.

114. J. Itoh, R. Kusaka and Y. Saito, J. Phys. Soc. Jap. 17, 463 (1962).

115. J. Itoh and Y. Yamagata, ibid. 17, 481 (1962).

116. R.E. Richards and T. Schaefer, Trans. Faraday Soc. 57, 210 (1961).

117. H. Abe and H. Shirai, J. Phys. Soc. Jap. 15, 1711 (1960).

118. H.A. Levy and S.W. Peterson, J. Chem. Phys. 21, 336 (1953), Phys. Rev. 86, 766 (1952); 83, 1270 (1951).

APPENDIX B

ALGORITHM OF THE COMPUTATIONAL METHOD FOR SHP OF IONS WITH $S > \frac{1}{2}$

Here, the simplified algorithm of the computational method for fitting the SHP of ions with $S > \frac{1}{2}$ in an orthorhombic or higher symmetry of crystalline field, is given. The computer program can be written easily from it for the calculation of 2S spin-Hamiltonian parameters from the 2S values of observed resonance fields for single orientation of $\vec{H}$. More than 2S spin Hamiltonian parameters can be fitted using data ror resonance fields at more than one orientation of for $\vec{H}$ This fitting method is considerably fast as all the parameters get fitted simultaneously.

Steps for Computation :

(1) Express the spin Hamiltonian (SH) matrix as : $\mathcal{H} = \sum_{i=1}^{2S} x_{(i)} T^{(i)}$ and define the $T^{(i)}$ operator matrices and $x_{(i)}$ parameters to be fitted.

(2) Read 2S experimental resonance fields and matching microwave quantum.

(3) Assign initial values $x_{(i)}^{(o)}$ to the $x_{(i)}$ parameters.

(4) Construct the SH matrix using the initial estimates $x_{(i)}^{(o)}$ for SHP.

(5) Compute the values of 2S theoretical resonance fields (H_j^T) by matching the separation between the levels corresponding to $\Delta M_s = \pm 1$.

(6) Choose a positive integer M (usually = 10) and define 2S increments $(\Delta H_j) = (H_j^o - H_j^T)/M$.

(7) Assign L = 1 i.e. step first .

(8) Compute 2S step fields $H_j^{(L)} = H_j^T + L.(\Delta H_j)$.

(9) Assign N = 1 (i.e. first iteration).

(10) Do the following for j = 1, 2S :

(i) Construct SH matrix with $H = H_j^{(L)}$ and $x_i = x_i^{(o)}$.

(ii) Diagonalize to obtain 2S+1 eigen values E_k and the eigen vector matrix C such that $C^{\dagger} \mathcal{H} C = \mathcal{H}_{diagonal}$

(iii) Evaluate functions; $F_j = \left(\left| E_k - E_{k+1} \right| - \frac{h\nu}{\beta} \right)^2$ and

$$R_{ik} = \sum_{p,q}^{2S+1} C_{pk} C_{qk} T^{(i)} \; ; \; k=j,j+1; \; i=1,\ldots 2S.$$

(iv) $\Delta R_{ij} = R_{ij} - R_{i(j+1)}, \; i=1,\ldots,2S$

(11) Compute F : $F = \sum_{j=1}^{2S} F_j$

(12) Evaluate the following functions for k=1,...,2S and i=1,...,2S :

(i) $B_{ik} = \sum_{j=1}^{2S} R_{kj} \, \Delta R_{ij}$ and

(ii) $D_i = \sum_{j=1}^{2S} F_j \, \Delta R_{ij}$

(13) Construct set of linear equations :

$$\sum_{k=1}^{2S} B_{ik} \, \Delta x_i = D_i \; , \; i=1,\ldots,2S$$

(14) Solve for Δx_i and construct modified values for initial estimates :

$$x_i^{(N)} = x_i^{(o)} + \Delta x_i \quad , \quad i = 1, 2S$$

(15) Replace $x_i^{(o)}$ by $x_i^{(N)}$ for next iteration

i.e. $x_i^{(o)} = x_i^{(N)}$.

(16) Define convergence limit ΔF (usually 10^{-2} to 10^{-3})

If $F \leqslant \Delta F$ go to step 17.

If $F > \Delta F$ then put N = N + 1 and go to 10.

(17) If L = M go to 18 and if L $\lessdot$ M assign L = L+1 and go to step 8.

(18) $x_i^{(N)}$ are the fitted SHP.

(19) STOP

(20) END

******